

# **Functionalization of Supramolecular Assemblies of Polyaromatic Oligophosphates and Energy Transfer in DNA-assembled Oligochromophores**

Inauguraldissertation  
der Philosophisch-naturwissenschaftlichen Fakultät  
der Universität Bern

vorgelegt von

Nutcha Bürki

von Worb BE

Leiter der Arbeit:

Prof. Dr. Robert Häner

Departement für Chemie, Biochemie und Pharmazie der Universität Bern

Original document saved on the web server of the University Library of Bern



This work is licensed under the  
Creative Commons Attribution-Non-Commercial 4.0 International License. To view a copy of this license, visit  
<https://creativecommons.org/licenses/by-nc/4.0/> or send a letter to Creative Commons, PO Box 1866, Mountain View, CA 94042, USA.

# Copyright Notice

This document is licensed under the Creative Commons Attribution-Non-Commercial 4.0 International License.  
<https://creativecommons.org/licenses/by-nc/4.0/>

## You are free to:



**Share** - copy and redistribute the material in any medium or format

**Adapt** - remix, transform, and build upon the material

## Under the following terms:



**Attribution** - You must give appropriate credit, provide a link to the license, and indicate if changes were made. You may do so in any reasonable manner, but not in any way that suggests the licensor endorses you or your use.



**NonCommercial** — You may not use the material for commercial purposes.

For any reuse or distribution, you must take clear to others the license terms of this work.

Any of these conditions can be waived if you get permission from the copyright holder.

Nothing in this license impairs or restricts the author's moral rights according to Swiss law.

The detailed license agreement can be found at:  
<https://creativecommons.org/licenses/by-nc/4.0/legalcode>



# **Functionalization of Supramolecular Assemblies of Polyaromatic Oligophosphates and Energy Transfer in DNA-assembled Oligochromophores**

Inauguraldissertation  
der Philosophisch-naturwissenschaftlichen Fakultät  
der Universität Bern

vorgelegt von

Nutcha Bürki

von Worb BE

Leiter der Arbeit:

Prof. Dr. Robert Häner

Departement für Chemie, Biochemie und Pharmazie der Universität Bern

Von der Philosophisch-naturwissenschaftlichen Fakultät angenommen.

Bern, 08.06.2021

Der Dekan

Prof. Dr. Zoltan Balogh

---

# Acknowledgements

First of all, I would like to thank Prof. Robert Häner for giving me the opportunity and the scientific freedom to do my PhD thesis in his research group for the past 4 years.

Furthermore, I want also to thank Dr. Christopher Serpell to act as an external co-referee for my thesis, and also sincere thanks to Prof. Andreas Türler to agree to be the chairman of my PhD defence.

I would also like to thank Prof. Thomas Feurer, Prof. Andrea Cannizzo and their coworkers for the collaboration in the context of the National Center of Competence in Research - Molecular Ultrafast Science and Technology (NCCR-MUST).

My thanks go also to all the past and current members of the research group, especially, I would like to thank Simon M. Langenegger for helping me with the illustrations, but also for the interesting and very helpful discussions through all these 4 years and Markus Probst for proofreading my thesis with patience. Additionally, I want to thank my master student Elena Grossenbacher (2019) for her help for my own work.

Financial support of the NCCR-MUST, the Swiss National Science Foundation (SNF) and the University of Bern are gratefully acknowledged.



---

# Contents

<b>Acknowledgements</b>	<b>i</b>
<b>Summary</b>	<b>1</b>
<b>1. General Introduction</b>	<b>2</b>
1.1. Supramolecular Polymers . . . . .	2
1.2. DNA . . . . .	4
1.2.1. Supramolecular DNA Based Architectures . . . . .	7
1.3. Energy Transfer and Light-Harvesting . . . . .	9
<b>2. Self-assembly of Polyaromatic Oligophosphates</b>	<b>11</b>
2.1. Introduction . . . . .	11
2.2. Aim of the Work . . . . .	13
2.3. Results & Discussion . . . . .	14
2.3.1. Approaches to Form Functionalized DNA-modified Nanosheets . . . . .	14
2.3.2. Self-assembly of Phenanthrene Trimer and DNA Phenanthrene Conjugates .	18
2.4. Conclusion . . . . .	23
2.5. Experimental Section . . . . .	25
<b>3. Functionalized Vesicles of Phenanthrene DNA Conjugates</b>	<b>27</b>
3.1. Introduction . . . . .	27
3.2. Aim of the Work . . . . .	29
3.3. Results & Discussion . . . . .	30
3.3.1. Formation of DNA-modified Vesicles . . . . .	30
3.3.2. Hybridization with Au Nanoparticles . . . . .	33
3.3.3. Energy Transfer . . . . .	34
3.3.4. Additional Experiment . . . . .	36

3.4. Conclusion . . . . .	39
3.5. Experimental Section . . . . .	41
<b>4. Self-assembly of Photocleavable Helical Ribbon Structures</b>	<b>43</b>
4.1. Introduction . . . . .	43
4.2. Aim of the Work . . . . .	45
4.3. Results & Discussion . . . . .	47
4.3.1. Self-assembly of 1D helical ribbons . . . . .	47
4.3.2. Irradiation of the ribbons . . . . .	49
4.4. Conclusion . . . . .	57
4.5. Experimental Section . . . . .	58
<b>5. Energy Transfer in DNA-assembled Oligochromophores</b>	<b>60</b>
5.1. Introduction . . . . .	60
5.2. Aim of the work . . . . .	62
5.3. Results & Discussion . . . . .	63
5.3.1. Limits of the Chromophore Segmentation . . . . .	63
5.3.2. DNA Duplexes containing Mismatches . . . . .	69
5.4. Conclusion . . . . .	73
5.5. Experimental Section . . . . .	74
<b>Bibliography</b>	<b>76</b>
<b>A. Appendix Chapter 2</b>	<b>86</b>
<b>B. Appendix Chapter 3</b>	<b>102</b>
<b>C. Appendix Chapter 4</b>	<b>117</b>
<b>D. Appendix Chapter 5</b>	<b>127</b>
<b>Curriculum Vitae</b>	<b>141</b>
<b>Erklärung</b>	<b>142</b>



---

# Summary

In the beginning of this thesis a general introduction is given to explain the main aspects of supramolecular polymers, the structure of the DNA and the advantages of combining the two into supramolecular assemblies and in the last part of the introduction the light-harvesting systems will be discussed.

Thereafter the experimental work of this thesis will be presented and can be separated into two main parts: In chapters 2 and 3 the formation and investigation of functionalized supramolecular assemblies of polyaromatic oligophosphates will be shown. In the second part, chapters 4 and 5, the energy transfer in DNA-assembled oligochromophores will be presented and discussed.

The first main part consists of three projects with the same goal: the functionalization of supramolecular polymers of polyaromatic oligophosphates. In chapter 3 the formation and investigation of DNA-modified vesicles will be discussed. In the last chapter an extension of previous studies of the group Häner will be shown, which is the incorporation of a photocleaver into a pyrene DNA-conjugate and the formation of DNA-modified fibres.

---

# 1. General Introduction

## 1.1. Supramolecular Polymers

Supramolecular polymers are built-up of repeating molecules that are held together by non-covalent interactions and are formed through self-assembly of building blocks.<sup>1-7</sup> In aqueous medium the self-assembly is based on Coulomb, van der Waals interactions, hydrogen bonds and hydrophobic effect.<sup>8,9</sup> In biology, chemistry and physics the ability of the self-assembly of molecules to form large clusters under equilibrium conditions is widely found. If the driving force for polymer growth is significantly contributed from the non-covalent interactions, the polymerization is considered to be a supramolecular polymerization.<sup>10</sup> Most of the supramolecular polymers are also reversible because of the before mentioned non-covalent interactions between the monomers.<sup>11</sup>

Classification of the supramolecular polymerizations is based on three different principles: (1) Physical origin classification; (2) structural monomer classification; (3) thermodynamical classification. Addition of a second or third dimension influences the free energy of the self-assembly of the polymer when changing the temperature or concentration, because of the additional interaction energies. So, depending on the dimension of the aggregate a fourth classification scheme is possible.<sup>2</sup>

Supramolecular polymerization growth can be divided into three mechanism: cooperative, isodesmic and ring-chain growth.<sup>1,2</sup> The isodesmic polymerization is characterized by a high polydispersity, the association constant of the monomer strongly affects the degree of polymerization (see Figure 1.1).<sup>2</sup> At all polymerization process step the reversible formation of a single non-covalent bond is identical. That means, the reactivity of the non-aggregated monomer with the growing polymer is not dependent on the length of the polymer chain.

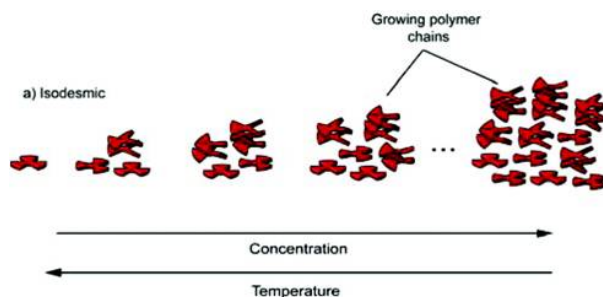


Figure 1.1.: Illustration of the supramolecular polymerization mechanisms. a) Isodesmic growth. The growth can be influenced by concentration or/and temperature. Adapted from reference<sup>2</sup>.

The next supramolecular polymerization mechanism is the ring-chain growth (see Figure 1.2). In this case, closed rings of monomers are in equilibrium with the linear polymers and oligomers. Small polymers chains react preferably with each other to form a closed ring, when the monomer concentration is below a certain point. In contrary, above a certain monomer concentration the polymer grow and the formation of linear chain is more favourable.<sup>2</sup>

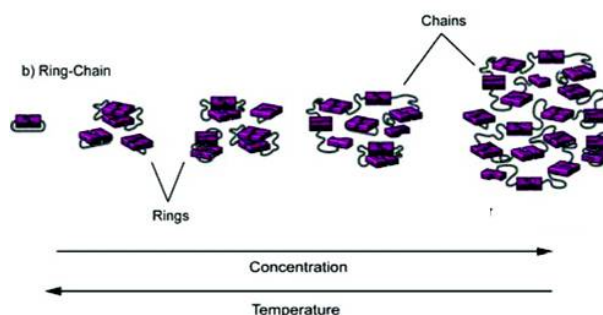


Figure 1.2.: Illustration of the supramolecular polymerization mechanisms. b) Ring-chain growth. The growth can be influenced by concentration or/and temperature. Adapted from reference<sup>2</sup>.

Supramolecular polymerization growth with the cooperative (nucleation-elongation) mechanism is slightly different (see Figure 1.3), to incorporate into the supramolecular polymers the monomers

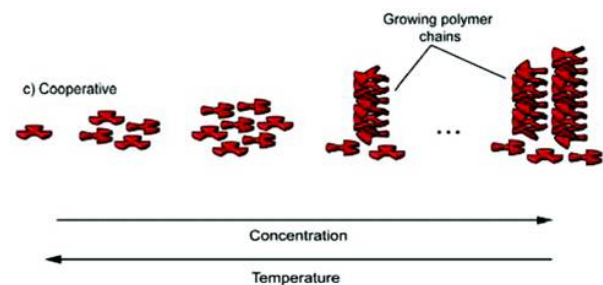


Figure 1.3.: Illustration of the supramolecular polymerization mechanisms. c) Cooperative mechanism. The growth can be influenced by concentration or/and temperature. Adapted from reference<sup>2</sup>.

need to adopt a high-energy conformation. Therefore, the formation starts very slowly, a stable nucleus has to be formed first, then additional monomers become favourable for the incorporation and the growing rate of the polymerization is higher.<sup>2,7</sup>

But all mechanisms have one thing in common; changing the condition, the concentration of the monomer, the temperature and/or changing the solvent, can have an impact on the polymerization degree or/and polymerization itself.<sup>7</sup>

Supramolecular polymers are very interesting soft materials, they are very interesting for biorelated and clinical applications, and can also act as soft electronics as well.<sup>12–14</sup>

## 1.2. DNA

Deoxyribonucleic acid, or abbreviated, DNA. For better understanding of the use of DNA in health, technology or generally speaking in science, it is necessary to understand the structure of DNA and its properties will be presented.

DNA can be separated basically in three main components, the nitrogen base, the deoxyribose sugar, and the phosphate group (see Figure 1.4).<sup>15</sup>

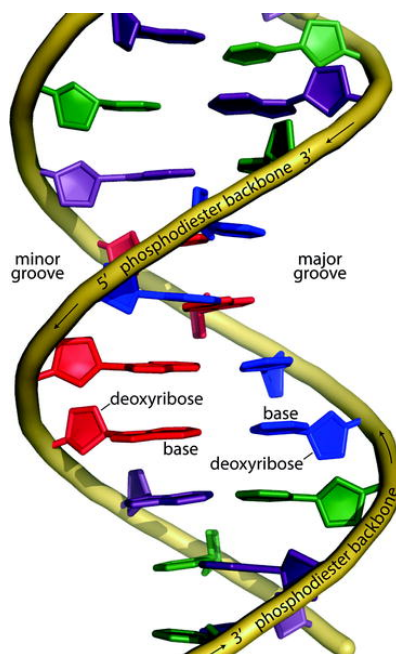


Figure 1.4.: Illustration of the main components of the DNA double helix. The colouration for the nucleobases are the same as in Figure 1.5. Figure from reference<sup>16</sup>.

With these three components it forms a long chain, the sugar and the phosphate are joined in alternating order in 3' 5' phosphate di-ester linkages, this part of the DNA is also called the backbone. One of the four different nitrogenous base is attached to each sugar, the four most common found in DNA are adenine (A) and guanine (G), which are the purines, and the other are thymine (T) and cytosine (C), which are the pyrimidines (see Figure 1.5). Because of the regular internucleotide linkage the chain is unbranched. As for the sequence of nucleic bases, the sequence of nucleic bases can be arranged completely arbitrarily, it only depends of the function of the DNA strand.<sup>15,17-20</sup>

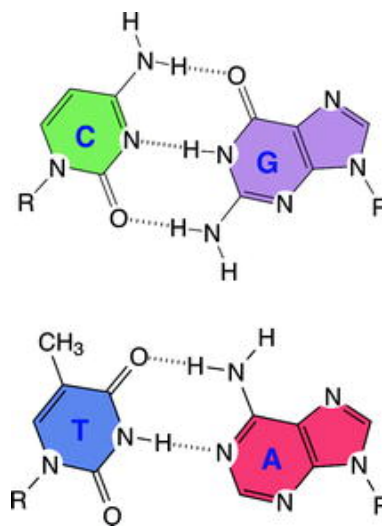


Figure 1.5.: Chemical structures of the four nucleobases. In green is cytosine (C), in violet is guanine (G), in blue thymine (T) and in red adenine (A). The nucleobases are paired according to the Watson-Crick base pairs rule. The hydrogen bonds are indicated in dotted lines. Figure from reference<sup>16</sup>.

According to the Watson-Crick base pairing rule, pyrimidines are only complementary with purines. So, two nucleotides, each on a different DNA strand, form via hydrogen bonds a base pair. Adenine pair with thymine using two hydrogen bonds, and cytosine forms via three hydrogen bonds with guanine the second base pair.<sup>15</sup> A - T pair rich DNA are more sensitive to denaturation and melting than DNA with higher G - C pair amount. The four nucleotides differ also in size, the pyrimidine nucleobases cytosine and thymine are molecules with a single aromatic ring, and the purine nucleobases, adenine and guanine, have two aromatic rings.<sup>20</sup>

Two complementary DNA strands hybridize to an antiparallel right-handed double-helix, where base pairs are centred on the helical axis and the sugar-phosphate backbones are on the outer part.<sup>15,16</sup> The driving force for this process of nucleation are the hydrophobic effect and base stacking, which the latter contributes to the duplex stability, rather than the hydrogen bonding.<sup>21-24</sup> The distance between the nucleotide bases is approximately 0.34 nm, one helical turn is 3.4 nm and consist  $\sim 10.3$  base pairs. The helix has a narrow minor groove and a wide major groove, the diameter of the double-helix is 2.0 nm.<sup>15,16</sup> As mentioned before the base stacking plays an important role to the stability of the duplex but there are other parameters like the sequence of the DNA itself, such as nucleobases and the length of the DNA strand. Even so the concentration of the DNA and if there is any cations present.<sup>25-28</sup>

Because of the interesting characteristics of the DNA, the DNA would make an interesting material for biotechnology and nanotechnology. It was tried to make use of the DNA characteristics, therefore, methods were explored to produce it synthetically; one of the methods to synthesis DNA is the phosphoramidite solid-phase synthesis.<sup>29</sup>

It must be mentioned that the phosphoramidite oligonucleotide synthesis procedure is from 3'- to 5'-direction, so the opposite to known DNA replication. The synthesis cycle has overall 4 steps (see Figure 1.6). But at the beginning of the cycle it starts first with the detritylation of the first DMT-protected nucleoside on the solid support. The first step of the synthesis cycle is then the activation and coupling of the next nucleoside phosphoramidite monomer. The second step is the capping of the unreacted 5'-OH groups with an acetyl group (reduction of side products), and the third is the oxidation of the phosphorus (III) triester to a phosphorus(V) triester. The last, the fourth step is detritylation of the DMT-protected nucleoside again. These four steps will be repeated until the configured sequence is synthesized. After the solid-phase synthesis the oligonucleotide has to be cleaved from the solid support, and the phosphodiester backbone and also the bases have to be deprotected.<sup>29</sup>

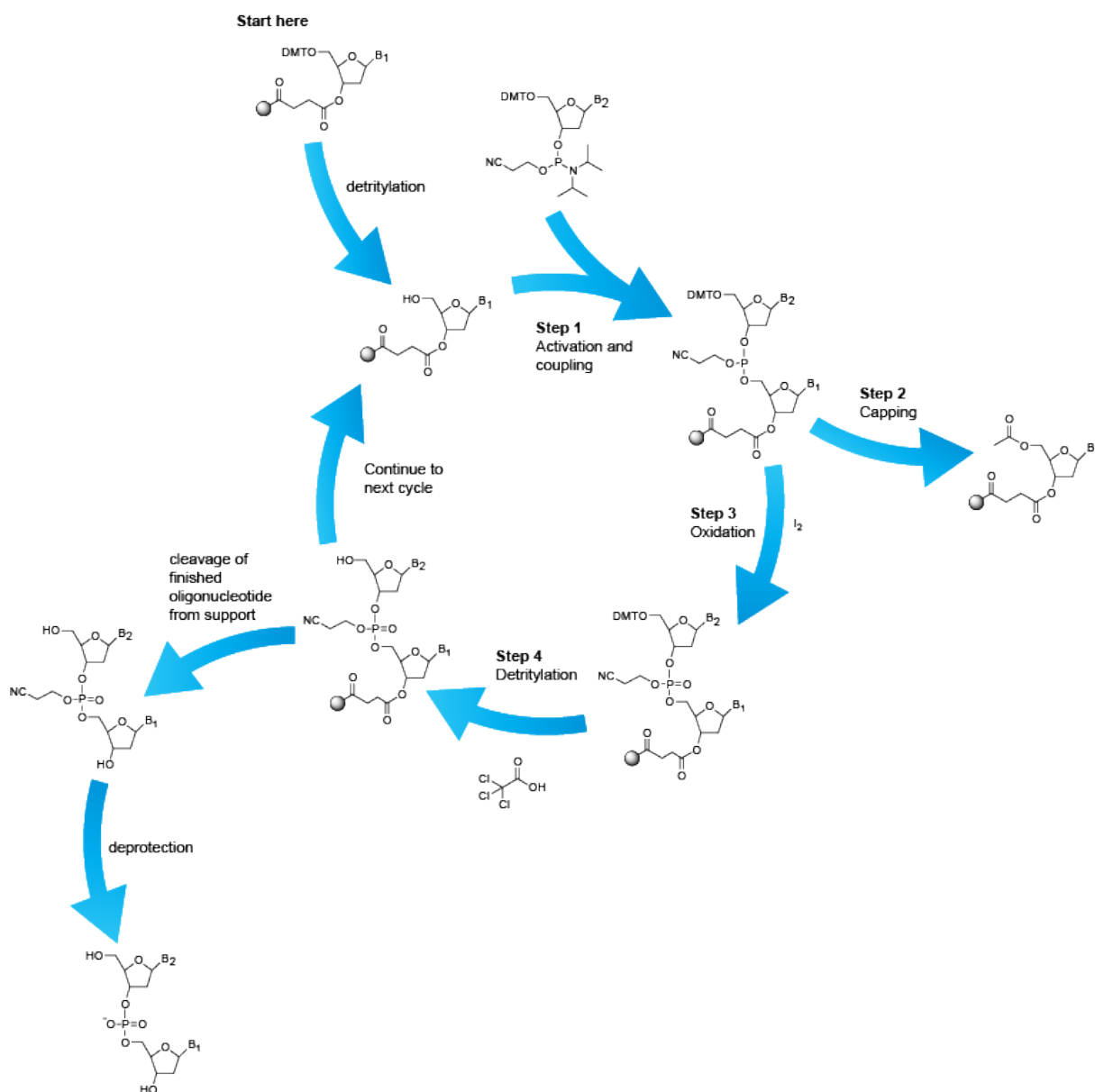


Figure 1.6.: The phosphoramidite oligonucleotide synthesis consists of cycles of a series of steps.  $B_{1,2}$  = nucleobase (A,T,G or C) and DMT = [bis-(4-methoxyphenyl)phenylmethyl]. Figure from reference<sup>29</sup>.

### 1.2.1. Supramolecular DNA Based Architectures

Shortly after the synthesis of DNA strands was well established, the research interest to modify DNA quickly evolved. Larger and more complex DNA structures, and even multidimensional nanostructures were designed.<sup>30–33</sup> Artificial DNA nucleotides were designed and merged with natural DNA, which are also called DNA conjugates. The involved additional features are of a great interest in the field of nanotechnology and material sciences.<sup>34–37</sup> Here, the DNA conjugates can be used as monomers to form supramolecular polymers, which would open up a wide new

range of possibilities. But what are the advantages of using modified DNA or DNA conjugates to form supramolecular polymers? One would be, that the presence of DNA in the nanostructures allows for further functionalization.<sup>38</sup> The advantages are the addressability, so, hybridization with a complementary single strand DNA (ssDNA); specificity, as in the last subchapter discussed, based on the Watson-Crick base pairing, the ssDNA will only hybridize with the correct, so the complementary ssDNA. The last point is the reversibility of the assembly, the denaturation of the DNA double helix under controlled conditions of pH, ionic strength, or temperature (see Figure 1.7).<sup>39,40</sup>

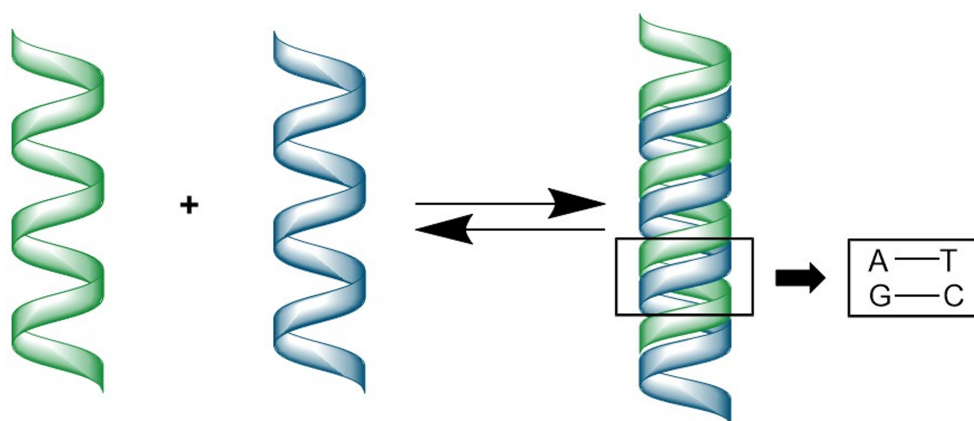


Figure 1.7.: A simple illustration of the hybridization and denaturation of two DNA single strands. For example: lowering the temperature can promote the hybridization of the DNA single strands, while heating leads to denaturation of the DNA duplex.

So, there are some advantages to modify supramolecular polymers with DNA and vice versa. Modification of DNA is not only possible with unnatural base pairs, also non-nucleosidic building blocks are possible.<sup>41–54</sup> These building blocks are linked to the DNA strand via a phosphate group and can have different property. For this work molecule with fluorescent character are of interest.<sup>55–61</sup>

In a previous study, phenanthrene and pyrene building blocks were incorporated into the center of a DNA duplex to form a DNA-based light-harvesting antenna (see Figure 1.8 and also next subchapter).<sup>62</sup> Units of  $\pi$ -stacked phenanthrene chromophores act as the light-collecting antenna, and the exciplex-forming pyrene act as the energy collector. Excitation at the wavelength of 320 nm leads to a fluorescence emission at 450 nm.



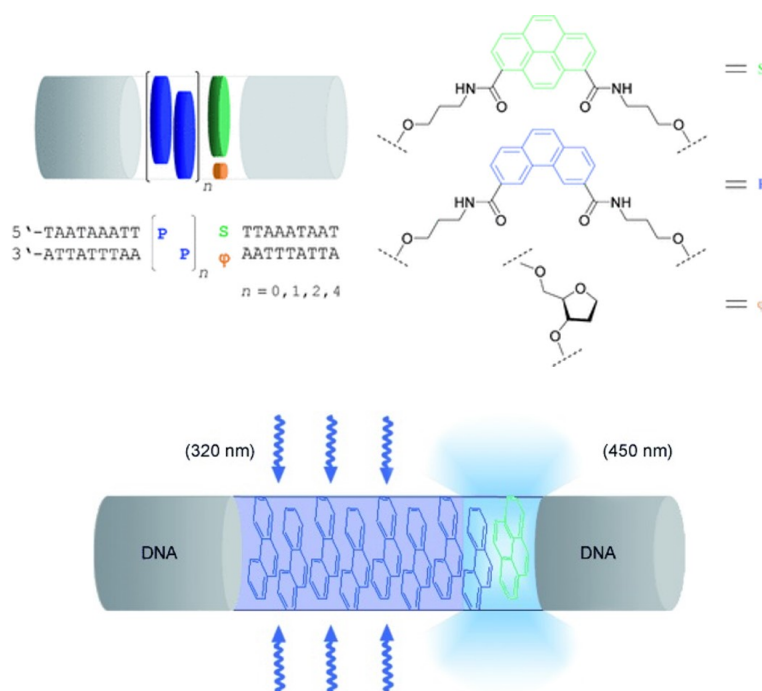


Figure 1.8.: Illustration of the DNA-based light-harvesting antenna. Fluorescence at the wavelength of 450 nm by excitation at 320 nm. Top right: Chemical structures of phenanthrene (P), pyrene (S) and an abasic side analogue  $\varphi$ . Adapted from the reference<sup>62</sup>.

### 1.3. Energy Transfer and Light-Harvesting

In the previous part, DNA modified supramolecular polymers were discussed. Modification with molecules with e.g. fluorescence properties can lead to systems where energy transfer or/and light-harvesting is possible.

The process in which the excitation energy is transferred from the initially excited molecular system (donor) to an acceptor is called excitation energy transfer (EET). The Förster resonance energy transfer (FRET) is distance-dependent and describe the EET, in cases where the electrostatic interactions between the molecular systems are weak.<sup>63</sup> The excitation hops from the donor to the acceptor and is based on electric dipole-dipole interactions. Förster explained the rate of FRET as a dependency on the inverse sixth power of intermolecular separation. If the donor and acceptor are placed within the Förster radius, FRET can be very efficient.<sup>64</sup>

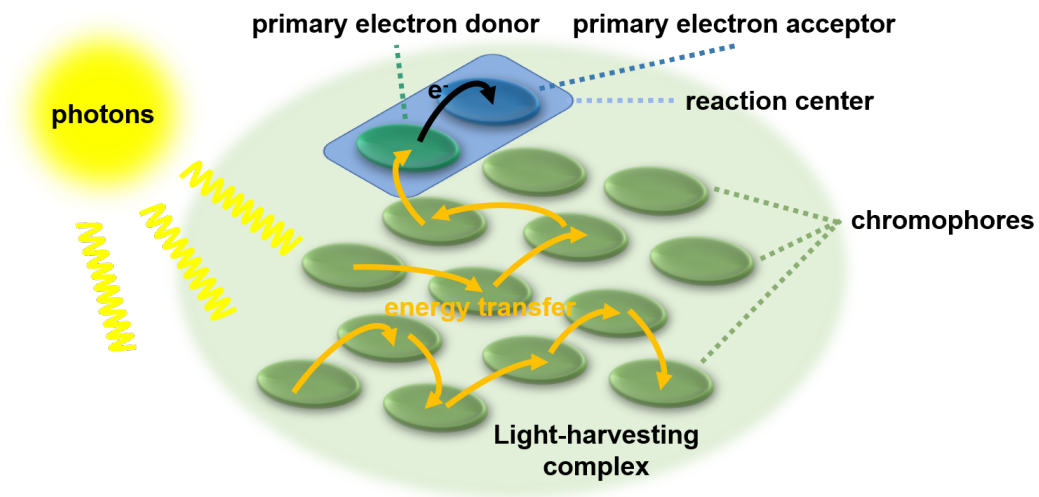


Figure 1.9.: Illustration of a light-harvesting complex. Chromophores absorb photons and the energy is transferred via other chromophores to the primary electron donor in the reaction center. The primary electron acceptor receive then the electron from the primary electron donor. Adapted from reference<sup>65</sup>.

In nature, plants, algae and some bacteria, convert energy in a process, called photosynthesis.<sup>66,67</sup> By using sunlight and carbon dioxide (CO<sub>2</sub>) they produce sugar and oxygen. For doing so, they have light-harvesting complexes (LHCs) to produce the substance they need.<sup>68</sup> The LHC contains proteins and chromophores, which absorb light for the photosynthesis and transfer the energy to photosystem reaction centres (see Figure 1.9). Chlorophyll, carotenoids, and phycobilins are the three major type of chromophores.

---

## 2. Self-assembly of Polyaromatic Oligophosphates

### 2.1. Introduction

Supramolecular polymers with functionalization possibility are of high interest. Assembly of  $\pi$ -conjugated molecules into defined structures are still attractive objects in materials sciences.<sup>3,69–81</sup> Therefore, incorporation of DNA provides an approach to functionalized supramolecular polymers and generates addressable nanoarchitectures with a variety of geometries.<sup>35,39,82–97</sup> One option to do so, is to dope or incorporate DNA conjugates, i.e. non-natural nucleobases are combined with natural DNA, into supramolecular polymers that are built of  $\pi$ -conjugated molecules. This approach was previously realized, the combination of a light-harvesting complex with DNA photonic wires was successfully formed from 3,6-dibutynylphenanthrene trimer, phenanthrene DNA conjugates and cyanine dyes (see Figure 2.1).<sup>98</sup> This construct shows a very efficient energy transfer from the phenanthrene donors to the dyes.

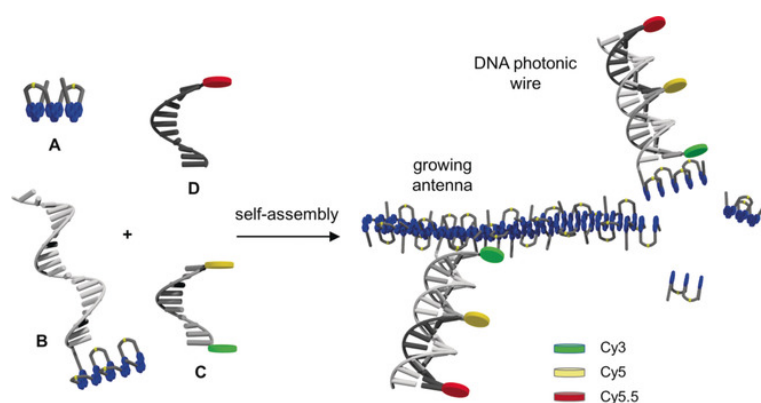


Figure 2.1.: Illustration of the self-assembly of phenanthrene trimer (A), phenanthrene DNA conjugates (B) and cyanine dyes attached to DNA strands (C,D). Figure from the reference<sup>98</sup>.

In the past, there were two supramolecular polymers that were formed from  $\pi$ -conjugated molecules that would be very interesting for this study and would be a great template for the assembly of functionalized supramolecular polymers. It was shown that phosphodiester-linked trimers of 1,6-dialkynyl-substituted pyrenes self-assemble into two-dimensional nanosheets in aqueous medium (see Figure 2.2).<sup>99,100</sup> The size of the nanosheets was controlled by changing the cooling temperature gradient.

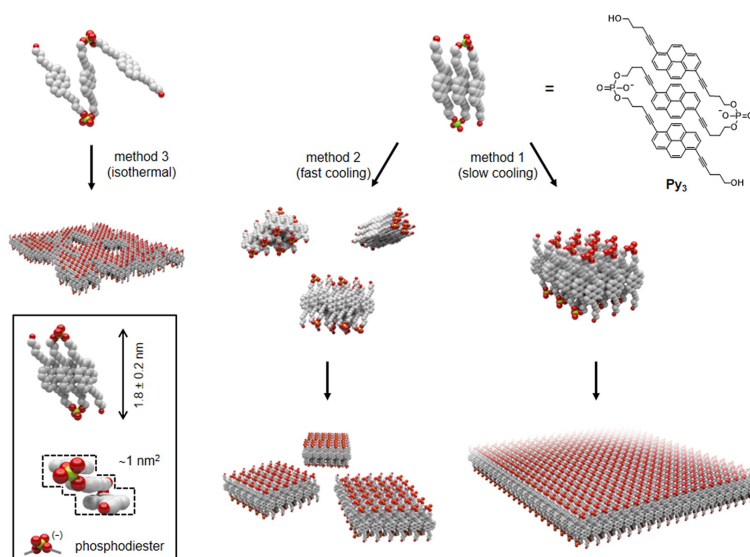


Figure 2.2.: Illustration of the **Py<sub>3</sub>** supramolecular polymerization pathway leading to two-dimensional nanosheets. Top right: Structure of **Py<sub>3</sub>**. Figure from the reference<sup>100</sup>.

The second study demonstrated that 2,7-disubstituted phosphodiester-linked phenanthrene trimers self-assemble into tubular structures (see Figure 2.3).<sup>101</sup>

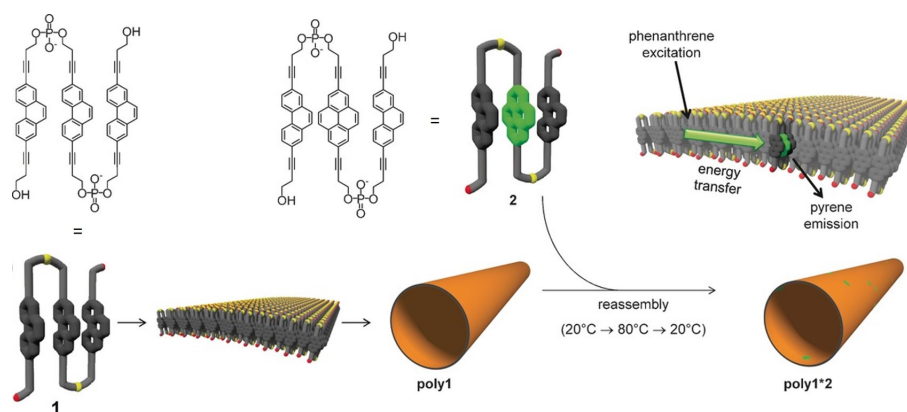


Figure 2.3.: Illustration of the supramolecular polymerization of the aromatic oligophosphates into a pyrene-doped phenanthrene nanotube. Energy is transferred from the excited phenanthrene (grey) to the pyrene acceptor (green) Top left: Structures of aromatic oligophosphates. Adapted from the reference<sup>101</sup>.

Formation of nanotubes with light-harvesting properties could be done by incorporating a pyrene (acceptor unit). Expanding these studies by doping the supramolecular polymers with DNA conjugates, would ideally result in functionalized nanosheets and/or functionalized nanotubes.

## 2.2. Aim of the Work

In this study, the aim was to obtain DNA functionalized supramolecular polymers. Therefore, different DNA conjugates were tested as potentially suitable candidates to dope the pyrene respectively phenanthrene trimers. Different conditions were tested to find an optimal condition to dope the nanosheets (see Figure 2.4) and nanotubes (see Figure 2.5). The formed supramolecular polymer structures were characterized by UV-vis spectroscopy and the visualisation of the DNA-modified nanotubes and nanosheets was done by atomic force microscopy (AFM). Furthermore, the functionalized nanosheets and nanotubes were hybridized with Au nanoparticles containing complementary DNA strand of the DNA conjugates.

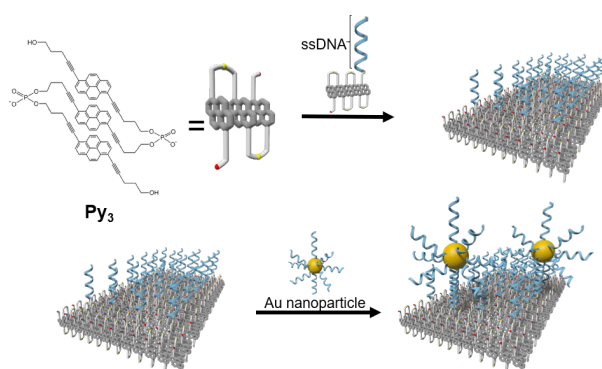


Figure 2.4.: Illustration of the supramolecular polymerization of functionalized DNA-modified nanosheets and the gold nanoparticles hybridization with the nanosheets.

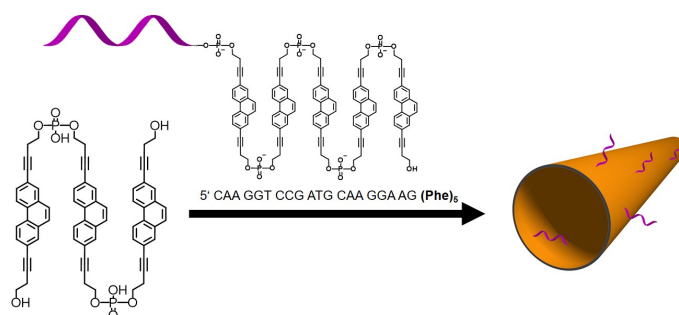


Figure 2.5.: Illustration of the supramolecular polymerization phenanthrene trimer and phenanthrene DNA conjugates into a DNA-modified phenanthrene nanotube. Adapted from the reference<sup>65,101</sup>.

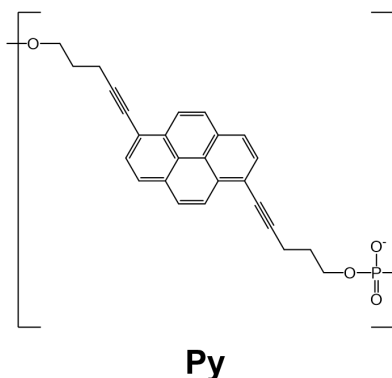
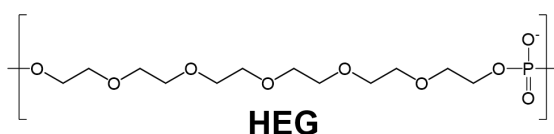
## 2.3. Results & Discussion

### 2.3.1. Approaches to Form Functionalized DNA-modified Nanosheets

Previously, it was already shown that doping the **Py**<sub>3</sub> (see chapter 2.1) with pyrene DNA conjugates to form DNA-modified nanosheets is a challenge.<sup>102</sup> In this previous study several pyrene DNA conjugates were tested: First, in between of the DNA single strand and the pyrene units a hexaethylene glycol linker (HEG) was integrated, to prevent steric hinderance. Second, also different lengths of the pyrene stack were tested. Unfortunately, in the end, the results were not conclusive and a new system had to be designed. In the present study, three such systems (pyrene DNA conjugates) therefore, were investigated (see Table 2.1).

Table 2.1.: The sequences of the synthesized compounds. Right: Chemical structure of the 1,6-dialkynylpyrene (**Py**) and hexaethylene glycol (HEG).

Oligomer	Sequence
<b>Py</b> <sub>3</sub>	Py-Py-Py
DNA-(HEG) <sub>1</sub> - <b>Py</b> <sub>7</sub>	3'-GAG TGC CTT C-(HEG)-Py-Py-Py-Py-Py-Py-Py
DNA- <b>Py</b> <sub>4</sub>	5'-CAA GGT CCG ATG CAA GGA GGA AG-Py-Py-Py-Py
DNA- <b>Py</b> <sub>5</sub>	5'-CAA GGT CCG ATG CAA GGA GGA AG-Py-Py-Py-Py-Py



In Table 2.1 are the oligomers that were used for this study. **DNA-(HEG)<sub>1</sub>-Py<sub>7</sub>** was synthesized in previous study.<sup>102</sup> **DNA-Py<sub>4</sub>** and **DNA-Py<sub>5</sub>** were synthesized according to the literature.<sup>99</sup> The pyrene DNA-conjugates consist of two, respectively three different parts. The first unit was built up of either four or five 1,6-pentynyl pyrenes. Next, was the single strand DNA (10, respectively 20 nucleobases) and in **DNA-(HEG)<sub>1</sub>-Py<sub>7</sub>** an additional hexaethylene glycol unit as introduced.

### Spectroscopic Characterisation

UV-vis spectrum of **Py**<sub>3</sub> doped with **DNA-(HEG)<sub>1</sub>-Py<sub>7</sub>** showed a J-band at 305 nm and at 335 nm a H-band, which was already observed before for the pyrene trimer (see Figure 2.6 a)).<sup>99</sup>

Doping the pyrene trimer with **DNA-Py<sub>4</sub>**, respectively **DNA-Py<sub>5</sub>** showed similar UV-vis spectra as with **DNA-(HEG)<sub>1</sub>-Py<sub>7</sub>**. By monitoring the temperature-dependent absorbance at the wave-

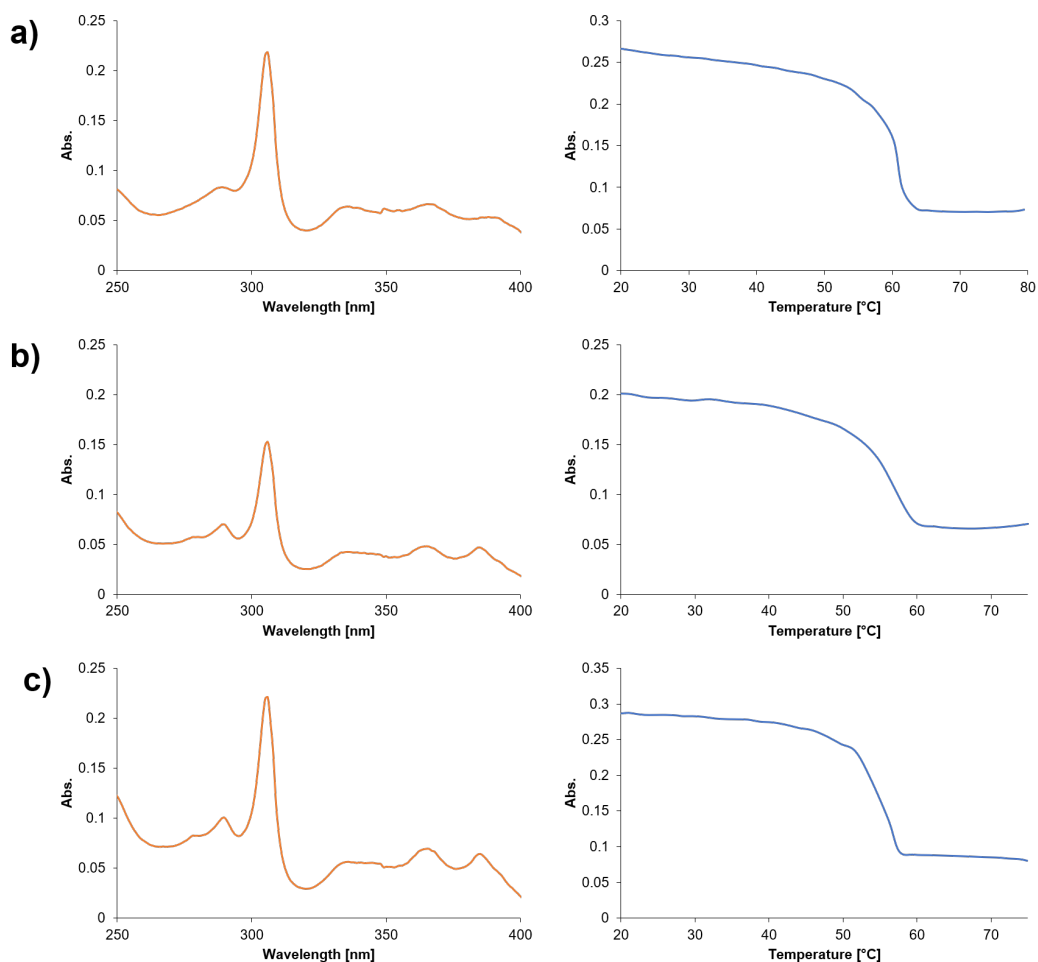


Figure 2.6.: Left: UV-vis spectra at 20 °C of  $2\mu\text{M}$  **Py**<sub>3</sub> and  $0.2\mu\text{M}$  a) **DNA-(HEG)<sub>1</sub>-Py<sub>7</sub>**; b) **DNA-Py<sub>4</sub>**; c) **DNA-Py<sub>5</sub>**, 10 mM sodium phosphate buffer, 10mM sodium chloride and 15% ethanol. Right: The cooling curve at 305 nm; temperature gradient: 15 °C/min.

length of 305 nm with a temperature gradient of 15°C/min, can give more information about the supramolecular polymerization mechanism of this system was obtained.<sup>7</sup> With the maximum of the first derivation of the cooling curves, it can be determined approximately where the transition from molecular dissolved state to the aggregated state takes place. The shape of the measured UV-vis cooling curve indicates a cooperative supramolecular polymerization process for all samples, i.e. a sharp bend in the curve. The “transition-temperatures” were determined as follows: **DNA-Py<sub>4</sub>** (59.5°C), **DNA-Py<sub>5</sub>** (57.6°C) and **DNA-(HEG)<sub>1</sub>-Py<sub>7</sub>** (56.9°C).

### Atomic Force Microscopy

Figure 2.7 reveals that **Py<sub>3</sub>** and **DNA-(HEG)<sub>1</sub>-Py<sub>7</sub>** formed supramolecular nanosheets. The AFM image shows a height of about 2 nm, which coincides with the nanosheets that were reported in the past.<sup>99</sup>.

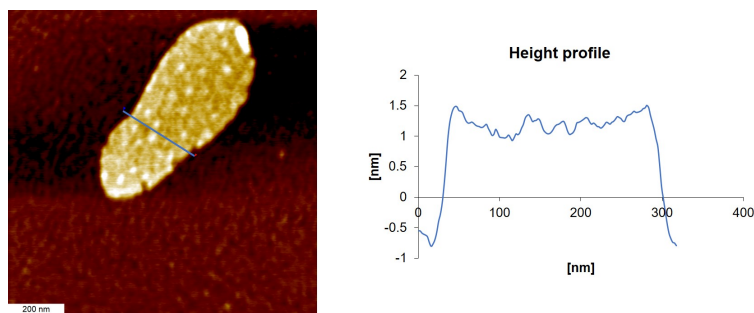


Figure 2.7.: AFM image of  $2\mu\text{M}$  **Py<sub>3</sub>** and  $0.2\mu\text{M}$  **DNA-(HEG)<sub>1</sub>-Py<sub>7</sub>** deposited on APTES-modified mica from aqueous solution containing 10 mM sodium phosphate buffer, 10mM sodium chloride and 15% ethanol. Right: corresponding height profile of the structure along the marked line in the AFM image.

The supramolecular nanosheets were hybridized with Au nanoparticles containing complementary DNA strand to investigate the presence of DNA on the nanosheets. The AFM image (see Figure 2.8) however, shows a random distribution of the AuNP-DNA on the APTES-mica, but an accumulation on the nanosheets was expected.

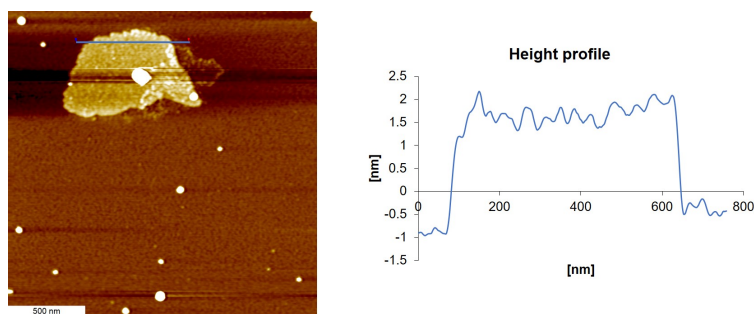


Figure 2.8.: AFM image of  $2\mu\text{M}$  **Py<sub>3</sub>** and  $0.2\mu\text{M}$  **DNA-(HEG)<sub>1</sub>-Py<sub>7</sub>**, after Au nanoparticles were added, deposited on APTES-modified mica from an aqueous solution containing 10 mM sodium phosphate buffer, 10mM sodium chloride and 15% ethanol. Right: corresponding height profile of the structure along the marked line in the AFM image.



The same experiment was done for **Py<sub>3</sub>** and **DNA-Py<sub>4</sub>**. Nanosheet-like structures could also be observed for this mixture and overall they look the same (see Figure 2.9), however, it seems that the nanosheet-like structures were larger than with **DNA-(HEG)<sub>1</sub>-Py<sub>7</sub>**. Investigation by AFM showed a random distribution of the Au nanoparticles after they were added to the preformed supramolecular polymers.

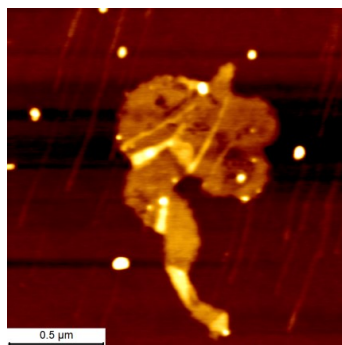


Figure 2.9.: AFM images of  $2\mu\text{M}$  **Py<sub>3</sub>** and  $0.2\mu\text{M}$  **DNA-Py<sub>4</sub>** treated with Au nanoparticles, deposited on APTES-modified mica from aqueous solution containing 10 mM sodium phosphate buffer, 10mM sodium chloride and 15% ethanol.

As previous study showed, with a different number of the pyrene building blocks, the behaviour of the self-assembly can change.<sup>83</sup> But, the AFM image (see Figure 2.10) of **Py<sub>3</sub>** and **DNA-Py<sub>5</sub>** showed also here a random distribution of the gold nanoparticles, same as for **Py<sub>3</sub>** and **DNA-Py<sub>4</sub>**.

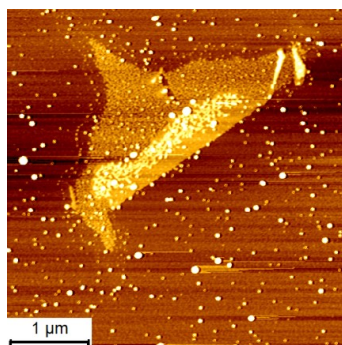


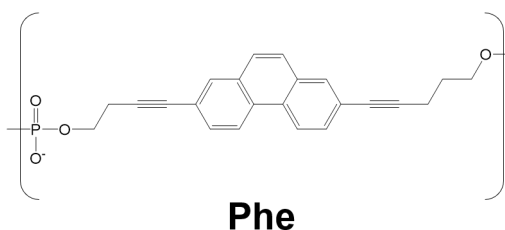
Figure 2.10.: AFM images of  $2\mu\text{M}$  **Py<sub>3</sub>** and  $0.2\mu\text{M}$  **DNA-Py<sub>5</sub>** treated with Au nanoparticles, deposited on APTES-modified mica from aqueous solution containing 10 mM sodium phosphate buffer, 10mM sodium chloride and 15% ethanol.

### 2.3.2. Self-assembly of Phenanthrene Trimer and DNA Phenanthrene Conjugates

This part of the study is similar to the previous one, however, here the main focus is on the self-assembly of functionalized supramolecular nanotubes. In Table 2.2 are the sequences of the **Phe<sub>3</sub>** and phenanthrene DNA conjugates (both phenanthrene DNA conjugates were synthesized, but not further characterized by a former group member Caroline D. Bösch, University of Bern, Department of Chemistry and Biochemistry, 2017). The oligomers were investigated in different aqueous solutions (see Table A.3 in Appendix A).

Table 2.2.: The sequences of the oligomers. Bottom: Chemical structure of the 2,7-dialkynylphenanthrene (**Phe**).

Oligomer	Sequence
Phe <sub>3</sub>	Phe-Phe-Phe
DNA-Phe <sub>3</sub>	5' CAA GGT CCG ATG CAA GGA AG Phe-Phe-Phe
DNA-Phe <sub>5</sub>	5' CAA GGT CCG ATG CAA GGA AG Phe-Phe-Phe-Phe-Phe



#### Phe<sub>3</sub> with DNA-Phe<sub>3</sub>

In the previous study, it was shown that in the presence of spermine tetrahydrochloride the **DNA-Phe<sub>3</sub>** formed vesicles.<sup>103</sup> Hence, the decision to start with a condition that also contains spermine.

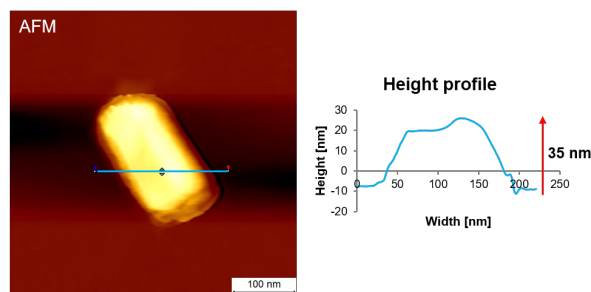


Figure 2.11.: AFM image of 0.5  $\mu\text{M}$  **Phe<sub>3</sub>** and 0.015  $\mu\text{M}$  **DNA-Phe<sub>3</sub>** deposited on APTES-modified mica from aqueous solution containing 10 mM sodium phosphate buffer, 0.1 mM spermine tetrahydrochloride and 20% ethanol. Temperature gradient: 15  $^{\circ}\text{C}/\text{min}$ . Right: corresponding height profile of the structure along the marked line in the AFM image.

The AFM image (see Figure 2.11) reveals that **Phe<sub>3</sub>** and **DNA-Phe<sub>3</sub>** in aqueous solution containing 10 mM sodium phosphate buffer, 0.1 mM spermine tetrahydrochloride and 20% ethanol, an almost rectangular structure was formed.

Lowering the polyamine concentration from 0.1 mM to 0.025 mM led to three different types of structures (see Figure 2.12): undefined structures, small, tube-like structures with a height of about 4 nm and sheet-like structures with a thickness of about 2 nm.

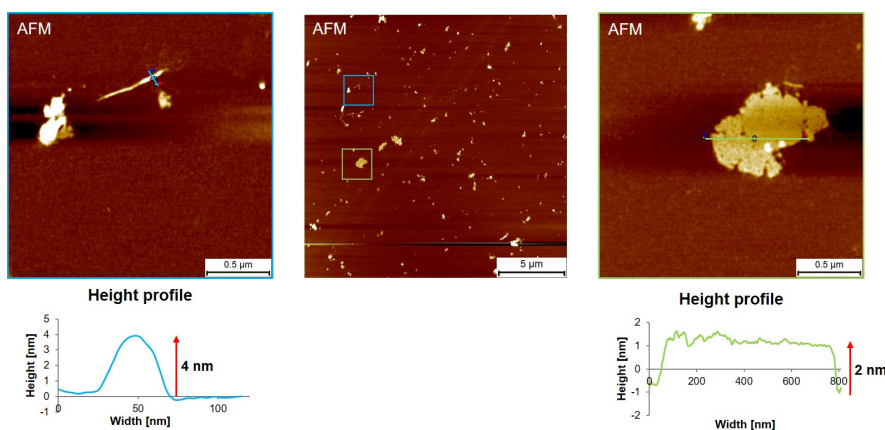


Figure 2.12.: AFM image of  $0.5\mu\text{M}$  **Phe<sub>3</sub>** and  $0.015\mu\text{M}$  **DNA-Phe<sub>3</sub>** deposited on APTES-modified mica. Condition: 10 mM sodium phosphate buffer, 0.025mM spermine tetrahydrochloride and 20% ethanol. Temperature gradient: 15 °C/min. Bottom: corresponding height profile of the structures along the marked line in the AFM image.

Now, with the same condition as before but with a higher **DNA-Phe<sub>3</sub>** concentration of  $0.03\mu\text{M}$  stripes and sheet-like structures were formed (see Figure 2.13).

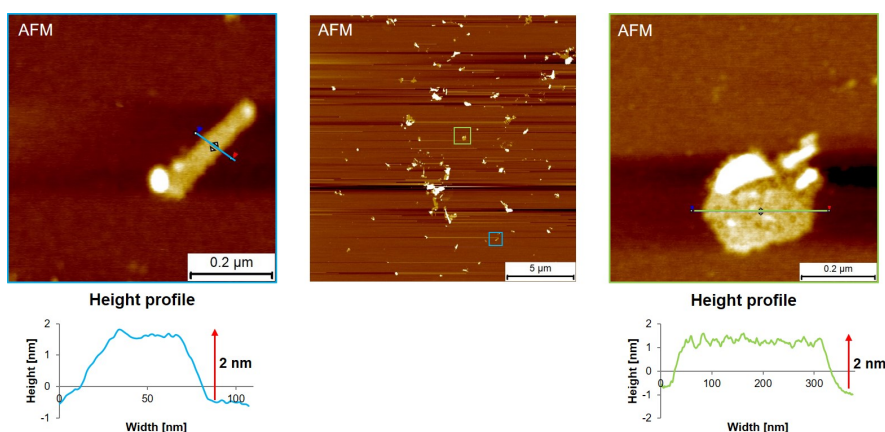


Figure 2.13.: AFM image of  $1\mu\text{M}$  **Phe<sub>3</sub>** and  $0.03\mu\text{M}$  **DNA-Phe<sub>3</sub>** deposited on APTES-modified mica. Condition: see Figure 2.12. Bottom: corresponding height profile of the structures along the marked line in the AFM image.

Zooming out, however, showed mostly undefined structures (see Figure 2.13). The structures that were observed, were most likely originating from the phenanthrene trimer only, due to its high concentration. In literature, and as already mentioned in the beginning, without the addition of spermine the **Phe<sub>3</sub>** would have formed nanotubes.<sup>101</sup> Therefore, rather tube-like structures were formed by lowering the spermine concentration as seen in Figure 2.12. Apparently the **DNA-Phe<sub>3</sub>** hinders the formation of the nanotubes as well, as seen in Figure 2.13. There, the tube-like structures disappear after increasing the **DNA-Phe<sub>3</sub>** concentration, which is disadvantageous to obtain functionalized supramolecular nanotubes. It seems like **DNA-Phe<sub>3</sub>** and the spermine disturbed the formation of the nanotubes and it was only possible to form rectangular- and stripe-like structures.

### **Phe<sub>3</sub> with DNA-Phe<sub>5</sub>**

In the following experiments, oligomer **DNA-Phe<sub>5</sub>** the number of phenanthrene was increased to five. **DNA-Phe<sub>5</sub>** in aqueous solution containing 10 mM sodium phosphate buffer, 0.1 mM spermine tetrahydrochloride and 20% ethanol showed sheet-like and tubular-like structures (see Figure 2.14) and at lower spermine concentration stripe structures can be observed (see Figure 2.15).

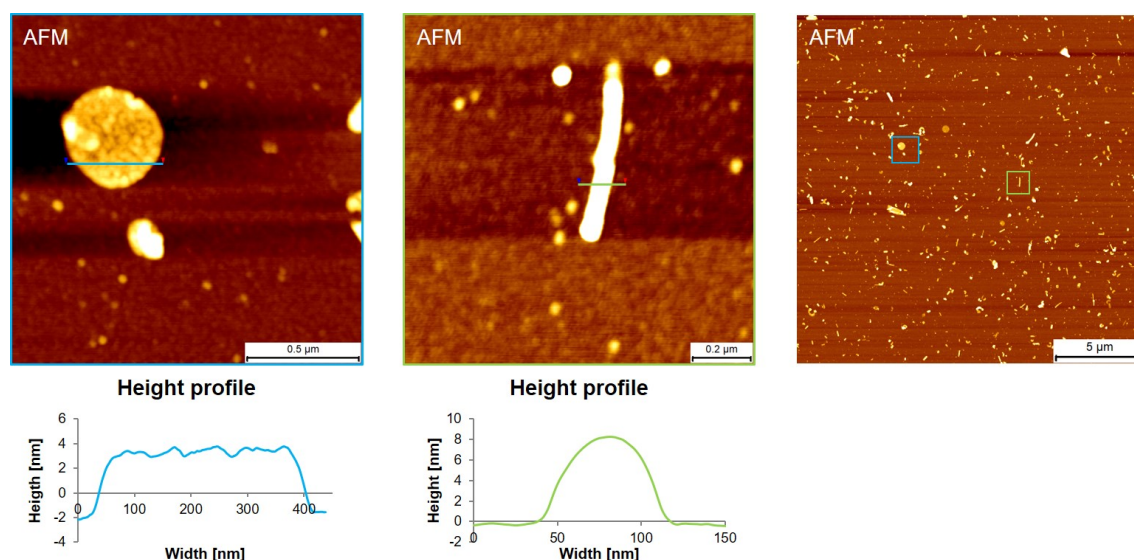


Figure 2.14.: AFM image of  $1\mu\text{M}$  **Phe<sub>3</sub>** and  $0.3\mu\text{M}$  **DNA-Phe<sub>5</sub>** deposited on APTES-modified mica. Condition: see Figure 2.11. Bottom: corresponding height profile of the structures along the marked line in the AFM image.

Figure 2.14 showed that in the presence of **DNA-Phe<sub>5</sub>** the formation of nanotubes is less disturbed than it was with **DNA-Phe<sub>3</sub>**. Surprisingly, shown in Figure 2.15, lowering the spermine concen-

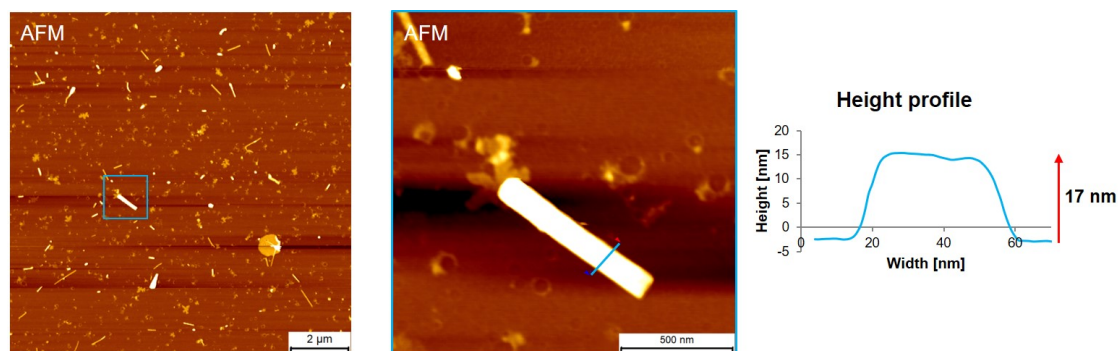


Figure 2.15.: AFM image of  $1\ \mu\text{M}$  **Phe<sub>3</sub>** and  $0.3\ \mu\text{M}$  **DNA-Phe<sub>5</sub>** deposited on APTES-modified mica. Condition: see Figure 2.12. Right: corresponding height profile of the structure along the marked line in the AFM image.

tration disturbed the formation of nanotubes much more, and without spermine flat tubular-like aggregates were formed (see Figure 2.16). The previous AFM measurements (see Figure 2.12 - Figure 2.15) revealed that there is a co-existence of these two types of structures, sheet-like and tubular-like (flat and non-flat). The sizes vary a lot and there were still undefined structures seen but certainly less than in the case of **DNA-Phe<sub>3</sub>**.

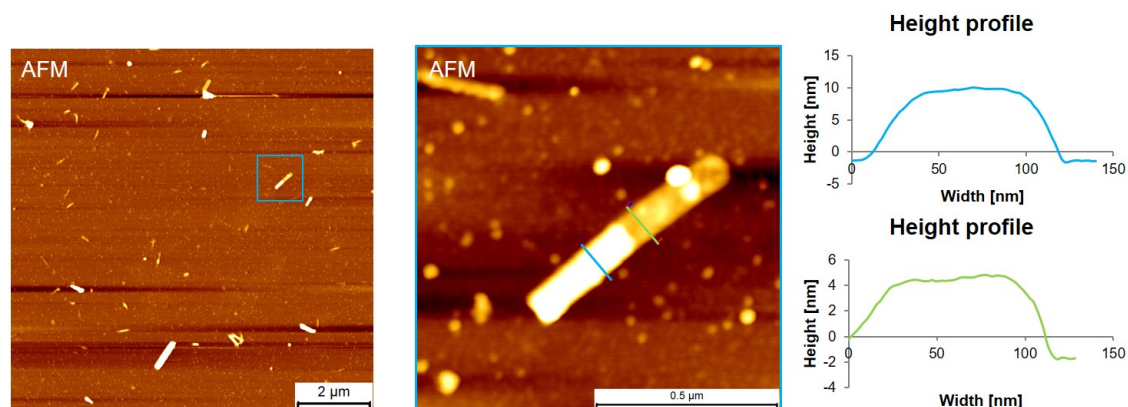


Figure 2.16.: AFM image of  $1\ \mu\text{M}$  **Phe<sub>3</sub>** and  $0.3\ \mu\text{M}$  **DNA-Phe<sub>5</sub>** deposited on APTES-modified mica. Condition: 10 mM sodium phosphate buffer and 20% ethanol. Temperature gradient:  $15\ \text{°C}/\text{min}$ . Right: corresponding height profile of the structure along the marked lines in the AFM image.

Further experiments were done with sodium chloride instead of polyamines. Because Au nanoparticles in the presence of polyamines tend to aggregate on their own (see next subchapter 2.3.2). However, the prerequisite is that with the application is also formed defined nanotubes. Figure 2.17 and Figure 2.18 show very large undefined structures and aggregates. Neither sheet-like nor tubular-like structures could be observed.

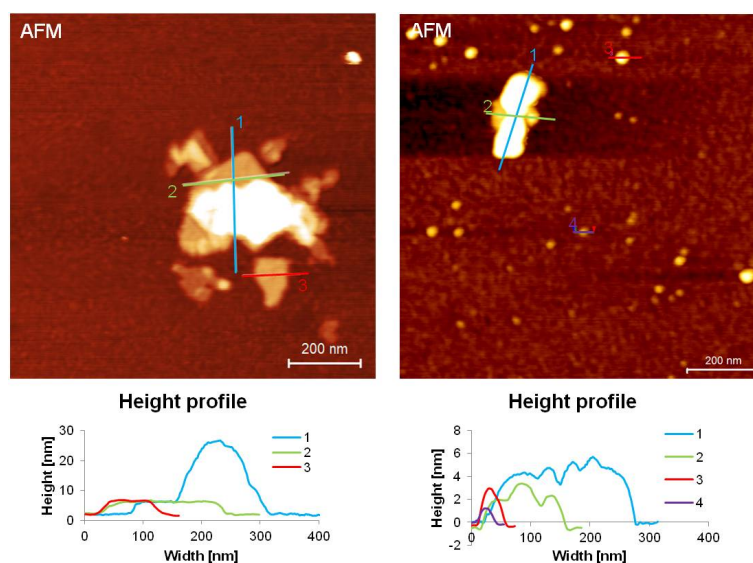


Figure 2.17.: AFM image of  $1\mu\text{M}$  **Phe<sub>3</sub>** and  $0.03\mu\text{M}$  **DNA-Phe<sub>5</sub>** deposited on APTES-modified mica. Condition: 10 mM sodium phosphate buffer and with a temperature gradient:  $1\text{ }^\circ\text{C}/\text{min}$ . Left: 200 mM NaCl. Right: 200 mM NaCl and 10% ethanol. Bottom: corresponding height profile of the structures along the marked lines in the AFM image.

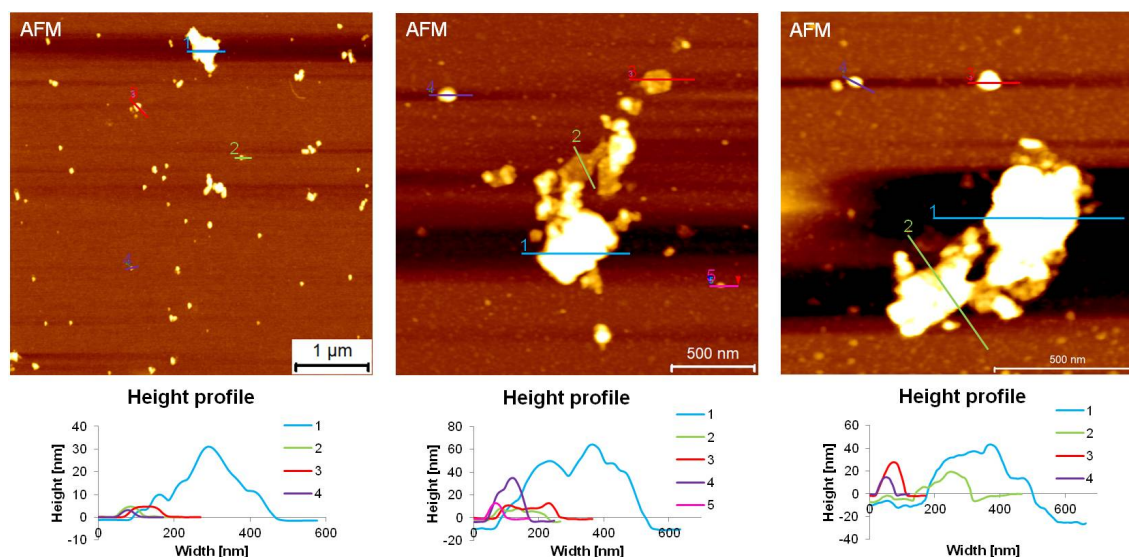


Figure 2.18.: AFM image of  $1\mu\text{M}$  **Phe<sub>3</sub>** and  $0.03\mu\text{M}$  **DNA-Phe<sub>5</sub>** deposited on APTES-modified mica. Condition: 10 mM sodium phosphate buffer and with a temperature gradient:  $1\text{ }^\circ\text{C}/\text{min}$ . Left: 100 mM NaCl. Middle: 100 mM NaCl and 10% ethanol. Right: 150 mM NaCl and 10% ethanol. Bottom: corresponding height profile of the structures along the marked lines in the AFM image.

### Problems of Au Nanoparticles in Presence of Polyamines

An additional experiment was carried out, where only **AuNP-DNA** was deposited on an APTES-mica under the condition of 10 mM sodium phosphate buffer, 0.1 mM spermine tetrahydrochloride and 20% ethanol. It showed that the **AuNP-DNA** formed in fact already large aggregates (see Figure 2.19 Left). By using only the bis(p-sulfonatophenyl)phenylphosphine (BSPP) stabilized gold nanoparticles at the same condition without any DNA, shows that polyamines have the tendency to induced the aggregation of **AuNP-DNA** (see Figure 2.19 Right). This matches the findings of other study.<sup>104</sup> To avoid this problem with cationic polyamines, the salt was changed to sodium chloride.

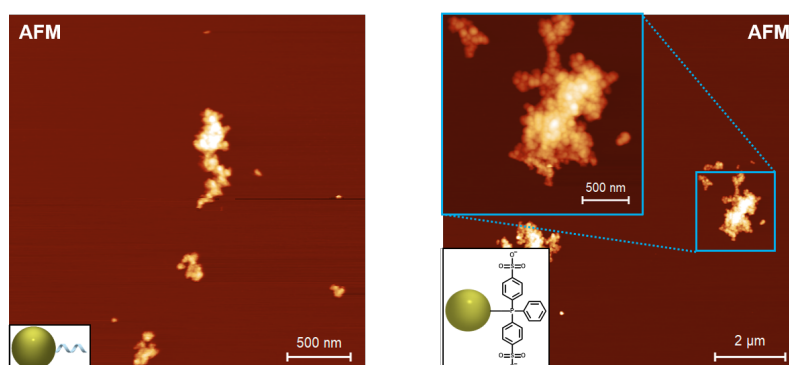


Figure 2.19.: AFM image of gold nanoparticles deposited on APTES-modified mica. Condition: 10 mM sodium phosphate buffer, 0.1 mM spermine tetrahydrochloride and 20% ethanol. Left: Gold nanoparticle modified with single strand DNA. Right: Gold nanoparticles stabilized with BSPP, no DNA.

## 2.4. Conclusion

The assembly of functionalized supramolecular polymers was at least partially demonstrated. Although, the atomic force microscopy revealed the formation of two-dimensional nanosheets with **Py<sub>3</sub>** and **DNA-(HEG)<sub>1</sub>-Py<sub>7</sub>/DNA-Py<sub>4</sub>/DNA-Py<sub>5</sub>**, unfortunately, the precise arrangement of gold nanoparticles by hybridization via the pyrene DNA conjugates did not work. The gold nanoparticles were randomly distributed and there was no accumulation of gold nanoparticles on the nanosheets. Therefore, there is no evidence that the supramolecular pyrene nanosheets were doped with the pyrene DNA conjugates. And even if the nanosheets were doped, there is still the possibility of steric hindrance for the gold nanoparticle, hence, they could not hybridize to the DNA on the nanosheets.

DNA-modified nanotubes were also not formed by using **Phe<sub>3</sub>** and **DNA-Phe<sub>3</sub>** at the tested conditions. There was a co-existence between two different types of structures, one was sheet-like, the other was tube-like or rectangular-shaped. Changing **DNA-Phe<sub>3</sub>** to **DNA-Phe<sub>5</sub>** did also not result in the formation of uniform nanotubes. Hybridization of gold nanoparticles to the DNA-modified structures only showed undefined aggregation of the gold nanoparticles induced by the presence of cationic polyamines. Replacing the polyamines with sodium chloride did not solve the problem, because there was no initial formation of defined nanotubes anymore.

Overall, it was shown that doping an existing system is influenced by many different factors. The right doping partner and the optimal conditions must be present. This study provide a good basis for further experiments though. For example, adjusting the DNA conjugates, and creating new designs may allow the incorporation into the preformed structures. To avoid the problem with polyamines, other salts can be tested as well. And assuming that the hybridization of the gold nanoparticles was sterically hindered, the design of the nanoparticles can be changed to allow for better chance of hybridization. For example, instead of fully modifying the gold nanoparticles with ssDNA, modifying the gold nanoparticles with a HEG spacer (hexaethylene glycol) would eventually help it from electrostatic repulsion of the nanosheets.



## 2.5. Experimental Section

### Material

All solvents and chemical reagents for the synthesis were purchased from commercial suppliers (Sigma Aldrich, TCI or Glen Research) and used without further purification.

### Synthesis

#### Synthesis of 1,6-dialkynylpyrene phosphoramidite

The pyrene building block was synthesized according to the literature.<sup>99,105</sup>

#### Synthesis of 2,7-dialkynylphenanthrene trimer

The 2,7-Bis(4-hydroxybut-1-yn-1-yl)phenanthrene was synthesized starting from 2,7-dibromophenanthrene, which is commercially available. The first reaction was Sonogashira reaction, then acetylation and phosphorylation were made to get 4-(7-(4-hydroxybut-1-yn-yl)phenanthrene-2-yl)but-3-yn-1-yl acetate and Bis(2-cyanoethyl)(phenanthrene-2,7-diylbis(but-3-yn-4,1-diyl)) bis(diisopropylphosphoramidite).

#### Synthesis of Pyrene Modified Solid-support

Pyrene-loaded controlled pore glass (CPG) support were needed for the solid-phase synthesis. The synthesis was according to the literature.<sup>101</sup>

#### Solid-phase synthesis

The oligomer were synthesized in a 1  $\mu$ M scale using the standard cyanoethyl phosphoramidite solid-phase synthesis protocol<sup>29</sup> on a ABI (Applied Biosystems Instruments) 394-DNA/RNA automated synthesizer.

#### Reversed Phase HPLC Purification

The HPLC purification was done on a Shimadzu HPLC system using ReproSil 100 C8, Lichrospher 100 RP-18, 5 $\mu$ m, 250 x 4mm column (Dr.Maisch GmbH). The mobile phase were: Solvent A: 0.1M

ammonium acetate buffer and solvent B: CH<sub>3</sub>CN for **Py<sub>3</sub>**. For **DNA-Py<sub>4</sub>** and **DNA-Py<sub>5</sub>**: Solvent A: 0.1M TEAA /acetonitrile 80:20 and solvent B: CH<sub>3</sub>CN.

### **Synthesis of Au Nanoparticles Modified with DNA**

The synthesis of the Au nanoparticles modified with DNA (AuNP-DNA) was done according to the literature<sup>106</sup>. The AuNP-DNA were synthesized by citrate reduction whereby tannic acid acts as co-reductant. The concentration of AuNP-DNA was determined in MilliQ by using a value of  $\epsilon^{520} = 1 \cdot 10^7 \text{ M}^{-1} \cdot \text{cm}^{-1}$  for 5 nm gold nanoparticles.

### **Mass Spectrometry**

The molecular mass were determined on Thermo Fisher LTQ Orbitrap XL using Nano Electrospray Ionization (NSI).

### **Sample Preparation**

The sample in the aqueous medium (10mM sodium phosphate buffer, 10mM sodium chloride and 15% ethanol) was heated up to 75 °C afterwards it was cooled down to 20 °C with a gradient of 15 °C/min.

### **Spectroscopic Characterisation**

UV-vis data were measured on a Cary 100 Bio spectrophotometer. For the measurement 1cm x 1cm quartz cuvettes were used.

### **Atomic Force Microscopy**

The mica substrates (20 × 20 mm<sup>2</sup>) were cleaved with Scotch tape. The mica surface was modified with N,N diisopropylethylamine and 3-aminopropyltriethoxy silane in the ration 1:3 as described in the reference<sup>107</sup>. Sample with DNA-modified gold nanoparticles (AuNP-DNA) were incubated for 10 minutes. 20 μL of the sample solution was drop-casted onto the mica substrate. After incubation, the modified mica sample was rinsed with 1 ml of MilliQ water and dried in an argon stream.

Details can be found in Appendix A.

---

## 3. Functionalized Vesicles of Phenanthrene DNA Conjugates

### 3.1. Introduction

Integration of DNA in nanotechnology is very promising for biofunctionalization in biotechnological approaches.<sup>108–111</sup> Supramolecular polymers formed of DNA conjugates, natural DNA combined with artificial DNA nucleotide surrogates, brings several advantages.<sup>34–37</sup> First, the supramolecular polymers entail a high degree of modularity because of their non-covalent interaction nature. Second, due to the presence of DNA it is possible to create properties like molecular recognition and allows for the construction of nanostructures with the potential of functionalization.<sup>38</sup> There are numerous studies about DNA-functionalized vesicles, the focus is mainly on DNA-functionalized liposomes and lipid-DNA conjugates.<sup>112–115</sup>

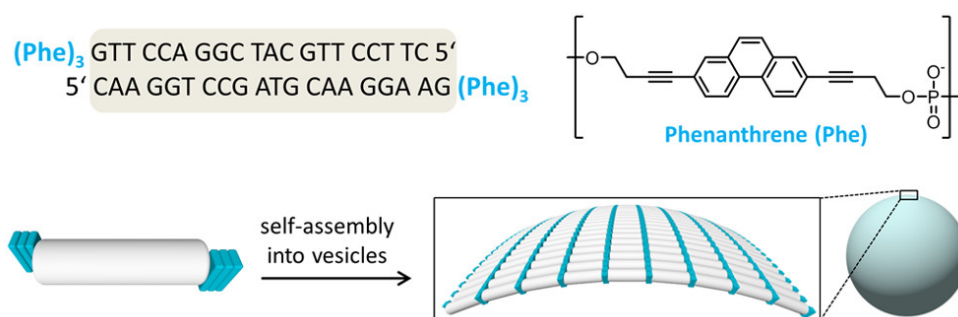


Figure 3.1.: Top: Sequence of the duplex with the phenanthrene overhangs and the 2,7-dialkynyl phenanthrene building block. Bottom: Illustration of the vesicle with a zoom-in of the surface. Figure is from reference<sup>103</sup>.

In a previous study, vesicle-shaped supramolecular polymers were formed by using DNA duplexes with phenanthrene overhangs at both ends (see Figure 3.1).<sup>103</sup> The vesicles showed a diameter in the range of 50-200 nm. They showed light-harvesting properties and transfer absorbed energy

to pyrene or Cy3, which act as an acceptor.

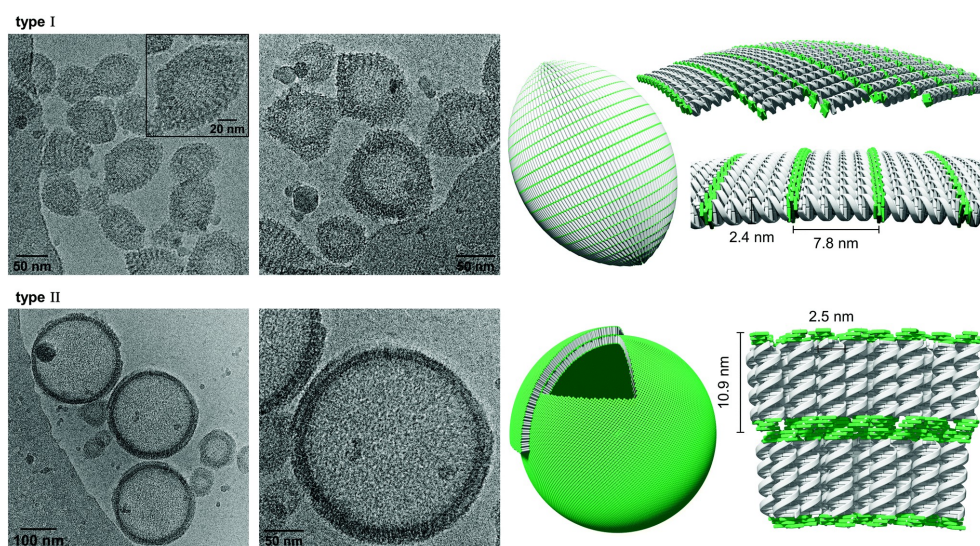


Figure 3.2.: Cryo-EM images and illustrations of prolate ellipsoids (type I) and spheres (type II) vesicles. Figure is from reference<sup>116</sup>.

Later, the phenanthrene units of the DNA hybrids were replaced by tetraphenylethylene (TPE) units resulting in two different vesicle morphologies.<sup>116</sup> The vesicles formed either prolate ellipsoids or spheres depending on the condition. The different types of vesicles suggest also a different orientation of the DNA. In both cases, the hydrophobic ends (TPE's) of the DNA duplexes were essential for the formation of the supramolecular structures.

### 3.2. Aim of the Work

DNA-phenanthrene conjugates **DNA-Phe<sub>5</sub>** were synthesized and form vesicular objects under optimized conditions (see Figure 3.3). The formed DNA-modified vesicles are investigated for functionalization by hybridization with single strand DNA with fluorescent dyes and Au nanoparticle-modified oligonucleotides. By excitation of the DNA-phenanthrenes an energy transfer from the phenanthrene to the fluorescent dye should occur. Additional experiments were done to check the possibility of encapsulation. The DNA-modified vesicles were characterized by UV-vis spectroscopy, fluorescence spectroscopy, atomic force microscopy (AFM) and transmission electron microscopy (TEM).

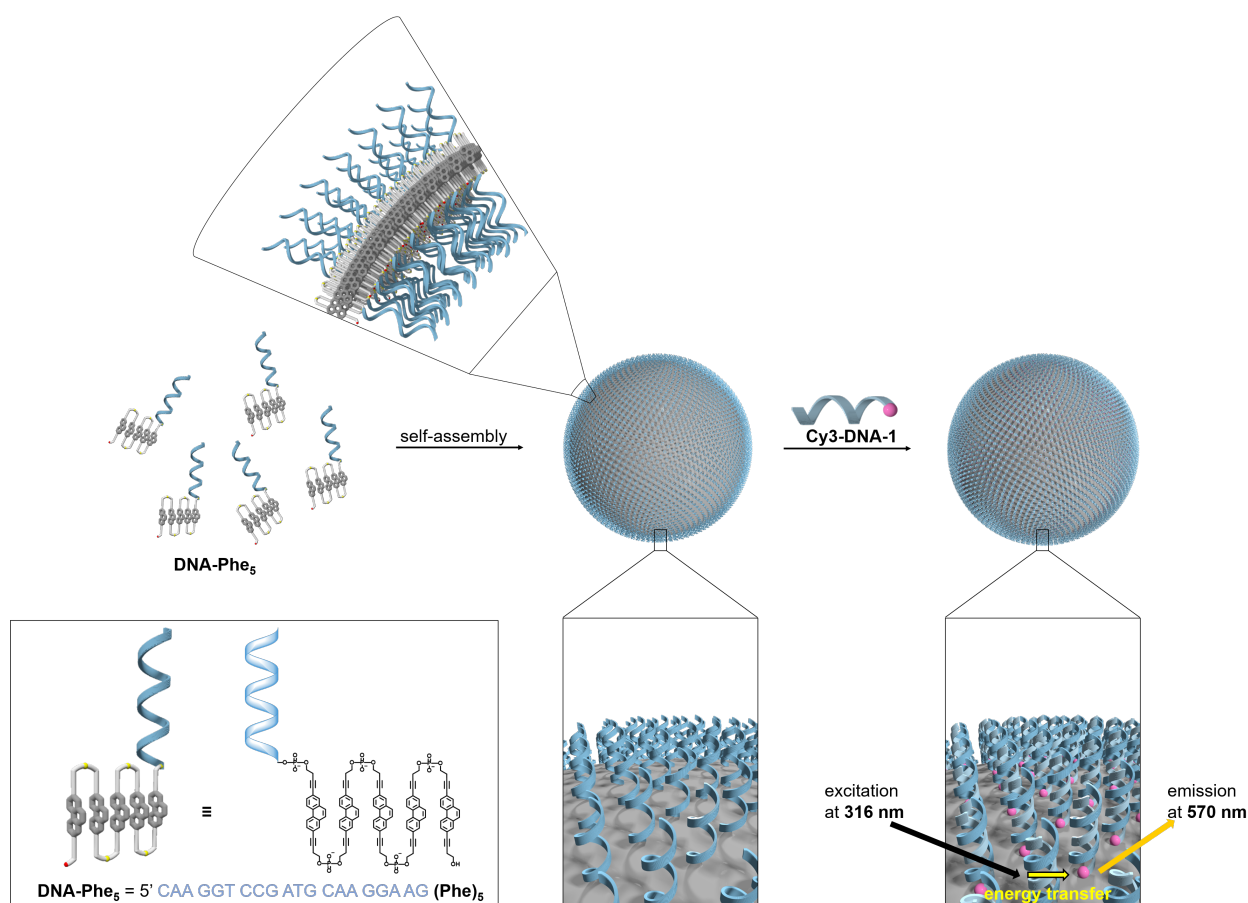


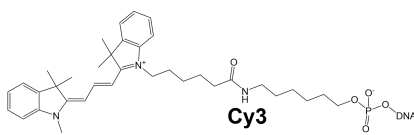
Figure 3.3.: Illustration of the self-assembly into a vesicle and hybridization with the single strand DNA with the fluorescent dye (**Cy3-DNA-1**, sequence see Table 3.1). Bottom left: Structure and sequence of **DNA-Phe<sub>5</sub>**.

### 3.3. Results & Discussion

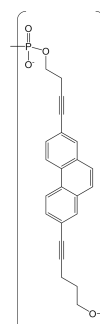
Table 3.1 shows the chemical structure and sequence of the oligomers that were used in this study. The 2,7-dialkynyl phenanthrene (**Phe**, see Table 3.1) building block was synthesized according to the literature.<sup>101</sup> The oligomers in this work were prepared by the phosphoramidite solid phase synthesis according to a published procedure.<sup>29</sup>

Table 3.1.: Sequences of the oligomers used in this study. Right & bottom: Chemical structures of the 2,7-dialkynylphenanthrene and Cy3 (from Microsynth GmbH, Switzerland, Balgach).

Oligomer	Sequence
DNA-Phe <sub>5</sub>	5' CAA GGT CCG ATG CAA GGA AG (Phe) <sub>5</sub>
AuNP-DNA	5' CTT CCT TGC ATC GGA CCT TG AuNP
AuNP-DNA-2	5' TCG ATG CAT GCA ATG TAC CA AuNP
Cy3-DNA-1	3' GTT CCA GGC TAC GTT CCT TC Cy3
Cy3-DNA-2	3' CAA GGT CCG ATG CAA GGA AG Cy3



**Cy3**



**Phe**

The same conditions, were applied as in the previous work.<sup>103</sup> However, other conditions (variation in concentration, other polyamines and salt) and different temperature gradients for the formation of vesicle structures were also tested (see Figure B.23 in Appendix B).

#### 3.3.1. Formation of DNA-modified Vesicles

The vesicle-shaped supramolecular polymers were self-assembled in aqueous solution in the presence of spermine. Monitoring the absorption at 260 nm, the vesicles were formed under controlled cooling from 70°C to 20°C with a temperature gradient of 1°C/min. Calculations of the first derivation of the cooling curves in Figure 3.4 showed formation temperatures at 57.4°C (pH 7.0), 51.1°C (pH 7.2), 49.2°C (pH 7.4) and 47.4°C (pH 7.6).

Therefore, there is a pH dependency at which temperature the supramolecular polymers were formed. Changes in the pH of the aqueous solution can influence the formation of this vesicle-shaped supramolecular polymer. Recording cooling curves of double strand DNA (dsDNA) reveal that the pH influences primarily the phenanthrene units and not the single strand DNA (see Figure 3.5). For the duplexes the formation temperatures were 53.3°C (pH 7.0), 55.4°C (pH 7.2),

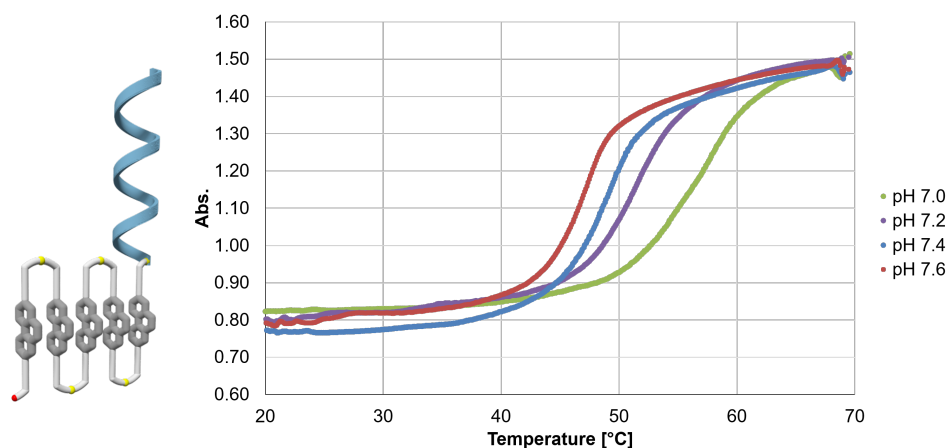


Figure 3.4.: Left: Illustration of **DNA-Phe<sub>5</sub>**. Right: Cooling curves of **DNA-Phe<sub>5</sub>** at different pH. Condition: 2.5  $\mu$ M **DNA-Phe<sub>5</sub>**, 10mM sodium phosphate buffer, 0.1mM spermine tetrahydrochloride and 20% ethanol. Cooling from 70°C to 20°C (temperature gradient: 1°C/min).

53.7°C (pH 7.4) and 53.0°C (pH 7.6), indicating no or only little pH dependency. Spermine is a tetraamine and can be sensitive to the pH of the environment, because of the pKa of one of the amine groups (pKa: 7.9, 8.4, 10.1 and 10.9).<sup>117</sup> Although, the difference seems to be modest (pH 7.0 to pH 7.6), it can influence the spermine and it can be "more" deprotonated with a slightly higher pH. As a result, the charge has to be compensated, therefore, an interaction between the polycation spermine and the phosphate group of phenanthrene becomes stronger. The effect of this interaction is visible in the cooling curves in Figure 3.4.

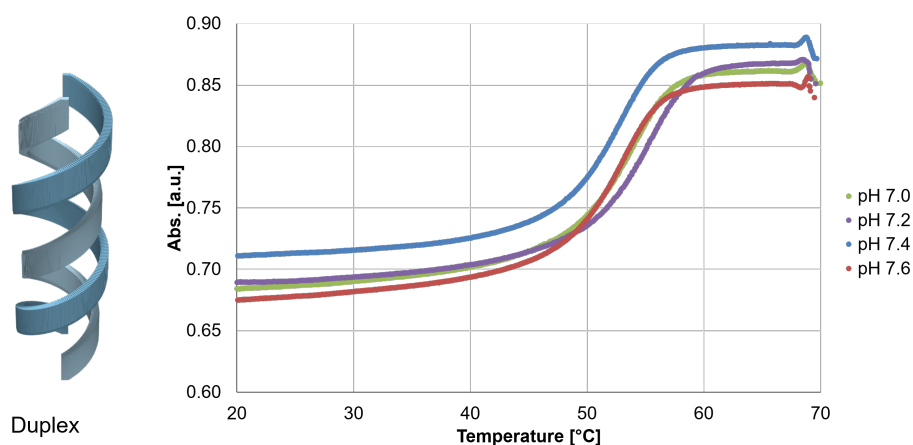


Figure 3.5.: Left: Illustration of dsDNA. Right: Cooling curves of dsDNA at different pH. Condition: see Figure 3.4.

The difference could not only be visually observed in the formation temperature, but also in a change in morphology. In Figure 3.6 AFM images reveal that at different pH the formation of

supramolecular polymers has also changed. The higher the pH, the more undefined structures were formed.

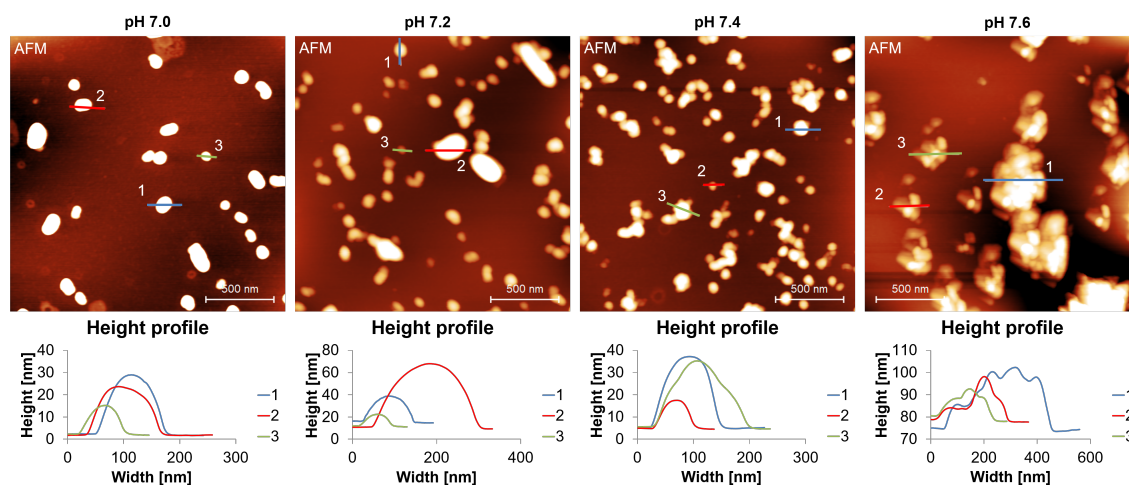


Figure 3.6.: AFM images of **DNA-Phe<sub>5</sub>** at different pH deposited on APTES-modified mica. Condition: see Figure 3.4. At the bottom the corresponding height profile along the line is shown in the insert of the AFM image.

In Figure 3.6 (first from left) and Figure 3.7 is the visualisation of the formed vesicle-shaped supramolecular polymers. It was done by atomic force microscopy (AFM) and transmission electron microscopy (TEM). The vesicles were formed under controlled cooling and deposited on a APTES-mica for AFM (for sample preparation see subchapter 3.5) and on a holey carbon grid for TEM (for sample preparation see subchapter 3.5).

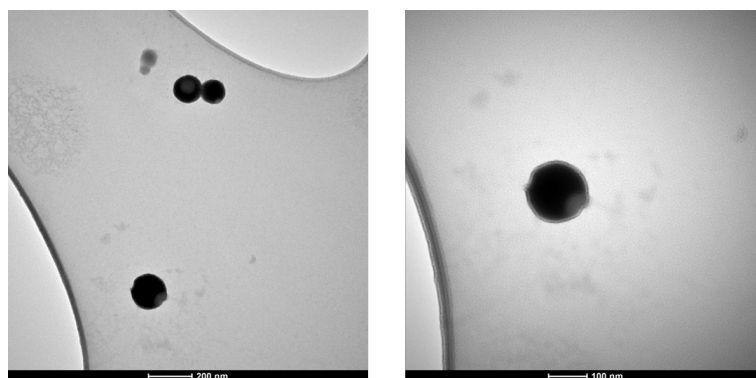


Figure 3.7.: TEM images of **DNA-Phe<sub>5</sub>** vesicles deposited on a holey copper carbon grid. Condition: see Figure 3.4. Right: Zoom-in of one of the vesicles in the left image.

AFM measurements revealed vesicles with a diameter of about 100 - 200 nm and a height of 15 - 70 nm. These results were also confirmed by TEM measurements.



### 3.3.2. Hybridization with Au Nanoparticles

If the single strand DNA that are tethered on the surface of the vesicles, they should be accessible and addressable. Therefore, the formed DNA-modified vesicles were investigated for functionalization by hybridization with gold nanoparticle-modified oligonucleotides. Gold nanoparticles with a complementary single strand DNA (**AuNP-DNA**) to **DNA-Phe<sub>5</sub>** were added in order to hybridize with the preformed vesicles. The **AuNP-DNA** seems also to form a large network not only with the DNA-modified vesicles but also on its own (see Figure 3.8 and Figure 3.9). This problem was already mentioned in previous studies (see subchapter 2.3.2).<sup>104</sup> Polyamines especially spermine have the tendency to induce the aggregation of gold nanoparticles.

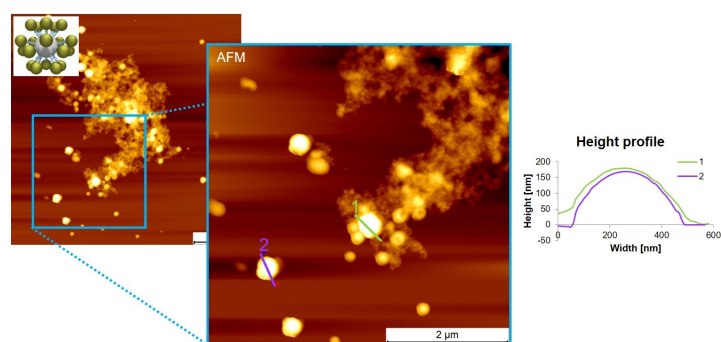


Figure 3.8.: AFM image of **DNA-Phe<sub>5</sub>** with **AuNP-DNA** deposited on APTES-modified mica. Condition: see Figure 3.4. Right: The height profile are shown that corresponding to the lines given in the AFM image.

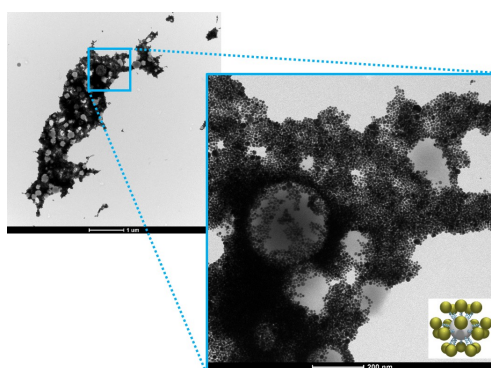


Figure 3.9.: TEM images of **DNA-Phe<sub>5</sub>** with  $0.25\mu\text{M}$  **AuNP-DNA** deposited on copper formvar carbon grid. Condition: see Figure 3.4.

The formation of clusters can not be inhibited in presence of polyamines and therefore, is inevitable. So showing the addressability and the accessibility of the DNA-modified vesicle could not be shown by hybridization with gold nanoparticles.

### 3.3.3. Energy Transfer

The functionalized vesicles were targeted with the complementary oligomer **Cy3-DNA-1**, which has the Cy3 dye at the 5' end (illustrated in Figure 3.10).

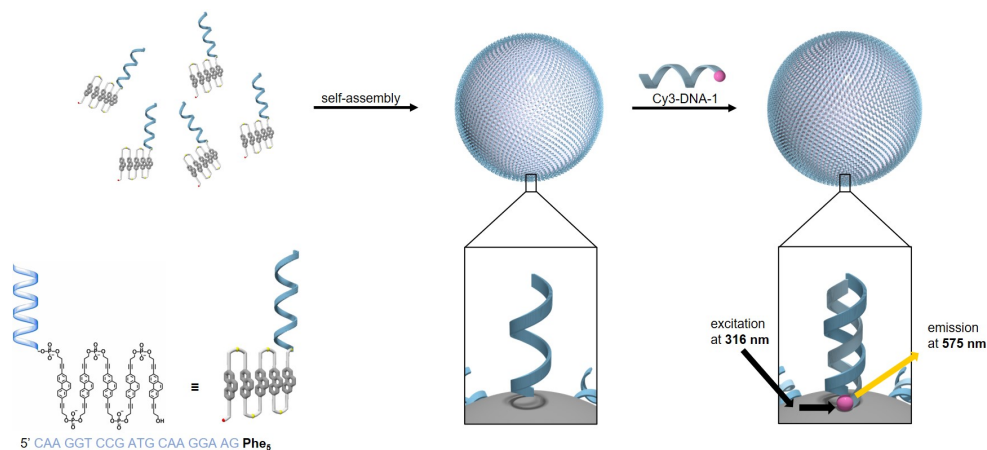


Figure 3.10.: Bottom left: Structure of the **DNA-Phe<sub>5</sub>**. Top: Simplified illustration of the self-assembly into a vesicle and hybridization with the single strand DNA with a fluorescent dye (**Cy3-DNA-1**).

The fluorescent dyes were added stepwise to the preformed DNA-modified vesicles (see Figure 3.11). By excitation of the phenanthrene in the shell (donor) at 316 nm the energy was transferred to Cy3 (acceptor), which was observed as an emission at 570 nm. The fluorescence spectra showed a Cy3 emission increase while the phenanthrene emission (376 nm and 395 nm) decreases with an increase in the concentration of **Cy3-DNA-1**. Emission at 570 nm (emission of Cy3) shows a stagnation at about 10% **Cy3-DNA-1** relative to the concentration of **DNA-Phe<sub>5</sub>**. The high negative charge density on the vesicle can have a negative impact on the hybridization of the dyes, therefore, only 10% of the DNA single strands were accessible by **Cy3-DNA-1**. As a control, non-complementary strand **Cy3-DNA-2** was used and no energy transfer could be observed (see Figure 3.11). Measurement with only **Cy3-DNA-1** showed also no energy transfer (see Figure B.18 in the Appendix B).

AFM measurements showed also that after the addition of over 10% **Cy3-DNA-1** to the DNA-modified vesicles, the shape stays mostly intact (see Figure 3.12 a). With 40% **Cy3-DNA-1** disc-like structures were observable on the surface of the mica (see Figure 3.12 c). The diameters of the vesicles were in the same range as before and the height profile of the disc-like structure was in the range of 1.5 – 2.7 nm. Also after heating/cooling of the same sample the vesicles were detected again (see Figure 3.12 b) and Figure 3.12 d). This observation was only made when

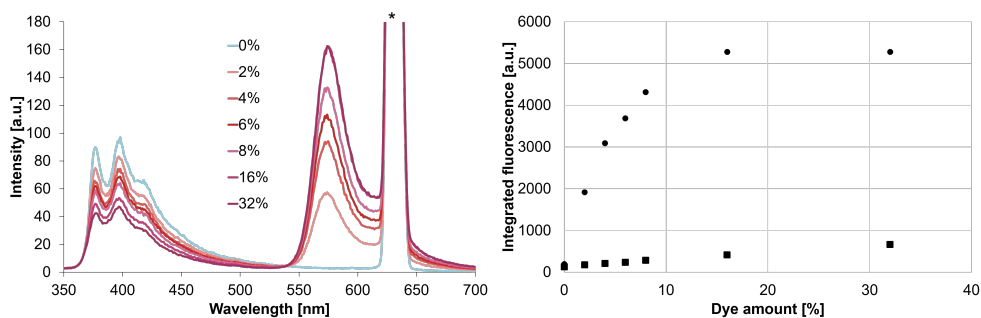


Figure 3.11.: Left: Fluorescence spectra of **DNA-Phe<sub>5</sub>** with stepwise addition of **1** to the preformed vesicles. Right: Integrated fluorescence (540 - 600 nm) of the stepwise addition of the complementary **Cy3-DNA-1** (●) and non-complementary **Cy3-DNA-2** (■).  $\lambda_{\text{exc}}$ : 316nm, 20°C. Excitation slit: 5 nm, emission slit: 5 nm. Condition: see Figure 3.4. \* in the spectrum mark a second harmonic order diffraction.

AFM was measured at the centre of the sample droplet (see Figure 3.13 Top). However, after the heating/cooling of the DNA-modified conjugates with 40% **Cy3-DNA-1**, the sample showed a different structure (see Figure 3.13 Bottom), but this structure could only be observed when measuring at the edge of the sample droplet. The mica surface seemed to be covered by large sheet-like structures and only a few vesicles. that "sat" on the sheets.

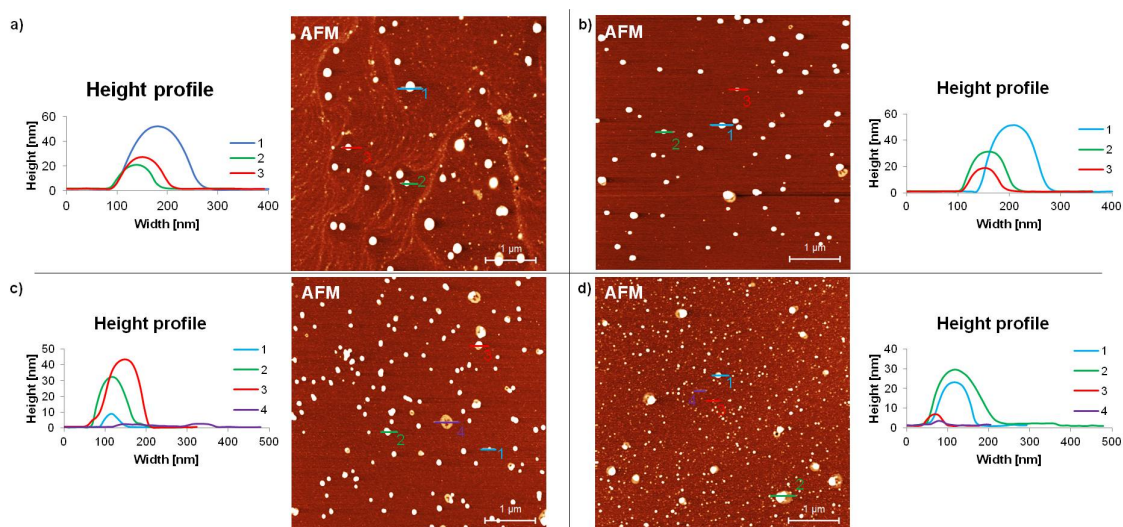


Figure 3.12.: AFM images of **DNA-Phe<sub>5</sub>** deposited on APTES-modified mica with the corresponding height profiles along the marked line in the AFM images. Condition: see Figure 3.4. a) after addition of 20% **Cy3-DNA-1**. b) with 20% **Cy3-DNA-1** after heating/cooling. c) after addition of 40% **Cy3-DNA-1**. d) with 40% **Cy3-DNA-1** after heating/cooling.

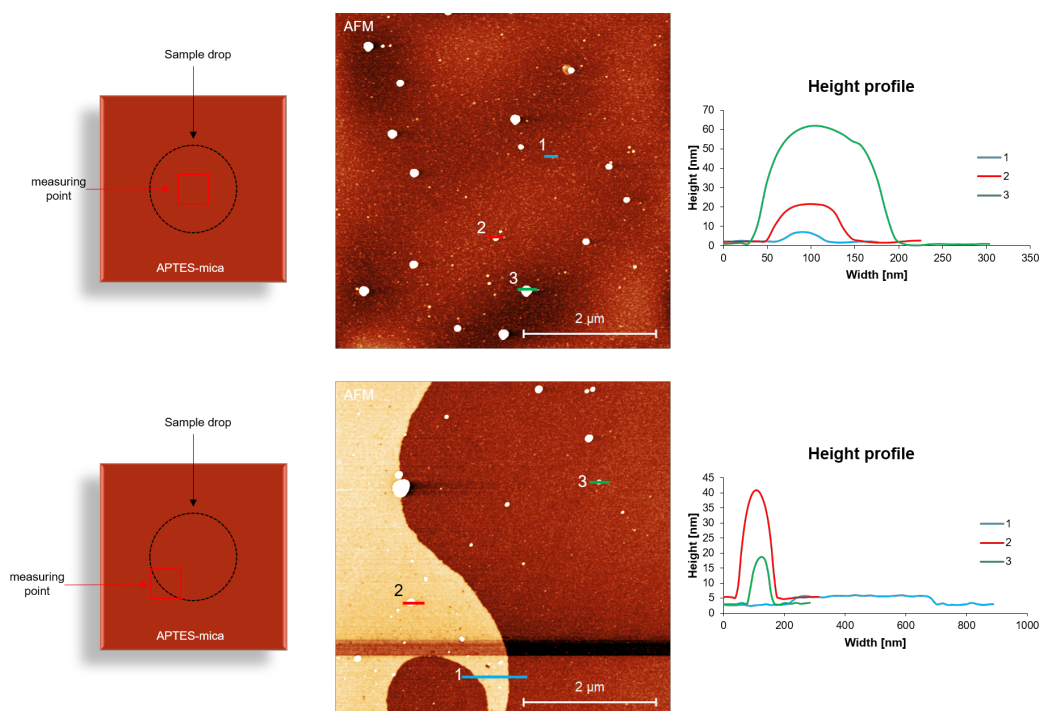


Figure 3.13.: Left: Illustration of the mica surface and the approximate position of the measurement. Middle: AFM images of **DNA-Phe<sub>5</sub>** with 40% **Cy3-DNA-1** deposited on APTES-modified mica. Condition: see Figure 3.4. Right: the corresponding height profiles along the marked lines of the AFM images.

### 3.3.4. Additional Experiment

#### Encapsulation

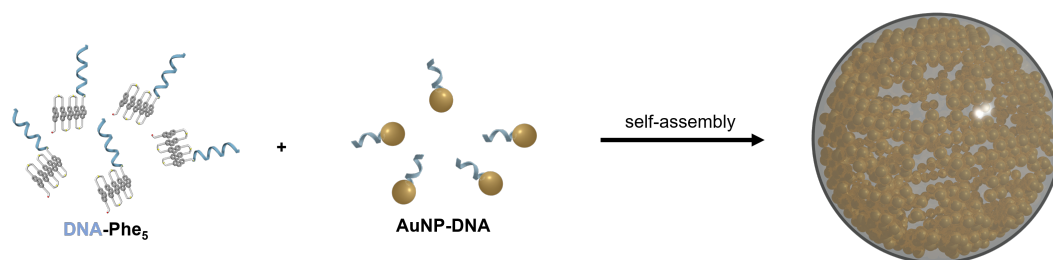


Figure 3.14.: Illustration of the gold nanoparticles (**AuNP-DNA**, simplified with only one ssDNA) encapsulated in the **DNA-Phe<sub>5</sub>** vesicle after the sample was heated up and cooled down.

Encapsulation of **AuNP-DNA** was attempted by heating/cooling of **DNA-Phe<sub>5</sub>** with **AuNP-DNA** (see Figure 3.14). Although, **AuNP-DNA** tends to make large network by itself, it was interesting to see the interaction of **DNA-Phe<sub>5</sub>** and **AuNP-DNA**.

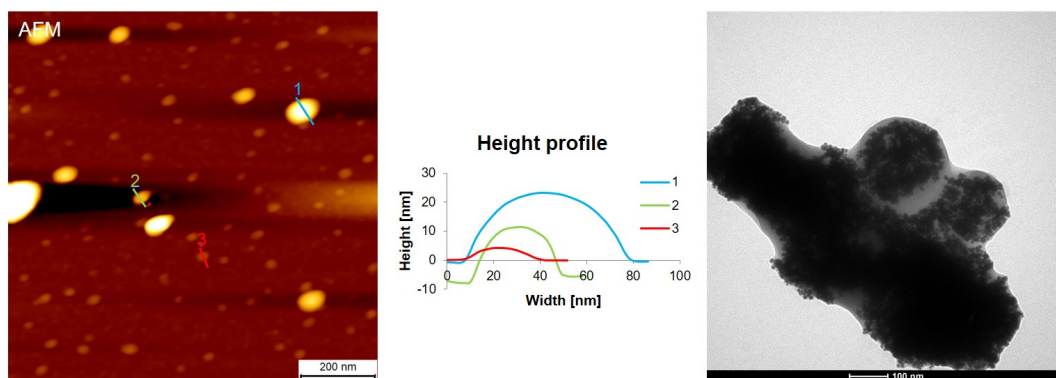


Figure 3.15.: AFM and TEM images of **DNA-Phe<sub>5</sub>** mixed with  $0.25\mu\text{M}$  **AuNP-DNA**. Condition: see Figure 3.4. Middle: the corresponding height profile along the marked lines of the AFM image.

In Figure 3.15 **AuNP-DNA** seems to be trapped in a shell of **DNA-Phe<sub>5</sub>**. But how the **DNA-Phe<sub>5</sub>** and **AuNP-DNA** were structurally ordered, is unknown.

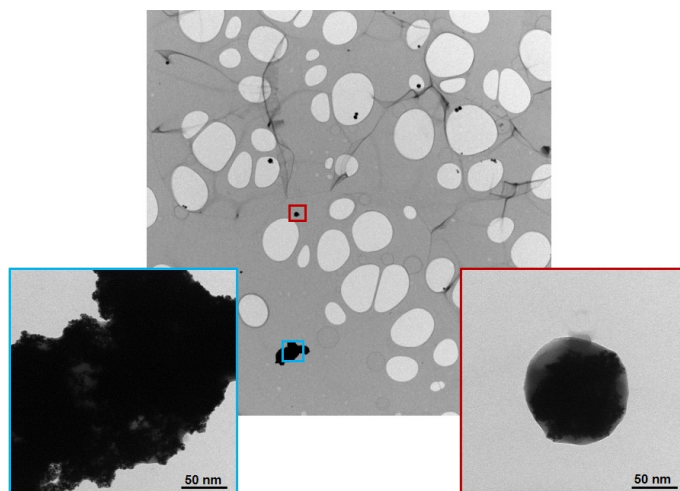


Figure 3.16.: TEM images of **DNA-Phe<sub>5</sub>** with  $0.1\mu\text{M}$  **AuNP-DNA** deposited on holey carbon grid. Condition: see Figure 3.4. Smaller images: Zoom-In.

In Figure 3.16 **AuNP-DNA** could be observed in the vesicle but also other undefined structures were formed and the gold nanoparticles seemed to be included in these aggregates. There was also an attempt to mix the DNA-modified vesicles, with the vesicles with the encapsulated **AuNP-DNA**, to investigate if there were interactions between the vesicles (see Figure 3.17): e.g., to observe an exchange of the gold nanoparticles between the vesicles. But no interactions between the encapsulated and the non-encapsulated vesicles were observed, the results were very similar to the previous TEM images in Figure 3.16.

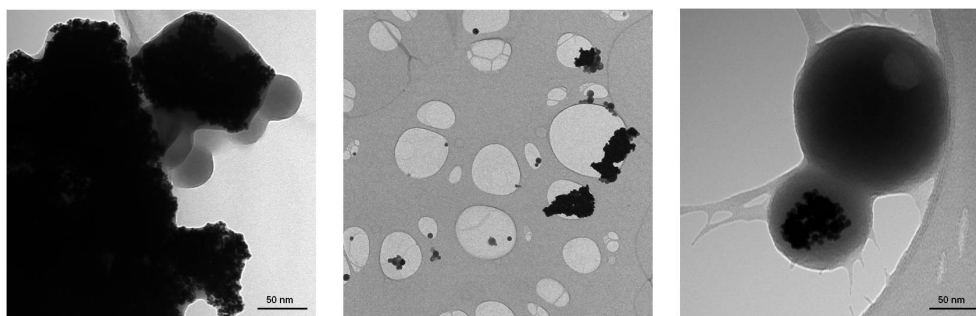


Figure 3.17.: TEM images of of  $2.5\mu\text{M}$  **DNA-Phe<sub>5</sub>** and  $2.5\mu\text{M}$  **DNA-Phe<sub>5</sub>** with **AuNP-DNA** encapsulated, deposited on holey carbon grid. Condition: see Figure 3.4.

The specificity of the encapsulation was verified by using non-complementary gold nanoparticles (**AuNP-DNA-2**). The non-complementary **AuNP-DNA-2** was heated/cooled down in the presence of **DNA-Phe<sub>5</sub>**.

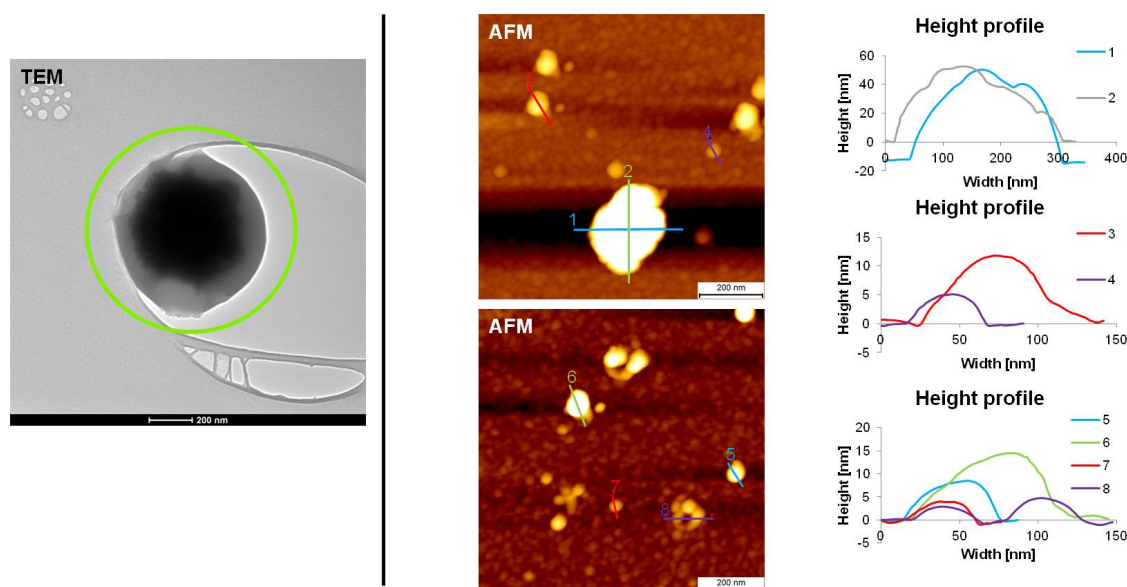


Figure 3.18.: Left: TEM image of  $2.5\mu\text{M}$  **DNA-Phe<sub>5</sub>** with complementary  $0.1\mu\text{M}$  **AuNP-DNA** encapsulated, deposited on holey carbon grid. Right: AFM images of  $2.5\mu\text{M}$  **DNA-Phe<sub>5</sub>** with complementary  $0.1\mu\text{M}$  **AuNP-DNA** deposited on APTES-modified mica. Condition: see Figure 3.4. Right: the corresponding height profiles along the marked lines of the AFM images.

Comparing the results shown in Figure 3.18 and Figure 3.19, it is obvious that with the non-complementary gold nanoparticles only undefined structures were be formed and/or vesicles with an irregular surface. In case of **AuNP-DNA** the TEM image showed the regularly round vesicle (Figure 3.18).

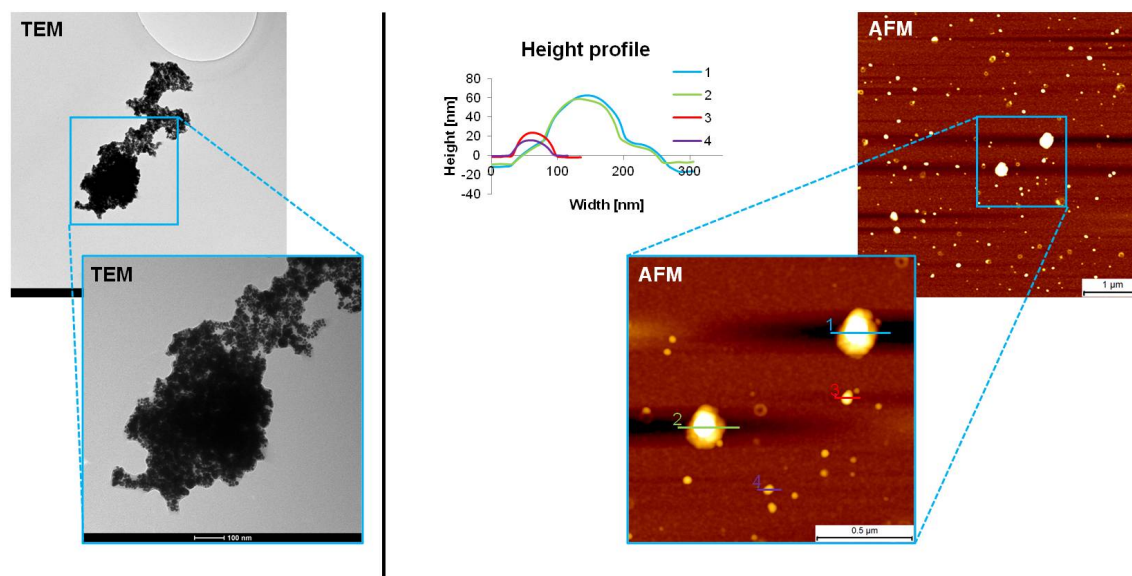


Figure 3.19.: Left: TEM images of of  $2.5\mu\text{M}$  **DNA-Phe<sub>5</sub>** with  $0.1\mu\text{M}$  **AuNP-DNA-2** deposited on holey carbon grid. Right: AFM images of  $2.5\mu\text{M}$  **DNA-Phe<sub>5</sub>** with  $0.1\mu\text{M}$  **AuNP-DNA-2** deposited on APTES-modified mica. Condition: see Figure 3.4. Middle: the corresponding height profiles along the marked lines of the AFM image.

### 3.4. Conclusion

In conclusion, phenanthrene DNA-conjugates self-assembled into DNA-modified vesicles (type I). TEM and AFM measurements confirmed the formation of vesicular-shaped supramolecular polymers with diameters of 100 to 200 nm. Hybridization with a complementary Cy3-modified DNA shows an energy transfer from the excited phenanthrenes to the Cy3, whereas non-complementary Cy3 modified DNA did not show the energy transfer.

The DNA-modified vesicles were also stable after the addition of the **Cy3-DNA-1**, however, after heating/cooling of the same sample sheet-like structures were formed, illustrated in Figure 3.20. This observation suggests a change in the arrangement of the oligomers after heating/cooling, leading to a sheet-like structure with a flat surface and vesicles (type II) with the same **DNA-Phe<sub>5</sub>** and **Cy3-DNA-1** arrangement as the sheet-like structure as illustrated in Figure 3.20. Similar structures were already observed for **DNA-Phe<sub>3</sub>**.<sup>103</sup>

Encapsulation of **AuNP-DNA** into the vesicles worked only partially, TEM images showed the encapsulated **AuNP-DNA** but the specificity could not be shown clearly. The images showed also the formation of other undefined structures. One reason for these aggregates and the non-

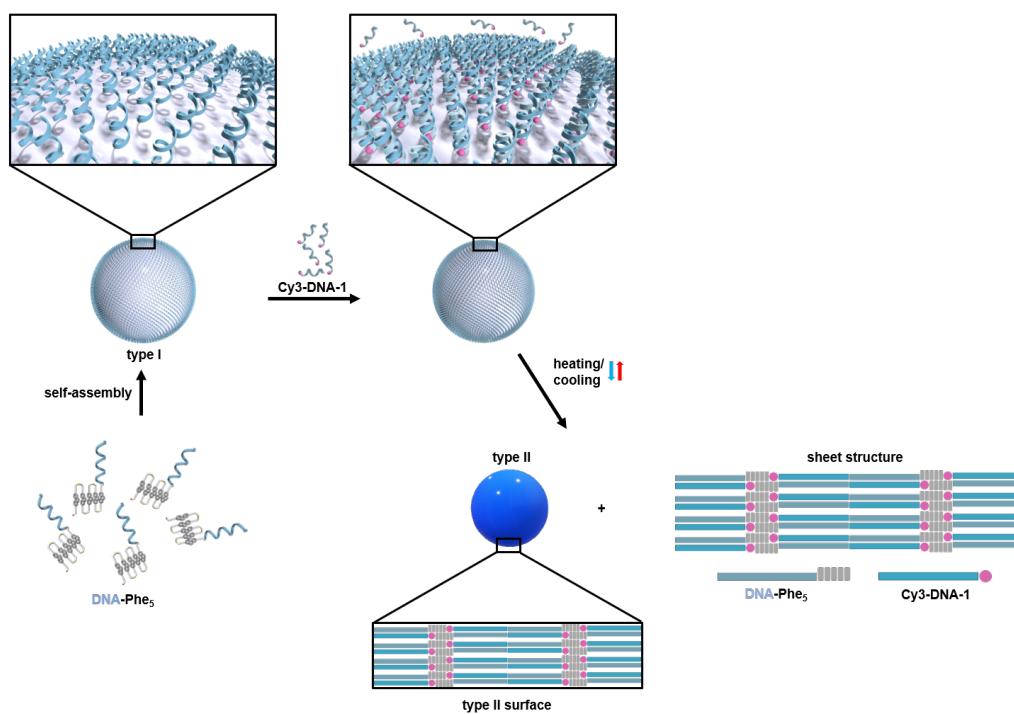


Figure 3.20.: Illustration of the formation of the DNA-modified vesicle (type I), sheet-like structure and vesicles with a different oligomer arrangement (type II).

specificity could be that the gold nanoparticles tend to form large networks on their own in the presence of spermine.<sup>104</sup> Hence, the **AuNP-DNA** start to aggregate as soon as they get in contact with the cationic polyamines, and the **DNA-Phe<sub>5</sub>** has little chance to actually interact specifically with the **AuNP-DNA**.



## 3.5. Experimental Section

### Synthesis of the Phenanthrene Building Block

#### Synthesis of the building block 2,7-phenanthrene

The 2,7-dialkynyl phenanthrene building block were synthesized according to the literature.<sup>101</sup>

#### Solid-phase synthesis

The oligos were synthesized in a 1  $\mu$ M scale using the standard phosphoramidite solid-phase synthesis protocol<sup>29</sup> on a ABI (Applied Biosystems Instruments) 394-DNA/RNA automated synthesizer.

#### HPLC Purification

The HPLC purification was done on a Shimadzu HPLC system using ReproSil 100 C18, Lichrospher 100 RP-18, 5 $\mu$ m, 250 x 4mm (Merck) . The mobile phase were: Solvent A: 0.1M TEAA /acetonitrile 80:20 and solvent B: CH<sub>3</sub>CN.

#### Synthesis of Au nanoparticles modified with DNA

The synthesis of the Au nanoparticles modified with DNA (**AuNP-DNA**) was done according to the literature<sup>106</sup>. The **AuNP-DNA** were synthesized by citrate reduction whereby tannic acid acts as co-reductant. The concentration of **AuNP-DNA** was determined in MilliQ by using a value of  $\epsilon^{520} = 1 \cdot 10^7 \text{ M}^{-1} \cdot \text{cm}^{-1}$  for 5 nm gold nanoparticles.

#### Sample preparation

The 2.5 $\mu$ M **DNA-Phe<sub>5</sub>**, 10mM sodium phosphate buffer, 0.1mM spermine tetrahydrochloride and 20% ethanol was heated up to 70 °C afterwards it was cooled down to 20 °C with a temperature gradient of 1 °C/min.

#### Sample preparation for the Atomic Force Microscopy

The mica substrates (20 x 20 mm<sup>2</sup>) were cleaved with Scotch tape. The mica surface was modified with N,N diisopropylethylamine and 3-aminopropyltriethoxy silane in the ration 1:3 as described in

the reference<sup>107</sup>. Sample that has to be hybridize with DNA-modified gold nanoparticles (AuNP-DNA) were incubated for 10 minutes after the addition of the AuNP-DNA solution. 20  $\mu\text{L}$  of the sample solution was drop-casted onto the mica substrate. After incubation time of 10 minutes, the modified mica sample was rinsed with 1 ml of MilliQ water and dried in an argon stream.

#### **Sample preparation for the Transmission electron microscopy**

The sample solution (5  $\mu\text{L}$ ) were put on the copper carbon grid/ copper formvar carbon grid/ copper holey carbon grid. It was incubated for 2-5 minutes then the solution was absorbed by a filter paper. The grid was then drawn through two different MilliQ water drop (each 10  $\mu\text{L}$ ), the solution was then absorbed with a filter paper each time. And in cases where there was no gold nanoparticles, the grid was then drawn through two different 0.5% uranyl acetate/UA zero solution drop (5  $\mu\text{L}$ ), the solution was absorbed with a filter paper.

Details can be found in Appendix B.

---

## 4. Self-assembly of Photocleavable Helical Ribbon Structures

### 4.1. Introduction

Supramolecular polymers that have functional characteristics are of a great interest.<sup>69,118–124</sup> Furthermore, supramolecular architectures with biological or optical properties can be an interesting material for nanotechnology.<sup>34,125–131</sup> Designing DNA conjugates, i.e. natural DNA nucleotides with artificial DNA nucleotide surrogates joined, which self-assemble via controlled arraying into supramolecular polymers with such characteristics is still a challenge.<sup>38,132–136</sup>

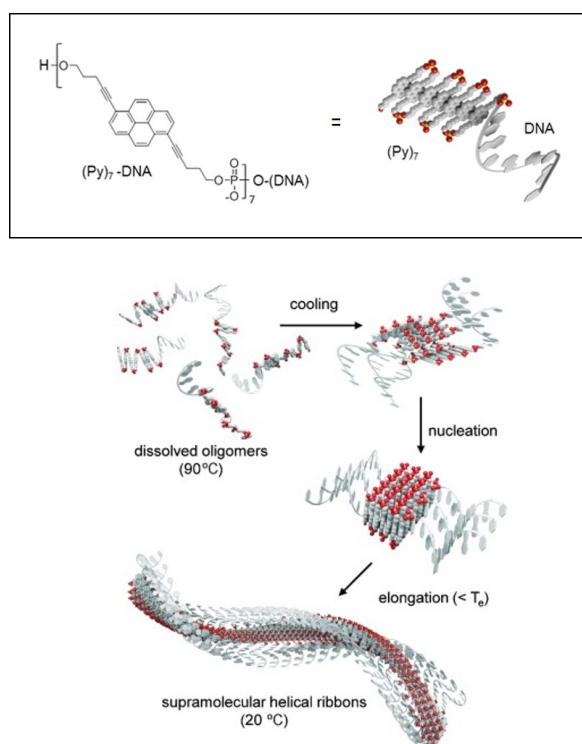


Figure 4.1.: Schematic illustration of the self-assembly of the pyrene-DNA oligomers into a helical ribbon structure. Top: Structure of the pyrene DNA conjugate. Adapted from the reference<sup>83,137</sup>.

Previously, it was shown that chimeric pyrene-DNA oligomers formed one-dimensional (1D) helical ribbon structures with a thickness of 2 nm (see Figure 4.1 and Figure 4.2).<sup>83,137,138</sup> The functionalization possibility of the helical ribbons was demonstrated by using gold nanoparticles with complementary DNA strands for hybridization with the supramolecular polymer.

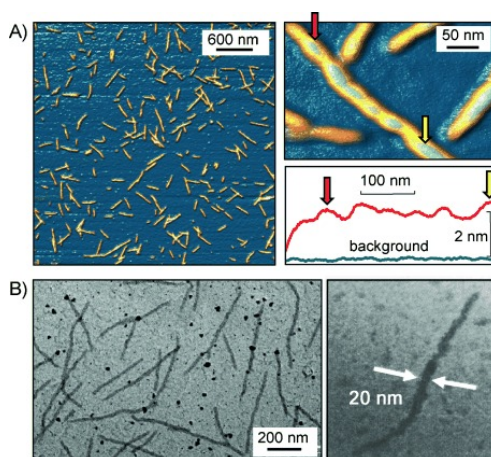


Figure 4.2.: A) AFM images of one-dimensional helical ribbons with the corresponding height profile. B) Transmission electron microscopy images with a zoom-in. Figure from the reference<sup>83</sup>.

In a second study, azobenzene functionalized benzene-1,3,5-tricarboxamide (BTA) self-assembled into a helical structure (see Figure 4.3).<sup>139</sup> Depolymerisation of the helical hydrogen-bonded polymers in methylcyclohexane was induced by UV light at the wavelength of 365 nm and can be reversed by irradiating at the wavelength of 455 nm.

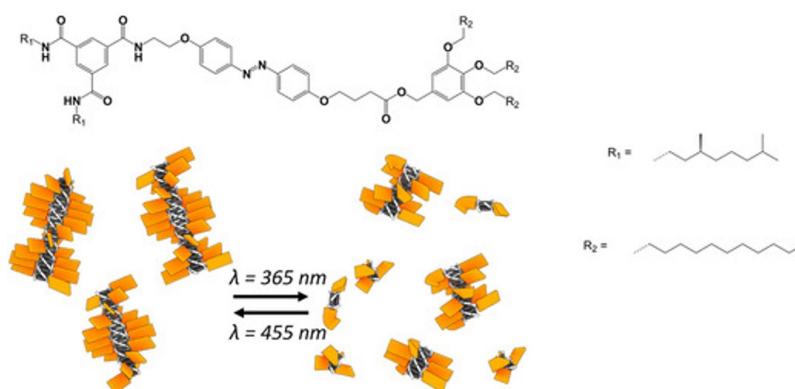


Figure 4.3.: Top: Chemical structure of azobenzene functionalized benzene-1,3,5-tricarboxamide (BTA). Bottom: Illustration of the superstructure and light-induced dissociation. Benzene rings of the BTA cores are (black disks), hydrogen bonds (white), and the azobenzenes (orange rectangles), trans-azobenzenes (flat rectangles), cis-azobenzenes (slightly twisted rectangles). Irradiation with UV-light (at 365 nm) leads to depolymerisation of the fibres, which can be reversed through irradiation at the wavelength of 455 nm or thermal relaxation. Figure from the reference<sup>139</sup>.

## 4.2. Aim of the Work

Here, in this study a photocleaver was incorporated into the before mentioned pyrene DNA conjugates (see Figure 4.1). It was expected that the new oligomer with the photocleaver should self-assemble into one-dimensional helical ribbon structures, like in the previous study. These ribbons are expected to be photocleavable, that means after the irradiation with UV-light the single strand DNA is supposed to be cleaved from the pyrenes, and thereby open up the option of influencing the structure of the supramolecular polymer. Atomic force microscopy should reveal the formation of the ribbon structures before and the resulting structures after the irradiation with UV-light. The addition of a dye (acceptor) attached to a complementary strand to the oligomer and then irradiating the pyrenes (donor), while measuring the dye emission was an additional experiment. After the irradiation of the photocleaver, the emission is expected to disappear. First, the self-assembly of a photocleavable ribbon is shown in this chapter.

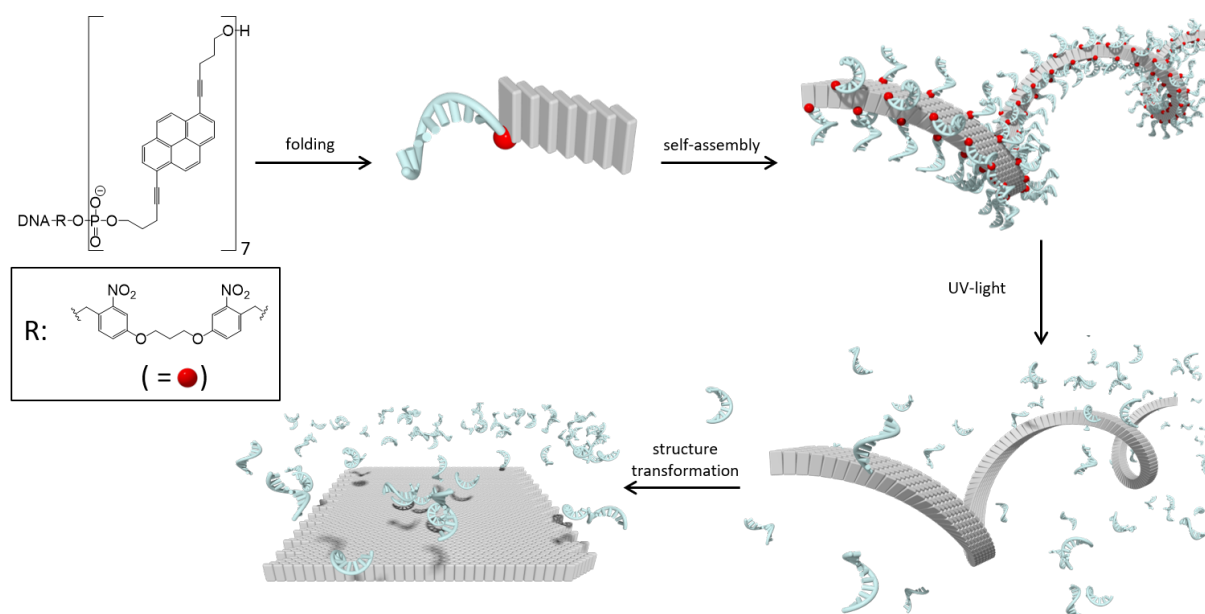


Figure 4.4.: Structure of the pyrene and photocleaver. Illustration of the folding, self-assembly and irradiation process. In blue is the DNA single strand (see Table 4.1). In grey are the pyrenes and the red dot as illustrated is the photocleaver.

By irradiation at the wavelength of 365 nm of the **DNA-R-Py<sub>7</sub>** a radical is formed. By radical-migration, H-migration, ring-closing reaction, and dissociation, it was expected to get DNA single strands and Py<sub>7</sub> in the end (see Figure 4.5). The DNA single strands and Py<sub>7</sub> are identified by mass spectrometry.

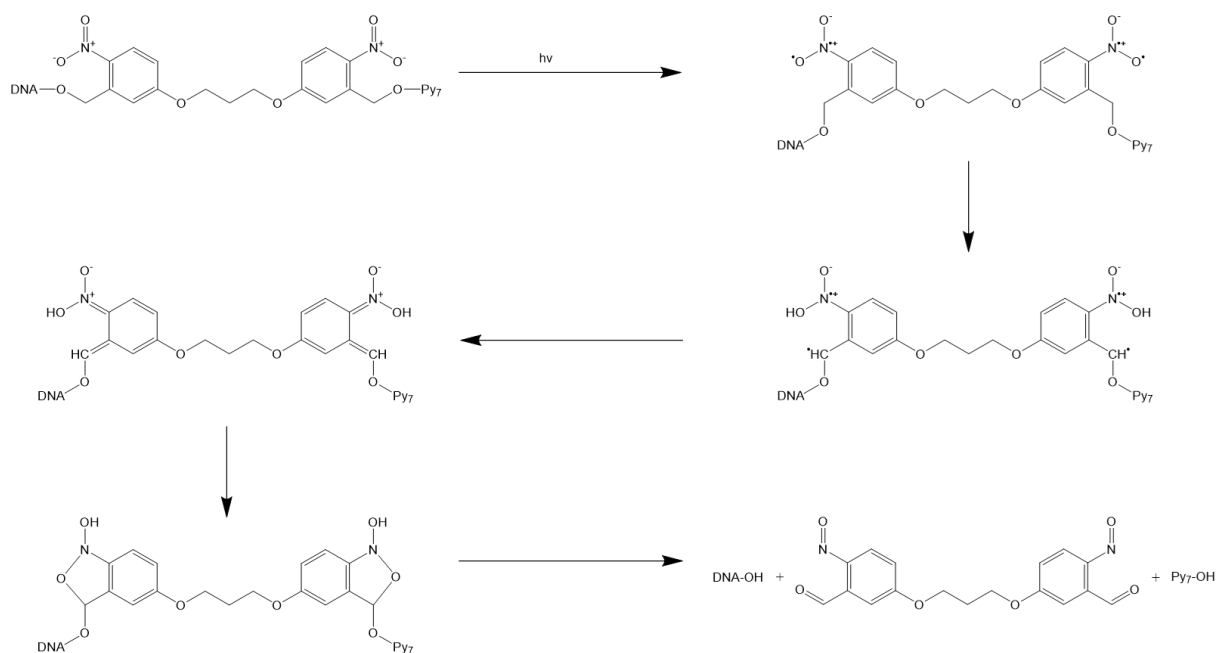


Figure 4.5.: Photoreaction of the photocleaver (5-[3-(3-Hydroxymethyl-4-nitro-phenoxy)-propoxy]-2-nitro-phenyl)-methanol).<sup>140,141</sup> Chemical structure of Py can be found in Figure 4.4.

## 4.3. Results & Discussion

### 4.3.1. Self-assembly of 1D helical ribbons

As mentioned in the introduction, it was found that DNA-pyrene conjugates based on 1,6-modified pentynyl pyrene self-assemble into helical ribbons. The 1,6-pyrene (**Py**, see Figure 4.4) and photocleaver (**R**, see Figure 4.4) building blocks were synthesized according to previous publications respectively according to a patent.<sup>105,140</sup> The oligomers that are used in this work were prepared by phosphoramidite solid phase synthesis according to published procedure.<sup>29</sup>

Table 4.1.: Oligomers that are used in this project with the corresponding sequences. Py = 1,6-pentynyl pyrene, R = photocleaver, Dyomics630 = dye, Cy5 = cyanine dye.

Oligomer	Sequence
DNA-R-Py <sub>7</sub>	Py-Py-Py-Py-Py-Py-Py-R - CTT CCG TGA G -3'
DNA-Py <sub>7</sub>	Py-Py-Py-Py-Py-Py-Py- CTT CCG TGA G -3'
DNA-Dyomics630	Dyomics630 - GAA GGC ACT C - 5'
DNA-Cy5	Cy5 - GAA GGC ACT C - 5'

Based on the previous study, the same condition was optimized and applied to this study.<sup>83,138</sup>

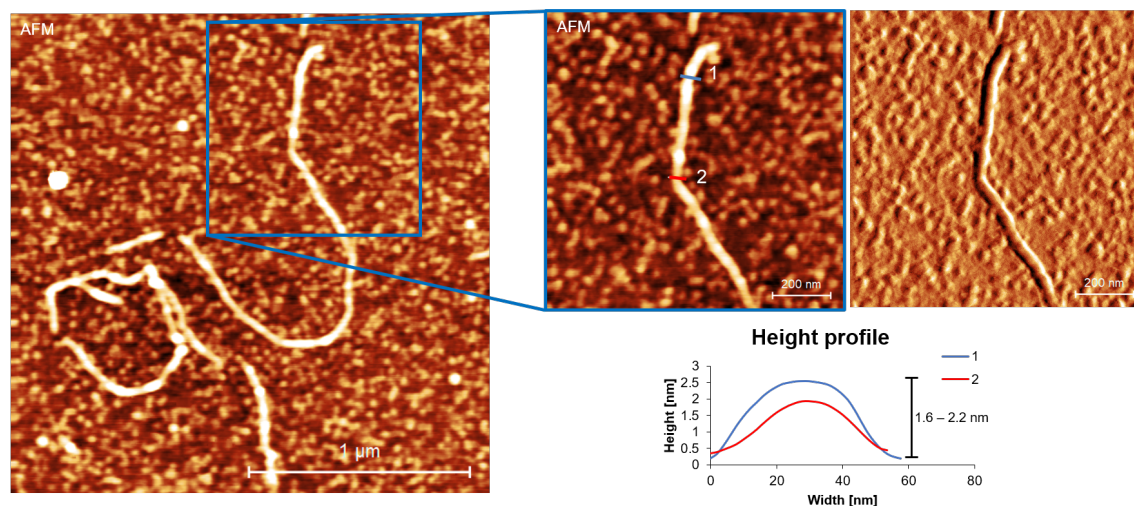


Figure 4.6.: AFM image of **DNA-R-Py<sub>7</sub>** ribbon structure deposited on APTES-modified mica (preparation see chapter 4.5). Condition: see Figure 4.7. Bottom right: corresponding height profile along the shown line in the insert of the AFM image.

The formation of the ribbons was achieved in aqueous medium with  $0.7 \mu\text{M}$  **DNA-R-Py<sub>7</sub>**, 10 mM sodium phosphate buffer (pH 7), 100 mM NaCl and by heating up to  $70^\circ\text{C}$  and cooling down to  $20^\circ\text{C}$  with a cooling rate of  $0.1^\circ\text{C}/\text{min}$  (see Figure 4.6).

In Figure 4.7, UV-vis spectra showed an appearing of a J-band at 305 nm and a H-band at 335 nm after the formation of the ribbons, as already observed in the literature.<sup>137</sup> These shifts are explained by a stair-like folding of the pyrene oligomers.<sup>83</sup>

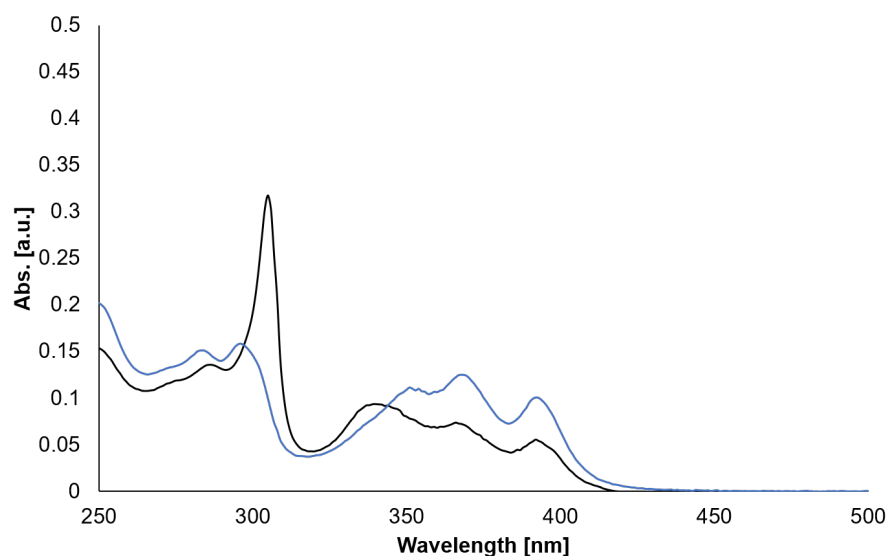


Figure 4.7.: UV-vis spectrum of **DNA-R-Py<sub>7</sub>** before (blue) after (black) the formation of ribbons. Condition: 0.7  $\mu$ M **DNA-R-Py<sub>7</sub>**, 10 mM sodium phosphate buffer (ph 7), 100 mM NaCl at 20°C.

The supramolecular polymerization process was observed by recording the UV-vis absorption at 305 nm, while the sample was heated up (70°C) and cooled down (20°C) (see Figure 4.8). Melting temperature was determined by heating up (70°C) the formed ribbons while recording the absorption at 305 nm, as well (see Figure 4.8).

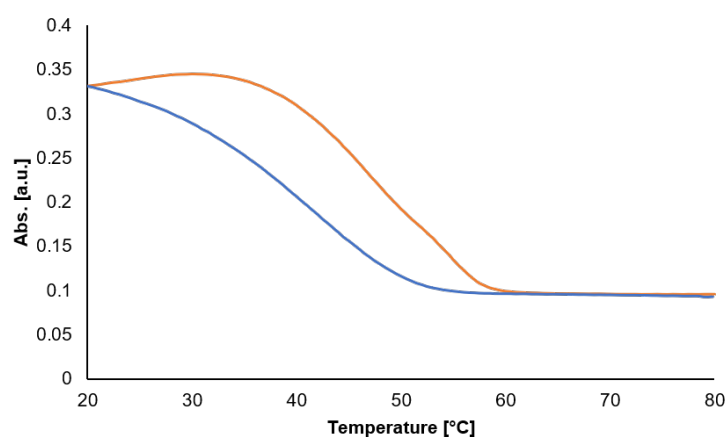


Figure 4.8.: Melting and cooling curves of **DNA-R-Py<sub>7</sub>**. Condition: see Figure 4.7, absorption at 305 nm. Blue: Cooling: 70°C to 20°C, cooling rate: 0.1°C/min. Orange: Heating: 20°C to 70°C, heating rate: 0.1°C/min.



These measurements give more information about the aggregation behaviour and the stability of the supramolecular polymers. The melting-cooling curves showed, the formation of the ribbons at 42.5°C (cooling ramp: 0.1°C/min) and a melting temperature of 48°C (heating ramp: 0.1°C/min).

#### 4.3.2. Irradiation of the ribbons

Observation of the melting-cooling curves at the wavelength at 305 nm for irradiated **DNA-R-Py<sub>7</sub>** showed not changes (see Figure 4.9). In a previous study, it was shown that the aqueous solution of a pyrene trimer required ethanol, in order to dissolve the pyrene aggregates, and to observe dissociation at a temperature below 70°C.<sup>99</sup> Here, a Py<sub>7</sub> unit was released after irradiation of the **DNA-R-Py<sub>7</sub>**, making it even more difficult to record a melting temperature in aqueous condition without the addition of ethanol.

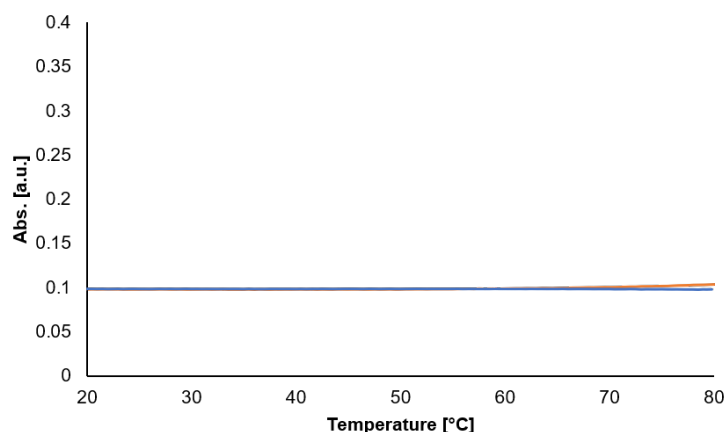


Figure 4.9.: Melting and cooling curves of **DNA-R-Py<sub>7</sub>** after irradiation for 30 min at the wavelength of 365 nm. Condition: see Figure 4.7, absorption at 305 nm. Blue: Cooling: 70°C to 20°C, cooling rate: 0.1°C/min. Orange: Heating: 20°C to 70°C, heating rate: 0.1°C/min.

Figure 4.10 shows the UV-vis absorption of **DNA-R-Py<sub>7</sub>** and **DNA-Py<sub>7</sub>** with different irradiation time. Irradiation at 365 nm had not only an influence to the oligomer with the photocleaver, but also to the one without. Increased irradiation time decreases the J-band and H-band, for the **DNA-R-Py<sub>7</sub>** more prominent than for **DNA-Py<sub>7</sub>**. It can not be excluded that the irradiation has also an impact on the pyrene. There is a significant decrease in the absorption for **DNA-Py<sub>7</sub>** from 30 min to 60 min irradiation time. Hence, the limit for the irradiation time was set to 30 min.

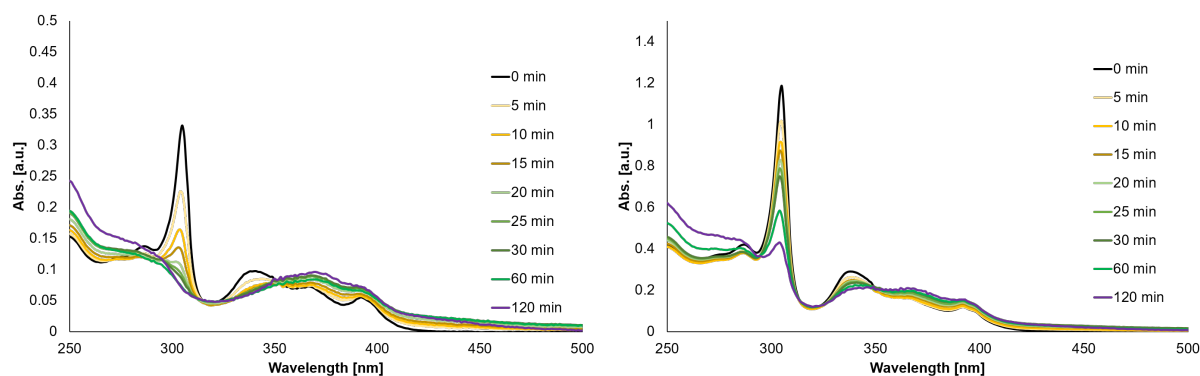


Figure 4.10.: UV-vis spectra of formed **DNA-R-Py<sub>7</sub>** ribbons (left) and **DNA-Py<sub>7</sub>** (right) after different irradiation times. After a certain time of irradiation (at 365 nm) the UV-vis absorption of the sample was measured. Condition: see Figure 4.7.

### High Performance Liquid Chromatography Experiments

The cleavage of **DNA-R-Py<sub>7</sub>** could also be observed in the HPLC chromatograms (see Figure 4.11). The **DNA-R-Py<sub>7</sub>** sample was irradiated at 365 nm for different times and via RP-HPLC it could be shown that the irradiation time has an influence on the cleavage. With increasing irradiation time, firstly, the retention time of the main peak (at about 15.8 min) shifted to the right and decreased in the intensity. Secondly, the peak at about 1.6 min appeared and increased in intensity.

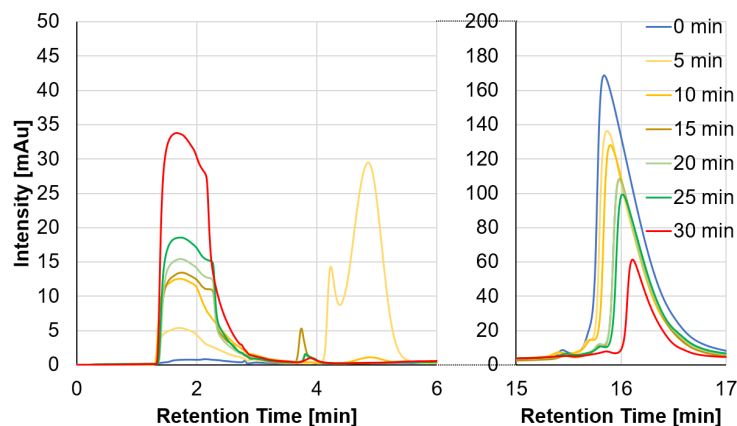


Figure 4.11.: HPLC traces of oligomer **DNA-R-Py<sub>7</sub>** after different irradiation times (irr. at 365 nm). Absorption at 260 nm was recorded. Zoom-in of the main peaks (about 1.6 min and 15.8 min).

Both mentioned peak were collected and to ensure the cleavage of the photocleaver mass spectroscopy (MS) was made and both mass could be found (see Table 4.2).

Table 4.2.: Calculated and measured mass of the collected peaks. Phosphate-Py<sub>7</sub> at about 15.8 min and ssDNA at about 1.6 min.

Oligomer	Calculated	Measured
DNA-R-Py <sub>7</sub>	6455.9926	6455.3028
Phosphate-Py <sub>7</sub>	3014.9107	3014.7750
ssDNA	3096.8669	3097.4424

### Atomic mass spectroscopy

Atomic force microscopy (AFM) showed the structures after irradiation. Samples were irradiated either in solution (condition see Figure 4.12) or on the APTES-mica (as in Figure 4.13, preparation see subchapter 4.5). In both cases, no ribbons were found, only small, irregular objects were observed.

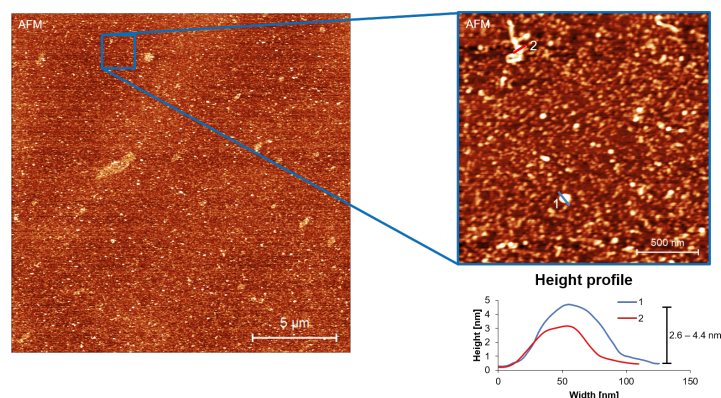


Figure 4.12.: AFM image of irradiated **DNA-R-Py<sub>7</sub>** sample deposited on APTES-modified mica. Condition: see Figure 4.7. Bottom right: corresponding height profile along the shown line in the insert of the AFM image.

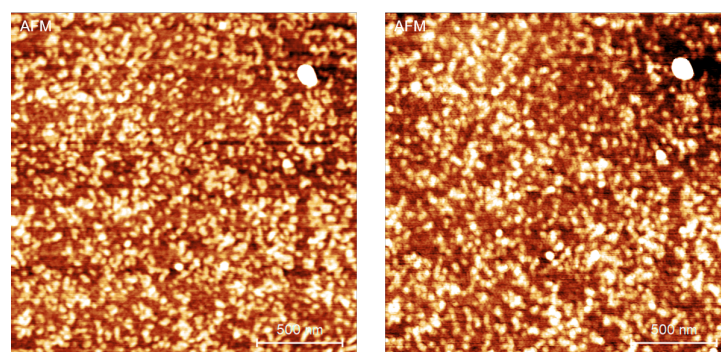


Figure 4.13.: AFM image of **DNA-R-Py<sub>7</sub>** sample deposited and irradiated on APTES-modified mica. Right: after the APTES-mica was washed again, in case there is any residue after the cleavage. Condition: see Figure 4.7.

## Spectroscopic Properties

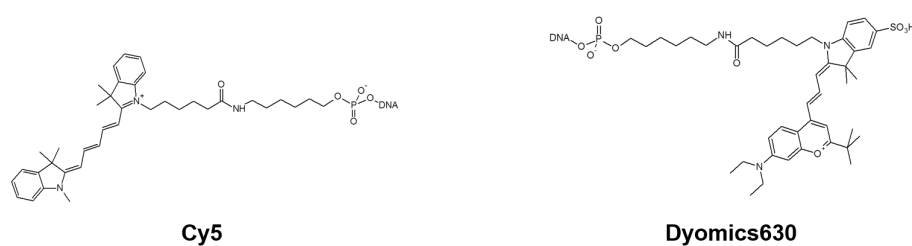


Figure 4.14.: Chemical structures of the commercially available Cy5 and Dyomics630 (from Mycrosynth GmbH, Bulgach, Switzerland).

Addition of a dye with a complementary DNA single strand to **DNA-R-Py<sub>7</sub>** should show the hybridization of the DNA and then the cleavage after the irradiation of the photocleaver at 365 nm. There were two dye candidates for these experiments (see Figure 4.14), the first one was Cy5, the second one was Dyomics630 (see Figure 4.14).

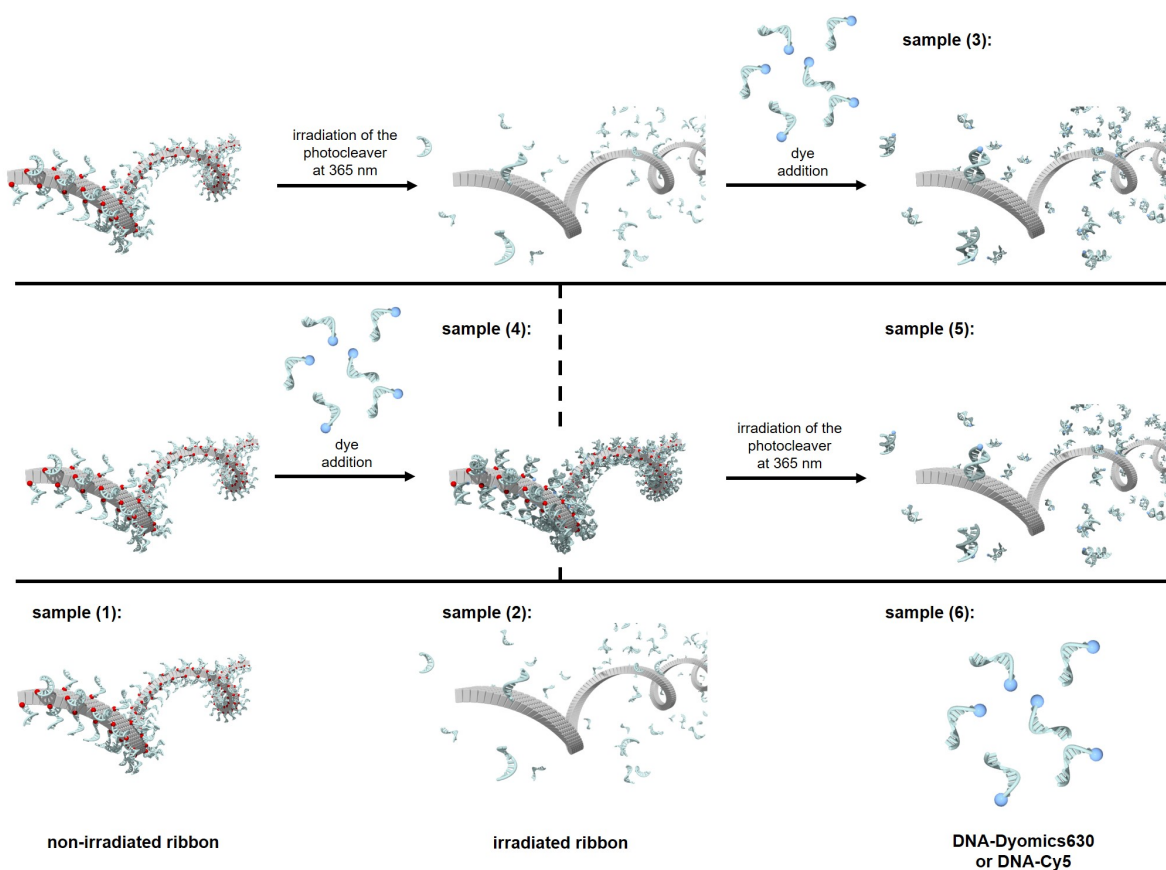


Figure 4.15.: Illustration of the different samples (explained next page). Top: sample (3), middle: sample (4) followed by sample (5) and bottom: sample (1): only non-irradiated ribbon, sample (2): only irradiated ribbon and sample (6): only dyes.

By excitation of the pyrenes at the wavelength of 365 nm, energy transfer should occur and an emission at 657 nm for Dyomics630 and 663 nm for Cy5 was observed.

In the following part, various samples were investigated: (see Figure 4.15). (1) Only non-irradiated preformed ribbons. (2) Photo cleaved ribbons. (3) Preformed ribbons were irradiated at 365 nm and then followed by the addition of **DNA-Cy5** or **DNA-Dyomics630**. (4) Non-irradiated preformed ribbons with **DNA-Cy5** or **DNA-Dyomics630**. (5) After the addition of **DNA-Cy5** or **DNA-Dyomics630** to the preformed ribbons, irradiation at 365 nm. (6) Only **DNA-Cy5** or **DNA-Dyomics630**.

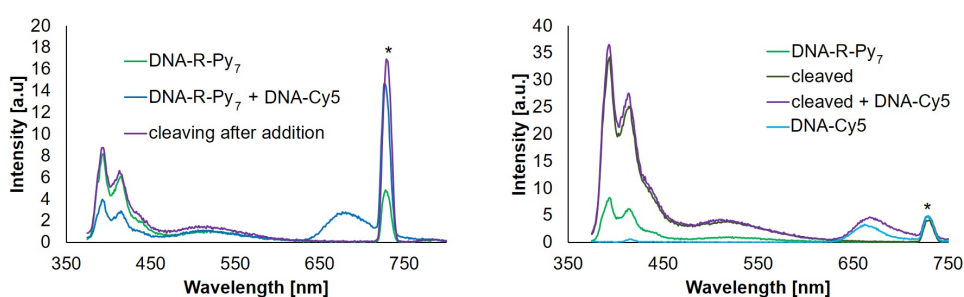


Figure 4.16.: Emission spectra of preformed **DNA-R-Py<sub>7</sub>** (green) and **DNA-Cy5** (blue). Left: Addition of 100% **DNA-Cy5** (dark blue) then irradiation at 365 nm for 30min (violet). Right: Irradiation at 365 nm for 30min (dark blue) then addition of 100% **DNA-Cy5** (violet). Condition: see Figure 4.7;  $\lambda_{\text{exc}}$ . 365 nm, 20°C; excitation slit: 5 nm, emission slit: 5 nm. \* in the spectrum marks a second-order diffraction.

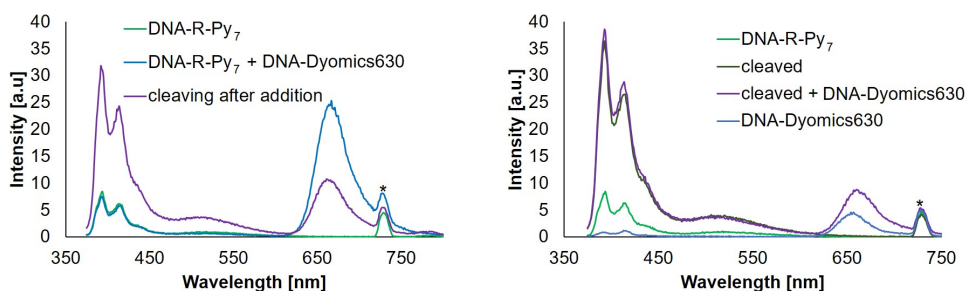


Figure 4.17.: Emission spectra of preformed **DNA-R-Py<sub>7</sub>** (green) and **DNA-Dyomics630** (blue). Left: Addition of 100% **DNA-Dyomics630** (dark blue) then irradiation at 365 nm for 30min (violet). Right: Irradiation at 365 nm for 30min (dark blue) then addition of 100% **DNA-Dyomics630** (violet). Condition: see Figure 4.16. \* in the spectrum marks a second-order diffraction.

Comparison of the two fluorescence measurements revealed that Cy5 (see Figure 4.16) was significantly less efficient than Dyomics630 (see Figure 4.17), plus Cy5 is not photostable, therefore, further experiments were done by using Dyomics630.

Stepwise addition of **DNA-Dyomics630** to the preformed ribbons showed a stagnation at about 40% **DNA-Dyomics630** (see Figure 4.18 and Figure 4.19). After 40% it was just a linear increase of the fluorescence emission.

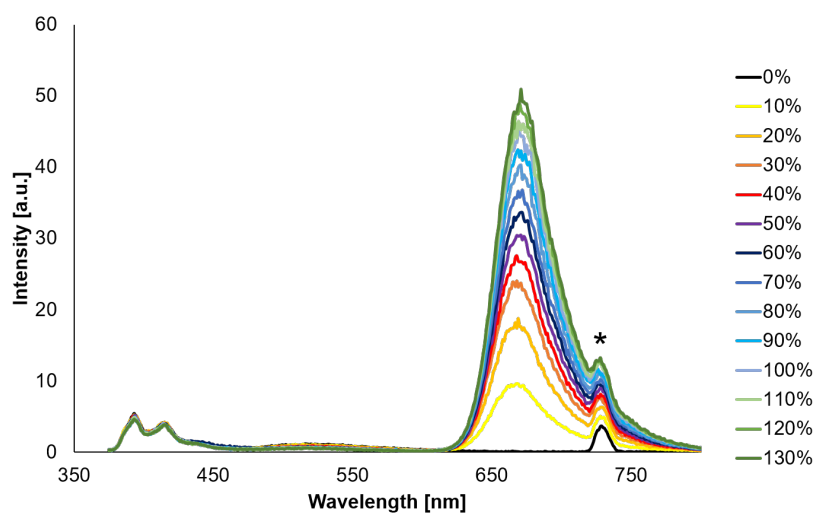


Figure 4.18.: Emission spectra of preformed **DNA-R-Py<sub>7</sub>** and stepwise addition of **DNA-Dyomics630**. Condition: same as in Figure 4.16. \* in the spectrum marks a second-order diffraction.

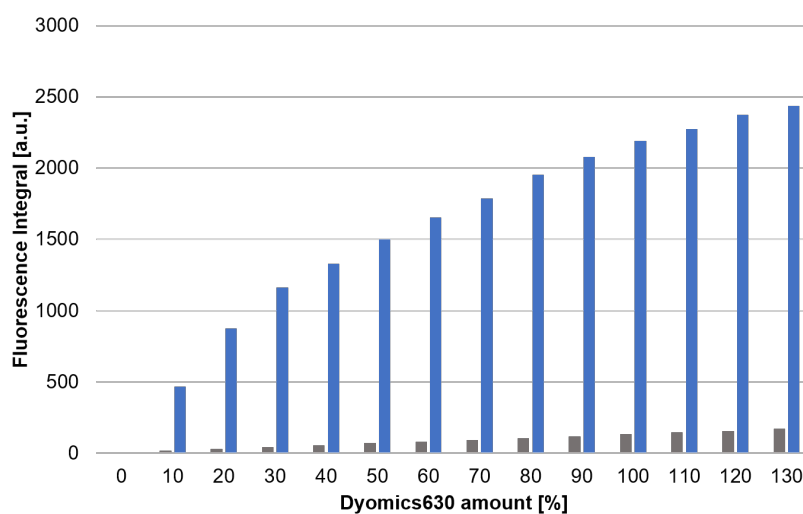


Figure 4.19.: Fluorescence integral of the emission spectra Figure 4.18 (emission from 620 nm -715 nm). Blue: **DNA-R-Py<sub>7</sub>**. Grey: only **DNA-Dyomics630**.

100% **DNA-Dyomics630** relative to the **DNA-R-Py<sub>7</sub>** concentration was added to the preformed ribbons. After addition and then after irradiation again the fluorescence were measured (sample (4) and (5), see Figure 4.20 left). In an other experiment, it was added to the irradiated sample, so after the **DNA-R-Py<sub>7</sub>** was cleaved (sample (3), see Figure 4.20 right).

After the irradiation the **DNA-Dyomics630** seems to have a higher emission intensity, when excited at the wavelength 365 nm.

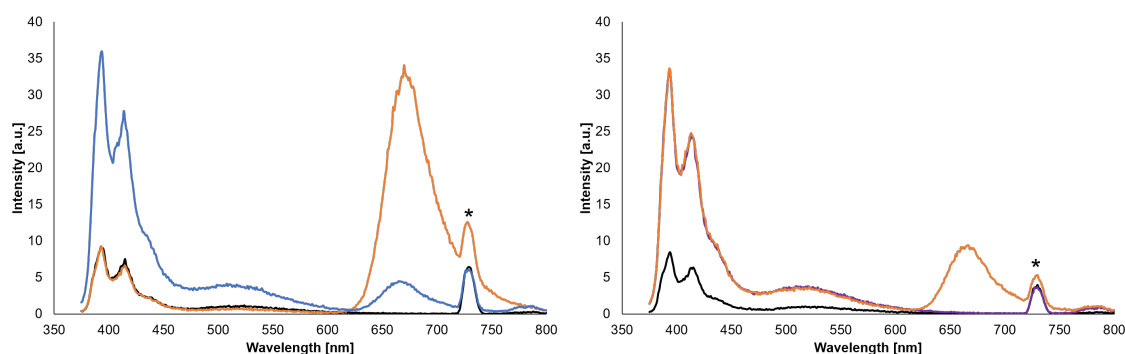


Figure 4.20.: Emission spectra of preformed **DNA-R-Py<sub>7</sub>** (black). Left: Addition of 100% **DNA-Dyomics630** (orange) then irradiation at 365 nm for 30min (blue). Right: Irradiation at 365 nm for 30min (violet) then addition of 100% **DNA-Dyomics630** (orange). Condition: see Figure 4.16. \* in the spectrum marks a second-order diffraction.

The cleaved **DNA-R-Py<sub>7</sub>** without **DNA-Dyomics630** showed a slightly higher fluorescence emission integral. As mentioned before, the sample (3) bar in Figure 4.21 shows the fluorescence integral after the addition of **DNA-Dyomics630** to the cleaved **DNA-R-Py<sub>7</sub>**. Surprisingly, the energy was still transferred to the Dyomics630. Addition of **DNA-Dyomics630** to the preformed ribbons (sample (4) bar in Figure 4.21) showed also an energy transfer to the

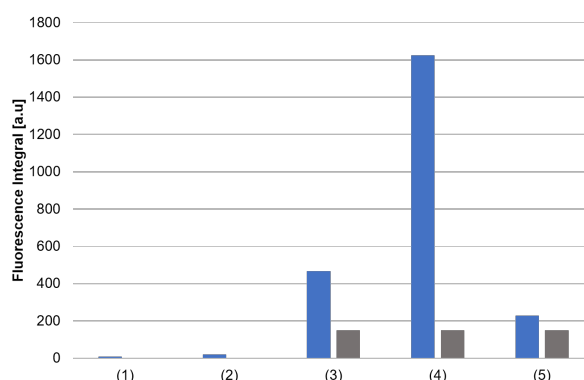


Figure 4.21.: Fluorescence integral of the emission spectra Figure 4.20 (emission from 620 nm - 715 nm). Approach of the bars/sample (1) to (5) is explained above. Blue: **DNA-R-Py<sub>7</sub>**. Grey: only **DNA-Dyomics630**.

Dyomics630, which is expected. However, there was still an emission observed after the ribbons with **DNA-Dyomics630** (sample (5), see Figure 4.20) (about 14% of the initial emission). In case the **DNA-R-Py<sub>7</sub>** was cleaved, a similar emission to the sample with only **DNA-Dyomics630** was expected (see Figure C.1 in Appendix C). As seen in Figure 4.21 (sample (2)) there was almost no emission for the cleaved ribbon and the **DNA-Dyomics630**.

From the result before (see Figure 4.18), it was decided to add **DNA-Dyomics630** where the fluorescence had the largest increase. So, the same experiment that was made with 100% **DNA-Dyomics630** was made with 10% **DNA-Dyomics630**. The measurement showed similar results with a less higher emission intensity. Also, in this case about 17% of the emission was still left after the cleaving of the ribbons (similar to Figure 4.20).

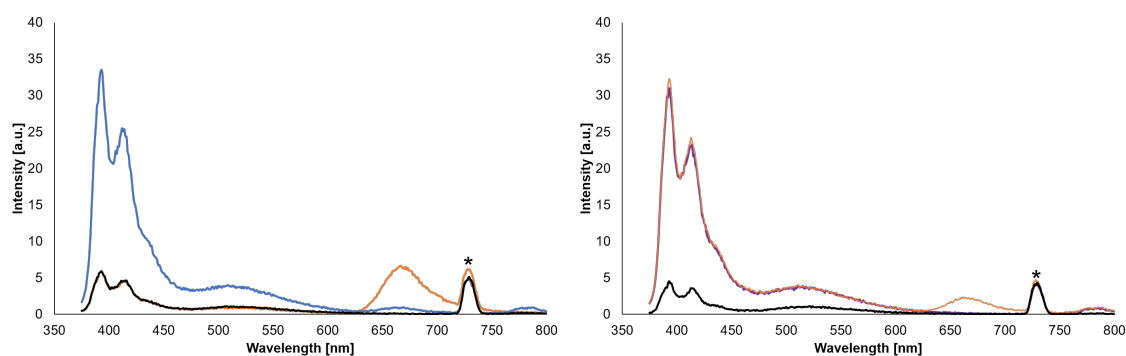


Figure 4.22.: Emission spectra of preformed **DNA-R-Py<sub>7</sub>** (black). Left: Addition of 10% **DNA-Dyomics630** (orange) then irradiation at 365 nm for 30min (blue). Right: Irradiation at 365 nm for 30min (violet) then addition of 10% **DNA-Dyomics630** (orange). Condition: see Figure 4.16. \* in the spectrum marks a second-order diffraction.

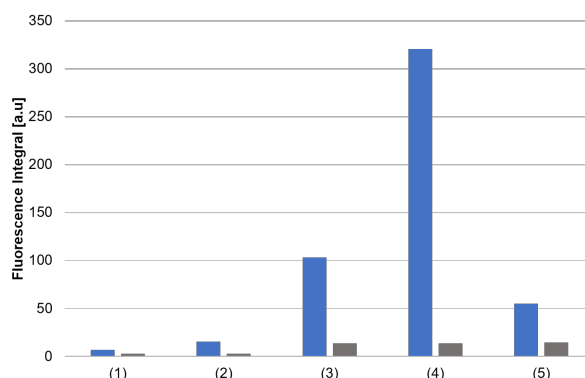


Figure 4.23.: Fluorescence integral of the emission spectra Figure 4.22 (emission from 620 nm - 715 nm). Approach of the bars/sample (1) to (5) is explained above. Blue: **DNA-R-Py<sub>7</sub>**. Grey: only **DNA-Dyomics630**.



A similar pattern as before is present, both experiments (10% and 100% **DNA-Dyomics630**) showed similar results but on a different intensity level. The residual emission (after irradiation of the photocleaver) could be observed in both cases. Therefore, it is evident that there was not 100% photo cleavage of the **DNA-R-Py<sub>7</sub>**.

#### 4.4. Conclusion

In conclusion, the photocleaver was successfully incorporated into the DNA-pyrene conjugates. AFM measurements showed that these DNA-pyrene conjugates with a photocleaver still self-assemble into helical ribbons. Fluorescence measurements revealed that the photocleaver could be irradiated and therefore that the helical ribbons are photocleavable. Also, AFM images showed that after irradiation the ribbons disappear and only undefined structures were found. Therefore, irradiation respectively cleaving of these DNA-pyrene conjugates with a photocleaver affects the structure of the supramolecular polymer. The results showed also that hybridization of a complementary DNA strand containing a dye affects the irradiation of the **DNA-R-Py<sub>7</sub>**. Surprisingly, addition of **DNA-Dyomics630** after **DNA-R-Py<sub>7</sub>** was cleaved, showed about two times more emission intensity compared to the emission of the sample, where the photocleaver of the oligomer **DNA-R-Py<sub>7</sub>** was irradiated after the addition of **DNA-Dyomics630**. This was unexpected, because the final result of the oligomer irradiation should be the same (in the end, there are Py<sub>7</sub> and ssDNA). Fluorescence spectra revealed also that after the photo-cleaving the energy was still transferred to the dyes. There are several reasons for these unexpected results, first, it was not possible to cleave all the **DNA-R-Py<sub>7</sub>**. And secondly, as mentioned before, it made a difference if the dye was hybridized to the ribbons or not, when **DNA-R-Py<sub>7</sub>** was cleaved before the addition of **DNA-Dyomics630**.

The incorporation of such a photocleaver can also be applied to other systems and/or DNA conjugates such as e.g. the demonstrated DNA-modified vesicles in chapter 3.

## 4.5. Experimental Section

### Material and General Methods

All required solvents and chemical reagents for the synthesis were purchased from commercial suppliers (Aldrich, Merck, TCI, Glen Research, Microsynth) and used without further purification. Mica plates ("V1", 20mmx20mm, thickness: 0.25mm) are from Plano GmbH.

### Synthesis

#### Synthesis of the photocleaver building block

The (5-(3-(3-Hydroxymethyl-4-nitro-phenoxy)-propoxy)-2-nitro-phenyl)-methanol (1) was synthesized starting from 3-Hydroxymethyl-4-nitro-phenol, which is commercially available. The first reaction was Finkelstein reaction, then tritylation and phosphorylation were made to get (5-(3-(3-(Bis-(4-methoxy-phenyl)-phenyl-methoxymethyl)-4-nitro-phenoxy)-propoxy)-2-nitro-phenyl)-methanol and then Diisopropyl-phosphoramidous acid 5-(3-(3-(bis-(4-methoxy-phenyl)-phenyl-methoxymethyl)-4-nitro-phenoxy)propoxy)-2-nitro-benzyl ester 2-cyano-ethyl ester. This reaction is according to a patent.<sup>140</sup>

#### Synthesis of the pyrene building block

The pyrene building block was synthesized according to literature.<sup>83,105</sup>

#### Solid-phase Synthesis

The oligos were synthesized in a 1  $\mu$ M scale using the standard phosphoramidite solid-phase synthesis protocol<sup>29</sup> on a ABI (Applied Biosystems Instruments) 394-DNA/RNA automated synthesizer.

#### HPLC Purification

The HPLC purification was done on a Shimadzu HPLC system using LiChroCART 250-4; LiChrospher 100, RP-18, 5  $\mu$ m column (Merck). The mobile phase were: Solvent A: HFIP buffer (ph 8) and solvent B: CH<sub>3</sub>CN.

### **Mass Spectrometry**

The molecular mass were determined on Thermo Fisher LTQ Orbitrap XL using Nano Electrospray Ionization (NSI).

### **Sample Preparation**

The sample in aqueous medium (0.7  $\mu\text{M}$  of the oligomer, 10 mM sodium phosphate buffer (ph 7), 100 mM NaCl ) was heated up to 70 °C afterwards it was cooled down to 20 °C with a temperature gradient of 0.1 °C/min.

### **Spectroscopic Characterisation**

UV-vis data were measured on a Cary 100 Bio spectrophotometer. Fluorescence and excitation data were measured on a Cary Eclipse spectrofluorimeter. The settings are as described in the corresponding spectra. For the measurement 1cm x 1cm quartz cuvettes were used.

### **Sample Preparation for the Atomic Force Microscopy**

The mica substrates (20 × 20 mm<sup>2</sup>) were cleaved with Scotch tape. The mica surface was modified with N,N diisopropylethylamine and 3-aminopropyltriethoxy silane in the ration 1:3 as described in the reference<sup>107</sup>. 20  $\mu\text{L}$  of the sample solution was drop-casted onto the mica substrate. After incubation time of 10 minutes, the modified mica sample was rinsed with 1 ml of MilliQ water and dried in an argon stream.

Details is in the Appendix C.

---

## 5. Energy Transfer in DNA-assembled Oligochromophores

Part of this work is based on a master thesis (Elena Grossenbacher, University of Bern, Department of Chemistry and Biochemistry, 2019). This study was performed in collaboration with Prof. Thomas Feurer, Prof. Andrea Cannizzo (Institute of Applied Physics, University of Bern, Switzerland) and the National Center of Competence in Research - Molecular Ultrafast Science and Technology (NCCR-MUST).

The results are published in:

*DNA-organized artificial LHCs - testing the limits of chromophore segmentation*

N. Bürki, E. Grossenbacher, A. Cannizzo, T. Feurer, S. M. Langenegger, R. Häner, *Org. Biomol. Chem.*, 2020, **18**, 6818.

### 5.1. Introduction

The formation of collectively excited states of multi-chromophores in a precise manner is of a great interest but is still a challenge.<sup>70,142–152</sup> In nature, light harvesting complexes (LHC) collect light by protein-bound chromophores.<sup>153–159</sup> The excited chromophores transfer this absorbed energy to a photosynthetic reaction center. LHC belongs to the functional unit of photosynthesis.<sup>66,67,153</sup> Inspired by nature, this well-evolved and highly efficient photosynthetic system was taken as the basis for artificial light harvesting complexes.<sup>160–163</sup> By using DNA as a supramolecular scaffold for the construction of definite arrays of aromatic dyes can be a helpful tool to control the assembly of well-organized artificial light harvesting system by making use of the hybridization of complementary strands.<sup>49,82,84,164–182</sup>

In the past, we showed in study a DNA-based hybrids built from homo- and hetero-multi-chromophores.<sup>183</sup> Electron-rich pyrene and electron-poor perylene-3,4,9,10-tetracarboxylic diimide (PDI) were incorporated into complementary DNA strands. These DNA-polycyclic aromatic hydrocarbon hybrids were used to test the degree of electronic coupling among the dye molecules. The study showed also that different number of pyrene-PDI interactions can directly influence the hybrid stability.

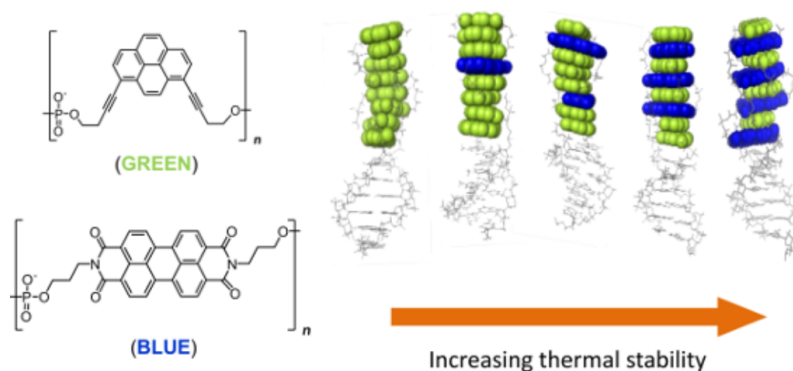


Figure 5.1.: Left: Structures of perylene-3,4,9,10-tetracarboxylic diimide (blue) and 1,8-dialkynylpyrene (green). Right: DNA-polycyclic aromatic hydrocarbon hybrids with different number of pyrene-PDI interactions, from left to right, increasing the number of interactions leads to an increasing thermal stability. Figure is from reference<sup>183</sup>.

Previously, we also reported a DNA-based light-harvesting antennae with phenanthrene donors and pyrene acceptor dye.<sup>184</sup> Different arrangements of light-absorbing phenanthrenes and pyrene were tested; stepwise an increasing number of intervening A-T base pairs were placed between a

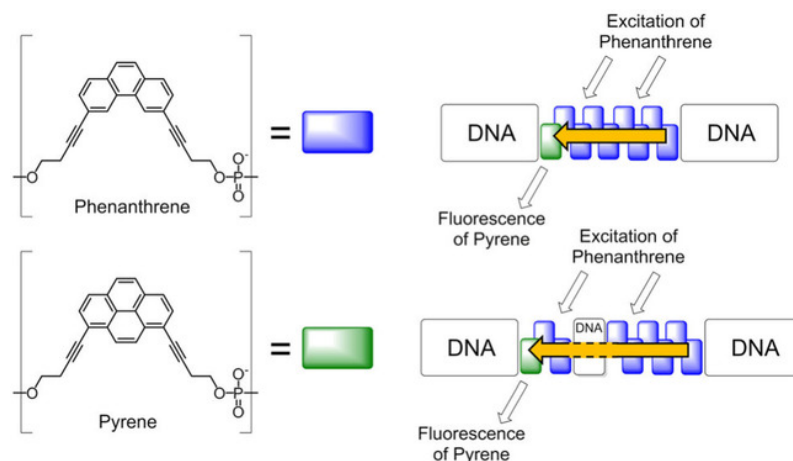


Figure 5.2.: Left: Structures of the building blocks; top: 3,6-dialkynylphenanthrene (blue); bottom: 1,8-dialkynylpyrene (green). Right: Schematic illustration of DNA-based light-harvesting antennae; top: without separating base pairs between phenanthrene units; bottom: with separating base pairs between phenanthrene units. Yellow arrows indicate energy transfer. Figure is from reference<sup>184</sup>.

block of six phenanthrenes and the pyrene. By exciting the phenanthrenes the energy will be transferred to the acceptor. The energy transfer could still be detected even after the phenanthrenes were separated by 5 A-T base pairs.

## 5.2. Aim of the work

In this study the limits of chromophore segmentation in DNA-organized artificial light harvesting complexes were tested. 1,8-dialkynylpyrene and 3,6-dialkynylphenanthrene were synthesized and incorporated into DNA strands. Fluorescence experiments should show the energy transfer from the excited phenanthrenes (donor) to the pyrene (acceptor) (see Figure 5.3) The efficiency of the chromophore segmentation is determined by quantum yield measurements.

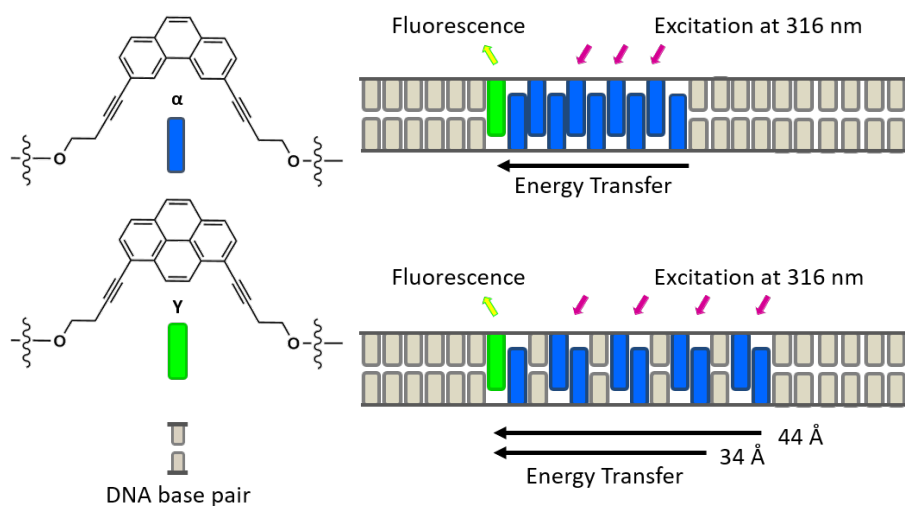


Figure 5.3.: Left: Structures of the building blocks; 3,6-dialkynylphenanthrene (blue); 1,8-dialkynylpyrene (green); and DNA base pair (grey). Right: Illustration of the two different arranged phenanthrene antennas in DNA-organized artificial LHCs. Bottom: phenanthrene stack and base pairs are alternated arranged; top: Single, contiguous phenanthrene stack. Figure can also be found in reference<sup>185</sup>.

### 5.3. Results & Discussion

The results are presented in two parts: In the first part the limitations of chromophore segmentation will be shown. In the second, results of the selectivity of the duplexes will be presented.

#### 5.3.1. Limits of the Chromophore Segmentation

*This part of the work was mainly carried out by Elena Grossenbacher (supervised by Nutchä Bürki, University of Bern, Department of Chemistry and Biochemistry, in 2019).*

Strand	Duplex	Sequence
S1	1	5' GGC TAA YTA AAT TTA AAT CGC 3'
S2		3' CCG ATT $\alpha$ AT TTA AAT TTA GCG 5'
S3	2	5' GGC TAA YT $\alpha$ AAT TTA AAT CGC 3'
S4		3' CCG ATT $\alpha$ A $\alpha$ TTA AAT TTA GCG 5'
S5	3	5' GGC TAA YT $\alpha$ A $\alpha$ T TTA AAT CGC 3'
S6		3' CCG ATT $\alpha$ A $\alpha$ T $\alpha$ A AAT TTA GCG 5'
S7	4	5' GGC TAA YT $\alpha$ A $\alpha$ T $\alpha$ TA AAT CGC 3'
S8		3' CCG ATT $\alpha$ A $\alpha$ T $\alpha$ A $\alpha$ AT TTA GCG 5'
S9	5	5' GGC TAA YT $\alpha$ A $\alpha$ T $\alpha$ T $\alpha$ AAT CGC 3'
S10		3' CCG ATT $\alpha$ A $\alpha$ T $\alpha$ A $\alpha$ A $\alpha$ TTA GCG 5'
S11	Ref1	5' GGC TAA Y $\alpha\alpha$ $\alpha\alpha$ T TTA AAT CGC 3'
S12		3' CCG ATT $\alpha\alpha\alpha$ $\alpha\alpha$ A AAT TTA GCG 5'

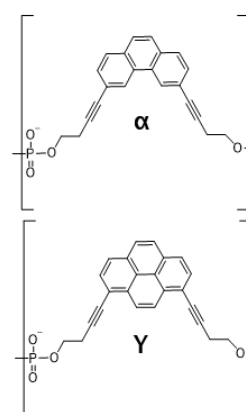


Figure 5.4.: Sequences of the modified DNA duplexes. Right: chemical structure of the pyrene and phenanthrene building blocks.

In Figure 5.4 are the sequences (**S1** - **S12**) of the phenanthrene- and/or pyrene-modified oligodeoxynucleotides that were synthesized and used in this project. Two complementary strands form a duplex (**1** - **5** & **Ref1**). The duplexes contain the acceptor 1,8-dibutynylpyrene (**Y**) and the donor chromophores 3,6-dibutynylphenanthrene ( $\alpha$ ). The design of the strands, in which the chromophores are separated by a varying number of DNA nucleotides, allows for a close interaction of the acceptor with at least one  $\alpha$  when the duplex is formed. **Ref1** serves as a reference for the duplex 5. Because of the well known quenching effect on the fluorescence of the nucleobase G, it was decided to use G-C base pairs at the end of the duplex to increase the stability, and incorporate A-T base pairs in between.<sup>62</sup>

### Spectroscopic Measurements

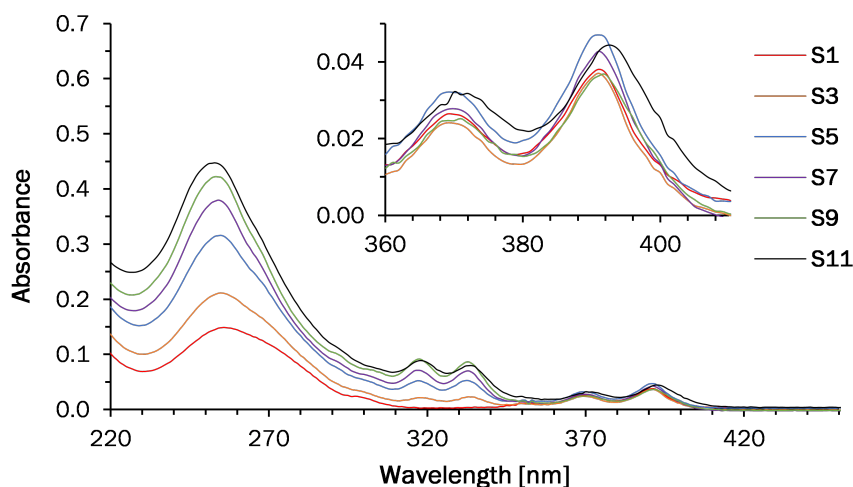


Figure 5.5.: UV-vis spectra of the single strands **S1**, **S3**, **S5**, **S7**, **S9** and **S11**. Conditions: 0.5  $\mu\text{M}$  strand, 10 mM sodium phosphate buffer (pH 7.0), 400 mM NaCl at 20°C.

Figure 5.5 shows the UV-vis spectra of the strands with one pyrene building block (**S1**, **S3**, **S5**, **S7**, **S9** and **S11**), all spectrum show similar vibronic bands at 370 nm and 391 nm which results from the pyrene. For **S11** it was slightly shifted and the maxima were 371 nm and 392 nm. Additional phenanthrene, in the strand led to a slight shift of the maxima. At about 260 nm, where pyrene, phenanthrene and the nucleobases absorb, the vibronic band starts at 256 nm for **S1** to 254 nm for **S9**, and for **S11** it was 251 nm. At 317 nm and 332 nm the maxima were similar for all strands, for **S11** it was 318 nm and 333 nm. The difference of **S11** are from the afore mentioned positioning of the pyrene and phenanthrene, where the other strands were separated by one DNA base pair, here they were positioned directly next to each other.

UV-vis spectra in Figure 5.6 show the single strands without any pyrene **S2** - **S12**. As in the previous UV-vis spectra, additional phenanthrene in the strand led to a slight shift of the vibronic band starting at 255 nm. The spectra in Figure 5.6 do not differ much from the spectra before (Figure 5.5) except the absence of the absorption bands of the pyrene of course. **S12** differs from the other strands because of the exact same mentioned reason stated before; the phenanthrenes are placed next to each other and are not separated by a DNA base pair.



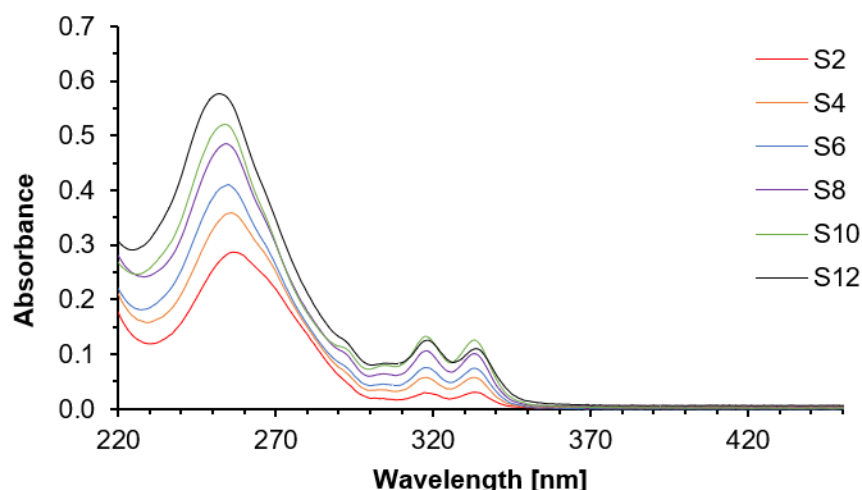


Figure 5.6.: UV-vis spectra of the strands **S2**, **S4**, **S6**, **S8**, **S10** and **S12**. Conditions: 0.5  $\mu\text{M}$  strand, 10 mM sodium phosphate buffer (pH 7.0), 400 mM NaCl at 20°C.

Figure 5.7 shows the UV-vis spectra of the duplexes (sample preparation see subchapter 5.5) **1** - **5** and **Ref1**. The spectra are similar to the UV-vis spectra before and only differ in the intensity. Vibronic bands of pyrene are at 370 nm and 391 nm, for phenanthrene the maxima are at 318 nm and 333 nm. At about 260 nm, the maxima are shifted with additional phenanthrene number, and without intervening A-T base pairs **Ref1** differs from the other duplexes and especially from duplex **5**. Therefore, a hypochromic effect is observed at 318 nm and a even more pronounced, at 333 nm.

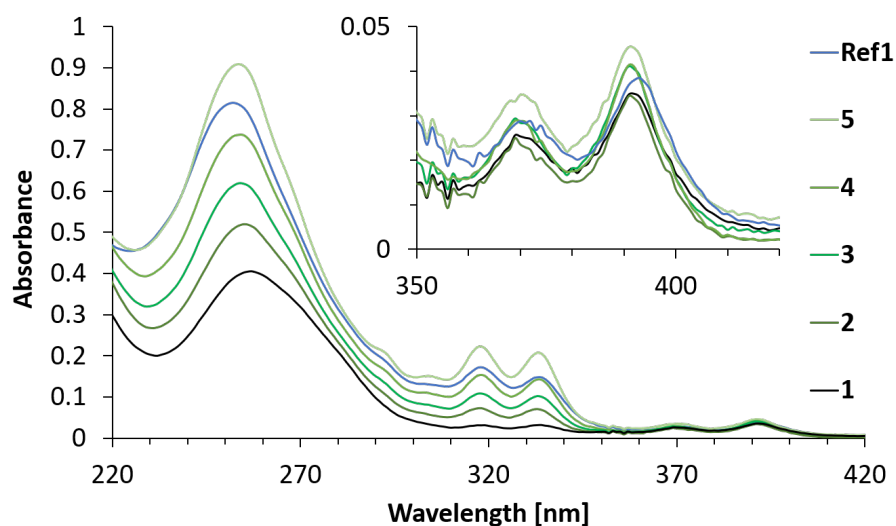


Figure 5.7.: UV-vis spectra of the duplex **1**, **2**, **3**, **4**, **5** and **Ref1**. Conditions: 0.5  $\mu\text{M}$  of each strand, 10 mM sodium phosphate buffer (pH 7.0), 400 mM NaCl at 20°C.

Duplex	Sequence	T <sub>m</sub> [°C]
1	5' GGC TAA YTA AAT TTA AAT CGC 3'	60.7
	3' CCG ATT αAT TTA AAT TTA GCG 5'	
2	5' GGC TAA YTα AAT TTA AAT CGC 3'	57.4
	3' CCG ATT αAα TTA AAT TTA GCG 5'	
3	5' GGC TAA YTα AαT TTA AAT CGC 3'	52.5
	3' CCG ATT αAα TαA AAT TTA GCG 5'	
4	5' GGC TAA YTα AαT αTA AAT CGC 3'	49.8
	3' CCG ATT αAα TαA αAT TTA GCG 5'	
5	5' GGC TAA YTα AαT αTα AAT CGC 3'	42.6
	3' CCG ATT αAα TαA αAα TTA GCG 5'	

Figure 5.8.: Melting temperatures (T<sub>m</sub>) of the duplex **1 - 5** and **Ref1**. Conditions: 0.5 μM of each strand, 10 mM sodium phosphate buffer (pH 7.0).

The stability of the duplexes can be determined by measuring the melting temperature (T<sub>m</sub>). The absorption during heating-cooling-cycles (80°C → 20°C, 20°C → 80°C, temp. rate of 0.5 °C/min) was recorded by monitoring the absorbance at 260 nm of the duplex **1 - 5** and **Ref1**, these melting curves can be found in the appendix D. The maximum of the first derivation of the melting curves is the T<sub>m</sub> (see Figure 5.8). It revealed, with increasing number of phenanthrenes the T<sub>m</sub> decreases, with each additional replacement of an A-T base pair with a pair of α results in a significant decrease in stability of 3-7°C. Duplexes **Ref1**, which has no nucleobases in between the modifications, and **5** have the same number of pyrene and phenanthrenes, but differ severely in duplex stability. The T<sub>m</sub> of duplex **5** is 42.6 °C and the T<sub>m</sub> of **Ref1** is 64°C, which is in the same range as the duplex **1**.

By excitation of the phenanthrenes at 316 nm, an emission of the acceptor pyrene can be observed. Fluorescence spectra (Figure 5.9) of the strands **S1**, **S3**, **S5**, **S7** and **S9** all containing one pyrene, show a maximum at 402 nm and a band that starts at about 426 nm and slightly shifted to 422 nm with each additional phenanthrene. So, the pyrene emission is mainly observed. It must also be mentioned, that the strand **S1** emits at about 425 nm when excited at 316 nm, this emission is not caused by energy transfer nor by light-harvesting. This is simply a result of the pyrene that also absorbs at 316 nm and has an emission with a maximum at 402 nm. The emission of the strand **S11** differs distinctly from the other strands. The maximum is at about 424 nm and at around 410 nm, a shoulder appears with a tailing up to 580 nm.

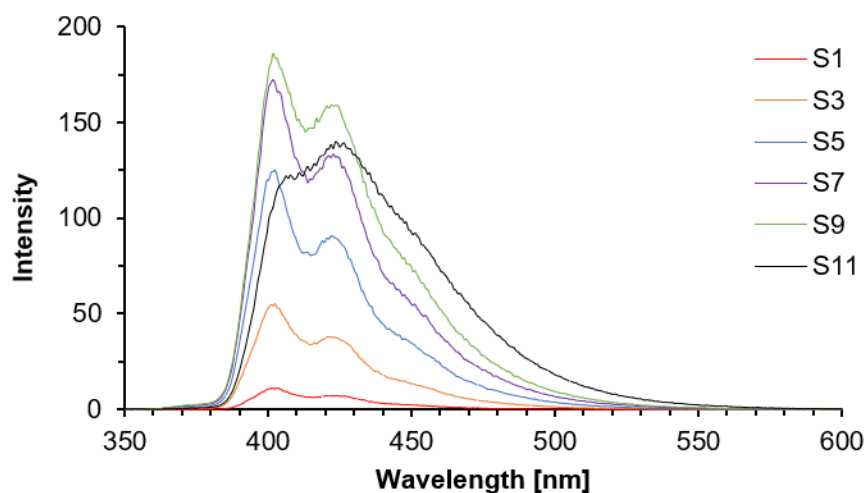


Figure 5.9.: Fluorescence spectra of the strands **S1**, **S3**, **S5**, **S7**, **S9** and **S11**. Conditions: 0.5  $\mu\text{M}$  strand, 10 mM sodium phosphate buffer (pH 7.0), 400 mM NaCl.  $\lambda_{\text{exc}}$ . 316 nm, 20°C; excitation slit: 2.5 nm, emission slit: 5 nm.

The strands **S2**, **S4**, **S6**, **S8** and **S10** only have phenanthrenes, therefore, fluorescence spectra (Figure 5.10) show only a very small emission intensity, because of the absence of the acceptor pyrene. The maxima are at 374 nm and 387 nm. Again, the strand **S12** differs and it shows a broad emission spectrum with a maximum at 397 nm since here, there is a stack of five phenanthrene present.

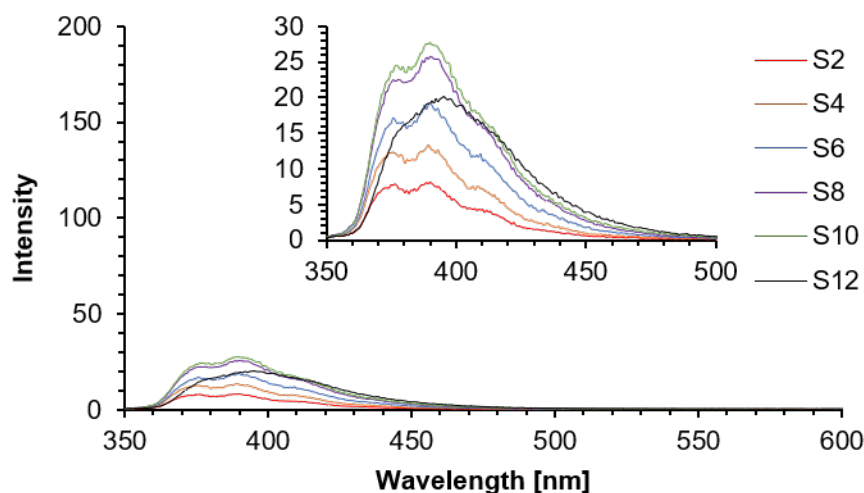


Figure 5.10.: Fluorescence spectra of the strands **S2**, **S4**, **S6**, **S8**, **S10** and **S12**. Conditions: 0.5  $\mu\text{M}$  strand, 10 mM sodium phosphate buffer (pH 7.0), 400 mM NaCl.  $\lambda_{\text{exc}}$ . 316 nm, 20°C; excitation slit: 2.5 nm, emission slit: 5 nm.

Fluorescence spectra (Figure 5.11) of the duplexes **1**, **2**, **3**, **4**, and **5** show significant pyrene

emission with the maximum at 402 nm and a second band that is now shifted, from 426 nm to 422 nm. Duplex **Ref1** on the other hand showed a broad band at about 430 nm. Almost no phenanthrene emission at 365-380 nm could be observed for the duplexes **1**, **2** and **3**. A small signal could be observed for duplex **4**, and for duplex **5** the signal was even more intense. Which means that phenanthrene itself emitted a part of the excitation energy, instead transferring it to the acceptor. From duplex **1** to duplex **4** the intensity of pyrene fluorescence increases gradually; for duplex **5** no further growth could be observed. An extended tailing with a shoulder at around 450 nm can be seen for all emission spectra, this is because of the phenanthrene excimer and/or phenanthrene-pyrene exciplex formation.<sup>186</sup>

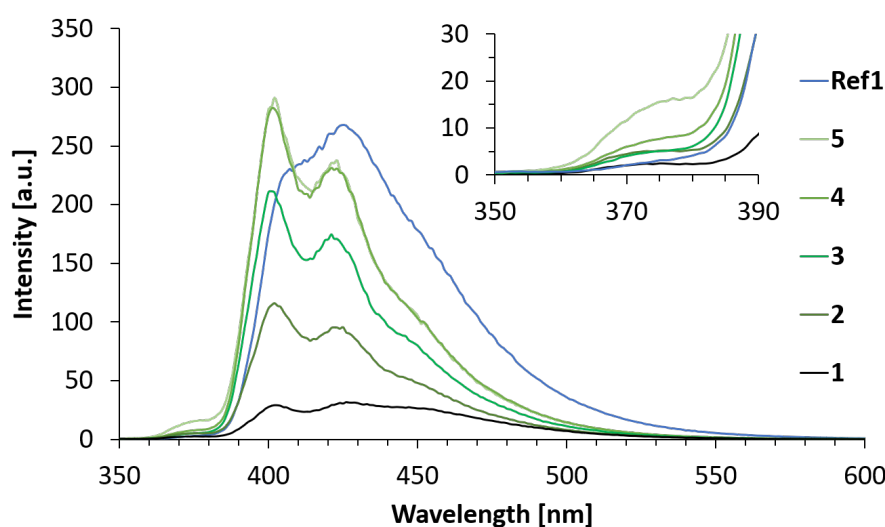


Figure 5.11.: Fluorescence spectra of duplex **1**, **2**, **3**, **4**, **5** and **Ref1**. Conditions: 0.5  $\mu\text{M}$  of each strand, 10 mM sodium phosphate buffer (pH 7.0), 400 mM NaCl.  $\lambda_{\text{exc}}$ . 316 nm, 20°C; excitation slit: 2.5 nm, emission slit: 5 nm.

The emission spectrum of duplex **Ref1** is similar to the single strand **S11** (see Figure 5.9), it has a maximum at 425 nm with a shoulder at about 410 nm and a tailing up to 580 nm. Due to the stacking arrangement and the resulting electronic coupling of the phenanthrenes, the duplex **Ref1**, which has an uninterrupted phenanthrene stack, shows little similarity to the other duplexes.

### Quantum Yields

Quantum yields ( $\phi_F$ ) were measured for duplexes **1** - **5** and **Ref1** using quinine sulfate as a reference (see subchapter 5.5). Table 5.1 shows an increasing quantum yield for duplexes **1** to **3** (approx. 68%) and starts to level off for duplex **4** and **5**. These findings match with the observed

fluorescence spectra (see Figure 5.11). Hence, the maximum length of such a interrupted phenanthrene antenna is reached at duplex **4**, where energy is still harvested by light absorption and the energy is transferred to the pyrene-acceptor since the quantum yield of duplex **5** is decreased by about 20% therefore, less efficient than duplex **4**. The highest quantum yield has **Ref1**, where the phenanthrene units are not interrupted by DNA base pair, as expected.

Table 5.1.: Quantum yields ( $\phi_F$ ) of the duplex **1** - **5** and **Ref1**. Conditions: 0.5  $\mu$ M of each strand, 10 mM sodium phosphate buffer (pH 7.0), 400 mM NaCl.

Duplex	Sequence	$\phi_F$ [%] (SD)
1	5' GGC TAA YTA AAT TTA AAT CGC 3'	47.2 ( $\pm$ 2.2)
	3' CCG ATT $\alpha$ AT TTA AAT TTA GCG 5'	
2	5' GGC TAA YT $\alpha$ AAT TTA AAT CGC 3'	51.0 ( $\pm$ 2.7)
	3' CCG ATT $\alpha$ A $\alpha$ TTA AAT TTA GCG 5'	
3	5' GGC TAA YT $\alpha$ A $\alpha$ T TTA AAT CGC 3'	68.1 ( $\pm$ 3.2)
	3' CCG ATT $\alpha$ A $\alpha$ T $\alpha$ A AAT TTA GCG 5'	
4	5' GGC TAA YT $\alpha$ A $\alpha$ T $\alpha$ TA AAT CGC 3'	64.0 ( $\pm$ 2.1)
	3' CCG ATT $\alpha$ A $\alpha$ T $\alpha$ A $\alpha$ AT TTA GCG 5'	
5	5' GGC TAA YT $\alpha$ A $\alpha$ T $\alpha$ T $\alpha$ AAT CGC 3'	46.3 ( $\pm$ 2.3)
	3' CCG ATT $\alpha$ A $\alpha$ T $\alpha$ A $\alpha$ A $\alpha$ TTA GCG 5'	
Ref1	5' GGC TAA Y $\alpha\alpha$ $\alpha\alpha$ T TTA AAT CGC 3'	70.0 ( $\pm$ 3.0)
	3' CCG ATT $\alpha\alpha\alpha$ $\alpha\alpha$ A AAT TTA GCG 5'	

### 5.3.2. DNA Duplexes containing Mismatches

In the previous subchapter, it was shown that the maximum length of 'interrupted' phenanthrene antenna is reached by duplex **4**. The question of the selectivity of this duplex was answered by adding mismatches to one of the strands. Therefore, three additional strands (**S13**, **S14** and **S15**) were synthesized (see Table 5.2), two of them have one mismatch but at different positions. The third one has two mismatches.

The same strand **S7** from the previous subchapter was also used here. Duplexes **6** to **8** have the exact same sequence as duplex **4** except with one or two base pair mismatches (see Table 5.2).

### Spectroscopic Measurements

In Figure 5.12 are the absorption spectra of all duplexes. Duplexes **6** to **8** show the same absorption profile as duplex **4**. Vibronic bands at 333 nm and 318 nm (phenanthrene) and the pyrene with

Table 5.2.: Sequence of duplexes **6** - **8**. Chemical structure of  $\alpha$  and  $\mathbf{Y}$  see Figure 5.4. In red are the mismatches.

Strand	Duplex	Sequence
S7	6	5' GGC TAA YT $\alpha$ A $\alpha$ T $\alpha$ TA AAT CGC 3'
S13		3' CCG ATT $\alpha$ T $\alpha$ T $\alpha$ A $\alpha$ AT TTA GCG 5'
S7	7	5' GGC TAA YT $\alpha$ A $\alpha$ T $\alpha$ TA AAT CGC 3'
S14		3' CCG ATT $\alpha$ A $\alpha$ T $\alpha$ T $\alpha$ AT TTA GCG 5'
S7	8	5' GGC TAA YT $\alpha$ A $\alpha$ T $\alpha$ TA AAT CGC 3'
S15		3' CCG ATT $\alpha$ T $\alpha$ T $\alpha$ T $\alpha$ AT TTA GCG 5'

maxima at 370 nm and 391 nm. Duplexes **7** and **8** show a slightly lower phenanthrene absorption bands (333 nm and 318 nm) than duplexes **4** and **6**.

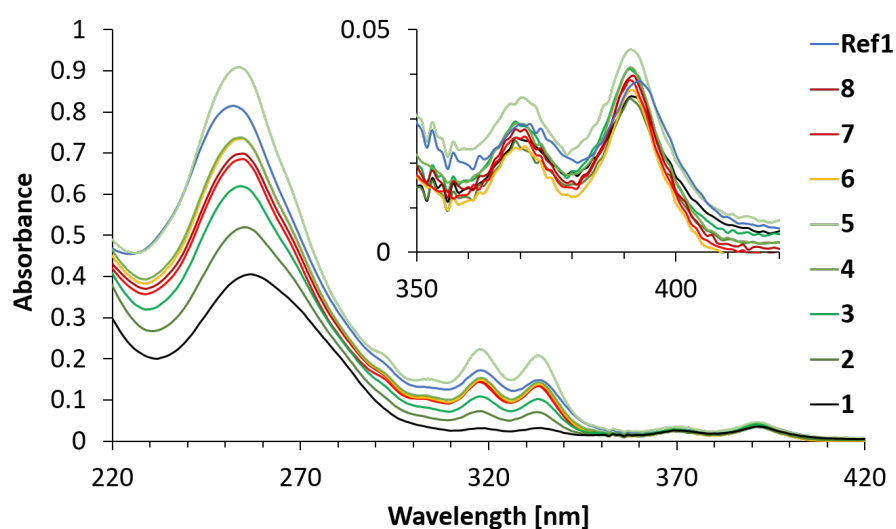


Figure 5.12.: UV-vis spectra of all duplexes investigated in this study. Conditions: 0.5  $\mu$ M of each strand, 10 mM sodium phosphate buffer (pH 7.0), 400 mM NaCl at 20°C.

Table 5.3.: Melting temperatures ( $T_m$ ) of the duplex **6**, **7** and **8**. Conditions: 0.5  $\mu$ M of each strand, 10 mM sodium phosphate buffer (pH 7.0).

Duplex	Sequence	$T_m$ [°C]
6	5' GGC TAA YT $\alpha$ A $\alpha$ T $\alpha$ TA AAT CGC 3'	50.7
	3' CCG ATT $\alpha$ T $\alpha$ T $\alpha$ A $\alpha$ AT TTA GCG 5'	
7	5' GGC TAA YT $\alpha$ A $\alpha$ T $\alpha$ TA AAT CGC 3'	48.3
	3' CCG ATT $\alpha$ A $\alpha$ T $\alpha$ T $\alpha$ AT TTA GCG 5'	
8	5' GGC TAA YT $\alpha$ A $\alpha$ T $\alpha$ TA AAT CGC 3'	51.3
	3' CCG ATT $\alpha$ T $\alpha$ T $\alpha$ T $\alpha$ AT TTA GCG 5'	

$T_m$  values were also determined for the duplexes **6** to **8** (see Table 5.3). In comparison to the fully complementary duplex **4** with a  $T_m$  of 49.8°C, the  $T_m$  of duplexes **6** and **7** each with one base

pair mismatch (T-T) are almost unchanged. Astonishing is the fact that the duplex **8** seems to be slightly more stable than the duplex **4**, although duplex **8** has two base pair mismatches. The assumption is that the mismatched base pairs are flipped out of the helix duplex. The flipping may result in additional  $\pi$ - $\pi$  interactions between the adjacent phenanthrene units which would be beneficial for the stability.<sup>187</sup> This can also be an explanation for duplexes **6** and **7**, although they have a mismatch base pair it seems not to affect the stabilisation, even though a mismatch usually tends to destabilize the DNA.

In Figure 5.13 the fluorescence spectra of **6** and **8** show an increase of the intensity in comparison to duplex **4**. Duplex **7** has also a similar shape as duplex **4** but in this case a lower pyrene fluorescence.

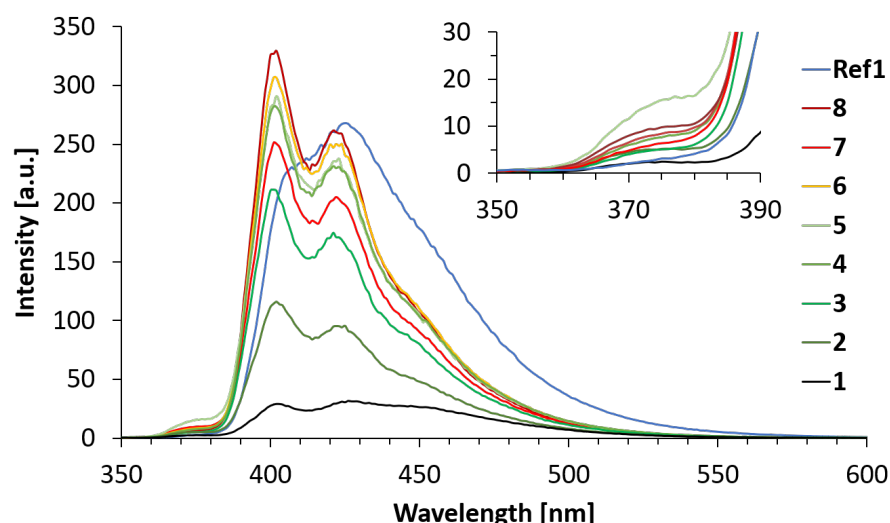


Figure 5.13.: Fluorescence spectra of all duplexes. Conditions: 0.5  $\mu$ M of each strand, 10 mM sodium phosphate buffer (pH 7.0), 400 mM NaCl.  $\lambda_{\text{exc}}$ . 316 nm, 20°C; excitation slit: 2.5 nm, emission slit: 5 nm.

### Quantum Yields

$\phi_F$  were measured for duplexes **6** - **8** using quinine sulfate as a standard (see subchapter 5.5) and are given in Table 5.4. The expectation for the duplexes with the mismatches was a decrease in the quantum yield, but surprisingly, they show a slightly higher or similar quantum yield than duplex **4** with a quantum yield of 64%. Also here, these findings maybe explained with the "flipped out" conformation of the mismatched DNA base pair (see above).

Table 5.4.: Quantum yields ( $\phi_F$ ) of the duplex **6**, **7** and **8**. Conditions: 0.5  $\mu$ M of each strand, 10 mM sodium phosphate buffer (pH 7.0), 400 mM NaCl.

Duplex	Sequence	$\phi_F$ [%] (SD)
6	5' GGC TAA YT $\alpha$ A $\alpha$ T $\alpha$ TA AAT CGC 3'	65.1 ( $\pm$ 0.6)
	3' CCG ATT $\alpha$ T $\alpha$ T $\alpha$ A $\alpha$ AT TTA GCG 5'	
7	5' GGC TAA YT $\alpha$ A $\alpha$ T $\alpha$ TA AAT CGC 3'	54.6 ( $\pm$ 0.6)
	3' CCG ATT $\alpha$ A $\alpha$ T $\alpha$ T $\alpha$ AT TTA GCG 5'	
8	5' GGC TAA YT $\alpha$ A $\alpha$ T $\alpha$ TA AAT CGC 3'	69.6 ( $\pm$ 1.2)
	3' CCG ATT $\alpha$ T $\alpha$ T $\alpha$ T $\alpha$ AT TTA GCG 5'	

### Summary of the data

The fluorescence emission signal was integrated over the range from 350 nm to 600 nm, the data is presented in Figure 5.14. Starting from duplex **1**, the fluorescence emission steadily increases, till duplex **4**. From these results, it can be concluded that each phenanthrene unit contributes approximately 2000 intensity units. As already shown in Figure 5.11 there was no increase of the fluorescence intensity from duplex **4** to duplex **5**. Although, duplex **Ref1** has also nine phenanthrene units (as duplex **5**), there was an increase of 4000 intensity units, 2000 units per additional phenanthrene, in comparison to duplex **4**. Even separated by A-T base pairs, the absorbed energy leads to an increasing pyrene fluorescence by increasing the number of phenanthrenes. However, the number of segmentation is limited, further addition of phenanthrenes, more than four segments (duplex **4**), does not increase the energy transfer to the pyrene anymore. In Figure 5.14, showing duplexes with mismatches, the fluorescence intensities are in the same range as duplex **4** (except duplex **7**). There are several reasons for the decrease of the energy transfer efficiency from duplex **4** to duplex **5**: i.) The simplest explanation is the increase in the distance between the last donor and the pyrene in duplex **5** compared to duplex **4**. The distance for duplex **4** would be 34 Å and for duplex **5** 44 Å, in assumption of a length of 3.4 Å per unit. ii.) The lower duplex stability, with additional phenanthrene segments, maybe another reason. Reduced molecular interactions between the two strands, including reduced stacking interactions between phenanthrenes, leads to the lower duplex stability, therefore, also a less efficient energy transfer to the pyrene.



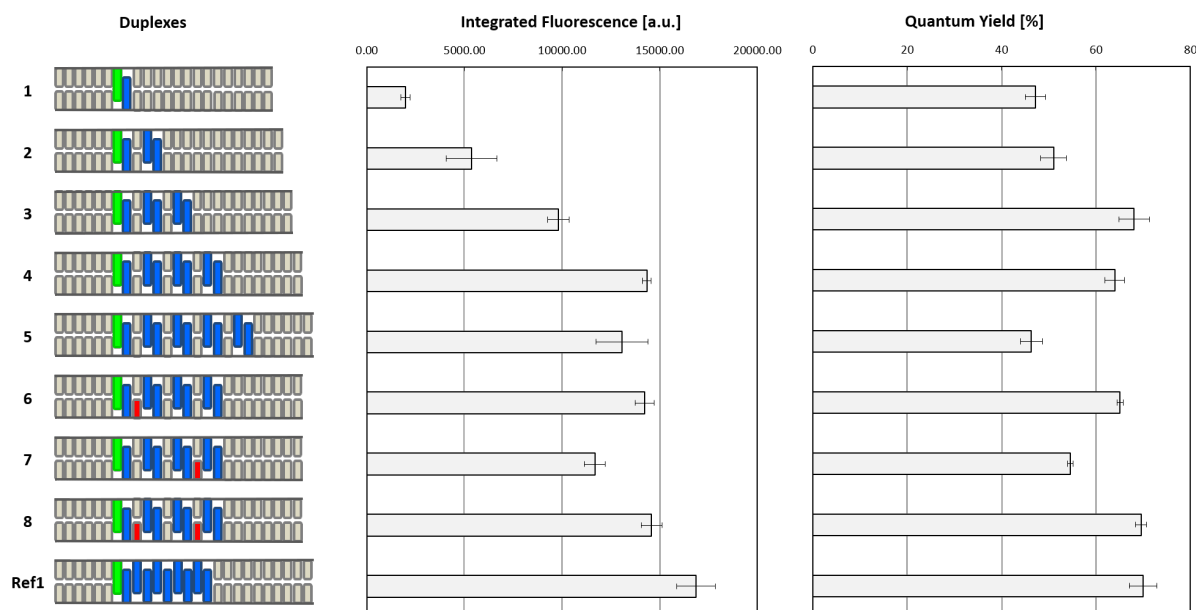


Figure 5.14.: Schematic illustration of the duplexes (blue: phenanthrene, green: pyrene, red: mismatch, grey: nucleobase). Middle & Right: Fluorescence Integral (350-600 nm) and quantum yields (quinine sulfate taken as a standard) of all duplexes in this study. Conditions:  $0.5 \mu\text{M}$  of each strand, 10 mM sodium phosphate buffer (pH 7.0), 400 mM NaCl.  $\lambda_{\text{exc.}}$  316 nm,  $20^\circ\text{C}$ ; excitation slit: 2.5 nm, emission slit: 5 nm.

## 5.4. Conclusion

In conclusion, DNA single strands, which were modified with a different number of phenanthrenes (donor) and one pyrene (acceptor) chromophores, were synthesized. The phenanthrenes were separated by integrating DNA nucleotides in between. The phenanthrenes in the DNA duplex serve as a light harvesting antenna. Although, the phenanthrene stack is interrupted by DNA base pairs, the energy was still efficiently transferred to a pyrene acceptor chromophore. All segmented oligochromophores showed an efficient light-harvesting with quantum yields ranging from 47% to 68%. The segmentation limit of A-T base pairs was reached after three to four chromophore segments (one segment = two chromophores and two base pair, one in each strand), after that, there was a decrease in the LHCs efficiency. Duplexes with mismatches showed almost the same efficiency as the duplex with no mismatches, indicating the strong interaction between the phenanthrenes.

## 5.5. Experimental Section

### Material

All required solvents and chemical reagents for the synthesis were purchased from commercial suppliers (Aldrich, Merck, TCI or Glen Research) and used without further purification.

### Synthesis

The 1,8-dialkynylpyrene phosphoramidite and 3,6-dialkynylphenanthrene phosphoramidite were synthesized according to the literature.<sup>105,188</sup>

### Solid-phase synthesis

The oligochromophores were synthesized in a 1  $\mu$ M scale using the standard cyanoethyl phosphoramidite solid-phase synthesis protocol<sup>29</sup> on a ABI (Applied Biosystems Instruments) 394-DNA/RNA automated synthesizer.

### Reversed Phase HPLC Purification

The HPLC purification was done on a Shimadzu HPLC system using LiChroCART 250-4; LiChrospher 100, RP-18, 5  $\mu$ m column (Merck). The mobile phase were: Solvent A: 0.1 M aqueous ammonium acetate and Solvent B: CH<sub>3</sub>CN.

### Mass Spectrometry

The molecular mass were determined on Thermo Fisher LTQ Orbitrap XL using Nano Electrospray Ionization (NSI).

### Sample Preparation - Duplex

The sample in aqueous medium (0.5  $\mu$ M each strand, 10 mM sodium phosphate buffer pH = 7.0, 400 mM NaCl) was heated up to 80 °C afterwards it was cooled down to 20 °C with a temperature gradient of 0.5 °C/min.

## Spectroscopic Characterisation

UV-vis data were measured on a Cary 100 Bio spectrophotometer. Fluorescence and excitation data were measured on a Cary Eclipse spectrofluorimeter. The settings are as described in the corresponding spectra. For the measurement 1 cm x 1 cm quartz cuvettes were used.

## Quantum Yield Determination

Quantum yields ( $\phi_F$ ) were calculated relative to quinine sulfate in 0.5 M H<sub>2</sub>SO<sub>4</sub> as a standard according to described procedure in literature.<sup>189</sup>  $\phi_F$  was determined by integration of the fluorescence emission area from 350 - 600 nm. The quinine sulfate and duplex absorption at the excitation wavelength at 316 nm were measured. Calculation were done with the following formula:

$$\phi_F = \frac{I_C \cdot A_R}{A_C \cdot I_R} \cdot \phi_R$$

$I_C$ : fluorescence emission area (350 – 600 nm) of the samples

$I_R$ : fluorescence emission area (350 – 600 nm) of quinine sulfate

$A_C$ : Absorption of the samples at 316 nm

$A_R$ : Absorption of the quinine sulfate at 316 nm

$\phi_R$ : quantum yield of quinine sulfate = 0.546

Detailed description can be found in Appendix D.

---

## Bibliography

- (1) A. Harada, *Supramolecular Polymer Chemistry*, 2012.
- (2) T. F. De Greef, M. M. Smulders, M. Wolfs, A. P. Schenning, R. P. Sijbesma and E. Meijer, *Chem. Rev.*, 2009, **109**, 5687–5754.
- (3) F. J. Hoeben, P. Jonkheijm, E. Meijer and A. P. Schenning, *Chem. Rev.*, 2005, **105**, 1491–1546.
- (4) C. Wang, Z. Wang and X. Zhang, *Acc. Chem. Res.*, 2012, **45**, 608–618.
- (5) L. Brunsveld, B. Folmer, E. W. Meijer and R. Sijbesma, *Chem. Rev.*, 2001, **101**, 4071–4098.
- (6) T. E. Kaiser, H. Wang, V. Stepanenko and F. Würthner, *Angew. Chem.*, 2007, **119**, 5637–5640.
- (7) M. M. Smulders, M. M. Nieuwenhuizen, T. F. de Greef, P. van der Schoot, A. P. Schenning and E. Meijer, *Chem. - Eur. J.*, 2010, **16**, 362–367.
- (8) L. Brunsveld, J. Vekemans, J. Hirschberg, R. Sijbesma and E. Meijer, *Proc. Natl. Acad. Sci. U. S. A.*, 2002, **99**, 4977–4982.
- (9) A. Arnaud, J. Belleney, F. Boué, L. Bouteiller, G. Carrot and V. Wintgens, *Angew. Chem., Int. Ed.*, 2004, **43**, 1718–1721.
- (10) D. Zhao and J. S. Moore, *Org. Biomol. Chem.*, 2003, **1**, 3471–3491.
- (11) J.-M. Lehn, *Angew. Chem., Int. Ed.*, 2015, **54**, 3276–3289.
- (12) X. Dai, L.-B. Huang, Y. Du, J. Han and J. Kong, *Composites Communications*, 2021, **24**, 100654.
- (13) B. Zhang, J. He, M. Shi, Y. Liang and B. Guo, *Chemical Engineering Journal*, 2020, **400**, 125994.

- (14) L. Li, J. M. Scheiger and P. A. Levkin, *Adv. Mater.*, 2019, **31**, 1807333.
- (15) J. D. Watson and F. H. Crick, Cold Spring Harbor symposia on quantitative biology, 1953, vol. 18, pp. 123–131.
- (16) J. C. Bowman and L. D. Williams, *Nucleic Acids*, Springer Berlin Heidelberg, 2011, pp. 1141–1147.
- (17) J. D. Watson and F. H. Crick, *Nature*, 1953, **171**, 737–738.
- (18) R. Wing, H. Drew, T. Takano, C. Broka, S. Tanaka, K. Itakura and R. E. Dickerson, *Nature*, 1980, **287**, 755–758.
- (19) M. Mandelkern, J. G. Elias, D. Eden and D. M. Crothers, *J. Mol. Biol.*, 1981, **152**, 153–161.
- (20) H. J. Cleaves, in *Watson–Crick Pairing*, Springer Berlin Heidelberg, 2011, pp. 1775–1776.
- (21) P. Yakovchuk, E. Protozanova and M. D. Frank-Kamenetskii, *Nucleic Acids Res.*, 2006, **34**, 564–574.
- (22) A. Ghosh and M. Bansal, *Acta Crystallogr., Sect. D: Biol. Crystallogr.*, 2003, **59**, 620–626.
- (23) G. Bonner and A. M. Klibanov, *Biotechnol. Bioeng.*, 2000, **68**, 339–344.
- (24) R. R. Sinden, C. E. Pearson, V. N. Potaman and D. W. Ussery, in *Adv. Genome Biol.* Elsevier, 1998, vol. 5, pp. 1–141.
- (25) A. Panjkovich and F. Melo, *Bioinformatics*, 2005, **21**, 711–722.
- (26) A. Panjkovich, T. Norambuena and F. Melo, *Nucleic Acids Res.*, 2005, **33**, W570–W572.
- (27) J. SantaLucia, H. T. Allawi and P. A. Seneviratne, *Biochemistry*, 1996, **35**, 3555–3562.
- (28) R. Owczarzy, B. G. Moreira, Y. You, M. A. Behlke and J. A. Walder, *Biochemistry*, 2008, **47**, 5336–5353.
- (29) *Solid-phase oligonucleotide synthesis*, <https://www.atdbio.com/content/17/Solid-phase-oligonucleotide-synthesis>, Accessed: 2021-03-14.
- (30) N. C. Seeman, *DNA Cell Biol.*, 1991, **10**, 475–486.
- (31) E. S. Andersen, M. Dong, M. M. Nielsen, K. Jahn, R. Subramani, W. Mamdouh, M. M. Golas, B. Sander, H. Stark, C. L. Oliveira et al., *Nature*, 2009, **459**, 73–76.
- (32) D. Han, S. Pal, J. Nangreave, Z. Deng, Y. Liu and H. Yan, *Science*, 2011, **332**, 342–346.
- (33) M. Li, H. Schnablegger and S. Mann, *Nature*, 1999, **402**, 393–395.

- (34) N. C. Seeman, *Annu. Rev. Biochem.*, 2010, **79**, 65–87.
- (35) E. Stulz, *Acc. Chem. Res.*, 2017, **50**, 823–831.
- (36) E. Stulz and G. H. Clever, *DNA Supramol. Chem. Nanotechnol.* John Wiley & Sons, 2015.
- (37) N. Appukkutti and C. J. Serpell, *Polym. Chem.*, 2018, **9**, 2210–2226.
- (38) M. Vybornyi, Y. Vyborna and R. Häner, *Chem. Soc. Rev.*, 2019, **48**, 4347–4360.
- (39) N. C. Seeman, *Nature*, 2003, **421**, 427–431.
- (40) K. V. Gothelf and T. H. LaBean, *Org. Biomol. Chem.*, 2005, **3**, 4023–4037.
- (41) M. Kirnos, I. Y. Khudyakov, N. Alexandrushkina and B. Vanyushin, *Nature*, 1977, **270**, 369–370.
- (42) S. C. Johnson, C. B. Sherrill, D. J. Marshall, M. J. Moser and J. R. Prudent, *Nucleic Acids Res.*, 2004, **32**, 1937–1941.
- (43) Y. Taniguchi and E. T. Kool, *J. Am. Chem. Soc.*, 2007, **129**, 8836–8844.
- (44) N. Zimmermann, E. Meggers and P. G. Schultz, *Bioorg. Chem.*, 2004, **32**, 13–25.
- (45) H. Liu, J. Gao, S. R. Lynch, Y. D. Saito, L. Maynard and E. T. Kool, *Science*, 2003, **302**, 868–871.
- (46) A. Ono and H. Togashi, *Angew. Chem.*, 2004, **116**, 4400–4402.
- (47) I. Hirao, T. Ohtsuki, T. Fujiwara, T. Mitsui, T. Yokogawa, T. Okuni, H. Nakayama, K. Takio, T. Yabuki, T. Kigawa et al., *Nat. Biotechnol.*, 2002, **20**, 177–182.
- (48) I. Hirao, M. Kimoto, T. Mitsui, T. Fujiwara, R. Kawai, A. Sato, Y. Harada and S. Yokoyama, *Nat. Methods*, 2006, **3**, 729–735.
- (49) V. L. Malinovskii, D. Wenger and R. Häner, *Chem. Soc. Rev.*, 2010, **39**, 410–422.
- (50) Y. Zheng, H. Long, G. C. Schatz and F. D. Lewis, *Chem. Commun.*, 2005, 4795–4797.
- (51) H. Kashida, M. Tanaka, S. Baba, T. Sakamoto, G. Kawai, H. Asanuma and M. Komiyama, *Chem. - Eur. J.*, 2006, **12**, 777–784.
- (52) R. L. Letsinger and T. Wu, *J. Am. Chem. Soc.*, 1995, **117**, 7323–7328.
- (53) U. B. Christensen and E. B. Pedersen, *Nucleic Acids Res.*, 2002, **30**, 4918–4925.
- (54) K. Berlin, R. K. Jain, M. D. Simon and C. Richert, *J. Org. Chem.*, 1998, **63**, 1527–1535.

- (55) D. Ward, E. Reich and L. Stryer, *J. Biol. Chem.*, 1969, **244**, 1228–1237.
- (56) M. E. Hawkins, *Cell Biochem. Biophys.*, 2001, **34**, 257–281.
- (57) N. J. Greco and Y. Tor, *J. Am. Chem. Soc.*, 2005, **127**, 10784–10785.
- (58) M. J. Rist and J. P. Marino, *Curr. Org. Chem.*, 2002, **6**, 775–793.
- (59) J. N. Wilson and E. T. Kool, *Org. Biomol. Chem.*, 2006, **4**, 4265–4274.
- (60) M. Wilhelmsson, *Q. Rev. Biophys.*, 2010, **43**, 159–183.
- (61) L. M. Wilhelmsson, A. Holmén, P. Lincoln, P. E. Nielsen and B. Nordén, *J. Am. Chem. Soc.*, 2001, **123**, 2434–2435.
- (62) F. Garo and R. Häner, *Angew. Chem., Int. Ed.*, 2012, **51**, 916–919.
- (63) T. Förster, *Ann. Phys.*, 1948, **437**, 55–75.
- (64) Z. G. Fetisova, A. M. Freiberg and K. E. Timpmann, *Nature*, 1988, **334**, 633–634.
- (65) C. D. Bösch, Dissertation, University of Bern, 2017.
- (66) E. Rabinowitch, *J. Phys. Chem.*, 1957, **61**, 870–878.
- (67) G. Tollin, *Radiat. Res., Suppl.*, 1960, **2**, 387–406.
- (68) D. C. Youvan and B. L. Marrs, *Sci. Am.*, 1987, **256**, 42–49.
- (69) S. Yagai, Y. Kitamoto, S. Datta and B. Adhikari, *Acc. Chem. Res.*, 2019, **52**, 1325–1335.
- (70) A. Wilson, G. Gasparini and S. Matile, *Chem. Soc. Rev.*, 2014, **43**, 1948–1962.
- (71) S. Sengupta and F. Würthner, *Acc. Chem. Res.*, 2013, **46**, 2498–2512.
- (72) A. Winter and U. S. Schubert, *Chem. Soc. Rev.*, 2016, **45**, 5311–5357.
- (73) P. A. Korevaar, T. F. de Greef and E. Meijer, *Chem. Mater.*, 2014, **26**, 576–586.
- (74) S. I. Stupp and L. C. Palmer, *Chem. Mater.*, 2014, **26**, 507–518.
- (75) T. Fenske, H.-G. Korth, A. Mohr and C. Schmuck, *Chem. - Eur. J.*, 2012, **18**, 738–755.
- (76) A. K. Geim and K. S. Novoselov, in *Nat. Sci. Technol.* World Scientific, 2009, pp. 11–19.
- (77) C. Li, M. Liu, N. G. Pschirer, M. Baumgarten and K. Mullen, *Chem. Rev.*, 2010, **110**, 6817–6855.
- (78) T. Aida, E. Meijer and S. Stupp, *Science*, 2012, **335**, 813–817.

- (79) L. Herkert, P. Selter, C. G. Daniliuc, N. Bäumer, J. P. Palakkal, G. Fernández and M. R. Hansen, *Chem. (Weinheim an der Bergstrasse, Germany)*, 2021, **27**, 4617.
- (80) Z. Chen, A. Lohr, C. R. Saha-Möller and F. Würthner, *Chem. Soc. Rev.*, 2009, **38**, 564–584.
- (81) L. Zang, Y. Che and J. S. Moore, *Acc. Chem. Res.*, 2008, **41**, 1596–1608.
- (82) Y. N. Teo and E. T. Kool, *Chem. Rev.*, 2012, **112**, 4221–4245.
- (83) Y. Vyborna, M. Vybornyi, A. V. Rudnev and R. Häner, *Angew. Chem., Int. Ed.*, 2015, **54**, 7934–7938.
- (84) M. Probst, S. M. Langenegger and R. Häner, *Chem. Commun.*, 2014, **50**, 159–161.
- (85) B. L. Cannon, L. K. Patten, D. L. Kellis, P. H. Davis, J. Lee, E. Graugnard, B. Yurke and W. B. Knowlton, *J. Phys. Chem. A*, 2018, **122**, 2086–2095.
- (86) R. Merindol, S. Loescher, A. Samanta and A. Walther, *Nat. Nanotechnol.*, 2018, **13**, 730–738.
- (87) V. Balzani, A. Credi and M. Venturi, *ChemSusChem*, 2008, **1**, 26–58.
- (88) N. L. Rosi and C. A. Mirkin, *Chem. Rev.*, 2005, **105**, 1547–1562.
- (89) J. M. Kinsella and A. Ivanisevic, *Langmuir*, 2007, **23**, 3886–3890.
- (90) J. K. Hannestad, P. Sandin and B. Albinsson, *J. Am. Chem. Soc.*, 2008, **130**, 15889–15895.
- (91) M. Endo and H. Sugiyama, *ChemBioChem*, 2009, **10**, 2420–2443.
- (92) Z. Hua, R. Keogh, Z. Li, T. R. Wilks, G. Chen and R. K. O'Reilly, *Macromol.*, 2017, **50**, 3662–3670.
- (93) N. C. Seeman, *Nano Lett.*, 2010, **10**, 1971–1978.
- (94) F. A. Aldaye, A. L. Palmer and H. F. Sleiman, *Science*, 2008, **321**, 1795–1799.
- (95) N. C. Seeman and N. R. Kallenbach, *Biophys. J.*, 1983, **44**, 201–209.
- (96) N. C. Seeman, *J. Theor. Biol.*, 1982, **99**, 237–247.
- (97) C. Lin, Y. Liu and H. Yan, *Biochemistry*, 2009, **48**, 1663–1674.
- (98) M. Kownacki, S. M. Langenegger, S.-X. Liu and R. Häner, *Angew. Chem.*, 2019, **131**, 761–765.



- (99) M. Vybornyi, A. V. Rudnev, S. M. Langenegger, T. Wandlowski, G. Calzaferri and R. Häner, *Angew. Chem., Int. Ed.*, 2013, **52**, 11488–11493.
- (100) M. Vybornyi, A. Rudnev and R. Häner, *Chem. Mater.*, 2015, **27**, 1426–1431.
- (101) C. D. Bösch, S. M. Langenegger and R. Häner, *Angew. Chem.*, 2016, **128**, 10115–10118.
- (102) N. Bürki, Master thesis, University of Bern, 2016.
- (103) C. D. Bösch, J. Jevric, N. Bürki, M. Probst, S. M. Langenegger and R. Häner, *Bioconjugate Chem.*, 2018, **29**, 1505–1509.
- (104) Z. De Liu, H. Y. Zhu, H. X. Zhao and C. Z. Huang, *Talanta*, 2013, **106**, 255–260.
- (105) H. Bittermann, D. Siegemund, V. L. Malinovskii and R. Häner, *J. Am. Chem. Soc.*, 2008, **130**, 15285–15287.
- (106) M.A., *Colloidal Gold: Principles, Methods, and Applications*, 1989, vol. 1, pp. 13–22.
- (107) L. S. Shlyakhtenko, A. A. Gall and Y. L. Lyubchenko, in *Mica functionalization for imaging of DNA and protein-DNA complexes with atomic force microscopy*, Springer, 2012, pp. 295–312.
- (108) J. Kim, A. S. Campbell, B. E.-F. de Ávila and J. Wang, *Nat. Biotechnol.*, 2019, **37**, 389–406.
- (109) C. Feng, H.-m. Ding, C.-l. Ren and Y.-q. Ma, *Sci. Rep.*, 2015, **5**.
- (110) C.-H. Lu, B. Willner and I. Willner, *ACS Nano*, 2013, **7**, 8320–8332.
- (111) X. Zhang, F. Wang, J.-L. Sheng and M.-X. Sun, *Curr. Med. Chem.*, 2019, **26**, 7147–7165.
- (112) A. Patwa, A. Gissot, I. Bestel and P. Barthélémy, *Chem. Soc. Rev.*, 2011, **40**, 5844–5854.
- (113) N. Dave and J. Liu, *ACS Nano*, 2011, **5**, 1304–1312.
- (114) M. Chung, R. D. Lowe, Y. H. M. Chan, P. V. Ganesan and S. G. Boxer, *J. Struct. Biol.*, 2009, **168**, 190–199.
- (115) E. Darley, J. K. D. Singh, N. A. Surace, S. F. Wickham and M. A. Baker, *Genes*, 2019, **10**, 1001.
- (116) S. Rothenbühler, I. Iacovache, S. M. Langenegger, B. Zuber and R. Häner, *Nanoscale*, 2020, **12**, 21118–21123.
- (117) R. A. Casero Jr and P. M. Woster, *J. Med. Chem.*, 2009, **52**, 4551–4573.
- (118) S. Datta, M. L. Saha and P. J. Stang, *Acc. Chem. Res.*, 2018, **51**, 2047–2063.

- (119) C. Lu, M. Zhang, D. Tang, X. Yan, Z. Zhang, Z. Zhou, B. Song, H. Wang, X. Li, S. Yin et al., *J. Am. Chem. Soc.*, 2018, **140**, 7674–7680.
- (120) G. Moad, *Polym. Chem.*, 2017, **8**, 177–219.
- (121) Y. Zheng, S. Li, Z. Weng and C. Gao, *Chem. Soc. Rev.*, 2015, **44**, 4091–4130.
- (122) L.-J. Chen and H.-B. Yang, *Acc. Chem. Res.*, 2018, **51**, 2699–2710.
- (123) W. Wang, Y. Zhang and W. Liu, *Prog. Polym. Sci.*, 2017, **71**, 1–25.
- (124) K. Thorkelsson, A. J. Mastroianni, P. Ercius and T. Xu, *Nano Lett.*, 2012, **12**, 498–504.
- (125) Y. Chen, D. Zhao and Y. Liu, *Chem. Commun.*, 2015, **51**, 12266–12269.
- (126) Y. Arisaka and N. Yui, *Macromol. Rapid Commun.*, 2019, **40**, 1900323.
- (127) X.-J. Chen, B. L. Sanchez-Gaytan, S. E. Hayik, M. Fryd, B. B. Wayland and S.-J. Park, *Small*, 2010, **6**, 2256–2260.
- (128) T. G. Edwardson, K. M. Carneiro, C. K. McLaughlin, C. J. Serpell and H. F. Sleiman, *Nat. Chem.*, 2013, **5**, 868.
- (129) J. List, M. Weber and F. C. Simmel, *Angew. Chem., Int. Ed.*, 2014, **53**, 4236–4239.
- (130) A. M. Breul, M. D. Hager and U. S. Schubert, *Chem. Soc. Rev.*, 2013, **42**, 5366–5407.
- (131) M. Irie, T. Fukaminato, K. Matsuda and S. Kobatake, *Chem. Rev.*, 2014, **114**, 12174–12277.
- (132) P. A. Beales, N. Geerts, K. K. Inampudi, H. Shigematsu, C. J. Wilson and T. K. Vanderlick, *J. Am. Chem. Soc.*, 2013, **135**, 3335–3338.
- (133) M.-M. Russew and S. Hecht, *Adv. Mater.*, 2010, **22**, 3348–3360.
- (134) K. C. Hannah and B. A. Armitage, *Acc. Chem. Res.*, 2004, **37**, 845–853.
- (135) Y.-W. Kwon, D. H. Choi and J.-I. Jin, *Polymer journal*, 2012, **44**, 1191–1208.
- (136) X. Lan, T. Liu, Z. Wang, A. O. Govorov, H. Yan and Y. Liu, *J. Am. Chem. Soc.*, 2018, **140**, 11763–11770.
- (137) Y. Vyborna, M. Vybornyi and R. Häner, *J. Am. Chem. Soc.*, 2015, **137**, 14051–14054.
- (138) Y. Vyborna, S. Altunbas, M. Vybornyi and R. Häner, *Chem. Commun.*, 2017, **53**, 12128–12131.

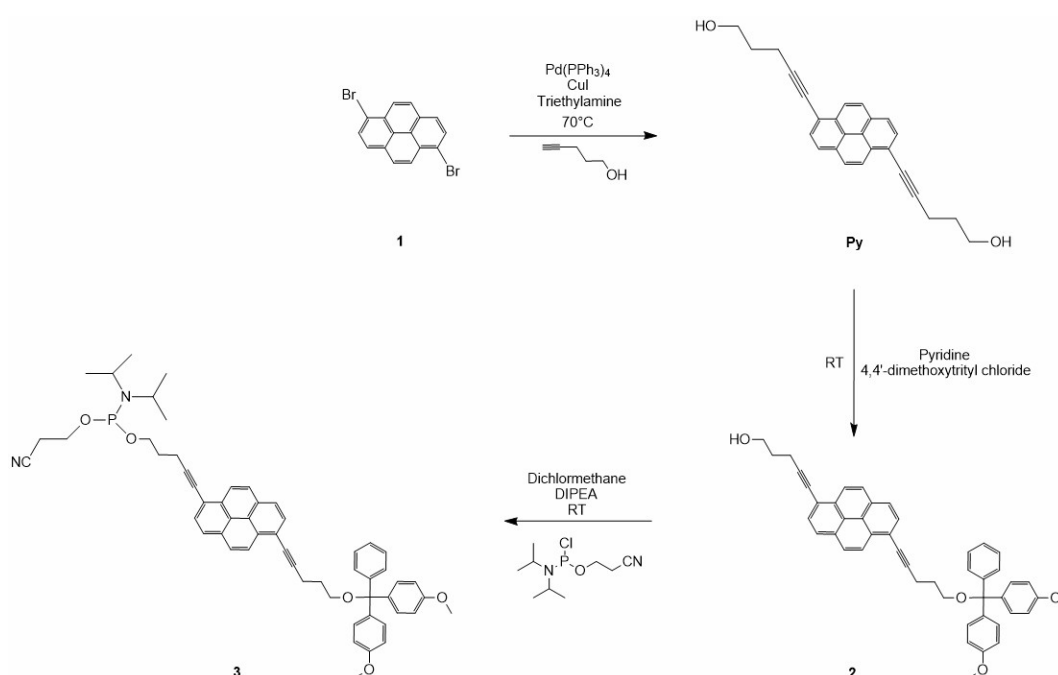
- (139) M. Gerth, J. A. Berrocal, D. Bochicchio, G. M. Pavan and I. K. Voets, *Chem. (Weinheim an der Bergstrasse, Germany)*, 2021, **27**, 1829.
- (140) F. Jean-Charles Natt, J. Hunziker, R. Häner and S. M. Langenegger, *Novel Compounds*, US2011/0092693 A1, US Pat., 2011.
- (141) A. Stutz, Dissertation, Eidgenössischen Technischen Hochschule Zürich, 2003.
- (142) G. Calzaferri, R. Méallet-Renault, D. Brühwiler, R. Pansu, I. Dolamic, T. Dienel, P. Adler, H. Li and A. Kunzmann, *ChemPhysChem*, 2011, **12**, 580–594.
- (143) S. Ghosh, X.-Q. Li, V. Stepanenko and F. Würthner, *Chem. - Eur. J.*, 2008, **14**, 11343–11357.
- (144) F. C. De Schryver, T. Vosch, M. Cotlet, M. Van der Auweraer, K. Müllen and J. Hofkens, *Acc. Chem. Res.*, 2005, **38**, 514–522.
- (145) G. J. Gabriel and B. L. Iverson, *J. Am. Chem. Soc.*, 2002, **124**, 15174–15175.
- (146) D. Beljonne, C. Curutchet, G. D. Scholes and R. J. Silbey, *J. Phys. Chem. B*, 2009, **113**, 6583–6599.
- (147) G. D. Scholes and G. Rumbles, *Materials For Sustainable Energy: A Collection of Peer-Reviewed Research and Review Articles from Nature Publishing Group*, 2011, 12–25.
- (148) H. Asanuma, T. Fujii, T. Kato and H. Kashida, *J. Photochem. Photobiol., C*, 2012, **13**, 124–135.
- (149) J. K. Klosterman, Y. Yamauchi and M. Fujita, *Chem. Soc. Rev.*, 2009, **38**, 1714–1725.
- (150) G. Scheibe, A. Schöntag and F. Katheder, *Naturwissenschaften*, 1939, **27**, 499–501.
- (151) A. Davydov, *Theory of molecular excitons*, Springer, 2013.
- (152) M. Kasha, *Radiation research*, 1963, **20**, 55–70.
- (153) F. Fassioli, R. Dinshaw, P. C. Arpin and G. D. Scholes, *J. R. Soc., Interface*, 2014, **11**, 20130901.
- (154) A. N. Melkozernov, J. Barber and R. E. Blankenship, *Biochemistry*, 2006, **45**, 331–345.
- (155) I. McConnell, G. Li and G. W. Brudvig, *Chemistry & biology*, 2010, **17**, 434–447.
- (156) D. Gust, T. A. Moore and A. L. Moore, *Acc. Chem. Res.*, 2001, **34**, 40–48.

- (157) G. D. Scholes, G. R. Fleming, A. Olaya-Castro and R. Van Grondelle, *Nat. Chem.*, 2011, **3**, 763–774.
- (158) B. Loll, J. Kern, W. Saenger, A. Zouni and J. Biesiadka, *Nature*, 2005, **438**, 1040–1044.
- (159) S. Ganapathy, G. T. Oostergetel, P. K. Wawrzyniak, M. Reus, A. G. M. Chew, F. Buda, E. J. Boekema, D. A. Bryant, A. R. Holzwarth and H. J. De Groot, *Proc. Natl. Acad. Sci. U. S. A.*, 2009, **106**, 8525–8530.
- (160) J. Su and L. Vayssieres, *ACS Energy Letters*, 2016, **1**, 121–135.
- (161) J. Barber, *Chem. Soc. Rev.*, 2009, **38**, 185–196.
- (162) D. G. Nocera, *Acc. Chem. Res.*, 2012, **45**, 767–776.
- (163) D. Gust, T. A. Moore and A. L. Moore, *Acc. Chem. Res.*, 2009, **42**, 1890–1898.
- (164) V. V. Filichev and E. B. Pedersen, *Wiley Encycl. Chem. Biol.*, 2008, 1–32.
- (165) E. Stulz, *Chem. - Eur. J.*, 2012, **18**, 4456–4469.
- (166) M. E. Østergaard and P. J. Hrdlicka, *Chem. Soc. Rev.*, 2011, **40**, 5771–5788.
- (167) H. Kashida, H. Asanuma and M. Komiyama, *Angew. Chem., Int. Ed.*, 2004, **43**, 6522–6525.
- (168) P. K. Dutta, R. Varghese, J. Nangreave, S. Lin, H. Yan and Y. Liu, *J. Am. Chem. Soc.*, 2011, **133**, 11985–11993.
- (169) N. S. Oltra, W. R. Browne and G. Roelfes, *Chem. Eur. J.*, 2013, **19**, 2457–2461.
- (170) T. S. Kumar, A. S. Madsen, M. E. Østergaard, J. Wengel and P. J. Hrdlicka, *J. Org. Chem.*, 2008, **73**, 7060–7066.
- (171) F. D. Lewis, L. Zhang, X. Liu, X. Zuo, D. M. Tiede, H. Long and G. C. Schatz, *J. Am. Chem. Soc.*, 2005, **127**, 14445–14453.
- (172) T. Takada, Y. Kawano, A. Ashida, M. Nakamura, K. Kawai, T. Majima and K. Yamana, *Tetrahedron Lett.*, 2013, **54**, 4796–4799.
- (173) I. K. Astakhova and J. Wengel, *Acc. Chem. Res.*, 2014, **47**, 1768–1777.
- (174) O. O. Adeyemi, V. L. Malinovskii, S. M. Biner, G. Calzaferri and R. Häner, *Chem. Commun.*, 2012, **48**, 9589–9591.
- (175) B. Albinsson, J. K. Hannestad and K. Börjesson, *Coord. Chem. Rev.*, 2012, **256**, 2399–2413.

- (176) J. G. Woller, J. K. Hannestad and B. Albinsson, *J. Am. Chem. Soc.*, 2013, **135**, 2759–2768.
- (177) C. M. Spillmann, M. G. Ancona, S. Buckhout-White, W. R. Algar, M. H. Stewart, K. Susumu, A. L. Huston, E. R. Goldman and I. L. Medintz, *ACS Nano*, 2013, **7**, 7101–7118.
- (178) C. V. Kumar and M. R. Duff Jr, *J. Am. Chem. Soc.*, 2009, **131**, 16024–16026.
- (179) K. Pan, E. Boulais, L. Yang and M. Bathe, *Nucleic Acids Res.*, 2014, **42**, 2159–2170.
- (180) C. M. Spillmann, S. Buckhout-White, E. Oh, E. R. Goldman, M. G. Ancona and I. L. Medintz, *Chem. Commun.*, 2014, **50**, 7246–7249.
- (181) R. Iwaura, H. Yui, Y. Someya and M. Ohnishi-Kameyama, *J. Photochem. Photobiol., B*, 2014, **130**, 199–204.
- (182) A. L. Stevens, P. G. Janssen, A. Ruiz-Carretero, M. Surin, A. P. Schenning and L. M. Herz, *J. Phys. Chem. C*, 2011, **115**, 10550–10560.
- (183) C. B. Winiger, S. M. Langenegger, O. Khorev and R. Häner, *Beilstein J. Org. Chem.*, 2014, **10**, 1589–1595.
- (184) C. D. Bösch, E. Abay, S. M. Langenegger, M. Nazari, A. Cannizzo, T. Feurer and R. Häner, *Helv. Chim. Acta*, 2019, **102**, e1900148.
- (185) N. Bürki, E. Grossenbacher, A. Cannizzo, T. Feurer, S. M. Langenegger and R. Häner, *Org. Biomol. Chem.*, 2020, **18**, 6818–6822.
- (186) S. M. Langenegger and R. Häner, *Bioorg. Med. Chem. Lett.*, 2006, **16**, 5062–5065.
- (187) T. A. Zeidan, M. Hariharan, K. Siegmund and F. D. Lewis, *Photochem. Photobiol. Sci.*, 2010, **9**, 916–922.
- (188) C. B. Winiger, S. M. Langenegger, G. Calzaferri and R. Häner, *Angew. Chem.*, 2015, **127**, 3714–3718.
- (189) S. Fery-Forgues and D. Lavabre, *J. Chem. Educ.*, 1999, **76**, 1260.
- (190) C. B. Winiger, S. Li, G. R. Kumar, S. M. Langenegger and R. Häner, *Angew. Chem., Int. Ed.*, 2014, **53**, 13609–13613.

## A. Appendix Chapter 2

### Synthesis of the 1,6-dialkynylpyrene phosphoramidite



Scheme A.1: Full reaction scheme of the 5-(6-(5-(Bis(4-methoxyphenyl)(phenyl)methoxy)pent-1-ynyl)pyren-1-yl)pent-4-ynyl 2-cyanoethyl diisopropylphosphoramidite synthesis.

#### 5,5'-(Pyrene-1,6-diyl)dipent-4-yn-1-ol (Py):

1,6- dibromopyrene (**1**) (1.5 g, 4.17 mmol), bis(triphenylphosphine)palladium(II) chloride (68.1 mg, 0.097 mmol) and copper(I) iodide (10.3 mg, 0.054 mmol) were dissolved in dry THF (34.1 mL) under argon and heated to 80 °C under reflux. After addition of triethylamine (20.5 mL) and 4-pentyn-1-ol (1.55 mL, 16.7 mmol) to the mixture it was stirred at this temperature overnight. After cooling to room temperature, the solvent was filtered through celite and removed under reduced pressure. Then it was dissolved in ethyl acetate (100ml), washed with 10% citric acid

and saturated carbonated. The organic phase was dried with sodium sulfated and was filtered. A column chromatography (CH<sub>2</sub>Cl<sub>2</sub>/PhMe/MeOH 87:10:3) was made and the collected fractions were evaporated, it gave a yellow solid (610 mg, 39.7%).

**Analytical data for Py:**

<sup>1</sup>H-NMR (300 MHz, DMSO) δ 8.50 (d, J = 9.2 Hz, 2H), 8.29 (d, J = 8.5 Hz, 4H), 8.13 (d, J = 8.0 Hz, 2H), 4.64 (t, J = 5.2 Hz, 1H), 3.66 (q, J = 6.2, 6.1 Hz, 2H), 2.72 (t, J = 7.1 Hz, 2H), 1.86 (p, J = 6.8 Hz, 2H).

**5-(6-(5-(Bis(4-methoxyphenyl)(phenyl)methoxy)pent-1-ynyl)pyren-1-yl)pent-4-yn-1-ol (2):**

Solid 4,4'-dimethoxytrityl chloride (560.9 mg, 1.66 mmol) was added in portion to a solution of **Py** (610 mg, 1.66 mmol) in pyridine (13 mL). The mixture was stirred overnight at room temperature. Dichloromethane (100 ml) was added to the mixture, washed with 10% citric acid and sodium hydrogen carbonate. The organic phase was dried with potassium carbonate and was filtered. A column chromatography (CH<sub>2</sub>Cl<sub>2</sub>/MeOH/NEt<sub>3</sub> 97/2/1) was made. The fractions containing **(2)** were collected and evaporated. Dichloromethane (filtered through ALOX) was added and the solution was evaporated, but not fully dry. Then it was put on the high vacuum. This gave a yellow foam (540mg, 48.6%).

**Analytical data for (2):**

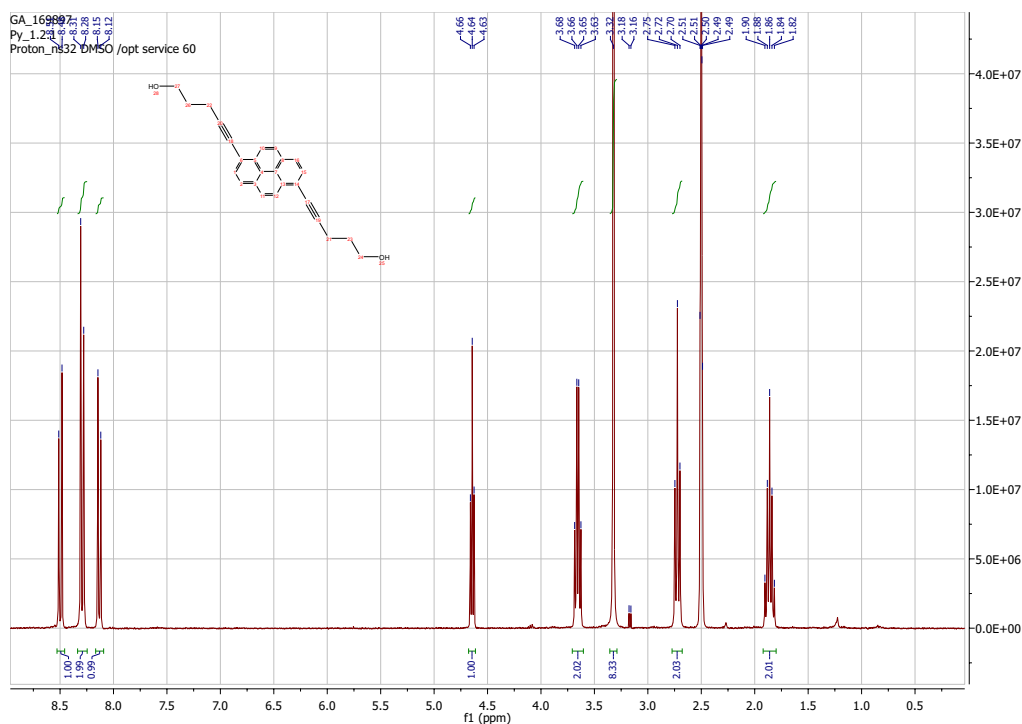
R<sub>f</sub> = 0.75 (CH<sub>2</sub>Cl<sub>2</sub>/MeOH/NEt<sub>3</sub> 97/2/1); <sup>1</sup>H NMR (300 MHz, DMSO) δ 8.50 (d, J = 9.1 Hz, 1H), 8.34 (d, J = 9.1 Hz, 1H), 8.28 (m, 3H), 8.16 (dd, J = 14.7, 8.6 Hz, 2H), 8.01 (d, J = 8.0 Hz, 1H), 7.43 (d, J = 7.3 Hz, 2H), 7.29 (m, 6H), 7.21 (m, 2H), 6.83 (d, J = 8.9 Hz, 4H), 5.33 (s, 7H) 4.67 (t, J = 5.2 Hz, 1H), 3.73 (s, 2H), 3.66 (m, 2H), 3.61 (s, 6H), 3.26 (t, J = 6.1 Hz, 2H), 2.81 (t, J = 6.1 Hz, 2H), 2.72 (t, J = 7.1 Hz, 2H), 2.43 (q, J = 7.0 Hz, 3H), 1.98 (m, 2H), 1.86 (p, J = 6.8 Hz, 2H), 1.23 (t, J = 7.3 Hz, 2H).

**5-(6-(5-(Bis(4-methoxyphenyl)(phenyl)methoxy)pent-1-ynyl)pyren-1-yl)pent-4-ynyl 2-cyanoethyl diisopropylphosphoramidite (3):**

(2) (500 mg, 0.75 mmol) was dissolved in CH<sub>2</sub>Cl<sub>2</sub> (15 mL). After addition of DIPEA (380 μL, 2.24 mmol), 2-cyanoethyl-N,N-diisopropylchlorophosphoramidite (229.3 mg, 0.97 mmol) was added. The mixture was stirred for 5 h at room temperature. The solution was evaporated and purified by a flash chromatography (hexane/ EtOAc/NEt<sub>3</sub> 50/49/1). The fractions were collected and it gave 93.1 mg (14.3%) of yellow solid (3).

**Analytical data for (3):**

R<sub>f</sub>= 0.72 (hexane/ EtOAc/NEt<sub>3</sub> 50/49/1); <sup>1</sup>H NMR (300 MHz, DMSO) δ 8.51 (d, J = 9.1 Hz, 1H), 8.34 (d, J = 9.1 Hz, 1H), 8.27 (m, 3H), 8.15 (dd, J = 15.0, 8.6 Hz, 2H), 8.01 (d, J = 8.0 Hz, 1H), 7.44 (d, J = 7.4 Hz, 2H), 7.29 (m, 8H), 7.07 (d, J = 8.9 Hz, 1H), 6.83 (m, 6H), 3.73 (d, J=1.6 Hz, 6H), 3.61 (s, 8H), 3.26 (t, J = 6.2 Hz, 3H), 2.78 (m, 8H), 1.99 (m, 4H), 1.35 (d, J = 11.2 Hz, 3H). <sup>31</sup>P NMR (121 MHz, DMSO) δ 146.75 (s).

Figure A.1.: <sup>1</sup>H-NMR of (Py).



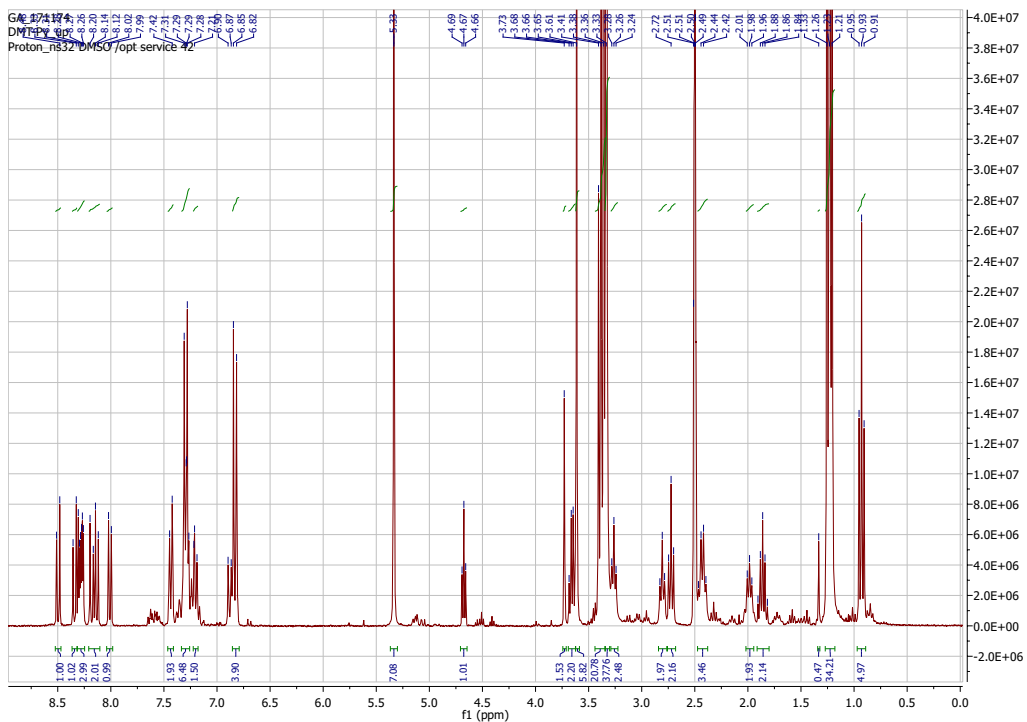


Figure A.2.: <sup>1</sup>H-NMR of (2).

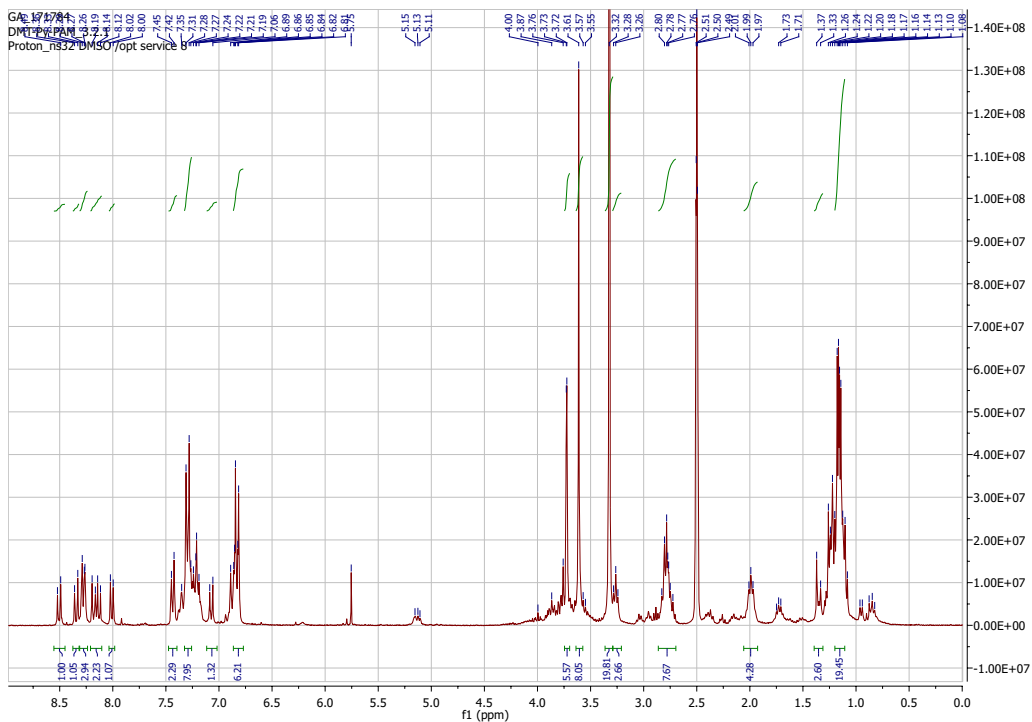


Figure A.3.: <sup>1</sup>H-NMR of (3).

## Synthesis of the Solid Support

This synthesis is according to the literature.<sup>101</sup>

(**2**) (30.8 mg, 0.046 mmol) was dissolved with dichloromethane (0.23 ml). Succinic anhydrid (4.7 mg) and DMAP (8.4 mg) were added. The mixture was stirred at room temperature for about 3.5 h. It was diluted with dichloromethane (10 ml), washed with 10% citric acid and brine and dried with sodium sulfate. The solvent was evaporated to dryness and dissolved with acetonitrile (5.97 ml). To 2 ml of this solution LCAA-CPG (308.1 mg) and HBTU (10.4 mg) were added. 1-methylimidazol (4  $\mu$ l) was added, the suspension was argonized and it was shaken overnight. The solid support was filtered and washed with dichloromethane. The solid support was added to DMAP (30.9 mg) and a mixture of pyridine/acetic acid anhydrid 3:1 (2.4 ml). The suspension was shaken for 2 h. It was filtered and washed with dichloromethane.

## DNA Synthesis

The 1,6-dialkynylpyrene phosphoramidite was used for the solid-phase oligonucleotide synthesis. The standard procedure as described was used.<sup>29</sup> The synthesis was done on the Applied Biosystems 394 DNA/RNA synthesizer using pyrene-loaded controlled pore glass (CPG) support (oligomer **Py**<sub>3</sub>, **DNA-Py**<sub>4</sub> and **DNA-Py**<sub>5</sub>). The average stepwise yield was between 94% and 100%. **DNA-(HEG)**<sub>1</sub>-**Py**<sub>7</sub> was already synthesized in the master thesis<sup>102</sup>, the procedure that was used for **DNA-Py**<sub>4</sub> and **DNA-Py**<sub>5</sub> can also adapt to this oligomer.

Table A.1.: The sequences of used oligomers.

Oligomer	Sequence
Py <sub>3</sub>	Py-Py-Py
DNA-(HEG) <sub>1</sub> -Py <sub>7</sub>	3'-GAG TGC CTT C-(HEG)-Py-Py-Py-Py-Py-Py-Py
DNA-Py <sub>4</sub>	5'-CAA GGT CCG ATG CAA GGA GGA AG-Py-Py-Py-Py
DNA-Py <sub>5</sub>	5'-CAA GGT CCG ATG CAA GGA GGA AG-Py-Py-Py-Py-Py

The cleavage of oligomer were done with 25% ammonium hydroxide for 16 hours at 55 °C in a closed vial with strong shaking. **Py**<sub>3</sub> was cleaved with 2 M ammonia in methanol for 7 hours. After the cleavage the oligomer were centrifuged (20 °C, 13000 rpm, for 3 min). After centrifugation, the supernatant was collected and the solid was washed 3 times with 1 ml MilliQ/ethanol 1:1 (**Py**<sub>3</sub>) or

1ml MilliQ (**DNA-Py<sub>4</sub>** and **DNA-Py<sub>5</sub>**). The crude oligomer were lyophilized overnight.

## HPLC Purification

After the solid-phase synthesis and the cleavage, the compounds have to be purified with HPLC (Dr.Maisch GmbH, ReproSil 100 C8, Lichrospher 100 RP-18, 5 $\mu$ m, 250 x 4mm). For the purification 0.1M ammonium acetate buffer (**Py<sub>3</sub>**) and 0.1M TEAA /acetonitrile 80:20 (compound **6** and **7**) were used; 1 ml/min; T = 50 °C; **Py<sub>3</sub>**: B[%] (t<sub>R</sub> [min]) = 50 (0); 100 (22); 50 (28); Compound **6** and **7**: B[%] (t<sub>R</sub> [min]) = 50 (22); 100 (26); 0 (32). The purities were determined with ESI mass spectroscopy (??).

**Py<sub>3</sub>** was dissolved in 1ml ethanol and oligomers **DNA-Py<sub>4</sub>** and **DNA-Py<sub>5</sub>** were dissolved in 1 ml 80:20 MilliQ/ethanol. The stock solution were diluted and the determination of the concentrations was achieved by using a value of  $\epsilon^{365}=35000 \text{ M}^{-1} \cdot \text{cm}^{-1}$  in ethanol for single pyrene unit.

## Synthesis of Au nanoparticles modified with DNA

300  $\mu$ l of HAuCl<sub>4</sub> (50 mM) and 49.7 ml MilliQ water were mixed and the solution was heated under reflux until boiling. 1 ml of 1 % CitNa and 3.5 ml 1 % tannic acid were mixed and heated. Both mixtures were put together after both were boiled. This mixture was heated under reflux and stirred for another 5 min. 10 ml of the prepared mixture was mixed with 10.9 mg of Bis(p-sulfonatophenyl)phenylphosphine dihydrate dipotassium (BSPP) and it was shaken overnight. The solution was filtered through a 0.22  $\mu$ m pore filter into a tube and a small amount of sodium chloride was added until the color changed to purple-brown. Then it was centrifuged for 20 min by 3000 u/min. The supernatant was removed, the AuNP was washed two times with 55  $\mu$ l 0.5x Tris/Borate/EDTA buffer solution (TBE) and 500  $\mu$ l 0.5 mM BSPP and centrifuged for 30 min at 13000 rpm. Then it was dissolved again with 55  $\mu$ l 0.5x TBE and 500  $\mu$ l 0.5 mM BSPP. The concentration of AuNP was determined in MilliQ by using a value of  $\epsilon^{520} = 1 \cdot 10^7 \text{ M}^{-1} \cdot \text{cm}^{-1}$  for 5 nm gold nanoparticles. The complementary single strand DNA modified with thiol (DNA-SH, 50  $\mu$ l, 69  $\mu$ M), 5x TBE (6,9  $\mu$ l), 159.5  $\mu$ l of the Au nanoparticles, 17.72  $\mu$ l NaCl (0.5M) and 2.77  $\mu$ l MilliQ were mix together. This mixture was shaken overnight at room temperature (24 °C) and 700 rpm. The mixture was then washed two times, each time with 200  $\mu$ l 0.5x TBE and centrifuge at 20 °C

and 13000 rpm for 30 min. Afterwards, it was dissolved in 100  $\mu\text{l}$  0.5x TBE. The concentration of the Au nanoparticles modified with DNA was determined by UV-vis spectroscopy.

## Mass Spectra

Table A.2.: The expected and measured mass of the oligomers.

Oligomer	Expected mass [g/mol]	Measured mass [g/mol]
Py <sub>3</sub>	1223.28	1222.38
DNA-Py <sub>4</sub>	7913.75	7913.47
DNA-Py <sub>5</sub>	8342.17	8342.62

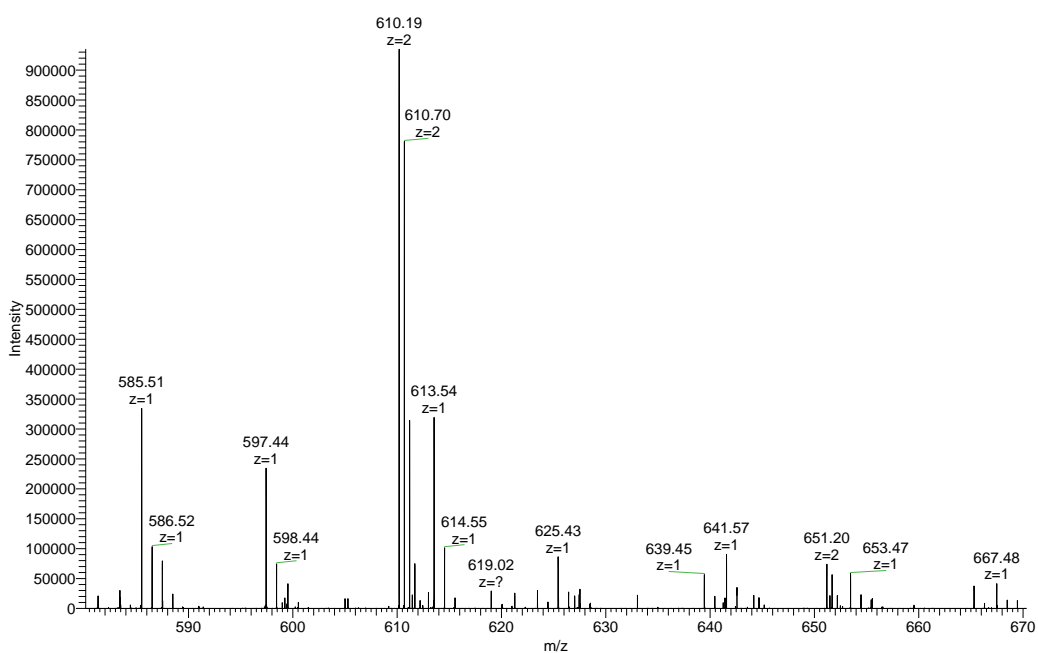


Figure A.4.: Mass spectrum of Py<sub>3</sub>.

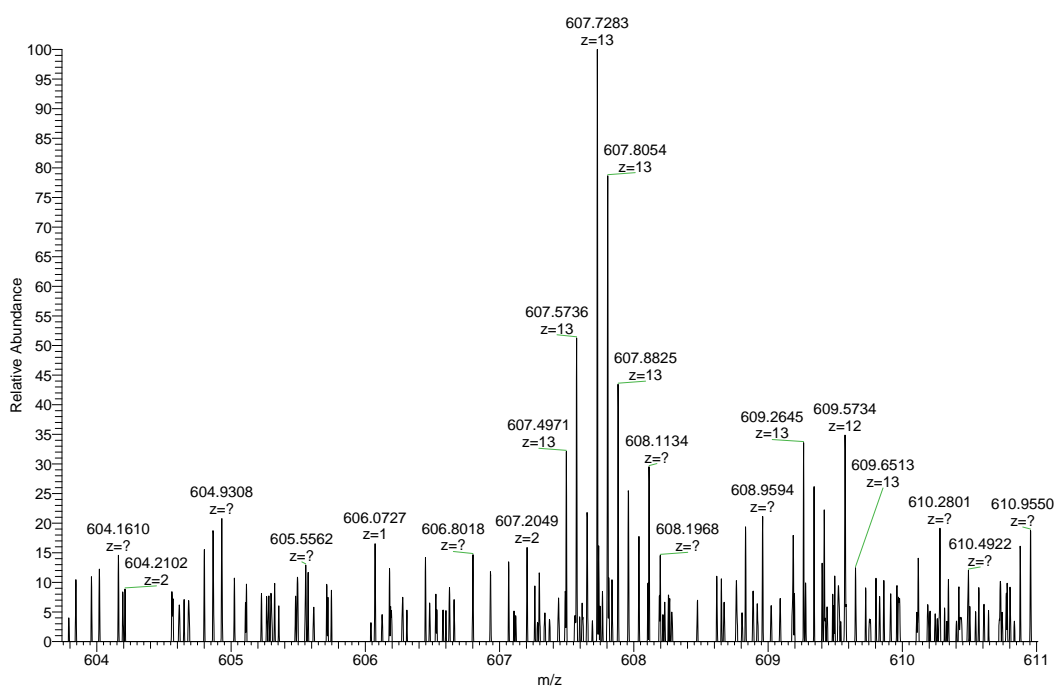


Figure A.5.: Mass spectrum of DNA-Py<sub>4</sub>.

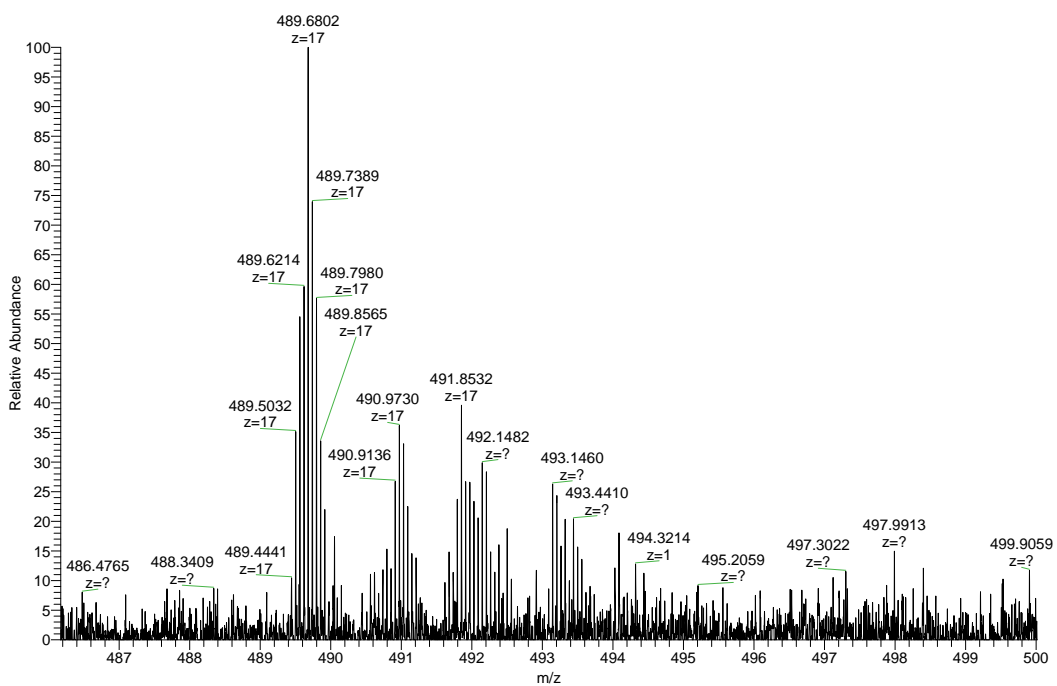


Figure A.6.: Mass spectrum of DNA-Py<sub>5</sub>.

## Tested Conditions

Table A.3.: Tested conditions of **Phe<sub>3</sub>** with **DNA-Phe<sub>3</sub>**. All conditions are with 10 mM sodium phosphate buffer (pH 7).

Condition	Phe <sub>3</sub> [μM]	DNA-Phe <sub>3</sub> [μM]	Temperature gradient [°C/min]	Morphology
0.1 mM spermine tetrahydrochloride & 20% EtOH	0.5	0.015	15	undefined
0.025 mM spermine tetrahydrochloride & 20% EtOH				tube-like & sheet-like
0.05 mM spermine tetrahydrochloride 20% EtOH	1	0.03		stripes & sheet-like
0.1 mM putrescine dihydrochloride & 20% EtOH				undefined

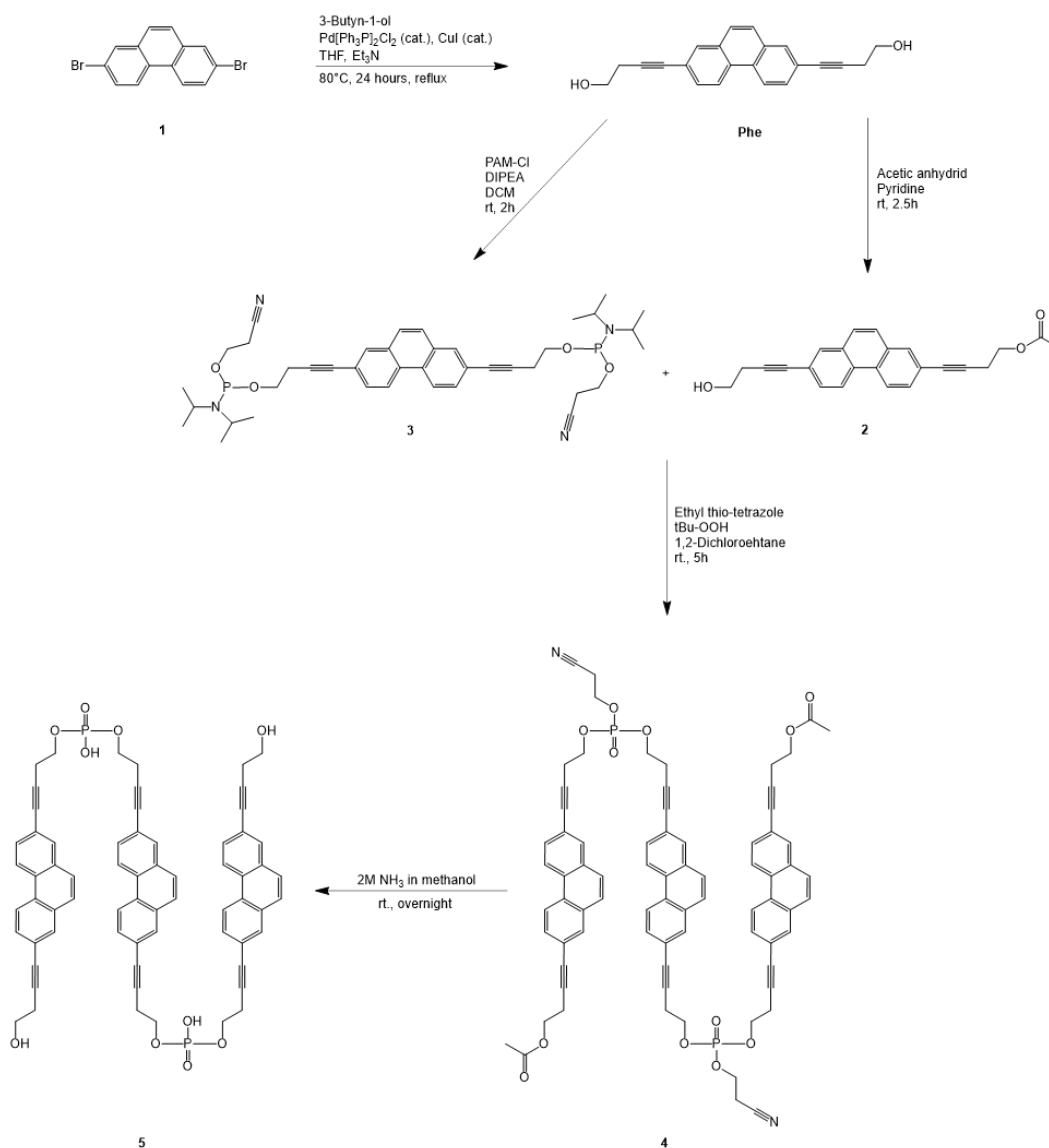
Table A.4.: Tested conditions of **Phe<sub>3</sub>** with **DNA-Phe<sub>5</sub>**. All conditions are with 10 mM sodium phosphate buffer (pH 7).

Condition	Phe <sub>3</sub> [μM]	DNA-Phe <sub>5</sub> [μM]	Temperature gradient [°C/min]	Morphology
0.1 mM spermine tetrahydrochloride & 20% EtOH	1	0.03	15	tube-like & sheet-like
			0.1	undefined
	-	1	15	undefined & vesicles
0.025 mM spermine tetrahydrochloride & 20% EtOH	1	0.03		stripes & sheet-like
20% EtOH				No hybridization
0.1 mM putrescine dihydrochloride & 20% EtOH				stripes
100 mM NaCl			tube-like & sheet-like	
100 mM NaCl and 10% ethanol	1	0.03	1	No hybridization
150 mM NaCl and 10% ethanol				undefined
200 mM NaCl				vesicle-like and sheet-like
200 mM NaCl and 10% ethanol				vesicle-like and undefined
				vesicle-like and sheet-like

## Synthesis of the Phenanthrene Trimer

### 2,7-Bis(4-hydroxybut-1-yn-1-yl)phenanthrene (Phe):

2,7-dibromophenanthrene (**1**) (594 mg, 1.77 mmol), bis(triphenylphosphine)palladium(II) dichloride (69 mg, 0.048 mmol) and copper(I) iodide (28 mg, 0.15 mmol) were dissolved in dry THF (13.8 mL) under argon and heated to 80 °C under reflux. After addition of triethylamine (6.9 mL)



Scheme A.2: Synthesis of 2,7-phenanthrene trimer

and 3-butyn-1-ol (0.4 mL, 5.47 mmol) to the mixture it was stirred at this temperature overnight. After cooling to room temperature, the solvent was removed under reduced pressure. Then it was dissolved in dichloromethane, washed with 10% citric acid and brine. The organic phase was dried with sodium sulfated and was filtered. A column chromatography (CH<sub>2</sub>Cl<sub>2</sub> (100%); CH<sub>2</sub>Cl<sub>2</sub>/MeOH 99:1 and CH<sub>2</sub>Cl<sub>2</sub>/MeOH 95:5) was made and the collected fractions were evaporated. The compound was dissolved with dichloromethane and hexane was added, the white precipitation was filtered and collected. It gave a white solid (384.1 mg, 69%).

**Analytical data for Phe:**

$^1\text{H-NMR}$  (300 MHz, DMSO)  $\delta$  8.75 (d,  $J$  = 8.6 Hz, 2H), 8.05 (d,  $J$  = 1.8 Hz, 2H), 7.84, 7.65 (dd,  $J$  = 8.5, 1.8 Hz, 4H), 4.95 (t,  $J$  = 5.6 Hz, 1H), 3.64 (td,  $J$  = 6.8, 5.6 Hz, 4H), 2.63 (t,  $J$  = 6.8 Hz, 4H).

**4-(7-(4-hydroxybut-1-yn-yl)phenanthrene-2-yl)but-3-yn-1-yl acetate (2):**

**Phe** (227 mg, 0.72 mmol) was dissolved with anhydrous pyridine (7.2 ml) under argon. 2M acetic anhydride (in anhydrous pyridine, 0.36 ml) was added dropwise to the **Phe** solution. The reaction mixture was stirred for 2.5 hours at room temperature under argon. The reaction mixture was diluted with dichloromethane (20 ml), washed with 0.5M HCl (20 ml), saturated  $\text{NaCO}_3\text{H}$  (20 ml) and brine (20 ml). The organic phase was dried with magnesium sulfate, filtered and evaporated. A column chromatography (hexane/ethyl acetate 3:2, dry loading) was made and the collected fractions were evaporated. This gave a white solid (99.2 mg, 39%).

**Analytical data for (2):**

$^1\text{H-NMR}$  (300 MHz, DMSO)  $\delta$  8.76 (dd,  $J$  = 8.9, 2.3 Hz, 2H), 8.06 (dd,  $J$  = 3.6, 1.7 Hz, 2H), 7.85, 7.66 (dd,  $J$  = 8.5, 1.8 Hz, 4H), 4.94 (t,  $J$  = 5.6 Hz, 1H), 4.22 (t,  $J$  = 6.6 Hz, 2H), 3.64 (td,  $J$  = 6.8, 5.6 Hz, 2H), 2.85 (t,  $J$  = 6.6 Hz, 2H), 2.63 (t,  $J$  = 6.8 Hz, 2H), 2.08 (s, 2H).

**Bis(2-cyanoethyl)(phenanthrene-2,7-diylbis(but-3-yne-4,1-diyl))  
bis(diisopropylphosphoramidite) (3):**

**Phe** (104.8 mg, 0.33 mmol) was dissolved in anhydrous THF (3.1 mL). After addition of  $\text{N,N}$ -Diisopropylethylamin (DIPEA) (0.57 ml, 3.33 mmol), 2-cyanoethyl- $\text{N,N}$ -diisopropylchlorophosphoramidite (PAM-Cl, 205.1 mg, 0.87 mmol) was added. The mixture was stirred for 2 hours at room temperature under argon. The solution was evaporated and purified by a flash chromatography (hexane/EtOAc 6:4 with 1% triethylamine). The fractions were collected, evaporated and it gave 179 mg (75%) of white oil (**3**).

**Analytical data for (3):**

$^1\text{H NMR}$  (300 MHz,  $\text{CDCl}_3$ )  $\delta$  8.53 (d,  $J$  = 8.7 Hz, 2H), 7.92 (d,  $J$  = 1.7 Hz, 2H), 7.72 – 7.56 (m, 4H), 3.87 (dtdd,  $J$  = 16.6, 8.1, 3.9, 1.9 Hz, 2H), 3.76 – 3.44 (m, 12H), 2.66 (td,  $J$  = 6.5, 2.7 Hz,



5H), 2.04, 1.53 – 1.35 (m, 10H), 1.24 (ddd,  $J = 16.6, 7.0, 3.9$  Hz).  $^{31}\text{P}$  (121 MHz,  $\text{CDCl}_3$ )  $\delta$  148.22, 14.17, 13.15, 7.68, 2.13.

**protected 2,7-phananthrene trimer (4):**

**(3)** (25 mg, 0.03 mmol) was dissolved in 1,2-dichloroethan (0.25 ml) and **(2)** (38 mg, 0.1 mmol) in 1,2-dichloroethan (0.5 ml). The dried ethyl thio-tetrazole (13.9 mg) was dissolved in 1,2-dichloroethan (0.43 ml) and it was added to the **(3)** solution. Then the **(2)** solution was added to the mixture and it was stirred at room temperature under argon. The reaction was controlled by TLC and it was stopped by adding t-Bu hydroxyperoxide solution (30  $\mu\text{l}$ ). The reaction mixture was diluted with chloroform (15 ml), washed twice with  $\text{NaCO}_3\text{H}$  (20 ml) and brine (20 ml). The organic phase was dried with magnesium sulfate, filtered and concentrated to dryness. The reaction mixture was dissolved with dichloromethane (1 ml). Prep TLC was made (dichloromethane/toluene/MeOH 86:10:4). The silica gel was washed two times with dichloromethane/MeOH 95:5 (30 ml) and filtered. The solution was concentrated and it gave **(4)** with a yield of 25%.

**Analytical data for (4):**

$^1\text{H}$  NMR (300 MHz,  $\text{CDCl}_3$ )  $\delta$  8.35 (d,  $J = 8.9$  Hz, 6H), 8.22 (d,  $J = 8.6$  Hz, 2H), 7.85 (d,  $J = 2.6$  Hz, 8H), 7.79, 7.54 (d,  $J = 9.5$  Hz, 18H), 7.47 (d,  $J = 3.4$  Hz, 4H), 4.43 – 4.25 (m), 4.07 (t,  $J = 6.6$  Hz, 2H), 2.98 – 2.87 (m), 2.80 (dt,  $J = 17.4, 6.5$  Hz), 2.12, 1.41 (d,  $J = 3.3$  Hz), 1.27 (d,  $J = 12.2$  Hz), 0.95 (d,  $J = 7.4$  Hz, 2H), 0.87 (d,  $J = 7.6$  Hz), 0.07.

**2,7-phananthrene trimer (5):**

2M  $\text{NH}_3$  in MeOH (5 ml) was added to the protected **(4)** (5.5 mg, 4.4  $\mu\text{mol}$ ) to dissolve **(4)** completely MeOH (2 ml) was added. The solution was stirred at room temperature under argon overnight. The crude product was lyophilized and then dissolved again with ethanol.

**Analytical data for (5):**

ESI-MS: found 1066.29; calculated 1066.30.

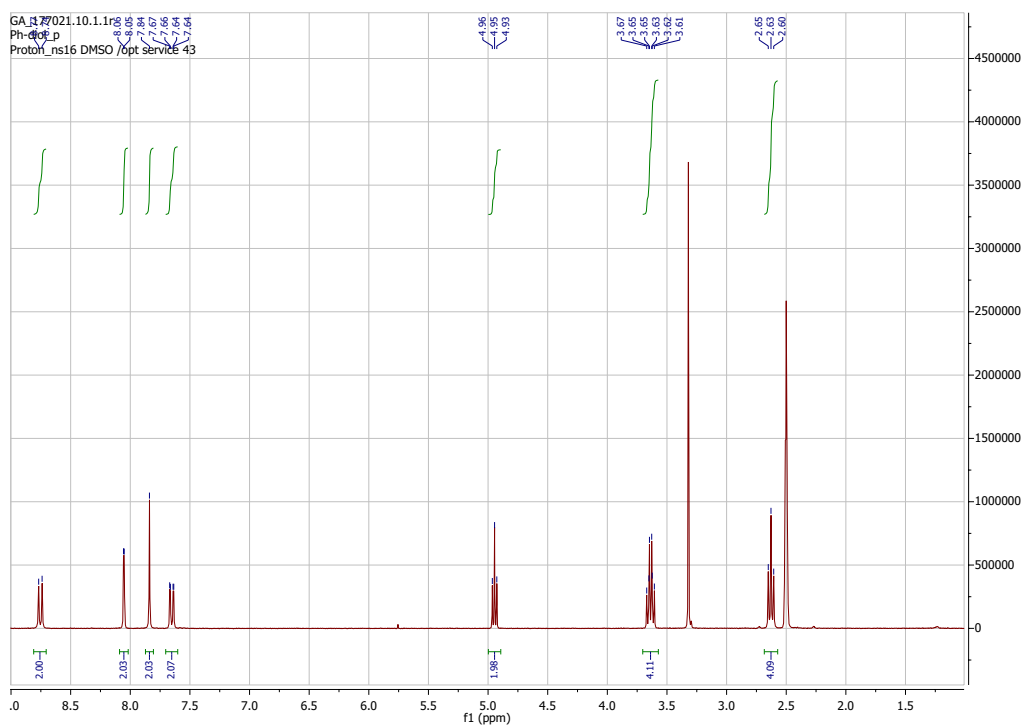


Figure A.7.:  $^1\text{H-NMR}$  of (2).

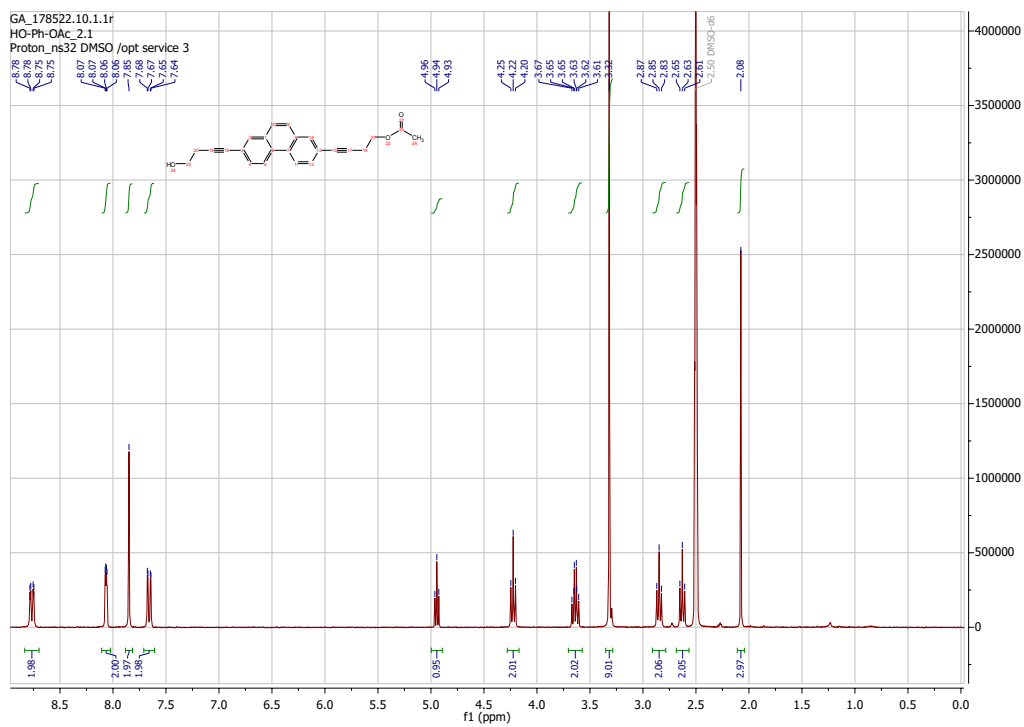


Figure A.8.:  $^1\text{H-NMR}$  of (2).

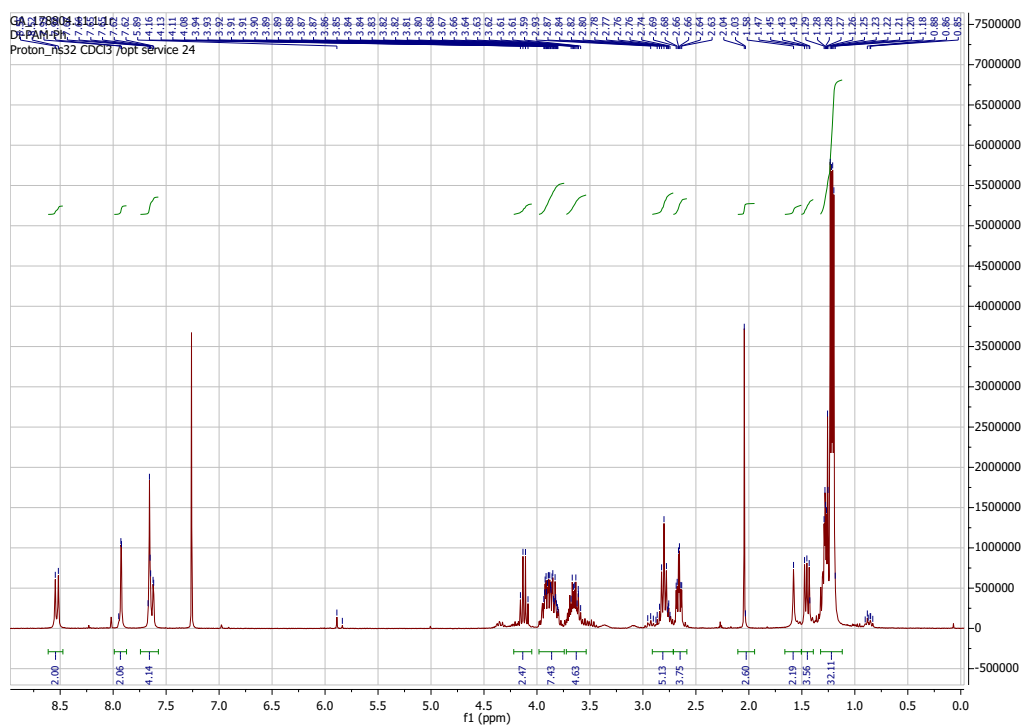


Figure A.9.:  $^1\text{H-NMR}$  of (3).

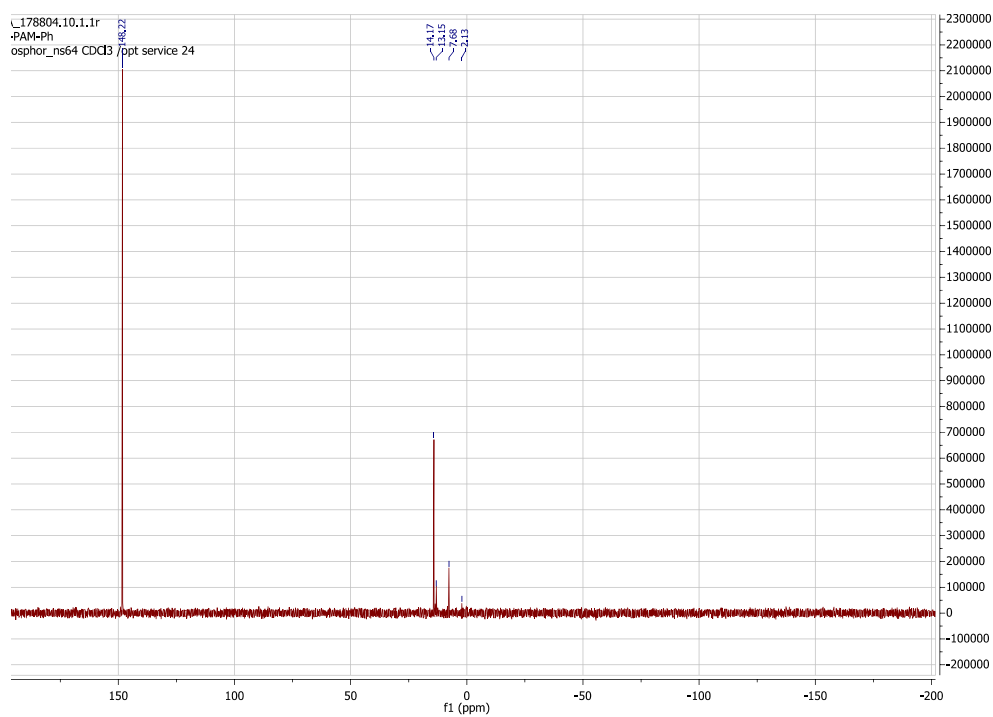


Figure A.10.:  $^{31}\text{P-NMR}$  of (3).

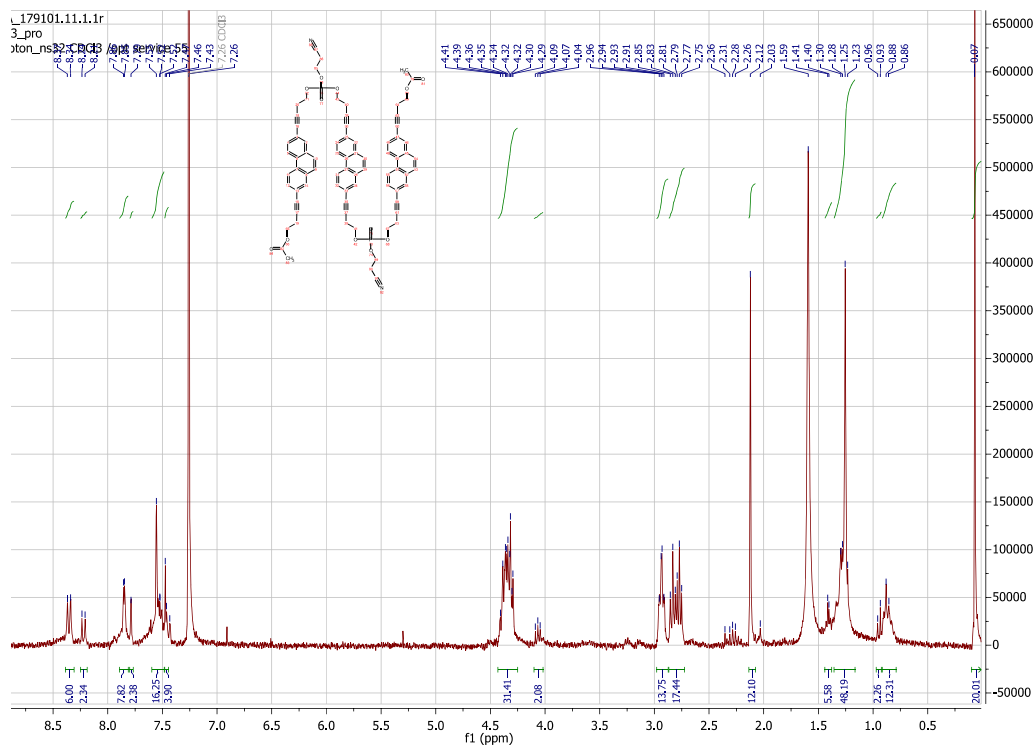


Figure A.11.: <sup>1</sup>H-NMR of (4).

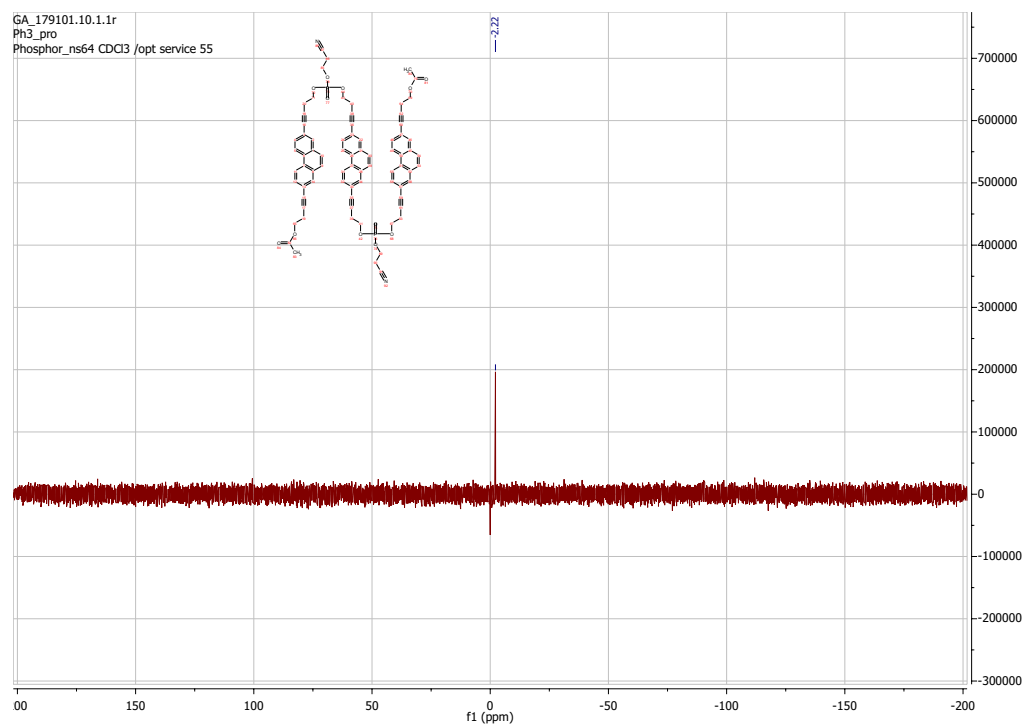


Figure A.12.: <sup>31</sup>P-NMR of (4).

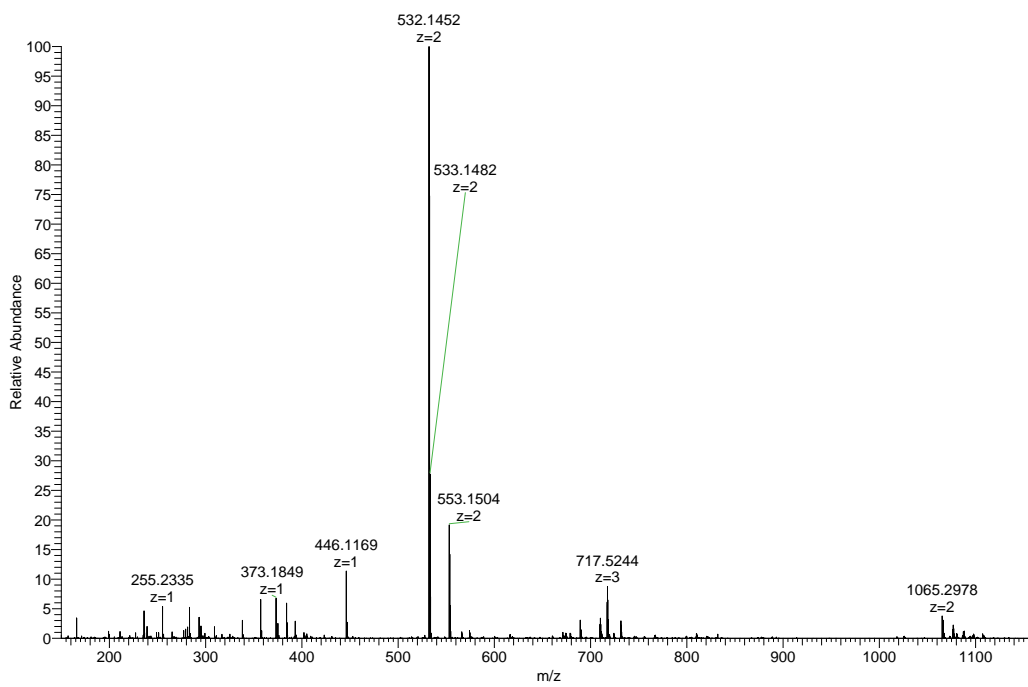


Figure A.13.: Mass spectrum of  $\text{Phe}_3$ .

## B. Appendix Chapter 3

### Tested Conditions

Table B.1.: Tested conditions for **DNA-Phe<sub>5</sub>**. All conditions were in 10 mM sodium phosphate buffer and with 2.5 $\mu$ M **DNA-Phe<sub>5</sub>**.

Condition	Morphology
100mM NaCl and 10% ethanol	sphere-like (not homogenous)
200mM NaCl and 10% ethanol	undefined
2mM MgCl <sub>2</sub> and 10% ethanol	sphere-like (not homogenous) & undefined
100mM NaCl, 2mM MgCl <sub>2</sub> and 10% ethanol	vesicles and undefined
100mM NaCl	undefined
2mM MgCl <sub>2</sub>	undefined
4mM MgCl <sub>2</sub>	undefined

Condition	Morphology
0.1mM putrescine dihydrochloride and 20% ethanol	vesicles and undefined
0.1mM putrescine dihydrochloride and 10% ethanol	undefined
10 $\mu$ M putrescine dihydrochloride and 10% ethanol	undefined
0.2mM putrescine dihydrochloride and 20% ethanol	vesicles and undefined
0.3mM putrescine dihydrochloride and 20% ethanol	vesicle-like and undefined
0.05mM spermidine trihydrochloride and 20% ethanol	vesicle-like and undefined
0.1mM spermidine trihydrochloride and 20% ethanol	vesicle-like and ring-like
0.2mM spermidine trihydrochloride and 20% ethanol	ring-like and undefined
0.1mM spermidine trihydrochloride and 10% ethanol	vesicle-like and undefined
0.2mM spermidine trihydrochloride and 10% ethanol	vesicle-like and undefined
0.4mM spermidine trihydrochloride and 10% ethanol	vesicle-like and undefined
0.2mM spermidine trihydrochloride	vesicle-like
0.3mM putrescine dihydrochloride, 20mM NaCl and 20% ethanol	vesicle-like and undefined
0.1mM spermidine trihydrochloride, 20mM NaCl and 20% ethanol	ring-like

## AFM Images

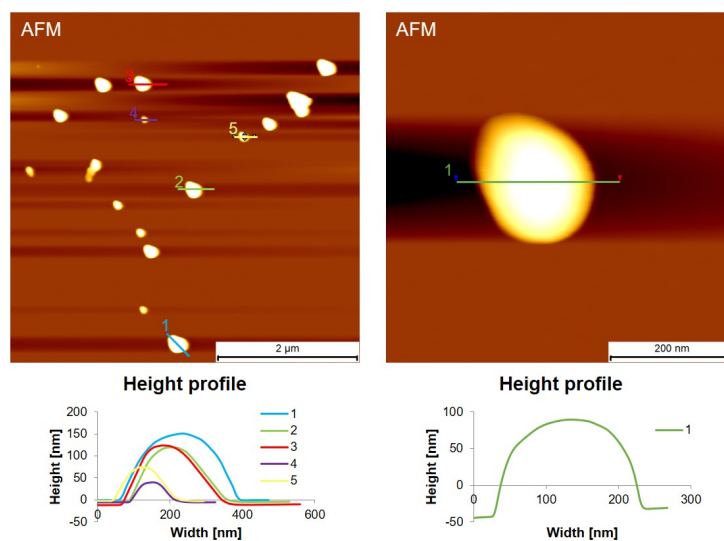


Figure B.1.: AFM images of  $2.5\mu\text{M}$  **DNA-Phe<sub>5</sub>** deposited on APTES-modified mica. Condition: 10 mM sodium phosphate buffer, 0.1mM spermine tetrahydrochloride and 20% ethanol. Temperature gradient:  $0.5\text{ }^\circ\text{C/min}$ . At the bottom the corresponding height profile along the line is shown in the insert of the AFM image.

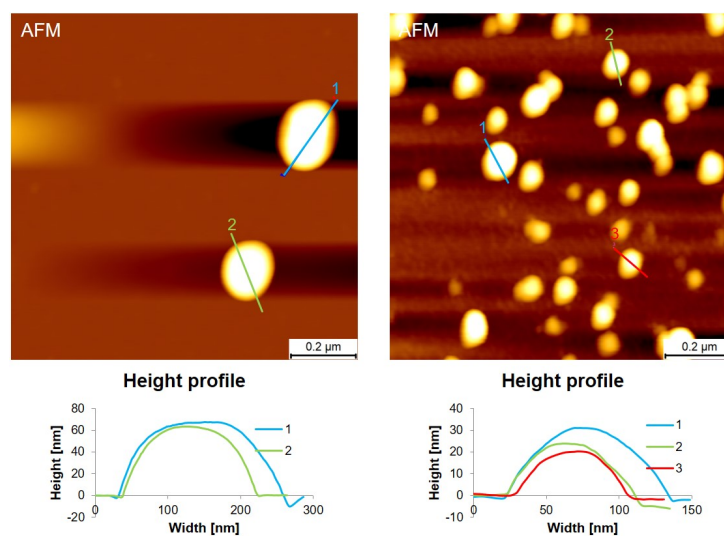


Figure B.2.: AFM image of  $2.5\mu\text{M}$  **DNA-Phe<sub>5</sub>** deposited on APTES-modified mica. Condition: see Figure B.1. Left: Temperature gradient:  $0.5\text{ }^\circ\text{C/min}$ . Right: Temperature gradient:  $15\text{ }^\circ\text{C/min}$ . At the bottom the corresponding height profile along the line is shown in the insert of the AFM image.

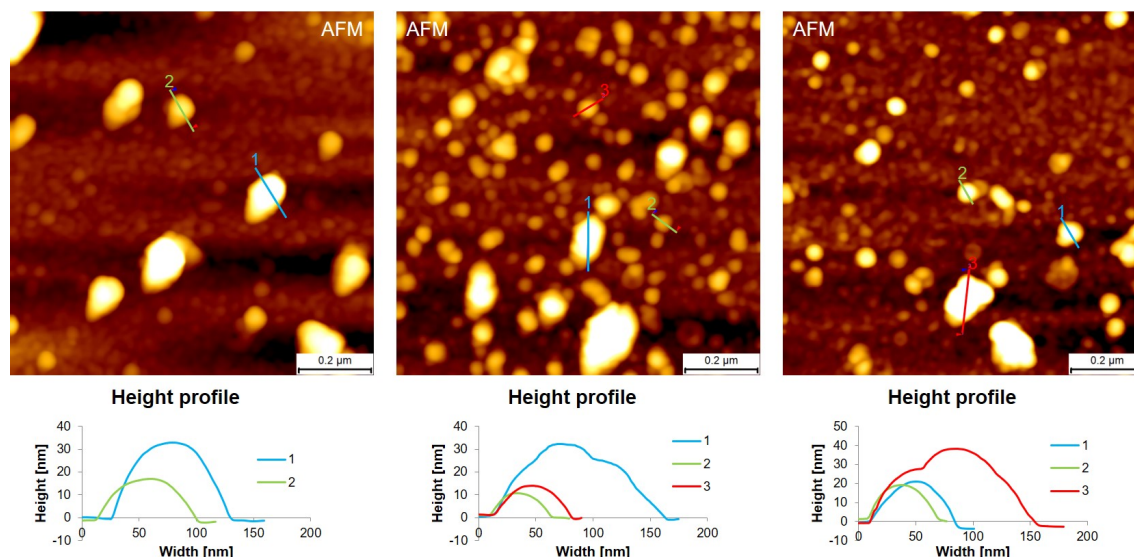


Figure B.3.: AFM images of  $2.5\mu\text{M}$  **DNA-Phe<sub>5</sub>** deposited on APTES-modified mica. Left: Condition: 10 mM sodium phosphate buffer, 100 mM NaCl and 10% ethanol. Middle: Condition: 10 mM sodium phosphate buffer, 2 mM MgCl<sub>2</sub> and 10% ethanol. Right: Condition: 10 mM sodium phosphate buffer, 100 mM NaCl, 2 mM MgCl<sub>2</sub> and 10% ethanol. Temperature gradient: 1 °C/min. At the bottom the corresponding height profile along the line is shown in the insert of the AFM image.

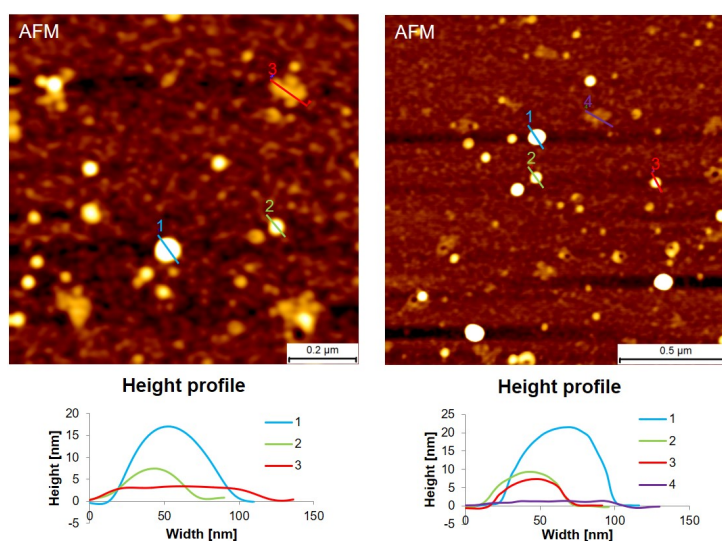


Figure B.4.: AFM images of  $2.5\mu\text{M}$  **DNA-Phe<sub>5</sub>** deposited on APTES-modified mica. Left: Condition: 10 mM sodium phosphate buffer, 0.1 mM putrescine dihydrochloride and 20% ethanol. Right: Condition: 10 mM sodium phosphate buffer, 0.2 mM putrescine dihydrochloride and 20% ethanol. Temperature gradient: 1 °C/min. At the bottom the corresponding height profile along the line is shown in the insert of the AFM image.



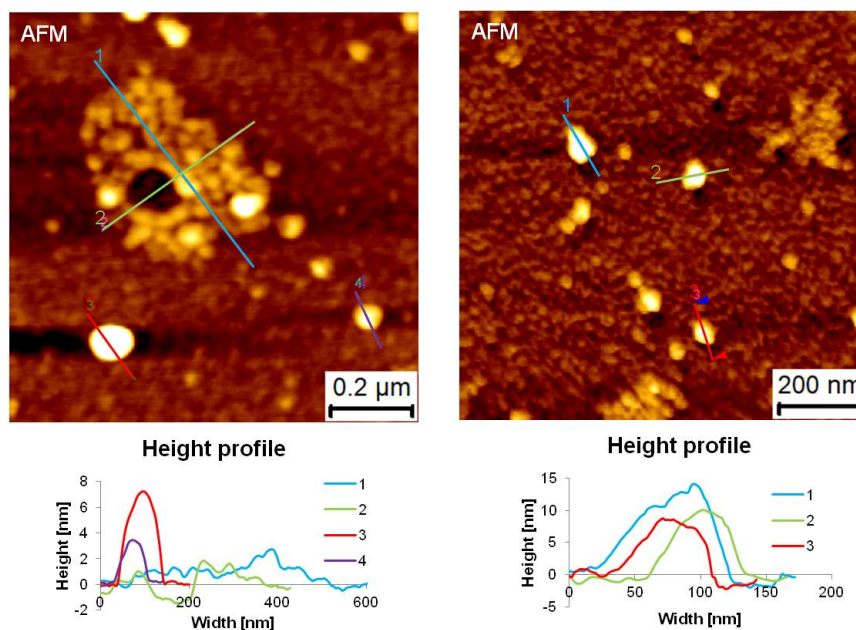


Figure B.5.: AFM images of  $2.5\mu\text{M}$  **DNA-Phe<sub>5</sub>** deposited on APTES-modified mica. Condition: 10mM sodium phosphate buffer pH 7. Temperature gradient:  $1^\circ\text{C}/\text{min}$ . Left: 0.3mM putrescine dihydrochloride and 20% ethanol. Right: 200mM NaCl and 10% ethanol.

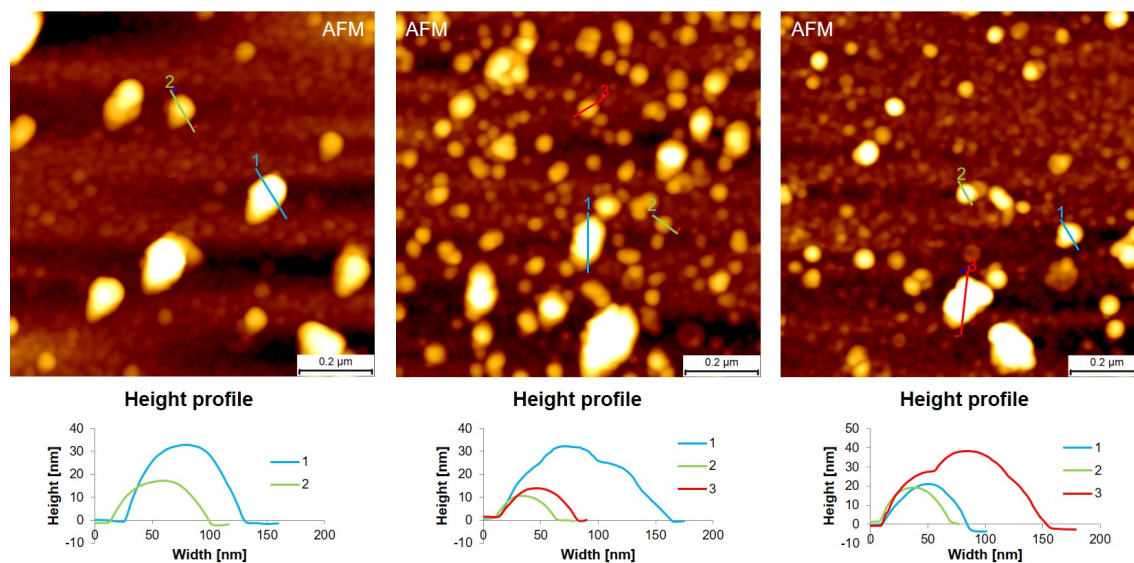


Figure B.6.: AFM images of  $2.5\mu\text{M}$  **DNA-Phe<sub>5</sub>** deposited on APTES-modified mica. Condition: 10mM sodium phosphate buffer pH 7. Temperature gradient:  $1^\circ\text{C}/\text{min}$ . Left: 100mM NaCl and 10% ethanol. Middle: 2mM  $\text{MgCl}_2$  and 10% ethanol. Right: 100mM NaCl, 2mM  $\text{MgCl}_2$  and 10% ethanol.

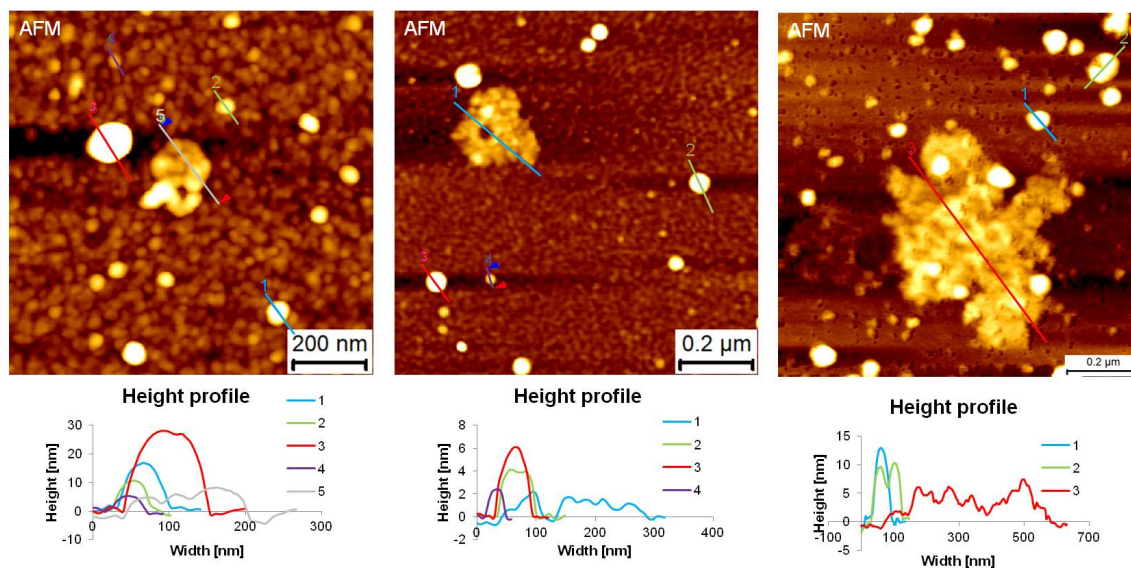


Figure B.7.: AFM images of  $2.5\mu\text{M}$  **DNA-Phe<sub>5</sub>** deposited on APTES-modified mica. Condition: 10mM sodium phosphate buffer pH 7 and 10% ethanol. Temperature gradient:  $1^\circ\text{C}/\text{min}$ . Left: 0.1mM spermidine trihydrochloride. Middle: 0.2mM spermidine trihydrochloride. Right: 0.4mM spermidine trihydrochloride.

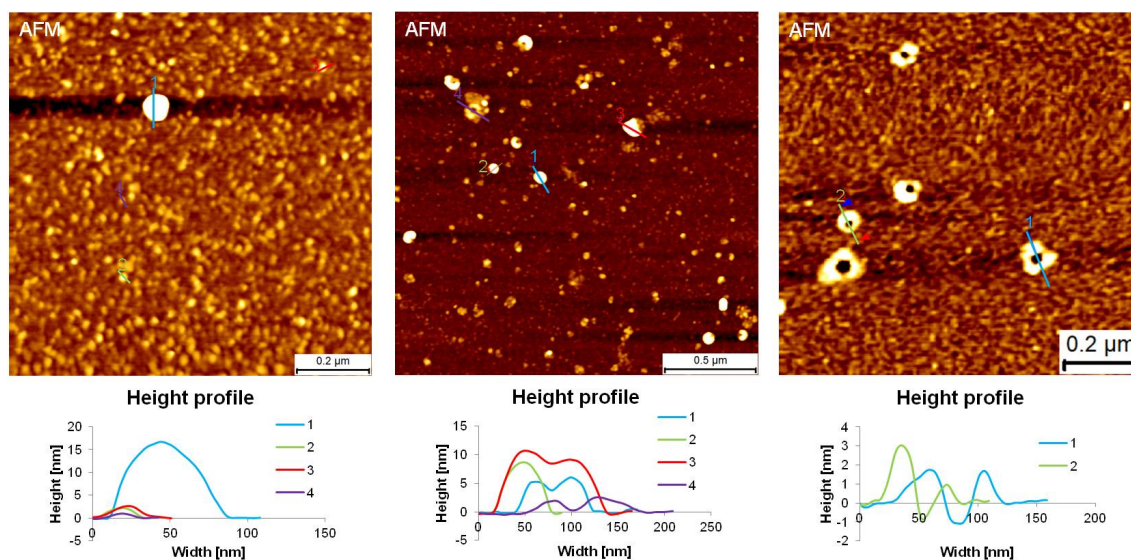


Figure B.8.: AFM images of  $2.5\mu\text{M}$  **DNA-Phe<sub>5</sub>** deposited on APTES-modified mica. Condition: 10mM sodium phosphate buffer pH 7. Temperature gradient:  $1^\circ\text{C}/\text{min}$ . Left: 0.2mM spermidine trihydrochloride. Middle: 0.3mM putrescine dihydrochloride, 20mM NaCl and 20% ethanol. Right: 0.1mM spermidine trihydrochloride, 20mM NaCl and 20% ethanol.

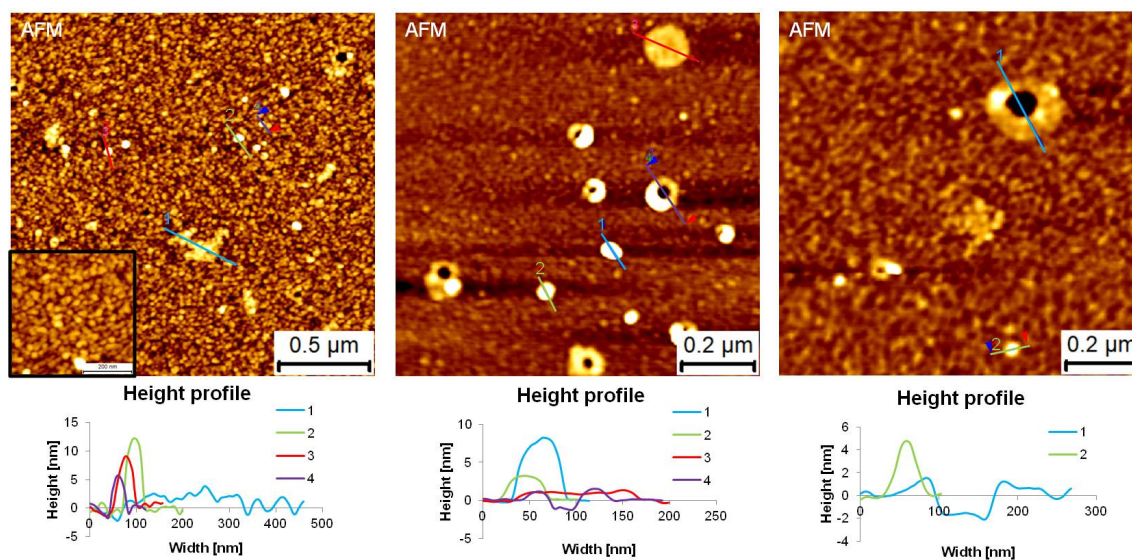


Figure B.9.: AFM images of  $2.5\mu\text{M}$  **DNA-Phe<sub>5</sub>** deposited on APTES-modified mica. Condition: 10mM sodium phosphate buffer pH 7 and 20% ethanol. Temperature gradient:  $1^\circ\text{C}/\text{min}$ . Left: 0.05mM spermidine trihydrochloride. Middle: 0.1mM spermidine trihydrochloride. Right: 0.2mM spermidine trihydrochloride.

### TEM Images

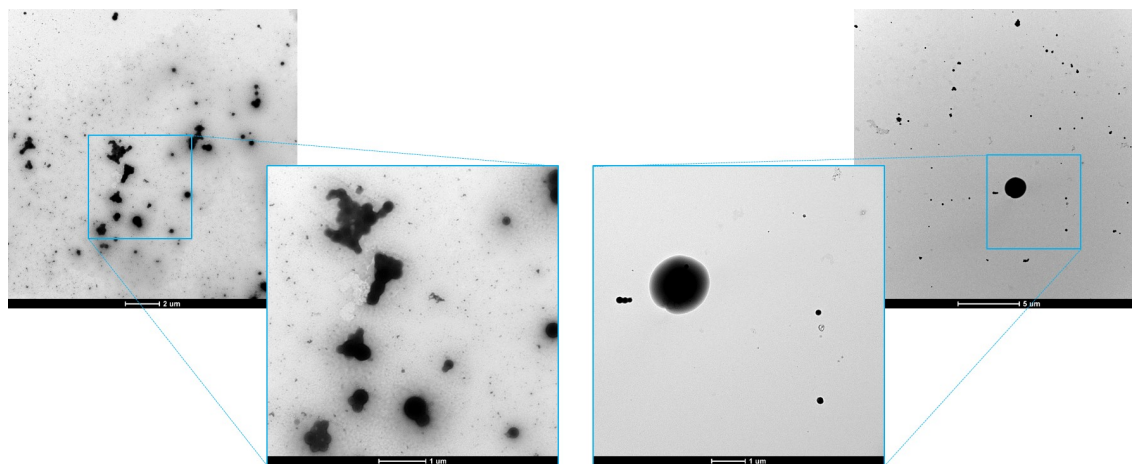


Figure B.10.: TEM images of  $2.5\mu\text{M}$  **DNA-Phe<sub>5</sub>** deposited on a copper carbon grid. Condition: see Figure B.1. Temperature gradient:  $0.5^\circ\text{C}/\text{min}$ . With the zoom-in.

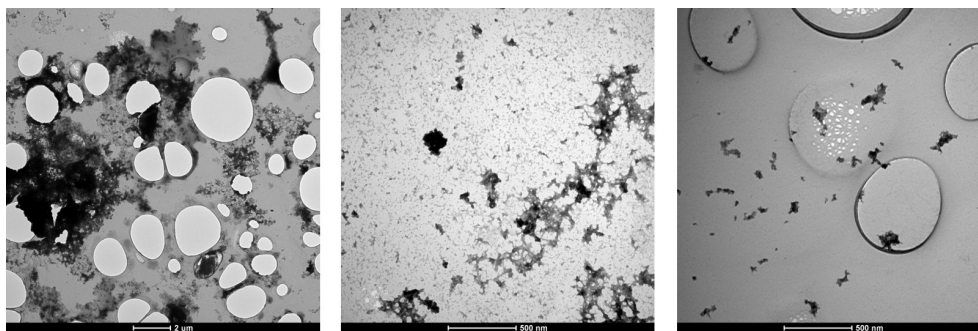


Figure B.11.: TEM images of 2.5 μM **DNA-Phe<sub>5</sub>** deposited on copper holey carbon grid. Left: Condition: 10 mM sodium phosphate buffer and 100 mM NaCl. Middle: Condition: 10 mM sodium phosphate buffer and 2 mM MgCl<sub>2</sub>. Right: Condition: 10 mM sodium phosphate buffer and 4 mM MgCl<sub>2</sub>. Temperature gradient: 1 °C/min.

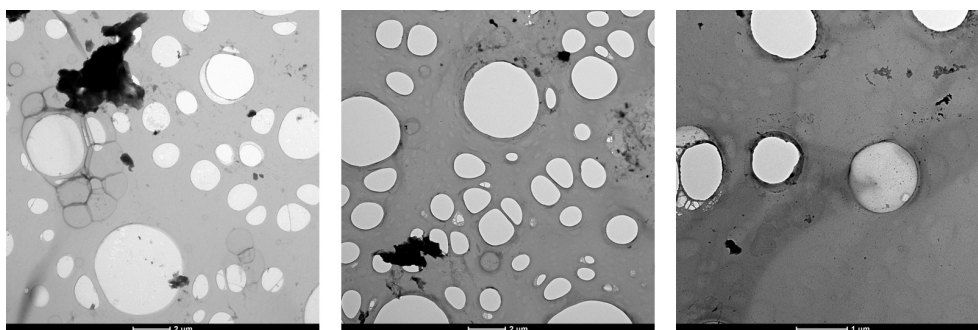


Figure B.12.: TEM images of 2.5 μM **DNA-Phe<sub>5</sub>** deposited on copper holey carbon grid. Left: Condition: 10 mM sodium phosphate buffer, 0.1 mM putrescine dihydrochloride and 20% ethanol. Middle: Condition: 10 mM sodium phosphate buffer, 0.1 mM putrescine dihydrochloride and 10% ethanol. Right: Condition: 10 mM sodium phosphate buffer, 10 μM putrescine dihydrochloride and 10% ethanol. Temperature gradient: 1 °C/min.

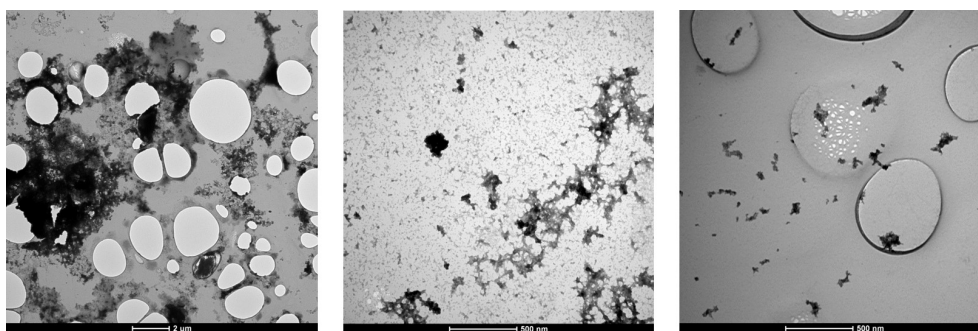


Figure B.13.: TEM images of of 2.5 μM **DNA-Phe<sub>5</sub>** deposited on holey carbon grid. Condition: 10mM sodium phosphate buffer pH 7. Temperature gradient: 1°C/min. Left: 0.1mM putrescine dihydrochloride and 20% ethanol. Middle: 0.1mM putrescine dihydrochloride and 10% ethanol. Right: 10 μM putrescine dihydrochloride and 10% ethanol.

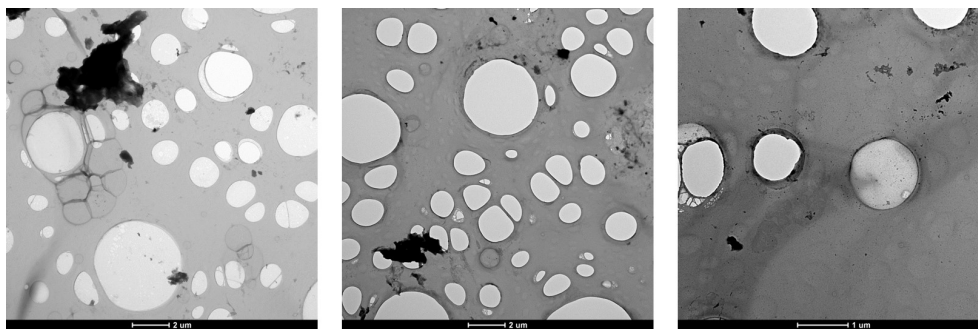


Figure B.14.: TEM images of of  $2.5\mu\text{M}$  **DNA-Phe<sub>5</sub>** deposited on holey carbon grid. Condition: 10mM sodium phosphate buffer pH 7. Temperature gradient:  $1^\circ\text{C}/\text{min}$ . Left: 100mM NaCl. Middle: 2mM  $\text{MgCl}_2$ . Right: 4mM  $\text{MgCl}_2$ .

## Spectroscopic Data

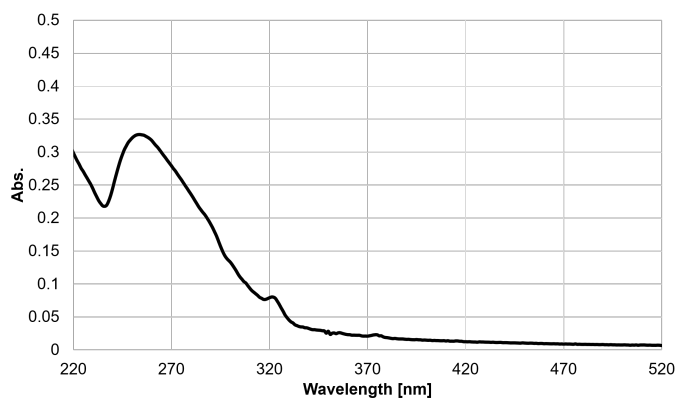


Figure B.15.: UV-vis spectrum of **DNA-Phe<sub>5</sub>**. Condition: see Figure B.1.

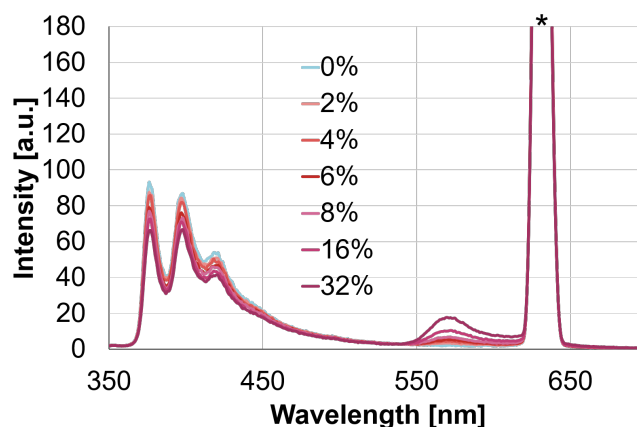
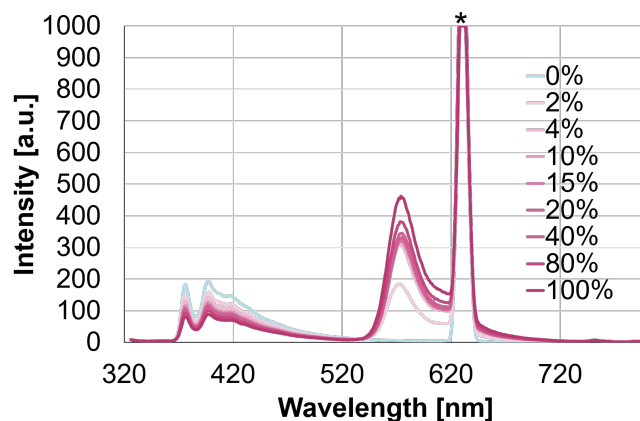
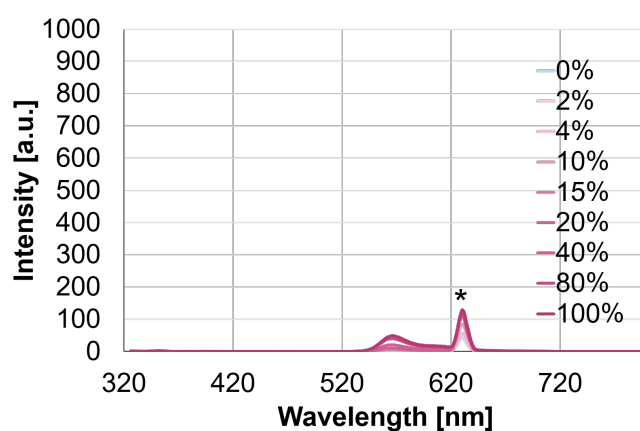
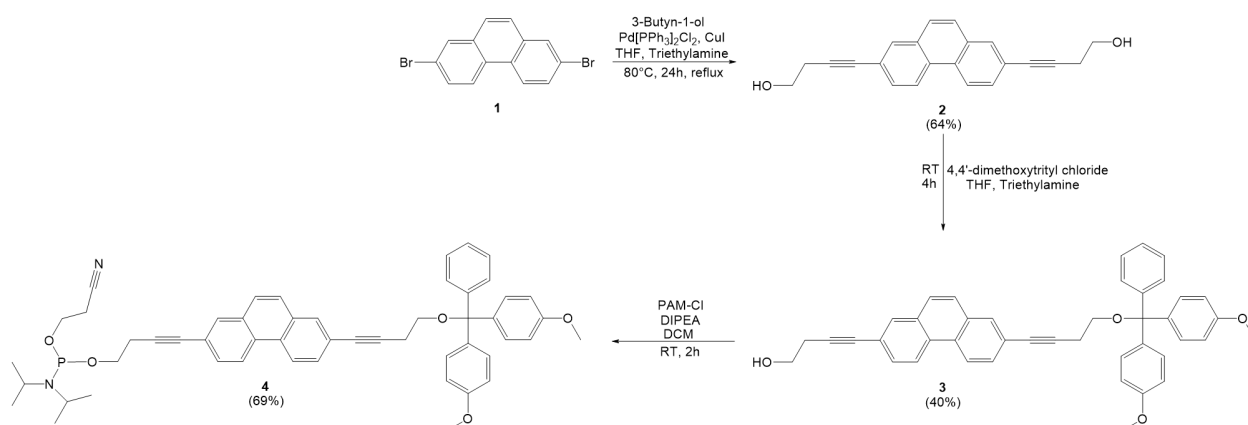


Figure B.16.: UV-vis spectra of **DNA-Phe<sub>5</sub>**. Stepwise addition of non-complementary **2**. Condition: see Figure B.1.

Figure B.17.: UV-vis spectra of **DNA-Phe<sub>5</sub>**. Stepwise addition of **1**. Condition: see Figure B.1.Figure B.18.: UV-vis spectra of the stepwise addition of **1**. Condition: see Figure B.1.

## Synthesis of the 2,7-dialkynylphenanthrene phosphoramidite



Scheme B.1: Synthesis steps of 2,7-phenanthrene building block

**2,7-Bis(4-hydroxybut-1-yn-1-yl)phenanthrene (2):**

2,7-dibromophenanthrene (**1**) (1254.4 mg, 3.73 mmol), bis(triphenylphosphine)palladium(II) dichloride (146 mg, 0.21 mmol) and copper(I) iodide (58 mg, 0.31 mmol) were dissolved in dry THF (29.2 mL) under argon and heated to 80 °C under reflux. After addition of triethylamine (14.6 mL) and 3-butyn-1-ol (0.9 mL, 11.55 mmol) to the mixture it was stirred at this temperature overnight. After cooling to room temperature, the mixture was filtered through Celite®. Then it was diluted with dichloromethane (HPLC quality, 70 ml), washed with 10% citric acid (80 ml) and saturated sodium hydrogen carbonate (80 ml). The organic phase was dried with sodium sulfate and was filtered. The crude product was evaporated to dryness, a column chromatography (eluent:CH<sub>2</sub>Cl<sub>2</sub>/MeOH 95:5; dry loading) was made and the collected fractions were evaporated. The compound was dissolved with dichloromethane and hexane was added, the white precipitation was filtered, collected and dried on the high vacuum. It gave a white solid (749.2 mg, 64%).

**Analytical data for Phe:**

<sup>1</sup>H-NMR (300 MHz, DMSO)  $\delta$  8.75 (d, J = 8.7 Hz, 2H), 8.05 (d, J = 1.8 Hz, 2H), 7.84, 7.65 (dd, J = 8.5, 1.8 Hz, 4H), 4.94 (t, J = 5.6 Hz, 1H), 3.64 (td, J = 6.8, 5.6 Hz, 4H), 2.63 (t, J = 6.8 Hz, 4H).

**2-[4-(4,4'-Dimethoxytriphenylmethoxy)but-1-yn-1-yl]-7-(4-hydroxyhex-1-yn-1-yl)phenanthrene (3):**

(**2**) (314.1 mg, 1 mmol) was dissolved with dry THF (8.4 ml) and triethylamine (1.7 ml) under argon. 4,4'-Dimethoxytrityl chloride (DMT-Cl, 338.9 mg, 1 mmol) was added slowly to the solution. The reaction mixture was stirred at room temperature under argon for 4 hours. After the reaction, it was diluted with dichloromethane (50 ml, HPLC quality), washed with 10% citric acid (50 ml) and saturated NaCO<sub>3</sub>H (50 ml). The organic phase was dried with potassium carbonate, filtered and evaporated. A column chromatography (hexane/ethyl acetate/triethylamine 1:1:0.02, loading as a liquid) was made and the collected fractions were evaporated. This gave a white/yellowish foam (245,8 mg, 40%).

**Analytical data for (3):**

$^1\text{H-NMR}$  (300 MHz, DMSO)  $\delta$  8.77 (dd,  $J = 8.9, 6.5$  Hz, 2H), 8.06 (t,  $J = 1.9$  Hz, 2H), 7.84, 7.66 (ddd,  $J = 8.7, 3.0, 1.9$  Hz, 4H), 7.50 – 7.44 (m, 2H), 7.32 (dd,  $J = 8.3, 4.5$  Hz, 6H), 7.23 (t,  $J = 7.3$  Hz, 1H), 6.90 (d,  $J = 8.9$  Hz, 4H), 4.95 (t,  $J = 5.6$  Hz, 1H), 3.73, 3.68 – 3.59 (m, 8H), 3.19 (t,  $J = 6.6$  Hz, 2H), 2.78 (t,  $J = 6.5$  Hz, 2H), 2.63 (t,  $J = 6.8$  Hz, 2H).

**4-(7-(4-(bis(4-methoxyphenyl)(phenyl)methoxy)but-1-yn-1-yl)phenanthren-2-yl)but-3-yn-1-yl (2-cyanoethyl) diisopropylphosphoramidite (4):**

(3) (211.7 mg, 0.34 mmol) was dissolved in dichloromethane (3.1 ml, HPLC quality and filtered through aluminium oxide) under argon. After addition of *N,N*-Diisopropylethylamin (DIPEA) (0.3 ml), 2-cyanoethyl-*N,N*-diisopropylchlorophosphoramidite (PAM-Cl, 0.09 ml, 0.36 mmol) was added. The mixture was stirred for 2 hours at room temperature under argon. The solution was evaporated and purified by a flash chromatography (hexane/EtOAc/ $\text{NEt}_3$  7:3:0.1, loading as liquid and a very short column). The fractions were collected, evaporated and it gave a white a bit oily foam (194 mg, 69%).

**Analytical data for (4):**

$^{31}\text{P}$  (121 MHz, DMSO)  $\delta$  147.16



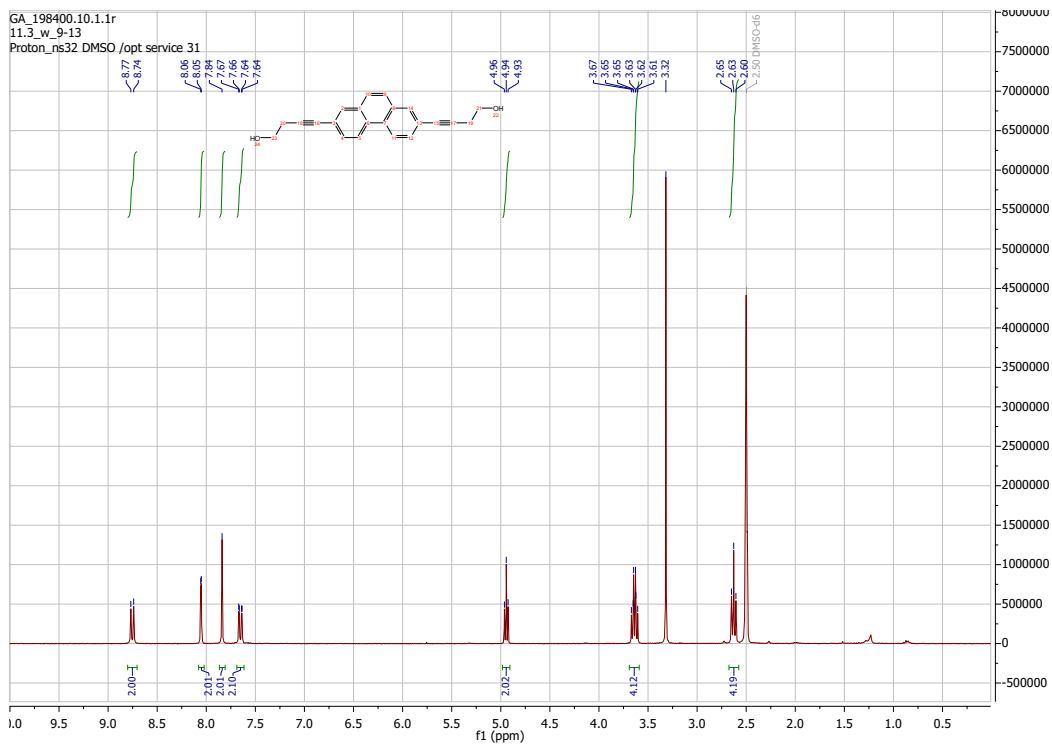


Figure B.19.: <sup>1</sup>H-NMR of (2).

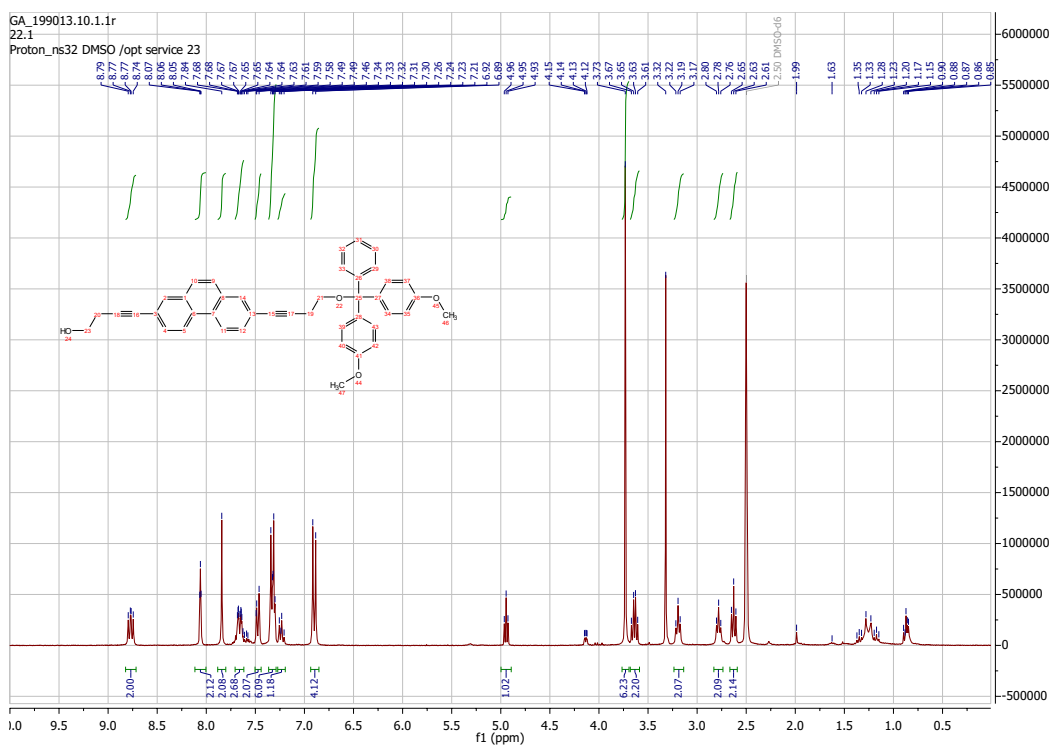
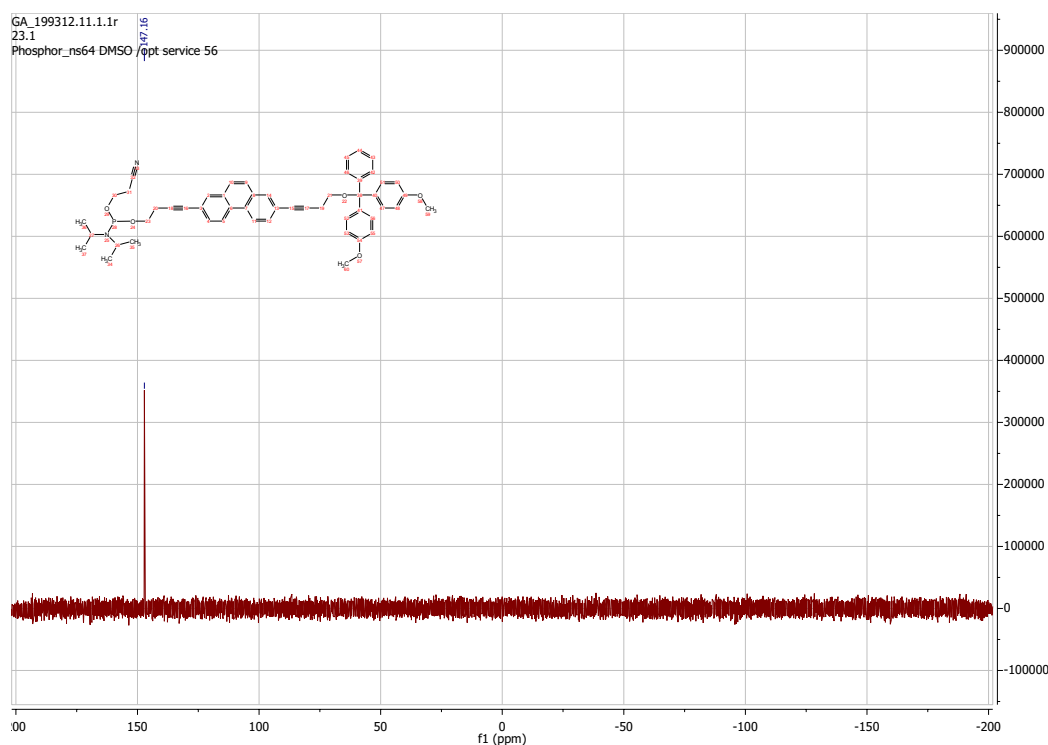


Figure B.20.: <sup>1</sup>H-NMR of (3).

Figure B.21.:  $^{31}\text{P}$ -NMR of (4).

### 2,7-Phanthrene-modified solid support

(3) (30.5 mg, 0.05 mmol) was dissolved with dichloromethane (0.25 ml, HPLC quality and filtered through aluminium oxide). Succinic anhydrid (5 mg) and DMAP (9.2 mg) were added. The mixture was stirred at room temperature for about 4.5 h. It was diluted with dichloromethane (10 ml, HPLC quality and filtered through aluminium oxide), washed with 10% citric acid and brine. Dried with magnesium sulfatate, filtered and the solvent was removed in vacuo. It was dissolved with acetonitrile (5 ml) under argon, 3.7 ml (0.0369 mmol of ester) of this solution was added to a round bottom flask with LCAA-CPG (300.3 mg, loading: 0.0246 mmol) and HBTU (28.1 mg). 1-methylimidazol (12  $\mu\text{l}$ ) was added, the suspension was argonized and it was shaken overnight. The solid support was filtered and washed with dichloromethane (HPLC quality and filtered through aluminium oxide). The solid support was added to DMAP (30.3 mg) and a mixture of pyridine/acetic acid anhydrid 3:1 (2.4 ml). The suspension was shaken for 2 h. It was filtered and washed with dichloromethane (HPLC quality and filtered through aluminium oxide). The solid support was collected in a small flask.

### Determination of the loading:

The solid support (2.3mg) was mixed with 3% TCA (10 ml). The absorption was measured, using  $\epsilon^{498}=70000 \text{ M}^{-1} \cdot \text{cm}^{-1}$  for single phenanthrene unit.

### Solid-phase Synthesis

The Solid-phase oligonucleotide synthesis was carried out by using compound 2,7-dialkynyl phenanthrene phosphoramidite as a building block for the oligomer **DNA-Phe<sub>5</sub>**. The standard procedure described in the reference<sup>29</sup> was used. The synthesis was done on the Applied Biosystems 394 DNA/RNA synthesizer using phenanthrene-loaded controlled pore glass (CPG) support (synthesis according to<sup>101</sup>). The average stepwise yield was between 94% and 100%.

The cleavage of **DNA-Phe<sub>5</sub>** and the single strand DNA were done with 28 - 30% ammonium hydroxide overnight at 55 °C in a closed vial with strong shaking (600 rpm). After the cleavage, the supernatant were collected in a 12 ml round-bottom tube. The solid supports were washed 3 times with 1ml MilliQ/ethanol 1:1 and each time they were centrifuged (20 °C, 13000 rpm, for 3 min). After centrifugation, the supernatant were collected in the respective round-bottom tube again and the oligos were lyophilized.

### HPLC Purification

After the solid-phase synthesis and the cleavage, **DNA-Phe<sub>5</sub>** has to be purified with HPLC (Dr.Maisch GmbH, ReproSil 100 C18, Lichrospher 100 RP-18, 5 $\mu\text{m}$ , 250 x 4mm). For the purification 0.1M TEAA /acetonitrile 80:20 were used; 1 ml/min; T = 40 °C; **DNA-Phe<sub>5</sub>**: B[%] ( $t_R$  [min]) = 50 (22); 50 (24); 100 (26); 100 (28); 0 (32). The purities were determined with ESI mass spectrometry. Expected mass: 8080.563 g/mol, measured 8081.411 g/mol.

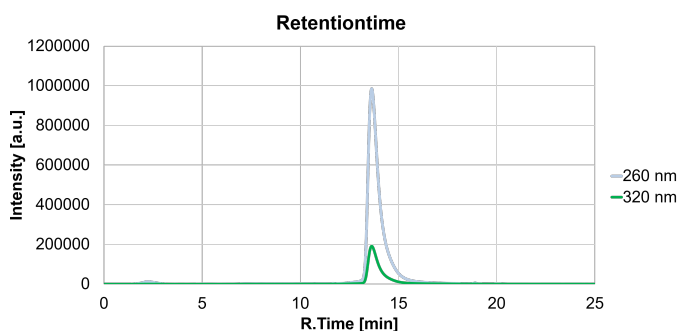


Figure B.22.: HPLC trace of **DNA-Phe<sub>5</sub>**.

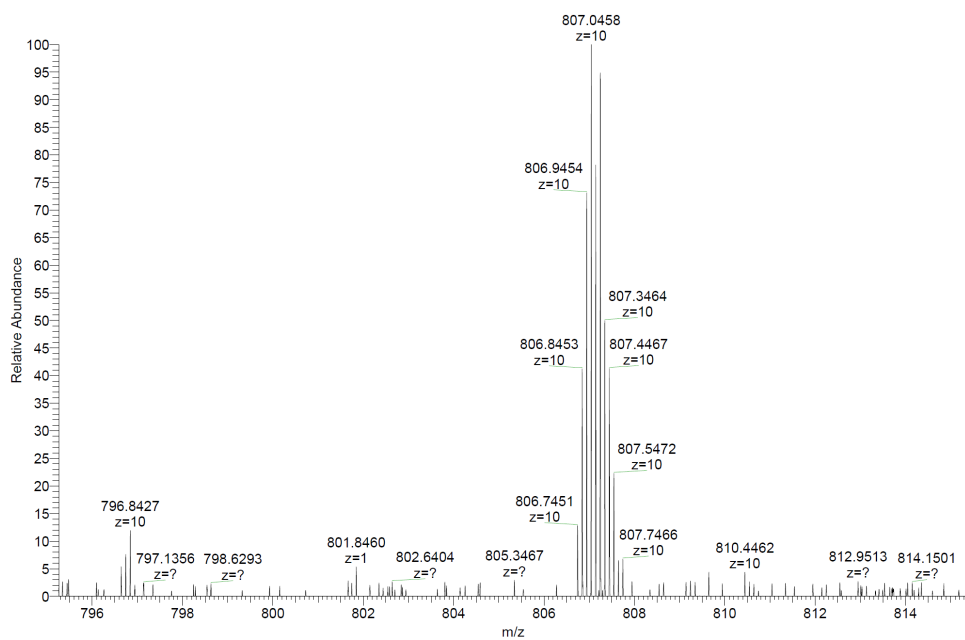


Figure B.23.: Mass spectrum of **DNA-Phe<sub>5</sub>**.

**DNA-Phe<sub>5</sub>** was dissolved with MilliQ. Determination of the concentrations were achieved by using a value of  $\epsilon^{260}=471600 \text{ M}^{-1}\cdot\text{cm}^{-1}$ .

---

## C. Appendix Chapter 4

### Spectra Data

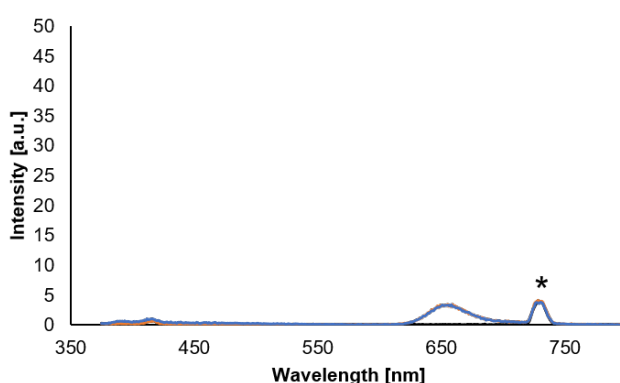


Figure C.1.: Emission spectra of **DNA-Dyomics630** (blue). After irradiation at 365 nm for 30min (orange). Condition: 0.7  $\mu\text{M}$  **DNA-R-Py<sub>7</sub>**, 10 mM sodium phosphate buffer (ph 7), 100 mM NaCl at 20°C;  $\lambda_{\text{exc}}$ . 365 nm, 20°C; excitation slit: 5 nm, emission slit: 5 nm. \* in the spectrum marks a second-order diffraction.

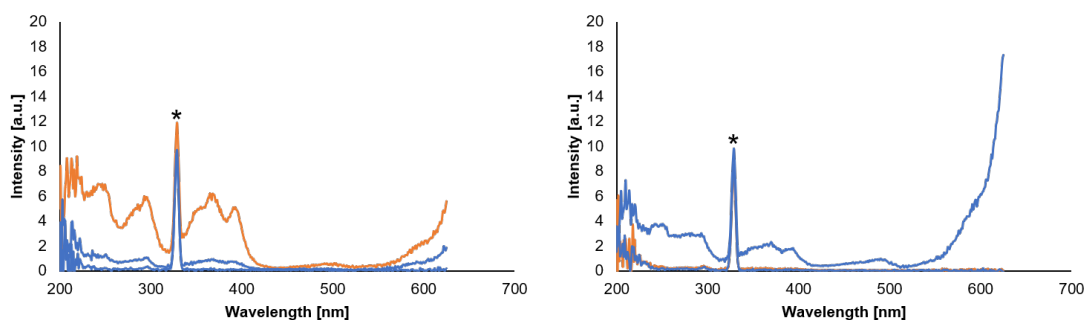


Figure C.2.: Excitation spectra of preformed **DNA-R-Py<sub>7</sub>** (dark blue). Left: Addition of 10% **DNA-Dyomics630** (dark blue) then irradiation at 365 nm for 30min (orange). Right: Irradiation at 365 nm for 30min (dark blue) then addition of 10% **DNA-Dyomics630** (orange). Conditions: see Figure C.1,  $\lambda_{\text{ex}}$  657 nm, 20°C. Excitation slit: 5 nm, emission slit: 5 nm. \* in the spectrum marks a second-order diffraction.

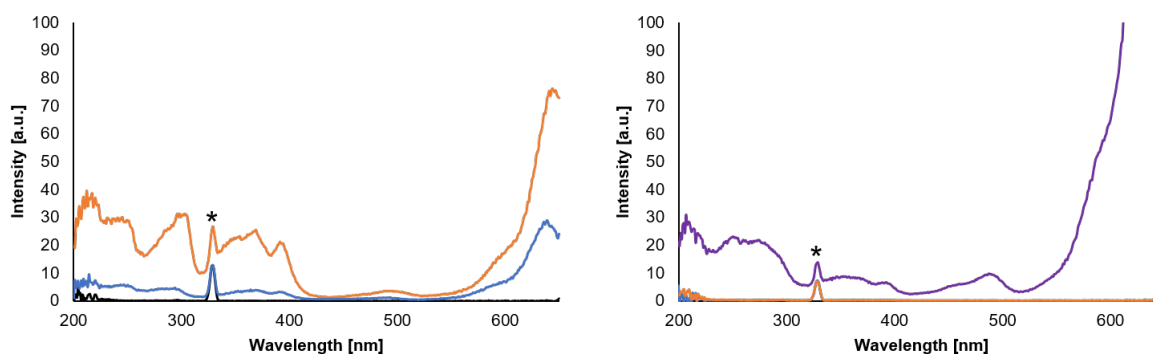


Figure C.3.: Excitation spectra of preformed **DNA-R-Py<sub>7</sub>** (black). Left: Addition of 100% **DNA-Dyomics630** (dark blue) then irradiation at 365 nm for 30min (orange). Right: Irradiation at 365 nm for 30min (orange) then addition of 100% **DNA-Dyomics630** (violet). Conditions: see Figure C.2. \* in the spectrum marks a second-order diffraction.

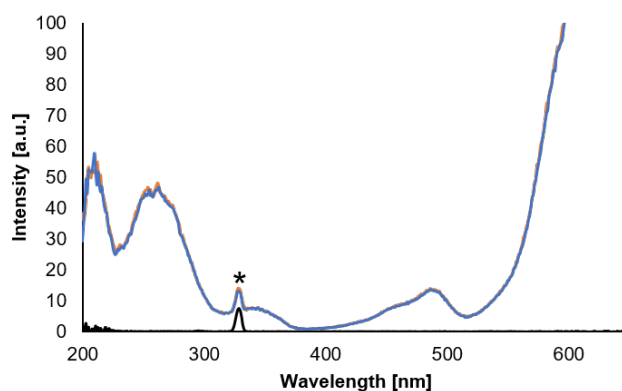


Figure C.4.: Excitation spectra of **DNA-Dyomics630**. Without **DNA-Dyomics630** (black), addition of 100% **DNA-Dyomics630** (dark blue) then irradiation at 365 nm for 30min (orange). Conditions: see Figure C.2. \* in the spectrum marks a second-order diffraction.

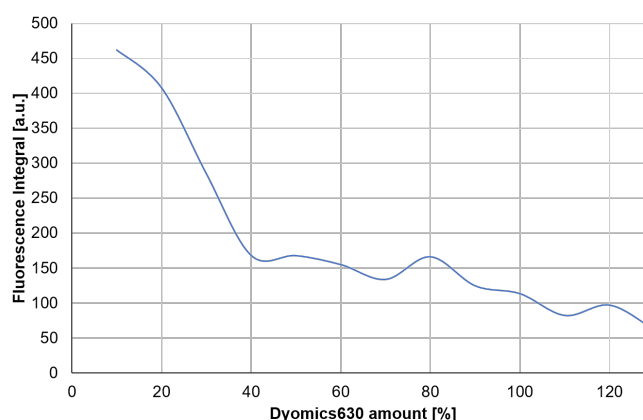


Figure C.5.: Development of the difference of the fluorescence integral of the stepwise addition of **DNA-Dyomics630**.

## Synthesis of the Photocleaver Building Block

### **(5-(3-(3-Hydroxymethyl-4-nitro-phenoxy)-propoxy)-2-nitro-phenyl)-methanol (26):**

3-Hydroxymethyl-4-nitro-phenol (1013.9 mg, 5.99 mmol) was dissolved in DMF (13 ml) under argon.  $K_2CO_3$  (994.8 mg), potassium iodide (104,8 mg) and 1,3-dibromopropane (0.28 ml) were added. The reaction mixture was stirred for 3 hours at 90°C under argon with reflux cooling. The cooled down solution was poured into distilled water (70 ml). The precipitate was filtered off with a filter crucible, washed with distilled water, saturated aqueous  $NaHCO_3$  solution and twice with distilled water. The gave a white/yellowish solid (883.8 mg, 87%).

#### **Analytical data for (26):**

$^1H$ -NMR (300 MHz, DMSO)  $\delta$  8.13 (d, J = 9.1 Hz), 7.37 (d, J = 2.8 Hz), 7.06 (dd, J = 9.1, 2.9 Hz), 5.58, 4.85, 4.30 (t, J = 6.2 Hz), 2.27 (p, J = 6.3 Hz).

### **(5-(3-(3-(Bis-(4-methoxy-phenyl)-phenyl-methoxymethyl)-4-nitro-phenoxy)-propoxy)-2-nitro-phenyl)-methanol (27):**

**(26)** (1000.2 mg, 2.64 mmol) was dissolved in pyridine (25 ml) under argon. 4,4'-dimethoxytritylchloride (DMT-Cl, 895.9 mg) was dissolved in pyridine (11 ml) and then it was added to the **(26)** solution. The reaction mixture was stirred overnight at room temperature under argon. The reaction mixture was controlled by TLC (eluent: EtOAc/hexane 1:1). The reaction mixture was diluted with EtOAc (120 ml), washed with 10% citric acid (120 ml), saturated aqueous  $NaHCO_3$  (120 ml), distilled water (120 ml) and brine (120 ml). The organic phase was dried with  $K_2CO_3$  and filtered. The solution was evaporated and purified by a flash column chromatography (EtOAc/hexane 1:3 with 1%  $NEt_3$  and EtOAc/hexane 1:1 with 1%  $NEt_3$ ). The fractions were collected, evaporated and it gave a white foam (759.0 mg, 42%).

#### **Analytical data for (27):**

$^1H$ -NMR (300 MHz, DMSO)  $\delta$  8.23 – 8.05 (m, 2H), 7.70 (d, J = 2.8 Hz, 1H), 7.47 (d, J = 7.5 Hz, 2H), 7.41 – 7.27 (m, 6H), 7.21 (d, J = 7.2 Hz, 2H), 6.99 – 6.71 (m, 6H), 5.00 (s, 2H), 4.65 (s, 2H), 4.33 (t, J = 6.0 Hz, 4H), 3.78 (s, 6H), 2.54 (s, 1H), 2.40 (p, J = 6.0 Hz, 2H).

**Diisopropyl-phosphoramidous acid 5-(3-(3-(bis-(4-methoxy-phenyl)-phenyl-methoxymethyl)-4-nitro-phenoxy)propoxy)-2-nitro-benzyl ester 2-cyano-ethyl ester (28):**

(27) (317.9 mg, 0.47 mmol) was dissolved in dichloromethane (1.9 ml, HPLC quality and filtered through aluminium oxide) under argon. N,N-Diisopropylethylamin (DIPEA) (0.2 ml) and 2-cyanoethyl-N,N-diisopropylchlorophosphoramidite (PAM-Cl, 125.9 mg) were added to the solution. The reaction mixture was stirred for 3 hours at room temperature under argon. The reaction mixture was controlled by TLC (eluent: EtOAc/hexane 1:1). The solvent of the reaction was reduced by evaporation and purified by a flash column chromatography (EtOAc/hexane 3:7 with 1% NEt<sub>3</sub>, loading as liquid and short column). The fractions were collected, evaporated and it gave a white foam (234.0 mg, 57%).

**Analytical data for (28):**

<sup>1</sup>H-NMR (300 MHz, DMSO)  $\delta$  8.22 – 8.07 (m, 1H), 7.52 – 7.44 (m, 1H), 7.44 – 7.17 (m, 7H), 6.84 (t, J = 9.8 Hz, 3H), 5.26 – 5.03 (m, 1H), 4.65 (s, 1H), 4.32 (t, J = 6.1 Hz, 2H), 3.78 (s, 1H), 3.78 (s, 3H), 2.61 (t, J = 6.3 Hz, 1H), 2.40 (t, J = 6.0 Hz, 1H), 1.21 (d, J = 6.8 Hz, 6H). <sup>31</sup>P NMR (121 MHz, DMSO)  $\delta$  149.00 (s).

## **Synthesis of the pyrene building block**

**5,5'-(Pyrene-1,6-diyl)dipent-4-yn-1-ol (Py):**

1,6- dibromopyrene (**1**) (1.5 g, 4.17 mmol), bis(triphenylphosphine)palladium(II) chloride (68.1 mg, 0.097 mmol) and copper(I) iodide (10.3 mg, 0.054 mmol) were dissolved in dry THF (34.1 mL) under argon and heated to 80 °C under reflux. After addition of triethylamine (20.5 mL) and 4-pentyn-1-ol (1.55 mL, 16.7 mmol) to the mixture it was stirred at this temperature overnight. After cooling to room temperature, the solvent was filtered through celite and removed under reduced pressure. Then it was dissolved in ethyl acetate (100ml), washed with 10% citric acid and saturated carbonated. The organic phase was dried with sodium sulfated and was filtered. A column chromatography (CH<sub>2</sub>Cl<sub>2</sub>/PhMe/MeOH 87:10:3) was made and the collected fractions were evaporated, it gave a yellow solid (610 mg, 39.7%).



**Analytical data for Py:**

$^1\text{H-NMR}$  (300 MHz,  $\text{CDCl}_3$ )  $\delta$  8.54 (d,  $J = 9.1$  Hz, 2H), 8.29 (d,  $J = 8.5$  Hz, 4H), 8.13 (d,  $J = 8.0$  Hz, 2H), 4.64 (t,  $J = 5.2$  Hz, 1H), 3.66 (q,  $J = 6.2, 6.1$  Hz, 2H), 2.80 (t,  $J = 7.0$  Hz, 2H), 1.86 (p,  $J = 6.8$  Hz, 2H).

**5-(6-(5-(Bis(4-methoxyphenyl)(phenyl)methoxy)pent-1-ynyl)pyren-1-yl)pent-4-yn-1-ol (2):**

Solid 4,4'-dimethoxytrityl chloride (560.9 mg, 1.66 mmol) was added in portion to a solution of **Py** (610 mg, 1.66 mmol) in pyridine (13 mL). The mixture was stirred overnight at room temperature. Dichloromethane (100 ml) was added to the mixture, washed with 10% citric acid and sodium hydrogen carbonate. The organic phase was dried with potassium carbonate and was filtered. A column chromatography ( $\text{CH}_2\text{Cl}_2/\text{MeOH}/\text{NEt}_3$  97/2/1) was made. The fractions containing **(2)** were collected and evaporated. Dichloromethane (filtered through ALOX) was added and the solution was evaporated, but not fully dry. Then it was put on the high vacuum. This gave a yellow foam (540mg, 48.6%).

**Analytical data for (2):**

$R_f = 0.75$  ( $\text{CH}_2\text{Cl}_2/\text{MeOH}/\text{NEt}_3$  97/2/1);  $^1\text{H NMR}$  (300 MHz, DMSO)  $\delta$  8.50 (d,  $J = 9.0$  Hz, 1H), 8.35 (d,  $J = 9.1$  Hz, 1H), 8.32 – 8.22 (m, 3H), 8.16 (dd,  $J = 14.9, 8.5$  Hz, 2H), 8.01 (d,  $J = 7.9$  Hz, 1H), 7.54 – 7.08 (m, 9H), 6.83 (d,  $J = 8.4$  Hz, 4H), 4.64 (t,  $J = 5.3$  Hz, 1H), 3.76 – 3.53 (m, 8H), 2.81 (t,  $J = 6.8$  Hz, 2H), 2.73 (t,  $J = 7.2$  Hz, 2H), 2.00 (d,  $J = 7.3$  Hz, 2H), 1.86 (p,  $J = 6.7$  Hz, 2H).

**5-(6-(5-(Bis(4-methoxyphenyl)(phenyl)methoxy)pent-1-ynyl)pyren-1-yl)pent-4-ynyl 2-cyanoethyl diisopropylphosphoramidite (3):**

**(2)** (500 mg, 0.75 mmol) was dissolved in  $\text{CH}_2\text{Cl}_2$  (15 mL). After addition of DIPEA (380  $\mu\text{L}$ , 2.24 mmol), 2-cyanoethyl-N,N-diisopropylchlorophosphoramidite (229.3 mg, 0.97 mmol) was added. The mixture was stirred for 5 h at room temperature. The solution was evaporated and purified by a flash chromatography (hexane/ EtOAc/ $\text{NEt}_3$  50/49/1). The fractions were collected and it gave 93.1 mg (14.3%) of yellow solid **(3)**.

**Analytical data for (3):**

$R_f = 0.72$  (hexane/ EtOAc/ $\text{NEt}_3$  50/49/1);  $^1\text{H}$  NMR (300 MHz, DMSO)  $\delta$  8.55 (d,  $J = 9.0$  Hz, 1H), 8.43 (d,  $J = 9.0$  Hz, 1H), 8.14 – 7.93 (m, 6H), 7.50 (d,  $J = 7.6$  Hz, 2H), 7.43 – 7.33 (m, 4H), 7.28 (d,  $J = 7.0$  Hz, 1H), 7.25 – 7.12 (m, 2H), 6.84 – 6.72 (m, 4H), 4.01 – 3.77 (m, 4H), 3.67 (s, 8H), 3.36 (t,  $J = 6.0$  Hz, 2H), 2.80 (dt,  $J = 13.5, 7.0$  Hz, 4H), 2.65 (t,  $J = 6.5$  Hz, 2H), 2.16 – 2.01 (m, 4H), 1.22 (dd,  $J = 6.8, 4.0$  Hz, 12H).  $^{31}\text{P}$  NMR (121 MHz, DMSO)  $\delta$  147.84 (s).

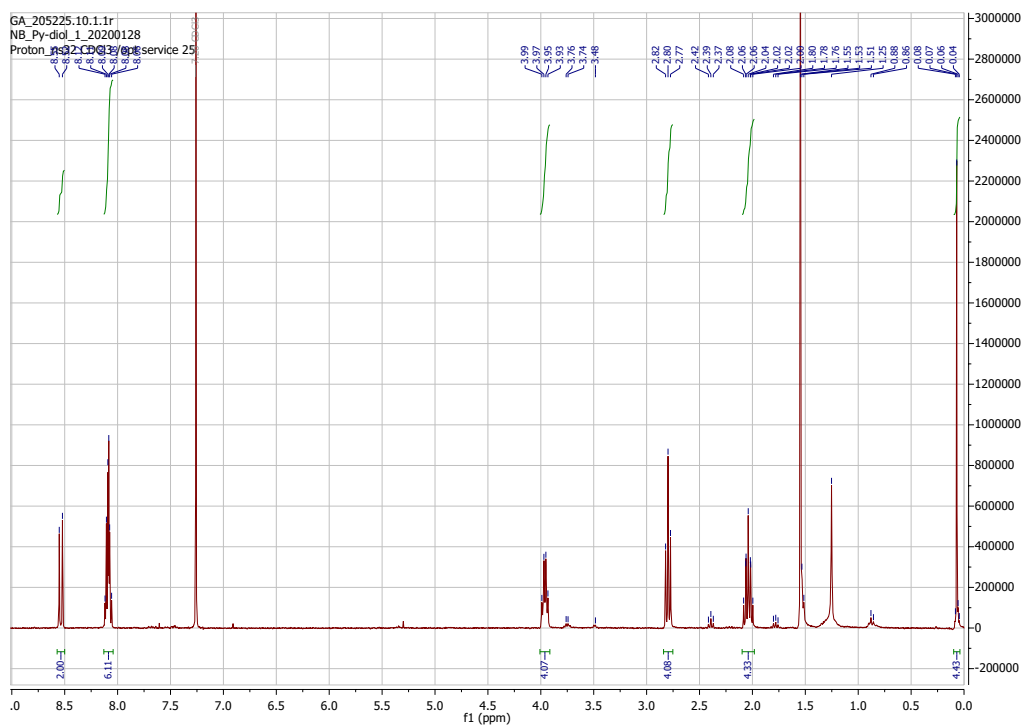


Figure C.6.:

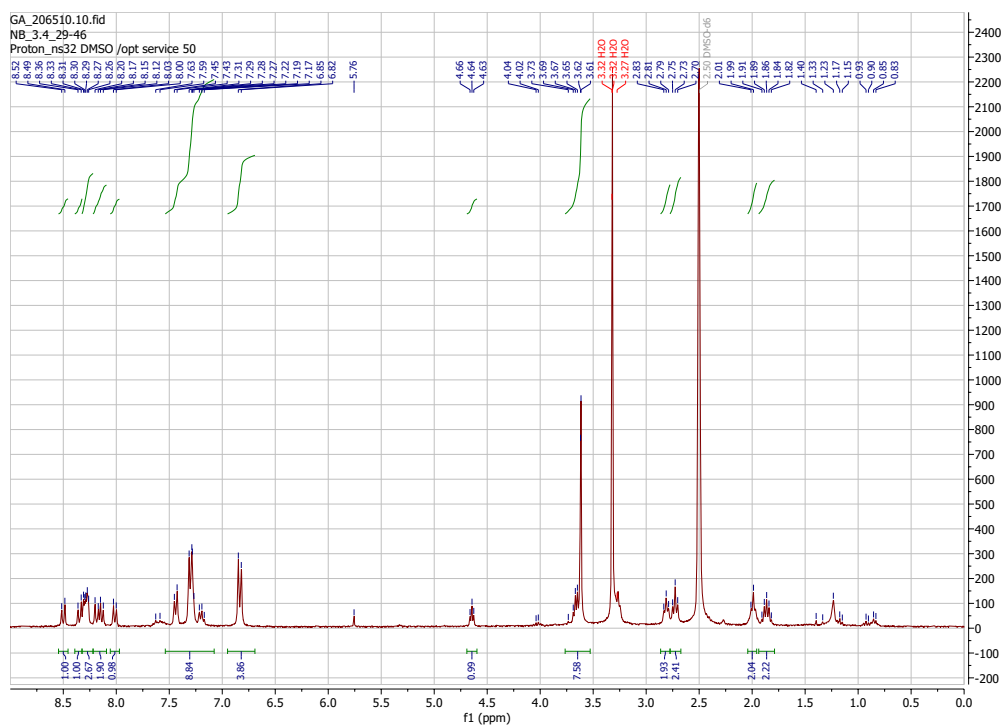


Figure C.7.:

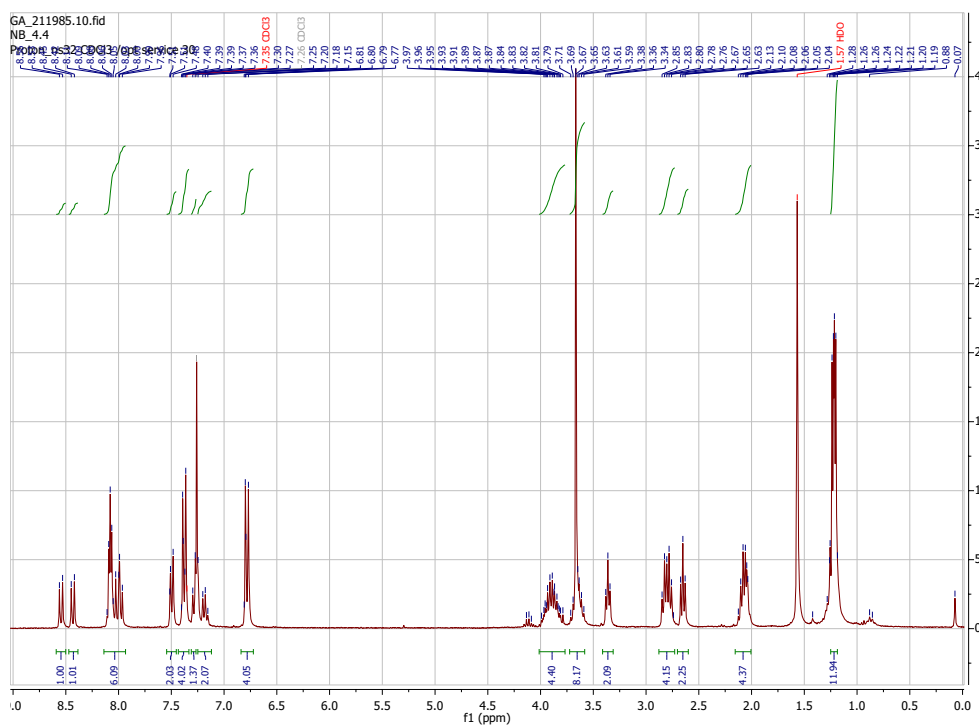


Figure C.8.:

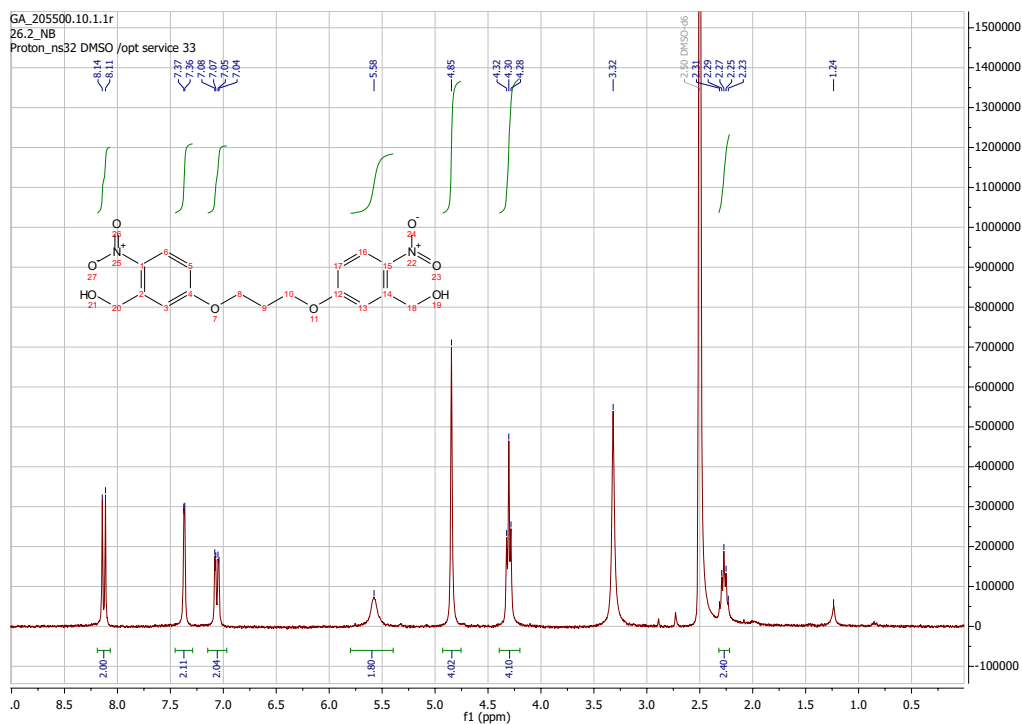


Figure C.9.:

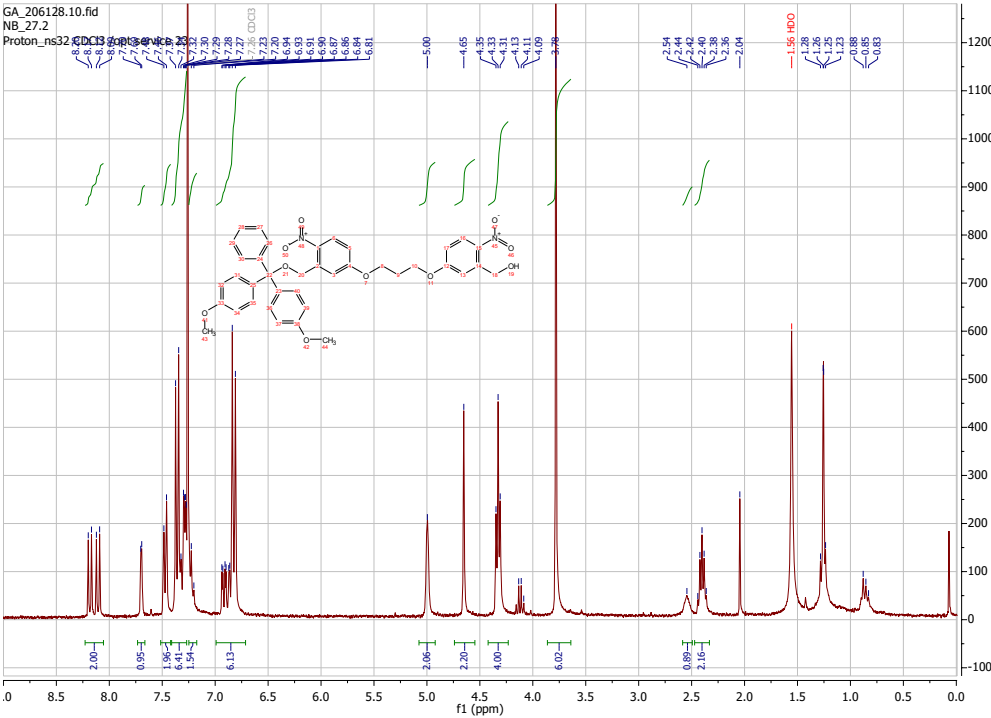


Figure C.10.:

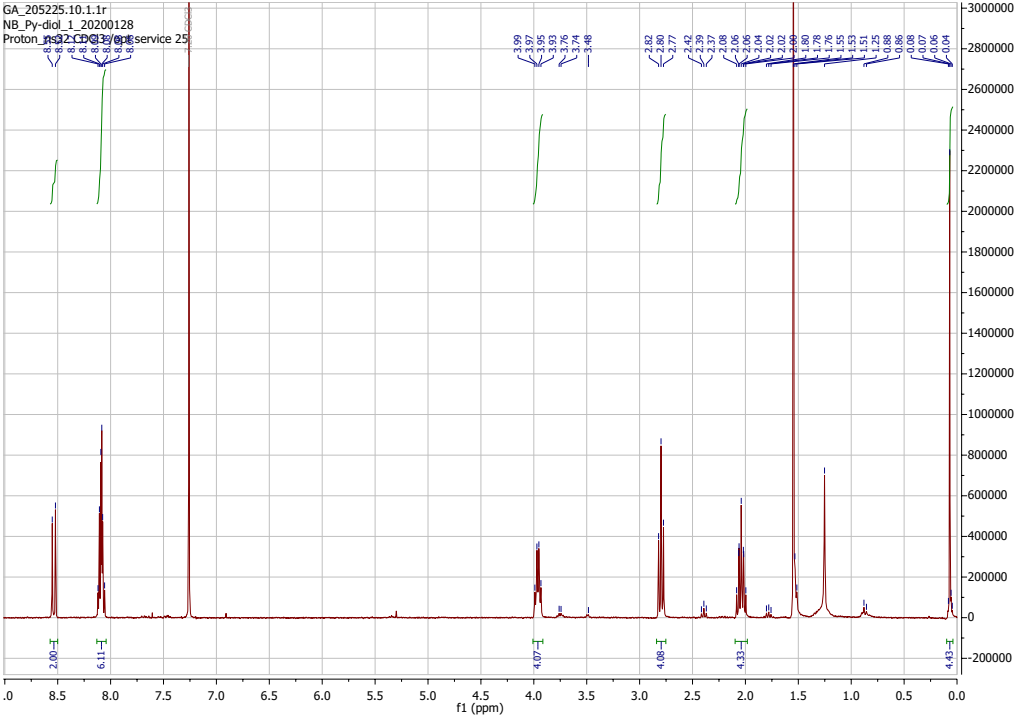


Figure C.11.:

## DNA Synthesis

The 1,6-dialkynylpyrene phosphoramidite (**3**) and the photocleaver (**28**) were used for the solid-phase oligonucleotide synthesis. The standard procedure as described was used.<sup>29</sup> The synthesis was done on the Applied Biosystems 394 DNA/RNA synthesizer using pyrene-loaded controlled pore glass (CPG) support (synthesized in previous study, see appendix A). Reverse phosphoramidite nucleobases were used. The average stepwise yield was between 93% and 100%.

The cleavage of oligomer were done with 28.0-30.0% ammonium hydroxide solution for 16 hours at 55 °C in a closed vial with strong shaking. After the cleavage the oligomer were centrifuged (20 °C, 13000 rpm, for 3 min). After centrifugation, the supernatant was collected and the solid support was washed 3 times with 1ml MilliQ/ethanol 2:8. The crude oligomer were lyophilized overnight.

## HPLC Purification

After the solid-phase synthesis and the cleavage, the compounds have to be purified with HPLC (LiChroCART 250-4; LiChrospher 100, RP-18, 5  $\mu$ m column, Merck). For the purification HFIP buffer (ph 8, 25mM HFIP, 2.1mM Et<sub>3</sub>N); 1 ml/min; T = 50 °C; B[%] (t<sub>R</sub> [min]) = 10 (0); 40 (24); 100 (25); 100 (28); 10 (30); 10 (39). The oligomer were washed 2 times with MillQ water. The purities were determined with ESI mass spectroscopy.

Table C.1.: Calculated and measured mass of **DNA-R-Py<sub>7</sub>** and **DNA-Py<sub>7</sub>**.

Oligomer	Calculated	Measured
DNA-R-Py <sub>7</sub>	6455.9926	6456.3466
DNA-Py <sub>7</sub>	6015.9222	6016.2509

The oligomer was dissolved in 8:2 MilliQ/ethanol. The stock solution were diluted and the determination of the concentrations was achieved by using a value of  $\epsilon^{365}=35000 \text{ M}^{-1} \cdot \text{cm}^{-1}$  in ethanol for single pyrene unit.

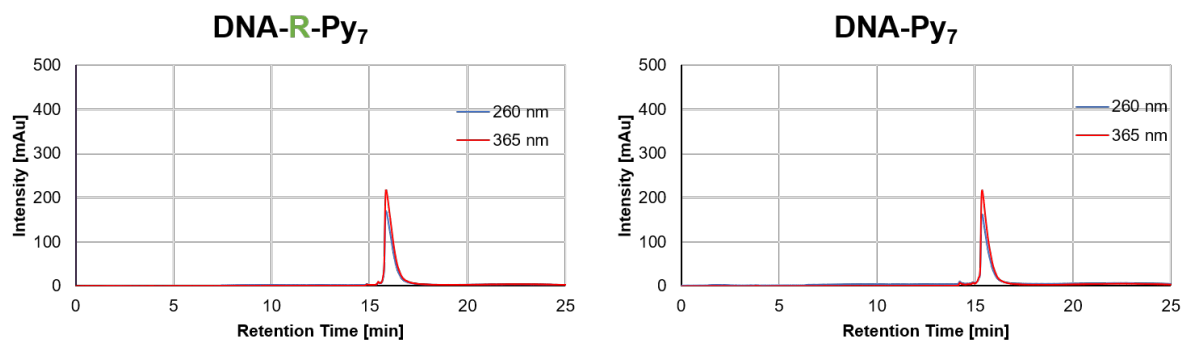


Figure C.12.: HPLC trace of **DNA-R-Py<sub>7</sub>**(left) and **DNA-Py<sub>7</sub>** (right).

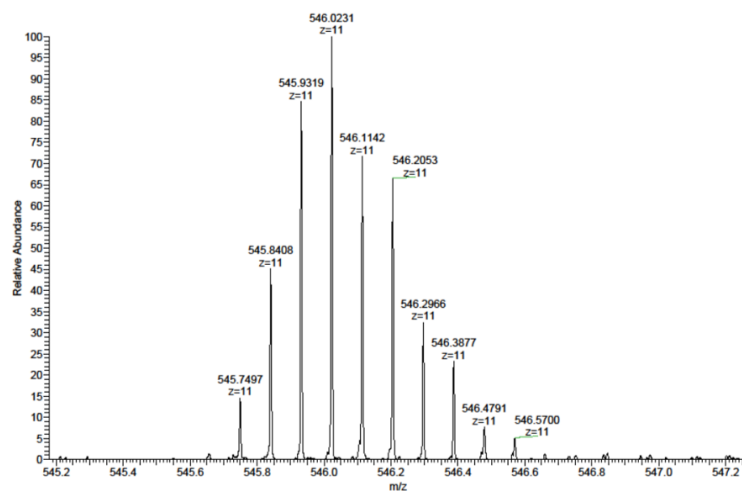


Figure C.13.: Mass spectrum of **DNA-R-Py<sub>7</sub>**.

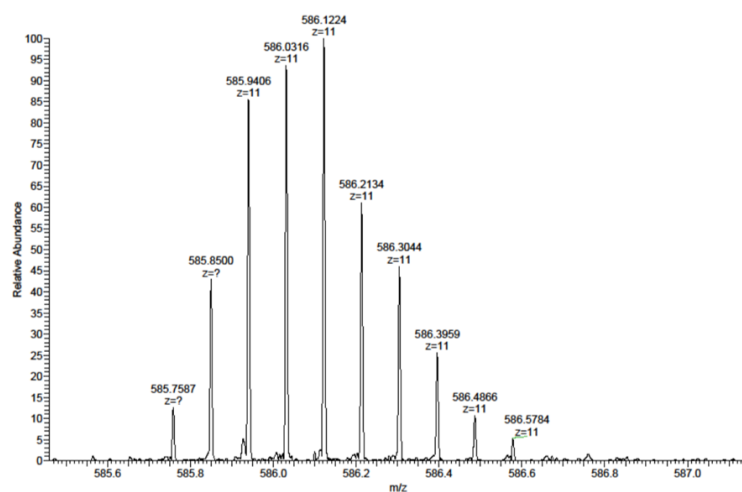


Figure C.14.: Mass spectrum of **DNA-Py<sub>7</sub>**.

## D. Appendix Chapter 5

### Spectroscopic Data

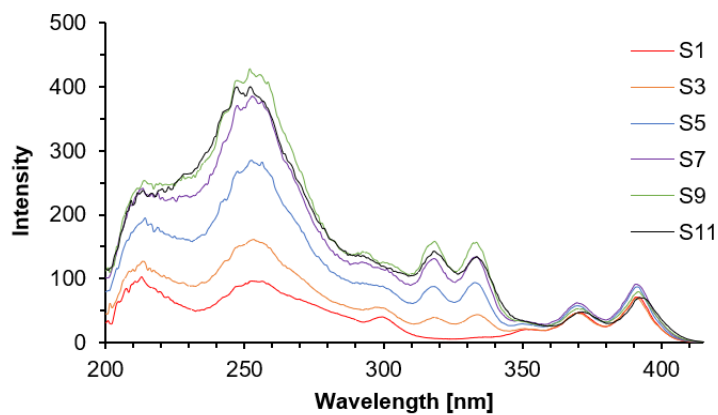


Figure D.1.: Excitation spectra of the strands **S1**, **S3**, **S5**, **S7**, **S9**, **S11**. Conditions: 0.5  $\mu\text{M}$  of the strand, 10mM sodium phosphate buffer (pH 7.0), 400mM NaCl,  $\lambda_{\text{em}}$  425 nm, 20°C. Excitation slit: 2.5 nm, emission slit: 5 nm.

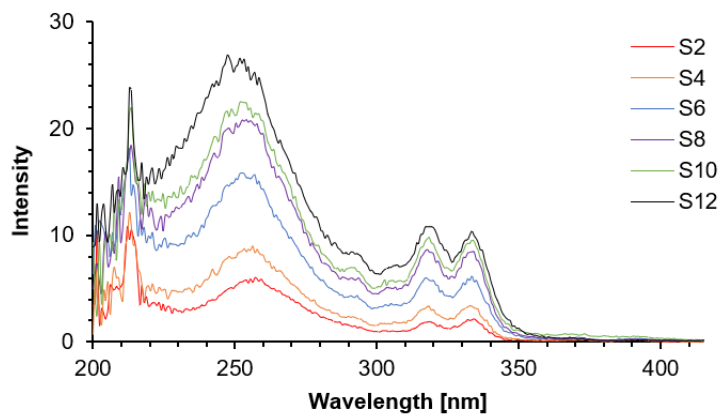


Figure D.2.: Excitation spectra of the strands **S2**, **S4**, **S6**, **S8**, **S10**, **S12**. Conditions: 0.5  $\mu\text{M}$  of the strand, 10mM sodium phosphate buffer (pH 7.0), 400mM NaCl,  $\lambda_{\text{em}}$  425 nm, 20°C. Excitation slit: 2.5 nm, emission slit: 5 nm.



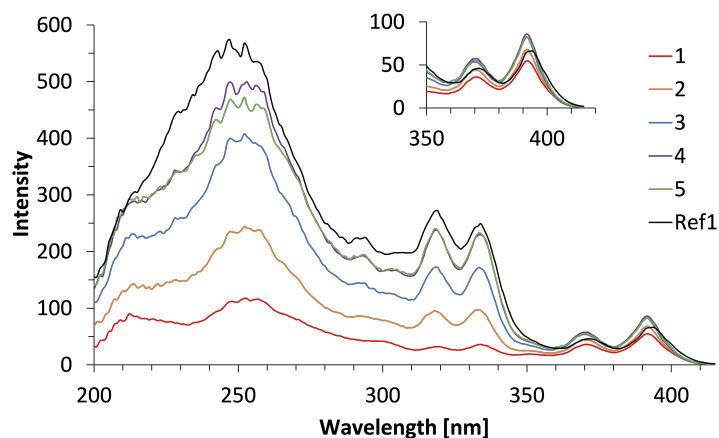


Figure D.3.: Excitation spectra of duplexes **1 – 5**, **Ref1**. Conditions: 0.5  $\mu\text{M}$  each strand, 10mM sodium phosphate buffer (pH 7.0), 400mM NaCl,  $\lambda_{\text{em}}$  425 nm, 20°C. Excitation slit: 2.5 nm, emission slit: 5 nm.

## Melting Curves

The duplexes were heated up to 80°C in the thermo-shaker for about 30 min before the cooling-heating curves were recorded. Absorption at 260 nm was monitored, where nucleobases, dialkynylpyrene and -phenanthrene absorb. Blue curve: Cooling stage (80 – 20°C), orange curve: heating stage (20 – 80°C). Conditions: Cooling/heating temp. rate= 0.5°C/min, 0.5  $\mu\text{M}$  each strand, 10mM sodium phosphate buffer (pH 7.0) and 400 mM NaCl.

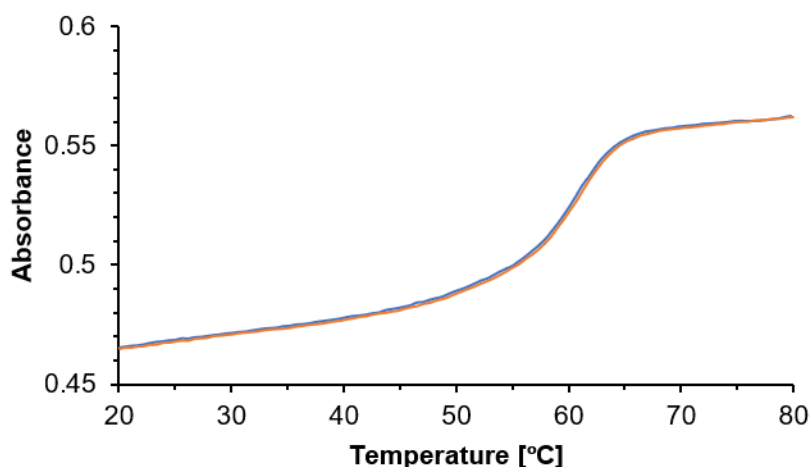


Figure D.4.: Cooling-heating curves of duplex **1**.

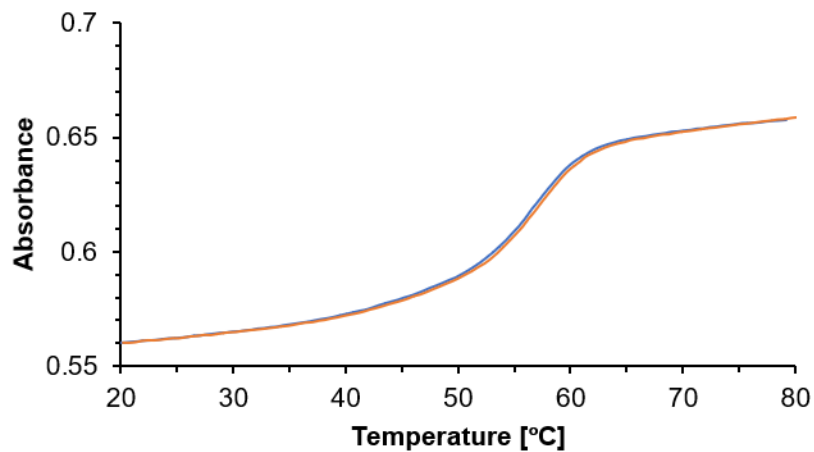


Figure D.5.: Cooling-heating curves of duplex 2.

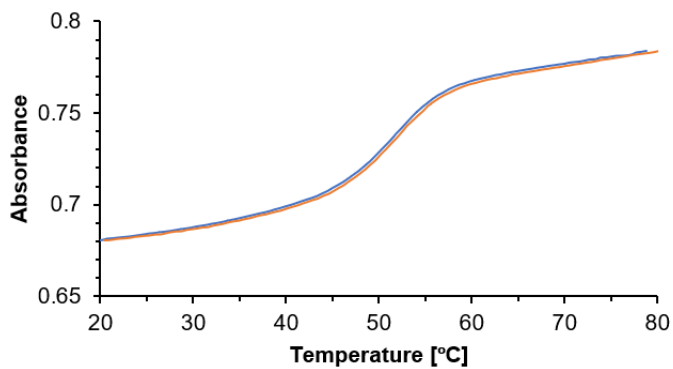


Figure D.6.: Cooling-heating curves of duplex 3.

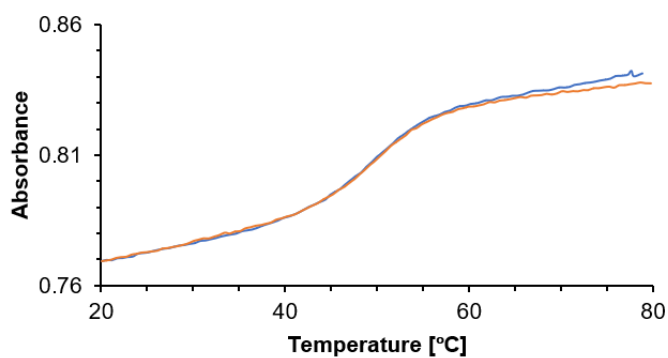


Figure D.7.: Cooling-heating curves of duplex 4.

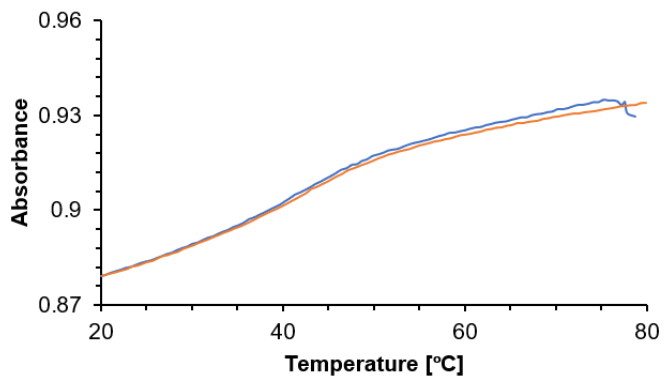


Figure D.8.: Cooling-heating curves of duplex 5.

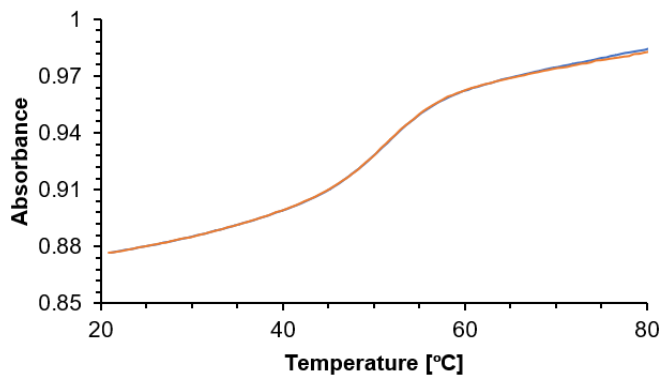


Figure D.9.: Cooling-heating curves of duplex 6.

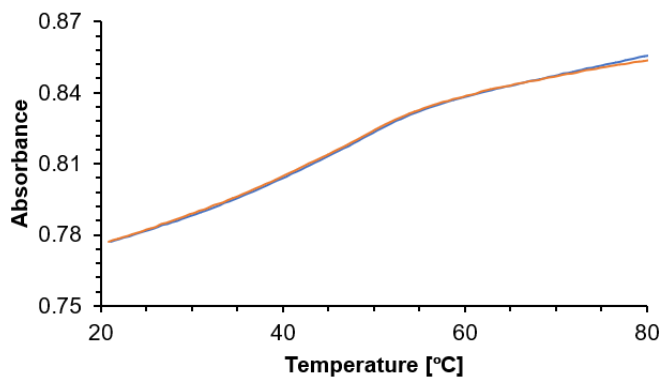
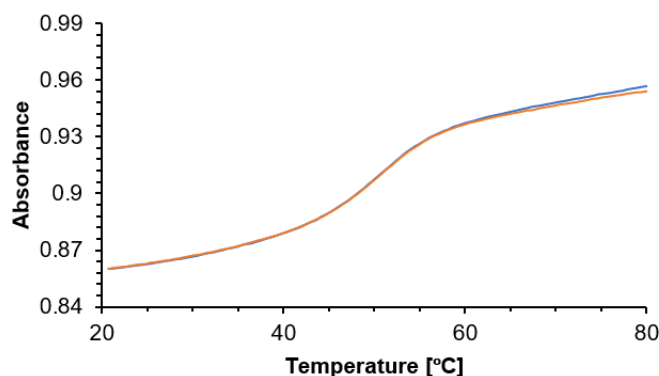


Figure D.10.: Cooling-heating curves of duplex 7.

Figure D.11.: Cooling-heating curves of duplex **8**.

## Synthesis

### Synthesis of the Synthesis of 1,8-dilakynylpyrene phosphoramidite

#### 4-(8-(4-(bis(4-methoxyphenyl)(phenyl)methoxy)but-1-yn-1-yl)pyren-1-yl)but-3-yn-1-yl (2-cyano-ethyl) diisopropylphosphoramidite (short: 1,8-dilakynylpyrene phosphoramidite):

4-(8-(4-(bis(4-methoxyphenyl)(phenyl)methoxy)but-1-yn-1-yl)pyren-1-yl)but-3-yn-1-ol (244.9 mg, 0.38 mmol, synthesized by Elena Grossenbacher) was dissolved in  $\text{CH}_2\text{Cl}_2$  (11 ml, HPLC quality and filtered through aluminium oxide). After addition of DIPEA (0.19 ml), 2-cyanoethyl-*N,N*-diisopropyl-chlorophosphoramidite (115.8 mg) was added. The mixture was stirred for 4 hours at room temperature under argon. The solution was evaporated and purified by a flash chromatography (hexane/EtOAc 1:1 with 1%  $\text{NEt}_3$ ). The fractions were collected and it gave 287.1 mg (91.1%) of **(1,8-dilakynylpyrene phosphoramidite)** green/yellowish oily foam.

#### Analytical data for (1,8-dilakynylpyrene phosphoramidite):

$^1\text{H-NMR}$  (300 MHz,  $\text{CDCl}_3$ )  $\delta$  8.70 – 8.53 (m, 2H), 8.15 – 7.96 (m, 6H), 7.62 – 7.52 (m, 2H), 7.49 – 7.40 (m, 4H), 7.36 – 7.27 (m, 2H), 7.25 – 7.18 (m, 1H), 6.89 – 6.78 (m, 4H), 4.08 – 3.79 (m, 5H), 3.77 (d,  $J = 1.3$  Hz, 6H), 3.67 (dt,  $J = 10.1, 6.8$  Hz, 2H), 3.46 (t,  $J = 6.7$  Hz, 2H), 2.96 (dt,  $J = 15.9, 6.8$  Hz, 4H), 2.62 (q,  $J = 6.1$  Hz, 2H), 1.22 (dd,  $J = 6.8, 4.0$  Hz, 12H).  $^{31}\text{P-NMR}$  (121 MHz,  $\text{CDCl}_3$ ) 148.29.

### **Synthesis of the 3,6-dilakynylphenanthrene phosphoramidite**

**4-(6-(4-(bis(4-methoxyphenyl)(phenyl)methoxy)but-1-yn-1-yl)phenanthren-3-yl)but-3-yn-1-yl (2-cyanoethyl) diisopropylphosphoramidite (short: 3,6-dilakynylphenanthrene phosphoramidite):**

4-(6-(4-(bis(4-methoxyphenyl)(phenyl)methoxy)but-1-yn-1-yl)phenanthren-3-yl)but-3-yn-1-ol (314.3 mg, 0.51 mmol, synthesized by Elena Grossenbacher) was dissolved in dichloromethane (4.6 ml) under argon. After addition of N,N-Diisopropylethylamin (DIPEA) (0.4 ml), 2-cyanoethyl-N,N-diisopropylchlorophosphoramidite (PAM-Cl, 146.5 mg) was added dropwise. The mixture was stirred for 3 hours at room temperature under argon. The solution was evaporated and purified by a flash chromatography (hexane/EtOAc 66:34 with 1% NEt<sub>3</sub>, loading as liquid and a very short column). The fractions were collected, evaporated and it gave a white a bit oily foam (394.2 mg, 95%).

#### **Analytical data for (3,6-dilakynylphenanthrene phosphoramidite):**

<sup>1</sup>H-NMR (300 MHz, CDCl<sub>3</sub>) δ 8.70 (d, J = 1.5 Hz, 2H), 7.78 (d, J = 8.2 Hz, 2H), 7.68 (s, 2H), 7.63 – 7.50 (m, 4H), 7.47 – 7.37 (m, 4H), 7.35 – 7.27 (m, 2H), 7.25 – 7.18 (m, 1H), 6.90 – 6.79 (m, 4H), 3.98 – 3.81 (m, 4H), 3.78 (s, 6H), 3.65 (dq, J = 10.2, 6.8 Hz, 2H), 3.37 (t, J = 7.0 Hz, 2H), 2.80 (dt, J = 11.1, 7.0 Hz, 4H), 2.69 – 2.60 (m, 2H), 1.29 – 1.15 (m, 17H). <sup>31</sup>P-NMR (121 MHz, CDCl<sub>3</sub>) 148.20, 139.04.

### **DNA Synthesis**

As already mentioned, a standard cyanoethyl phosphoramidite solid-phase synthesis protocol was used and beginning with nucleoside-loaded controlled pore glass (CPG) support. Cleavage and deprotection of the oligochromophores from the solid support was done by treatment with 28-30% NH<sub>4</sub>OH (aq) at 55°C overnight. The supernatants were collected, the solid support were washed two times with 1 ml H<sub>2</sub>O (MilliQ) and the crude oligomers were lyophilized.

## HPLC Purification

The crude oligomers were purified by reversed phase HPLC (Merck LiChroCART 250-4; LiChrospher 100, RP-18, 5  $\mu\text{m}$ ); solvent A: 0.1 M aqueous ammonium acetate; solvent B:  $\text{CH}_3\text{CN}$ ; 1 ml/min;  $T = 40^\circ\text{C}$ .

Table D.1.: HPLC solvent gradients used for the purification.

	Gradient 1	Gradient 2	Gradient 3
Time [min]	Solvent B in Solvent A [%]	Solvent B in Solvent A [%]	Solvent B in Solvent A [%]
0.01	0	0	0
2.00	0	0	5
22.00	30	40	50
24.00	100	100	100
26.00	100	100	100
28.00	0	0	0

The gradients were used as followed: **S1 - S4**: Gradient 1; **S5 and S6**: Gradient 2; **S7 - S15**: Gradient 3.

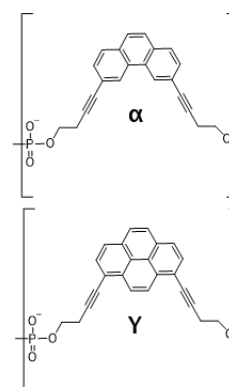
## Mass Spectra

Mass spectra **S1 - S12** are from Elena Grossenbacher (University of Bern, Department of Chemistry and Biochemistry, 2019).

The molecular mass of the oligomers were measured in negative ion mode in mixtures of water/acetonitrile/triethylamine.

Table D.2.: Calculated and measured masses of oligomer strands.

Strand	Sequence	Calculated mass	Measured mass
S1	5' GGC TAA YTA AAT TTA AAT CGC 3'	6524.1548	6524.0712
S2	3' CCG ATT $\alpha$ AT TTA AAT TTA GCG 5'	6482.1280	6482.0520
S3	5' GGC TAA Y $\alpha$ AAT TTA AAT CGC 3'	6587.0412	6587.1432
S4	3' CCG ATT $\alpha$ A $\alpha$ TTA AAT TTA GCG 5'	6554.0278	6554.1216
S5	5' GGC TAA Y $\alpha$ A $\alpha$ T TTA AAT CGC 3'	6649.9276	6649.1470
S6	3' CCG ATT $\alpha$ A $\alpha$ T $\alpha$ A AAT TTA GCG 5'	6625.9276	6625.1470
S7	5' GGC TAA Y $\alpha$ A $\alpha$ T $\alpha$ TA AAT CGC 3'	6721.8274	6722.1693
S8	3' CCG ATT $\alpha$ A $\alpha$ T $\alpha$ A $\alpha$ AT TTA GCG 5'	6688.8140	6689.1672
S9	5' GGC TAA Y $\alpha$ A $\alpha$ T $\alpha$ T $\alpha$ AAT CGC 3'	6784.7138	6785.2350
S10	3' CCG ATT $\alpha$ A $\alpha$ T $\alpha$ A $\alpha$ A $\alpha$ TTA GCG 5'	6760.7138	6760.2222
S11	5' GGC TAA Y $\alpha\alpha$ $\alpha\alpha$ T TTA AAT CGC 3'	6784.7138	6784.1983
S12	3' CCG ATT $\alpha\alpha\alpha$ $\alpha\alpha$ A AAT TTA GCG 5'	6760.7138	6761.2182



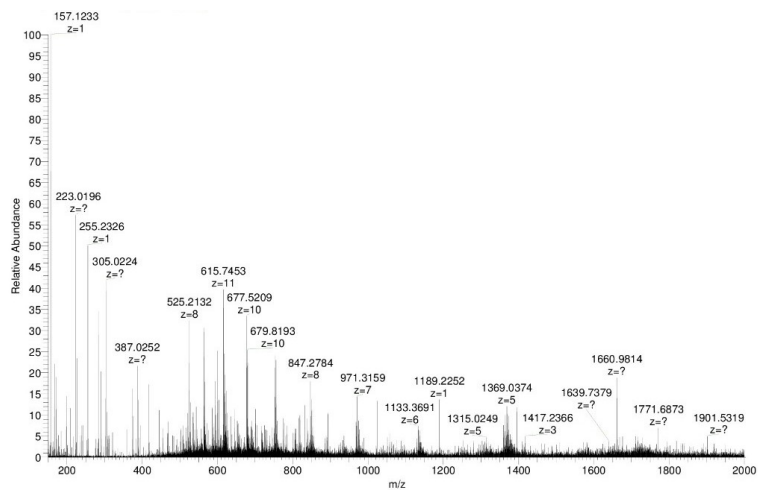


Figure D.12.: Mass spectrum of single strand S1.

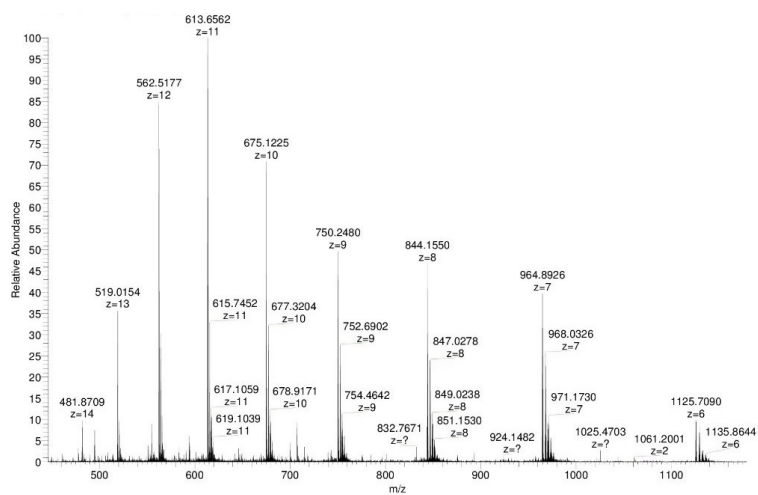


Figure D.13.: Mass spectrum of single strand S2.

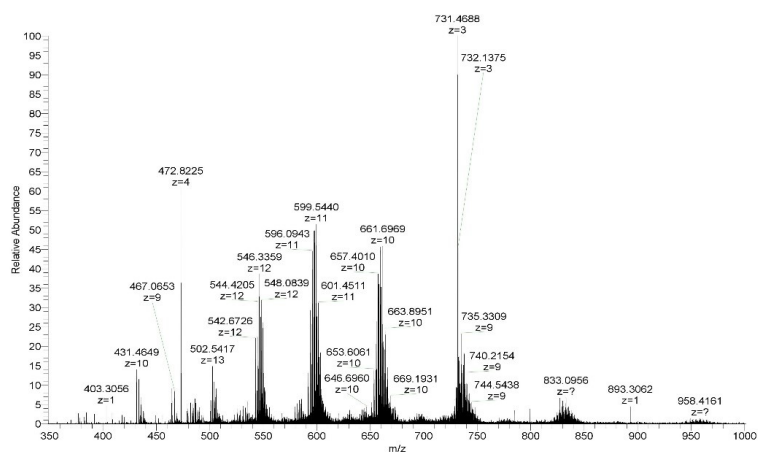


Figure D.14.: Mass spectrum of single strand S3.

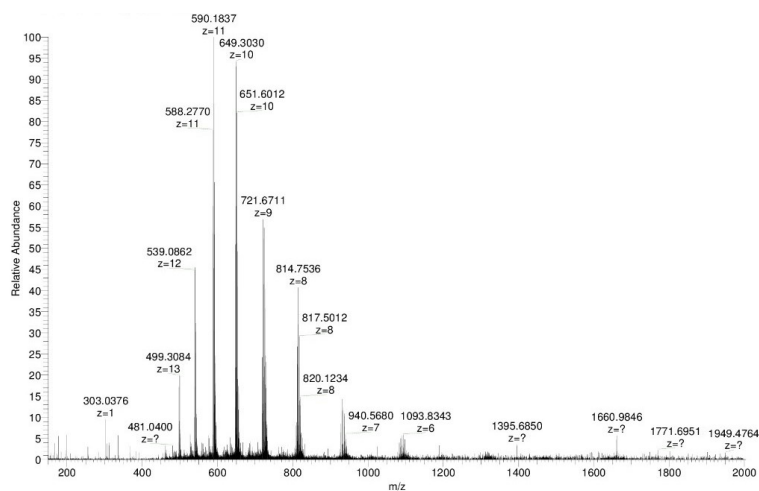


Figure D.15.: Mass spectrum of single strand S4.

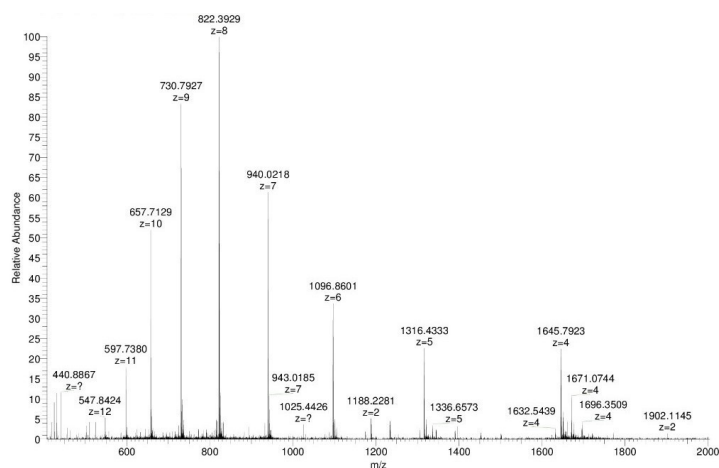


Figure D.16.: Mass spectrum of single strand S5.

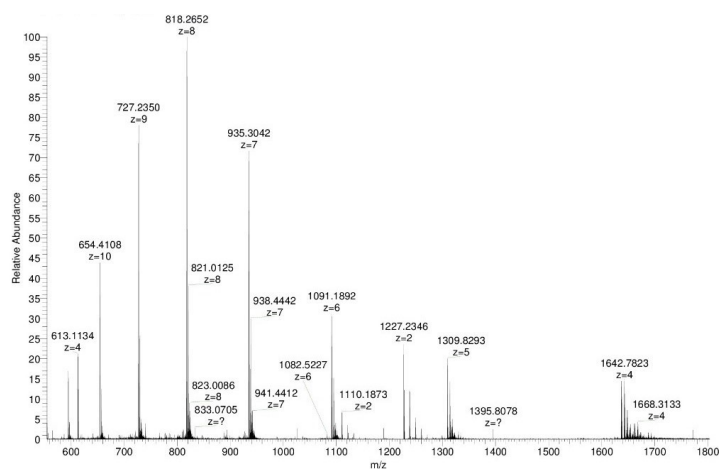


Figure D.17.: Mass spectrum of single strand S6.



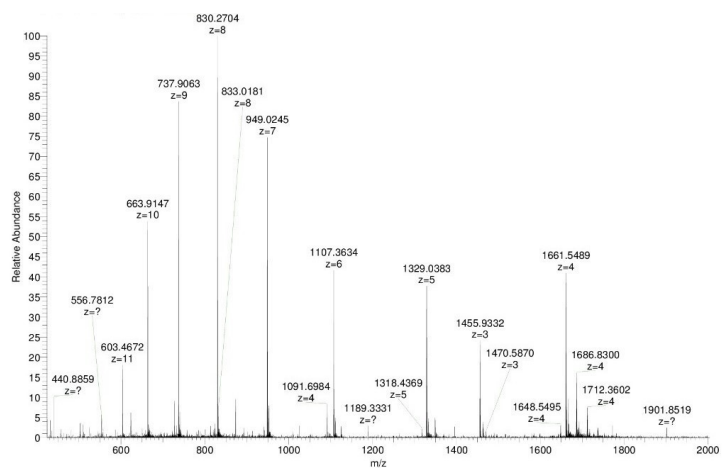


Figure D.18.: Mass spectrum of single strand S7.

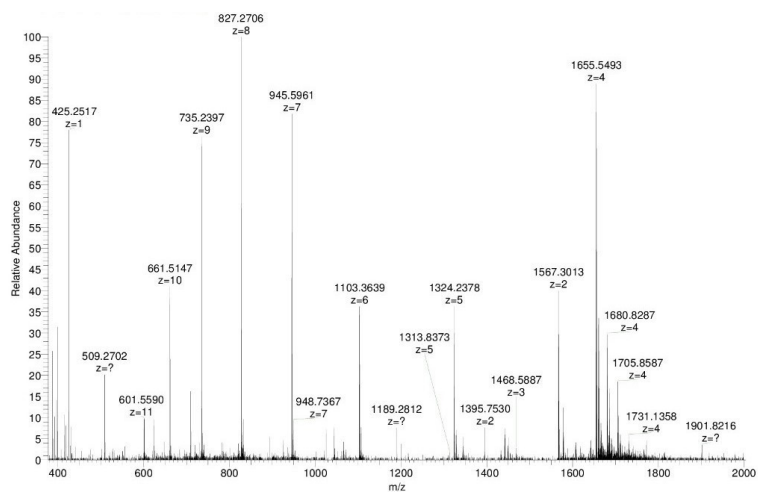


Figure D.19.: Mass spectrum of single strand S8.

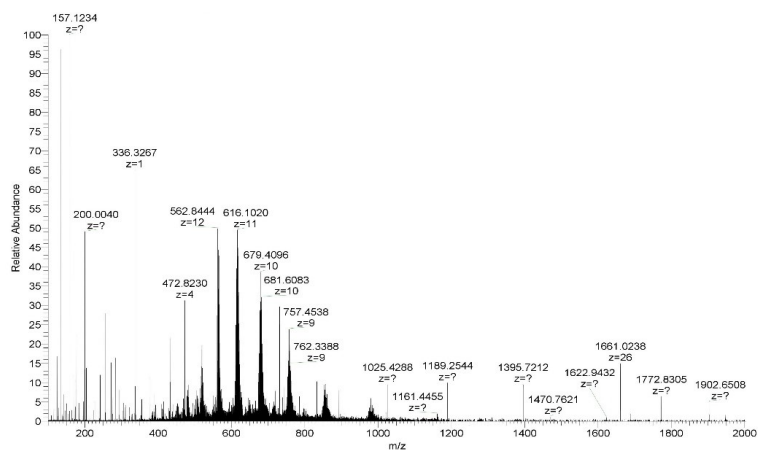


Figure D.20.: Mass spectrum of single strand S9.

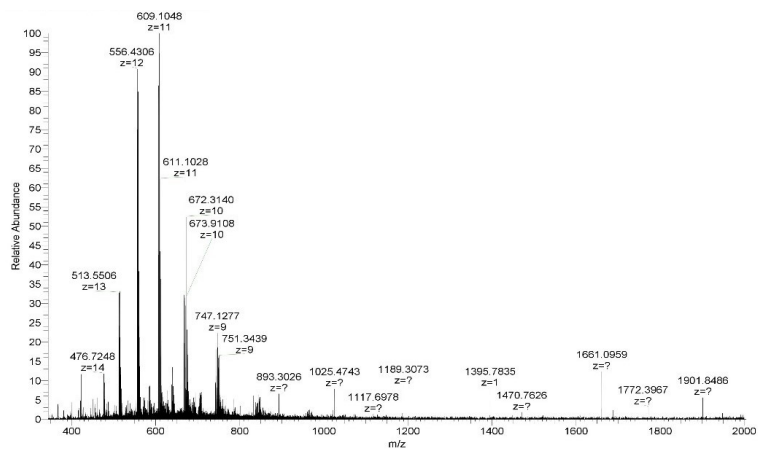


Figure D.21.: Mass spectrum of single strand S10.

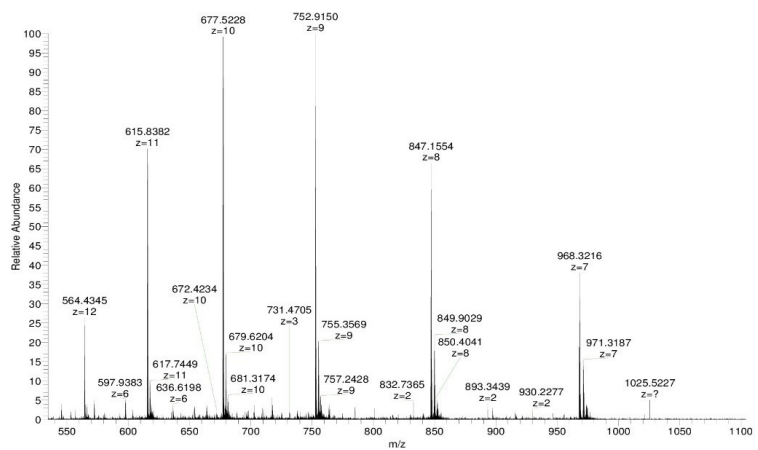


Figure D.22.: Mass spectrum of single strand S11.

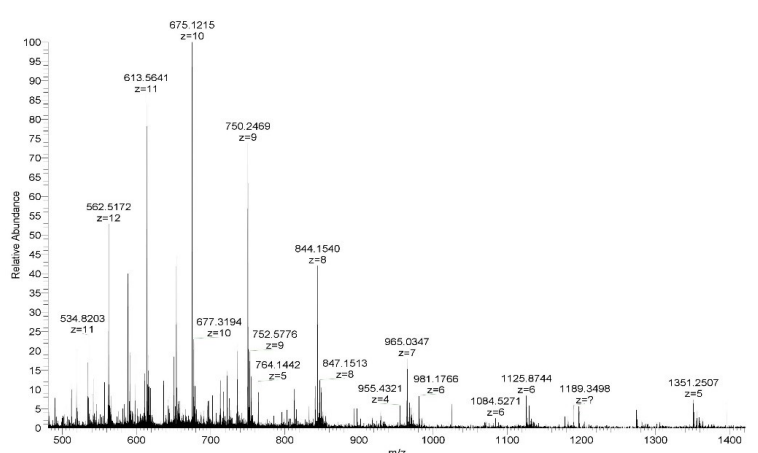


Figure D.23.: Mass spectrum of single strand S12.

## Oligomer Strand for Duplex with Mismatch

Here are the mass spectra of the oligomer strand for the duplex **6 - 8**.

Table D.3.: Calculated and measured masses of oligomer strands.

Strand	Sequence	Calculated mass	Measured mass
S13	3' CCG ATT $\alpha$ T $\alpha$ T $\alpha$ A $\alpha$ AT TTA GCG 5'	6679.8006	6680.1760
S14	3' CCG ATT $\alpha$ A $\alpha$ T $\alpha$ T $\alpha$ AT TTA GCG 5'	6679.8006	6680.1570
S15	3' CCG ATT $\alpha$ T $\alpha$ T $\alpha$ T $\alpha$ AT TTA GCG 5'	6670.7872	6670.1316

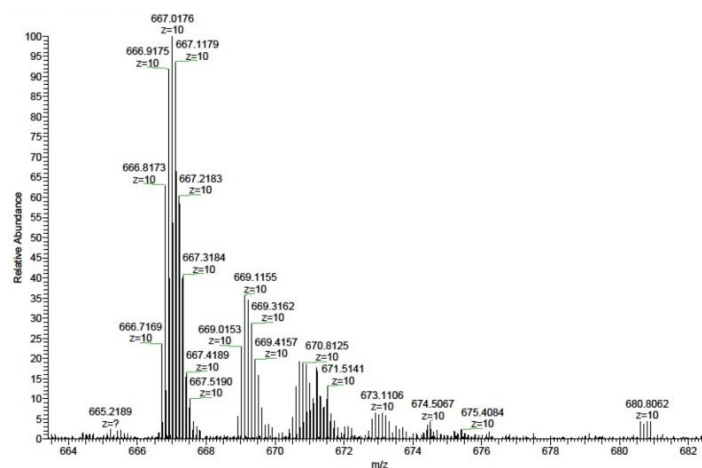


Figure D.24.: Mass spectrum of single strand **S13**.

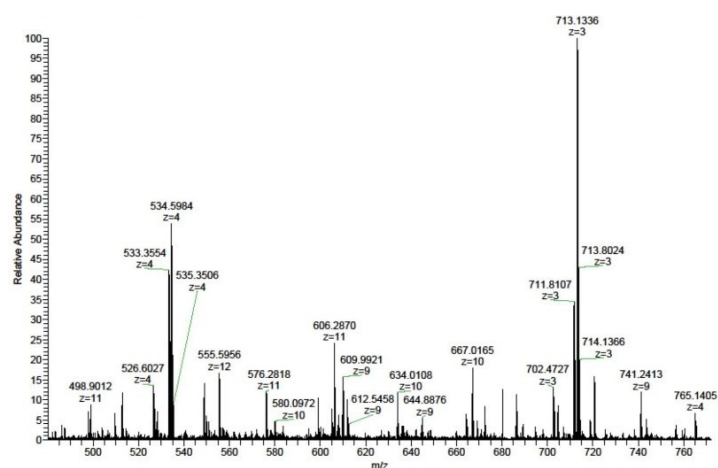
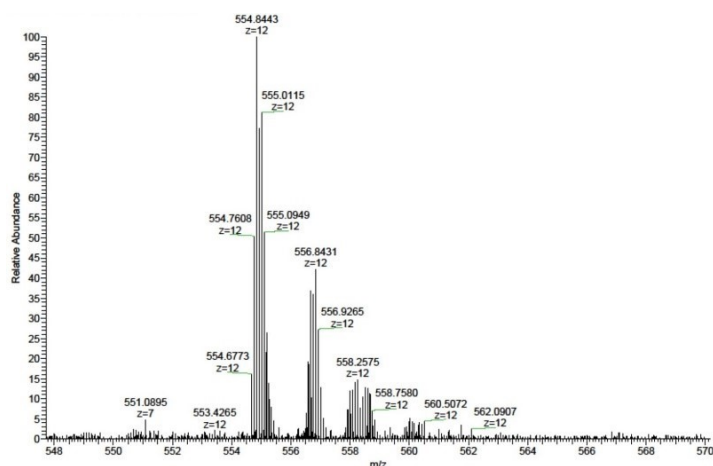


Figure D.25.: Mass spectrum of single strand **S14**.

Figure D.26.: Mass spectrum of single strand **S15**.

## Concentration Determination

The purified oligomers were dissolved in 1 ml MilliQ H<sub>2</sub>O. The absorbance at 326 nm of the diluted stock solutions were measured to determine the concentrations of oligomer strands S2 – S15, using the  $\epsilon_{326}$  value of 34'500 for 3,6-dialkynylphenanthrene.<sup>190</sup> Concentration of strand S1 was determined differently, because it does not contain 3,6-dialkynylphenanthrene. The molar absorption coefficient at 260 nm was calculated using the  $\epsilon_{260}$  values of 15'300, 11'700, 7'400 and 9'000 for A, G, C and T bases, respectively, and 30'000 for 1,8-dialkynylpyrene.

---

# Erklärung

gemäss Art. 18 PromR Phil.-nat. 2019

Name/Vorname: Bürki Nutcha

Matrikelnummer: 10-914-489

Studiengang: Chemie und Molekulare Wissenschaften

Bachelor

Master

Dissertation

Titel der Arbeit: Functionalization of Supramolecular Assemblies of Polyaromatic Oligophosphates and Energy Transfer in DNA-assembled Oligochromophores

LeiterIn der Arbeit: Prof. Dr. Robert Häner

Ich erkläre hiermit, dass ich diese Arbeit selbständig verfasst und keine anderen als die angegebenen Quellen benutzt habe. Alle Stellen, die wörtlich oder sinngemäss aus Quellen entnommen wurden, habe ich als solche gekennzeichnet. Mir ist bekannt, dass andernfalls der Senat gemäss Artikel 36 Absatz 1 Buchstabe r des Gesetzes über die Universität vom 5. September 1996 und Artikel 69 des Universitätsstatuts vom 7. Juni 2011 zum Entzug des Dokortitels berechtigt ist.

Für die Zwecke der Begutachtung und der Überprüfung der Einhaltung der Selbständigkeitserklärung bzw. der Reglemente betreffend Plagiate erteile ich der Universität Bern das Recht, die dazu erforderlichen Personendaten zu bearbeiten und Nutzungshandlungen vorzunehmen, insbesondere die Doktorarbeit zu vervielfältigen und dauerhaft in einer Datenbank zu speichern sowie diese zur Überprüfung von Arbeiten Dritter zu verwenden oder hierzu zur Verfügung zu stellen.

Bern, 18.03.2021

Ort/Datum

Unterschrift